MCEER
EARTHQUAKE ENGINEERING TO EXTREME EVENTS

ISSN 1520-295X

Remote Sensing for Resilient Multi-Hazard Disaster Response

Volume III: Multi-Sensor Image Fusion Techniques for Robust Neighborhood-Scale Urban Damage Assessment

by
Beverley J. Adams and Anneley McMillan

Technical Report MCEER-08-0022

November 17, 2008

This research was conducted at ImageCat Ltd. and was supported primarily by the Earthquake Engineering Research Centers Program of the National Science Foundation under award number EEC 9701471.

NOTICE

This report was prepared by ImageCat Ltd. as a result of research sponsored by MCEER through a grant from the Earthquake Engineering Research Centers Program of the National Science Foundation under NSF award number EEC-9701471 and other sponsors. Neither MCEER, associates of MCEER, its sponsors, ImageCat Ltd., nor any person acting on their behalf:

a. makes any warranty, express or implied, with respect to the use of any information, apparatus, method, or process disclosed in this report or that such use may not infringe upon privately owned rights; or

b. assumes any liabilities of whatsoever kind with respect to the use of, or the damage resulting from the use of, any information, apparatus, method, or process disclosed in this report.

Any opinions, findings, and conclusions or recommendations expressed in this publication are those of the author(s) and do not necessarily reflect the views of MCEER, the National Science Foundation, or other sponsors.

Remote Sensing for Resilient Multi-Hazard Disaster Response

Volume III: Multi-Sensor Image Fusion Techniques for Robust Neighborhood-Scale Urban Damage Assessment

by

Beverley J. Adams[1] and Anneley McMillan[2]

Publication Date: November 17, 2008
Submittal Date: April 8, 2008

Technical Report MCEER-08-0022

Task Number 10.3.1

NSF Master Contract Number EEC 9701471

1 Managing Director, ImageCat, Ltd.
2 Research Scientist, ImageCat, Ltd.

MCEER
University at Buffalo, State University of New York
Red Jacket Quadrangle, Buffalo, NY 14261
Phone: (716) 645-3391; Fax (716) 645-3399
E-mail: *mceer@buffalo.edu*; WWW Site: *http://mceer.buffalo.edu*

NTIS DISCLAIMER

- This document has been reproduced from the best copy furnished by the sponsoring agency.

Preface

The Multidisciplinary Center for Earthquake Engineering Research (MCEER) is a national center of excellence in advanced technology applications that is dedicated to the reduction of earthquake losses nationwide. Headquartered at the University at Buffalo, State University of New York, the Center was originally established by the National Science Foundation in 1986, as the National Center for Earthquake Engineering Research (NCEER).

Comprising a consortium of researchers from numerous disciplines and institutions throughout the United States, the Center's mission is to reduce earthquake losses through research and the application of advanced technologies that improve engineering, pre-earthquake planning and post-earthquake recovery strategies. Toward this end, the Center coordinates a nationwide program of multidisciplinary team research, education and outreach activities.

MCEER's research is conducted under the sponsorship of two major federal agencies: the National Science Foundation (NSF) and the Federal Highway Administration (FHWA), and the State of New York. Significant support is derived from the Federal Emergency Management Agency (FEMA), other state governments, academic institutions, foreign governments and private industry.

MCEER's NSF-sponsored research objectives are twofold: to increase resilience by developing seismic evaluation and rehabilitation strategies for the post-disaster facilities and systems (hospitals, electrical and water lifelines, and bridges and highways) that society expects to be operational following an earthquake; and to further enhance resilience by developing improved emergency management capabilities to ensure an effective response and recovery following the earthquake (see the figure below).

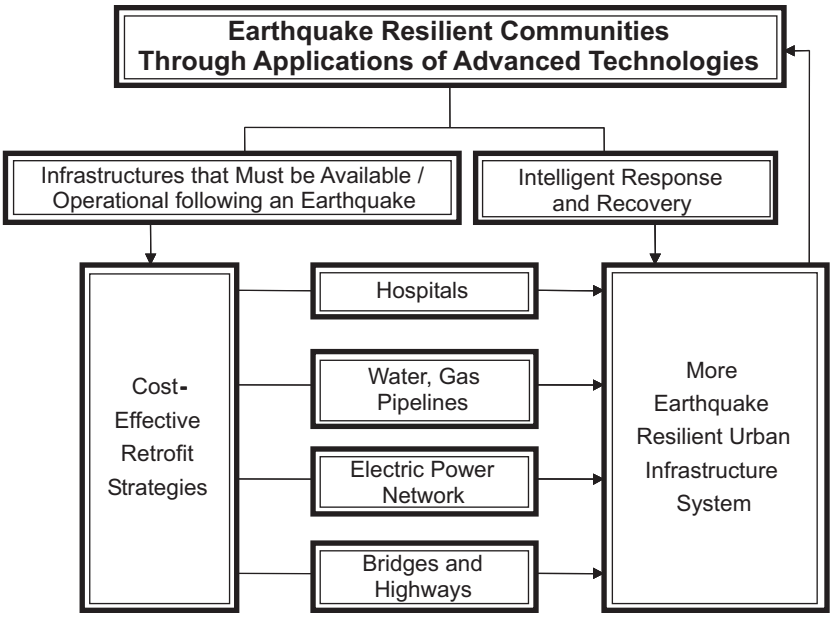

A cross-program activity focuses on the establishment of an effective experimental and analytical network to facilitate the exchange of information between researchers located in various institutions across the country. These are complemented by, and integrated with, other MCEER activities in education, outreach, technology transfer, and industry partnerships.

This report investigates multi-sensor pixel-based image fusion methodologies, combining 'before' and 'after' images from two different high-resolution optical satellites (Quickbird and IKONOS), to assess neighborhood damage extent and severity. The 2003 earthquake that struck Bam, Iran is used as a case study. Three different pixel-based methodological approaches were used to investigate damage-related changes: spectral comparison, textural comparison and edge-based comparison. The results showed that all three damage detection methods successfully identified building collapse within neighborhoods of Bam. This is Volume III of a five part series of reports that investigate the use of remote sensing techniques for resilient multi-hazard disaster response.

PREFACE

This preface introduces a five volume series, documenting scientific research conducted by MCEER researchers at ImageCat, Inc., investigating remote sensing techniques for resilient disaster response.

Volume I: INTRODUCTION TO DAMAGE ASSESSMENT METHODOLOGIES

Volume II: COUNTING THE NUMBER OF COLLAPSED BUILDINGS USING AN OBJECT-ORIENTED ANALYSIS: CASE STUDY OF THE 2003 BAM EARTHQUAKE

Volume III: MULTI-SENSOR IMAGE FUSION TECHNIQUES FOR ROBUST NEIGHBORHOOD-SCALE URBAN DAMAGE ASSESSMENT

Volume IV: A STUDY OF MULTI-TEMPORAL AND MULTI-RESOLUTION SAR IMAGERY FOR POST-KATRINA FLOOD MONITORING IN NEW ORLEANS

Volume V: INTEGRATION OF REMOTE SENSING IMAGERY AND VIEWS™ FIELD DATA FOR POST-HURRICANE CHARLEY BUILDING DAMAGE ASSESSMENT

The report series embraces MCEER's stated mission of pursuing *the discovery and development of new knowledge, tools and technologies that equip communities to become more disaster resilient in the face of earthquakes and other extreme events*. Accordingly, the research documented here is multi-hazard in nature, spanning international earthquake, flood and hurricane events. In all cases, the research is undertaken with the underlying goal of improving resilience, in particular the *rapidity* and *resourcefulness* of disaster response activities. Further, it is aimed at meeting stated User needs in the immediate aftermath of disasters, such as a rapid estimate of the number of collapsed/damaged structures, and the delineation of flood inundation zones.

These volumes represent a significant milestone in post-disaster damage assessment, constituting the culmination of seven years' research activities. During this time, we have witnessed the 'Coming of Age' of remote sensing technologies and analytical techniques within the disaster response arena. *Technology push* in the form of new sources of high-resolution imagery and increasingly advanced and analytical techniques has driven the development of new capabilities attuned to meet the needs of responders. This has been coupled with heightened *User pull* from sectors including the re/insurance industry, and with the onset of recent catastrophes such as hurricane Katrina, opportunities for operational implementation.

Research collaborations established by ImageCat, Inc. with multi-hazard researchers from the US, Italy and UK, underpin this report series. Through sharing and exchanging a wealth of experience and expertise, the teams of scientists and engineers have advanced the knowledge boundaries of remote sensing damage detection. Particular highlights include:

- ✓ The ability to rapidly count the number of collapsed buildings, where a building is treated as an 'object' within the digital image, rather than a group of pixels (Volume II in collaboration with the University of Bologna)
- ✓ The fusion of pre- and post-disaster imagery captured by different high resolution sensors to facilitate flexible damage mapping irrespective of which sensor passes first over the disaster zone (Volume III)
- ✓ The use of cloud-penetrating to assess flooding extent throughout storm-ridden areas (Volume IV in collaboration with University College London)
- ✓ HAZUS-compatible post-hurricane damage assessment based on remote sensing imagery, when access to the disaster zone is precluded (Volume V in collaboration with Texas Tech University).

In June 2006, MCEER launched its Remote Sensing Institute (RSI), which will *serve as a platform for developing and operationally implementing innovative multi-hazard techniques, strategies and products for rapidly assessing post-disaster impacts, modeling and quantifying the built environment, and monitoring recovery*. The RSI will continue to embrace fundamental and applied research activities to develop innovative new approaches to short- and long-term disaster management. Commercial products and services developed by MCEER researchers and available through RSI include: near real-time flood, surge, hurricane, earthquake and tsunami damage assessment through remote sensing-based damage scales and advanced image analysis techniques; and forensic GPS-registered damage assessment using the in-field VIEWS™ data collection and visualization system.

ABSTRACT

Volume III of this five volume damage detection report investigates multi-sensor pixel-based image fusion methodologies, combining 'before' and 'after' images from two *different* high-resolution optical satellites (Quickbird and IKONOS) to assess neighborhood damage extent and severity; the 2003 Bam (Iran) earthquake is employed as a case study.

Since the advent of high-resolution optical satellite imagery, a number studies have explored its use for multi-temporal damage detection (for details see the literature review in Volume I of this report series). Operationally, a significant challenge facing its implementation for post-disaster relief is the timeliness with which reliable damage information is distributed. One obvious way of improving timeliness and thereby *resilience* is to increase the rapidity of imagery acquisition after the event occurs. When detecting damage using satellite imagery, previous research has shown that the most accurate method of assessing changes is using a pair of 'before' and 'after' event scenes. Ideally, for ease of processing, these images would be collected by the same satellite. However, from a practical standpoint, the speed of response may be maximized by combining pre- and post-disaster images acquired by different sensors.

Conducting multi-temporal change/damage detection using images from different satellites poses significant technical challenges due to variations between their spatial, spectral, system and platform specifications. A review of previous studies integrating imagery from different sensors is initially presented. A series of pre-processing and processing steps are then introduced to counteract fundamental non-damage related differences between the images. These include: pan-sharpening, co-registration and resampling and histogram matching. Vegetation exclusion and roof\ inclusion masks are also presented, as they counteract both multi-sensor and non-disaster multi-temporal differences.

Having taken steps to mitigate multi-sensor effects, three different pixel-based methodological approaches are used to investigate damage-related changes:

i) Spectral comparison: Detects building collapse in terms of fundamental changes in DN values between the before and after imagery, testing the hypothesis that building collapse in Bam creates a reduction in reflectance within optical bands of the spectrum, where bright roofs of intact buildings are replaced by darker piles of rubble comprising the constituent materials.

ii) Textural comparison: Detects building collapse in terms of changes in the degree of homogeneity displayed by urban features, testing the hypothesis that chaotic piles of rubble associated with collapsed buildings will exhibit poorly-defined edge structures and high textural variability, which produces a statistically measurable difference in textural indicators

iii) Edge-based comparison: Detects building damage in terms of changes in the frequency of edges associated with intact versus collapsed structures, testing the hypothesis that collapsed buildings show fewer edges in the post-earthquake image, as distinct building boundaries are replaced by an indistinct and chaotic pattern of debris.

Validating the results against a visual inspection-based assessment of building damage from Yamazaki *et al.* (2004b), the processing steps undertaken to mitigate multi-sensor effects were largely successful. Further, all three damage detection methods successfully identified building collapse within neighborhoods of Bam.

Specifically, the results suggest that for the spectral comparison the working hypothesis can be accepted that a lower spectral response is associated with the debris of collapsed structures versus the homogenous roofs of non-damage buildings. For the textural analysis, the working hypothesis is rejected that chaotic piles of rubble associated with collapsed buildings exhibit poorly-defined edge structures and high textural variability. Alternative hypotheses are proposed that there is reduced chaos and lower dissimilarity, lower entropy and higher correlation within neighborhoods sustaining extreme building damage. For the edge-based comparison, the working hypothesis is accepted that collapsed buildings show fewer edges in the post-earthquake image, as distinct building boundaries are replaced by an indistinct and chaotic pattern of debris.

ACKNOWLEDGEMENT

This research was conducted at ImageCat, and was supported in whole or in part by the Earthquake Engineering Research Centers Program of the US National Science Foundation under award number EEC-9701471 to MCEER. We would like to thank MCEER Thrust Area III leader Kathleen Tierney for her continued guidance and support for this research.

Additionally, we would like to acknowledge the following individuals for their contributions to the work documented in these five volumes:

Gabriele Bitelli, DISTART, University of Bologna

Simon Chesworth, MDA Corporation

Shubharoop Ghosh, ImageCat, Inc.

Marjorie Greene, EERI

Charles K. Huyck, ImageCat, Inc.

Kishor Mehta, WISE Center, Texas Tech University

Jeremy Morley, Department of Geomatic Engineering, UCL

Keiko Saito, Cambridge University Centre for the Risk in the Built Environment (CURBE)

J. Arn Womble, WindForce Associates, Inc

Thuy Vu, GTRC, Japan

TABLE OF CONTENTS

TABLE OF CONTENTS (CONTINUED)

LIST OF ILLUSTRATIONS

LIST OF ILLUSTRATIONS (CONTINUED)

LIST OF ILLUSTRATIONS (CONTINUED)

LIST OF ILLUSTRATIONS (CONTINUED)

LIST OF ILLUSTRATIONS (CONTINUED)

LIST OF TABLES

LIST OF TABLES (CONTINUED)

SECTION 1
INTRODUCTION

1.1 Rationale and Literature Review

Volume III of this five volume damage detection report series documents research conducted by MCEER researchers at ImageCat, with the objective of *developing a multi-sensor pixel-based image fusion methodology, combining before and after images from different satellites to assess neighborhood damage extent and severity*. The 2003 Bam (Iran) earthquake is employed as a case study.

In the aftermath of a major earthquake, the rapid assessment of urban damage extent and severity is valuable because it may be used operationally for a range of applications, including:

- Identifying affected areas for assessing resource requirements
- Highlighting the hardest-hit locations for prioritizing the deployment of emergency teams and resources
- Establishing provisional indicators of damage and casualties, in order to communicate the scale of the disaster and to obtain support from national and international organizations including Governments and aid agencies.

There is growing recognition of the important role that remote sensing technology has to play in providing a quick-look post-disaster damage assessment. As noted in Chapter 2, this is a function of technology push and User pull (Adams, 2005). In the case of User pull, a remote sensing-based approach to damage detection offers a *resilient* assessment of the post-disaster situation, through *rapid* situation assessment and the implementation of a *resourceful* technique that is not affected by ground-access issues.

In the case of technology push, a considerable volume of research has been conducted during the 1990's and since the start of the new millennium, to develop techniques for rapid semi-automated multi-temporal damage assessment. As discussed by the literature review within Volume I, following events dating back to the 1995 Hyogoken-Nanbu (Kobe) earthquake, moderate resolution optical satellites have been successfully used to provide a broadscale indication of damage extent (Adams, 2004; Adams and Huyck, 2006; Adams *et al.*, 2004a; Eguchi *et al.*, 2000a, 2000b, 2003b; Estrada *et al.*, 2001b, 2003; Huyck *et al.*, 2002, 2004a; Kaya *et al.*, 2004, 2005; Kohiyama and Yamazaki, 2005a, 2005b; Kohiyama *et al.*, 2003; Matsuoka and Yamazaki, 1998, 2000b, 2002; Ozisik and Kerle, 2004; Tralli, 2000; Turker and San, 2003; Yamazaki, 2001). The utility of SAR systems for damage assessment has also been investigated (Aoki *et al.*, 1998; Archiniegas *et al.*, in press; EDM, 2000; Matsuoka and Yamazaki, 2002, 2003, 2004a, 2004b, 2005, 2006; Mansouri and Shinozuka, 2005; and Mansouri *et al.*, 2004, 2005).

Since the advent of high-resolution optical satellite imagery, a number studies have explored its use for multi-temporal damage detection at a Tier 2 Neighborhood scale within the tiered reconnaissance framework (see Volume I). Although progress has been made using multi-

temporal high-resolution imagery, a number of operational barriers persist, which have limited it use within the disaster response community. Operationally, one significant challenge is the timeliness with which reliable damage information is distributed. This is largely a function of the frequency of imagery acquisition, which is in turn determined by a number of factors including: satellite overpass schedules; flexibility with acquisition specifications (for example, can the system point); occurrence of obscuring effects such as cloud; and processing/delivery speed. One obvious way of improving timeliness and thereby resilience is to increase the rapidity of imagery acquisition after the event occurs. Practically, this may be achieved by increasing the number of orbiting sensors, or improving the ability to manipulate the acquisition specifications of existing sensors.

Effectively utilizing such an expanded imagery set is, however, also highly dependent on the availability of robust image processing algorithms. Robust processing is demanded because it may be necessary or advantageous to combine pre- and post-disaster images captured by two different sensors. Figure 1-1 provides a schematic illustration of the benefits offered by 'multi-sensor' analysis, over and above traditional single-sensor studies. Niemeyer and Canty (2003) emphasize the importance of flexible techniques which are robust. For example, new systems have a limited historic archive, so in many cases, multi-temporal damage assessment would require a 'before' image from an alternative sensor. Equally, there may simply be no pre-event archive for a given sensor, or the catalogue may comprise older images that are deemed unreliable. Combining images from two different sensors also presents an opportunity to improve accuracy levels by minimizing the effects of other non-disaster-related sources of change. To minimize seasonal sources of change between the images, the 'before' image is ideally either dated close to the disaster, or captured at a similar time of year. The most recent 'before' image may have been acquired by a different sensor to the first available 'after' scene. Flexibility in the choice of sensor could also help by mitigating other common sources of variability, such as atmospheric calibration, look angle and sun illumination (see, for example, Neilsen *et al.* 1998).

Conducting multi-temporal change/damage detection using images from different satellites poses significant technical challenges. In the case of high-resolution optical systems, the actual change detection process (such as differencing or correlation) that is applied to single source before and after data remains the same when images from different sensors are used. However, new challenges are encountered during the pre-processing and processing stages leading up to this point, due to differences between the spatial, spectral, system and platform specifications of the various sensors. These differences create new sources of compatibility issues between 'before' and 'after' data, in addition to familiar effects such as seasonal change and random variations in ground surface features detectable in high-resolution coverage (such as the movement of vehicles). For example, Quickbird acquires panchromatic and multispectral imagery at 0.6m/2.4m and IKONOS at 1m/4m. This poses a complex challenge of how to compare individual pixels that cover slightly different areas of the ground surface. Also, the wavelengths spanned by the blue, green, red and near infrared bands are slightly different. This requires a technique to accommodate subtle differences in the spectral return for each and every ground surface feature. Another source of variation is the processing routine employed to account for atmospheric effects. This may alter the brightness of each pixel value. These differences are listed in Section 1.2.

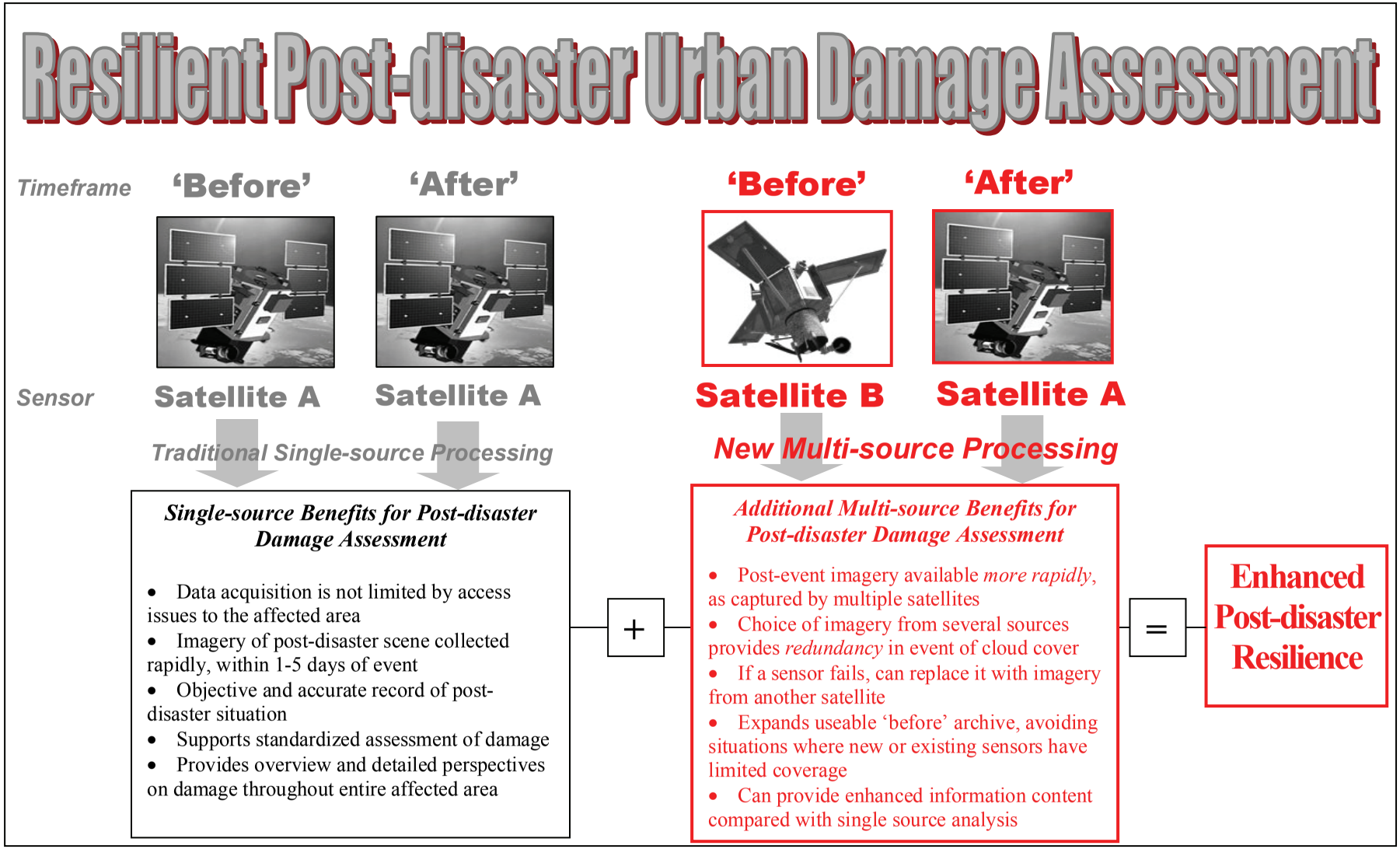

Figure 1-1 Schematic Representation of the Potential for Enhanced Post-Disaster Resilience Through More Rapid Urban Damage Detection Offered Through the Resourceful Fusion of Multi-Satellite Imagery (Multi-Source), versus Traditional Analysis Using Images from a Single-Satellite (Single-Source).

A multiplicity of terminology surrounds the use of data from different sources to gain enhanced output. A discussion of definitions is found in Pohl and van Genderen (1998). Terms such as 'data integration', 'data fusion', 'image fusion', 'image merging', 'image integration', 'cross-sensor' and 'multi-sensor' are all commonly used. 'Cross-sensor' has a connotation of examining the differences between two sensors, perhaps in relation to calibrating them (see, for example, Boccippio *et al.* 2000). *Multi-sensor* analysis suggests the use of two or more sensors in one study, generally with the aim of utilizing them to enhance data analysis or to create a new solution. As such, this definition is deemed appropriate for the current study.

The term 'data fusion' is defined as the process of dealing with data and information from multiple sources to achieve refined/improved information for decision making (Hall, 1992), and has been applied broadly to encompass the fusion of different types of information, for instance fusing raster imagery with digital elevation data, or vector data with raster (Ware 2003, Gens 2004). Data integration is generally linked with GIS applications (Pohl and van Genderen, 1998). Considering that the present study is concerned with the fusion of images captured by different sensors, the procedure may be better represented by the term *image fusion*, defined as 'the combination of two or more different images to form a new image by using a certain algorithm' (Pohl and van Genderen, 1994).

In general terms, data fusion encapsulates a diversity of procedures, offering the potential to create novel synergistic solutions where, by definition, the whole is greater than the sum of the parts. Table 1-1 cites a range of examples from the literature, and briefly describes the degree to which they have been used for disaster response activities. In summary, statistical methods to detect change involving multi-sensor information have been used, such as the multiplication of images, ratios, summation, and some normalization routines (for a review, see Pohl and van Genderen, 1998). Other examples include Price (1987), Ehlers (1991) Mouat *et al.* 1993, and Mangolini *et al.* (1993). In most cases, problems were encountered during processing, due to the amount of difference between the two images to be analyzed. Factors affecting compatibility for the change detection process ranged from viewing angle, illumination, and shadow to cloud cover.

Applications of these techniques range from flood mapping (Kuehn *et al.* 2002), topographic mapping/updating (Hellwich *et al.* 2007), and land use studies, to forestry (Kosaka *et al.* 2005). However, comparatively few of the documented integration processes or multi-temporal change detection methods have been applied in a post-disaster damage assessment context. Resolution or pan-sharpening is the most commonly used technique, although its prior implementation is limited to the enhancement of individual scenes (e.g. Zhang 2004; Guo and Pinliang, 1989; Pohl and van Genderen , 1998). Huyck *et al.* (2004a) and Stramondo *et al.* (2006a, 2006b) explore the potential of integrating optical and SAR imagery after the 1999 Marmara and 2003 Bam earthquakes. Huyck *et al.* (2005) conduct a preliminary study into the integration of high-resolution pre- and post-disaster optical imagery of Bam acquired by different sensors. However, this work is exploratory, and serves to highlight challenges associated with the integration process, which form the basis of the present study.

Table 1-1 Pixel-Based Image Fusion Techniques Documented in the Literature. Prior Use for Post-Disaster Response and Damage Assessment is Described.

Technique	Description	Prior use for disaster response	Citations
General Techniques			
a) Cross-sensor integration	• A common example of cross sensor integration is the fusion of Synthetic Aperture Radar (SAR) with optical data. Techniques include: overlay; colour transformation; subsititution; and PCA. Advantages of optical data include its high resolution, spectral properties and easy interpretability. Radar data may add additional information about the roughness and water content of the ground surface, and counteracts gaps in an analysis due to cloud cover or shadow (Pohl and van Genderen, 1998). Other examples include the combination of aerial imagery and SPOT satellite coverage, and aerial and TM data. • Techniques include: Brovey transformation; classification; thematic generalization, spatial aggregation, canononical correlation analysis (MAD transformation) and bayesian threshold determination.	• Exploratory study by Huyck *et al.* (2005) combining IKONOS and Quickbird imagery of the Bam earthquake. Identified processing issues requiring further research. • Stramondo *et al.* (2006a, 2006b) classify indices extracted from S AR and optical data to assess damage caused by the 1999 Marmara and 2003 Bam earthquakes. • Following the World Trade Center attack, optical aerial imagery was integrated with lidar, infra-red imagery and digital photography linked by GPS.	**General** Aschbacher & Lichtenegger, (1990), Brisco and Brown (1995), Corves (1994), Dallemand *et al.* (1992), Harris *et al.* (1990), Limpitlaw and Gens (2006), Neilsen *et al.* (1998), Petit and Lambin (2001) **Damage detection** Huyck *et al.* (2004a) , Rodarmel *et al.* (2002), Stramondo *et al.* (2006a, 2006b)
b) Multi-temporal change detection	• Multi-temporal changes are assessed by comparing images from two or more different dates. Statistical methods of comparison include the multiplication of images, ratios, summation, and some normalization routines.	• Single exploratory study after the Bam earthquake looking at the integration of Quickbird and IKONOS imagery (Huyck *et al.*, 2005).	**General** Ehlers (1991), Pohl and van Genderen (1998), Price (1987), Mouat *et al.* (1993), Mangolini *et al.* (1993) **Damage detection** Huyck *et al.* (2005)
Specific Techniques			
c) Resolution merge or pansharpening	• This utilizes the spectral properties of the multi-spectral bands of a sensor and the increased spatial resolution of the panchromatic band to better distinguish ground surface features (Gungor and Shan 2004). Documented techniques include RGBI, IHS, Brovey, YIQ, wavelet, ESST 3H and 3S, Smoothing Filter-Based Intensity Modulation (SFIM), and HPF additive. • A less common but still useful technique is to resolution merge two inputs from different satellites to create a sharpened or spectrally enhanced image.	• Widely used to maximize the information content of individual 'before' and 'after' high-resolution optical images. No examples combining high resolution sensors (e.g. Quickbird and IKONOS) into a single output. • Moderate resolution inputs from different satellites have been merged (e.g. SPOT and Landsat) to combine the higher panchromatic resolution of SPOT with the spectral range of Landsat.	**General** Gungor and Shan (2004) , Guo and Pinliang (1989), Pohl and van Genderen (1998), Shettigara (1992), Tu *et al.* (2005, 2006) **Damage detection** Not really used for damage detection on its own apart from in visual analysis.

Table 1-1 Pixel-Based Image Fusion Techniques Documented in the Literature. Prior Use for Post-Disaster Response and Damage Assessment is Described.

Technique	Description	Prior use for disaster response	Citations
d) False color composite	• A method of combining images of different dates (see Chapter 7), sensors (Suits *et al.* 1988, Welch *et al.* 1985, Chavez 1987) or imagery types (Aschbacher and Lichtenegger 1990, Comhaire *et al.* 1994, Pohl *et al.* 1994) to provide a visual interpretation of change as a function of variations in colour. • Involves assigning a different image band to each primary display colour. Input bands may include basic spectral bands or processed output (e.g. PCA analysis, texture).	• Used to enhance the visibility of change over time. Has been useful in a number of earthquake studies. • An example is the study of the Bhuj Earthquake in 2001. Useful for the study of hidden fault systems.	**General** Aschbacher and Lichtenegger (1990) Chavez (1987), Comhaire *et al.* (1994), Pohl *et al.* (1994), Suits *et al.* (1988) , Welch *et al.* (1985) **Damage detection** Wang *et al.* (2005), Verma and Rathore (2002), Chiroiu and Andre (2001)
e) Principal Component Analysis	• Principal components analysis (PCA) is a statistical technique for simplifying a data set, by reducing multidimensional data sets to lower dimensions for analysis.	• Has been utilized for post-flood damage evaluation using landsat TM and ETM	**General** Corner *et al.* (1999) **Damage detection** Gianinetto *et al.* (2006)
f) Substitution	• Regression Variable Substitution (or RVS), uses a multiple regression procedure to determine a linear combination (or replacement vector) of an image channel that can be replaced by another channel. (LeMoigne *et al.* 2001) • Canonical variate substitution produces new composite bands based on linear combinations of the original bands (Neilsen, 2002).	• Unmixing-based multi-sensor multi-resolution image fusion • Change detection in multispectral imagery from multi-sensor	**General** Zhukov *et al.* (1999), Nielsen (2002), Liao et al. (2005)

1.2 Approach

Given the pressing need for more robust semi-automated multi-sensor damage detection algorithms, a series of pixel-based methodologies are explored here using Quickbird and IKONOS imagery captured before and after the 2003 Bam earthquake. Table 1-2 identifies general multi-sensor variations between Quickbird and IKONOS imagery, with suggested procedures to account for these differences.

Table 1-2 General Multi-Sensor Differences Between IKONOS and Quickbird Imagery, and Suggested Procedures to Account for the Variation

Multi-sensor difference between IKONOS and Quickbird	**Suggested procedure to account for difference used in this study.**
Wavelength difference	Needs an approach which is less reliant on subtle spectral differences. Feature extraction (i.e. edge detection) suggested.
Atmospheric effects – i.e. cloud / haze	Difficult to account for in pre-processed imagery. Masking if warranted.
Resolution	Needs a re-sampling strategy to create a comparable pixel size.
Time of day when image was acquired – different shadows	Masking – explore shadow spectral signature.
Time of year when image was acquired - vegetation difference	Masking such as an NDVI approach to exclude from analysis.
Difference in look angle	Acquire near nadir imagery: only slight difference. Requires co-registration of images

Building on these considerations, as well as findings from prior research conducted by ImageCat researchers at MCEER (see, for example, Adams *et al.* 2004a, 2004b, Huyck and Adams 2004, Huyck *et al.*, 2004b, Huyck *et al.* 2005, Womble *et al.* 2006) three different approaches are investigated to detect change/damage at a Tier 2 Neighborhood scale. As shown by the methodology flow diagram in figure 1-2, these comprise:

1. Method 1: Spectral comparison
2. Method 2: Textural comparison
3. Method 3: Image primitive comparison through edge-detection

The spectral comparison examines the fundamental spectral response associated with intact and damage structures within the red, green, blue (and near-infrared for masking) bands of the pre- and post-event images, before going on to investigate differencing and classification techniques to extract change. Prior research following disasters including the 1995 Kobe, 1999 Marmara and 2001 Bhuj earthquake suggests that the spectral characteristics of buildings changes when damage is sustained (Chiroiu *et al.* 2002, 2006, Eguchi *et al.* 2002, 2003a, 2003b, Huyck *et al.* 2004a, Matsuoka and Yamazaki 1999, 2000b, Saito and Spence 2004, 2005, Saito *et al.* 2004). Potential issues were anticipated to come from the difference in sensor acquisition specifications,

as well as temporal differences causing shadow and illumination differences. This initial comparison seeks to determine specific changes accompanying adobe structures in Bam.

The textural comparison explores whether differences in texture measures from Quickbird and IKONOS imagery can be attributed to change due to building collapse. Prior research by Adams *et al.*, (2004a), Gusella *et al.* (2005a, 2005b) and Huyck *et al.* (2005) indicates that texture measures such as dissimilarity successfully distinguish between extreme - versus non-damaged states. This technique should rely less on specific spectral differences between the images, and more on the relationship of neighbouring pixel values. The edge detection method examines the use of edge detection filters, to ascertain if the occurrence of edges significantly varies between Quickbird and IKONOS inputs from pre and post earthquake imagery. As well as relying less on spectral properties, in theoretical terms, edge frequency may be expected to change with building collapse, since a single distinct structural boundary comprising perpendicular edges is replaced by piles of rubble that visually are characterised by less sharply defined edge gradients. However the direction of change in the number of edge pixels is difficult to predict as edges may be more frequent, but smaller. This will be interesting to investigate.

The following sections describe the pixel-based image processing and analysis techniques involved in the spectral comparison Method 1 and Results 1 (Section 2 and Section 3), textural Method 2 and Results 2 (Section 4 and 5) and edge-detection Method 3 and Results 3 (Section 6 and 7). In each case, the methodology employs a pair of multi-sensor IKONOS and Quickbird images of Bam, which are subject to the pre-processing steps described in Section 1.3. As a key component of methodology development, the research described in the following sections seeks to identify potential sources of non-compatibility between the multi-sensor input images, and incorporate techniques that accommodate the major sources of multi-sensor noise (see table 1-4). Data fusion techniques to promote compatibility are considered at each step of the pre-processing and methodological processing sequence. Discussion and key findings are reserved for Section 8, with directions for future research outlined in Section 9.

The pixel-based image pre-processing and processing techniques described here were conducted using Geomatica 10 and ENVI software (RSI, 2002). Visualization and accuracy assessments were conducted using ArcGIS.

1.3 Datasets and Pre-Processing

1.3.1 Imagery

Imagery from before the 2003 Bam earthquake was captured by the Quickbird satellite on the 3rd September 2003, and provided courtesy of the EERI Learning from Earthquakes Program. An IKONOS image was available from the 27th December 2003, one day after the earthquake struck. Validation datasets with which to compare damage assessment results were obtained from Yamazaki *et al.* (2004b) and USAID (2004).

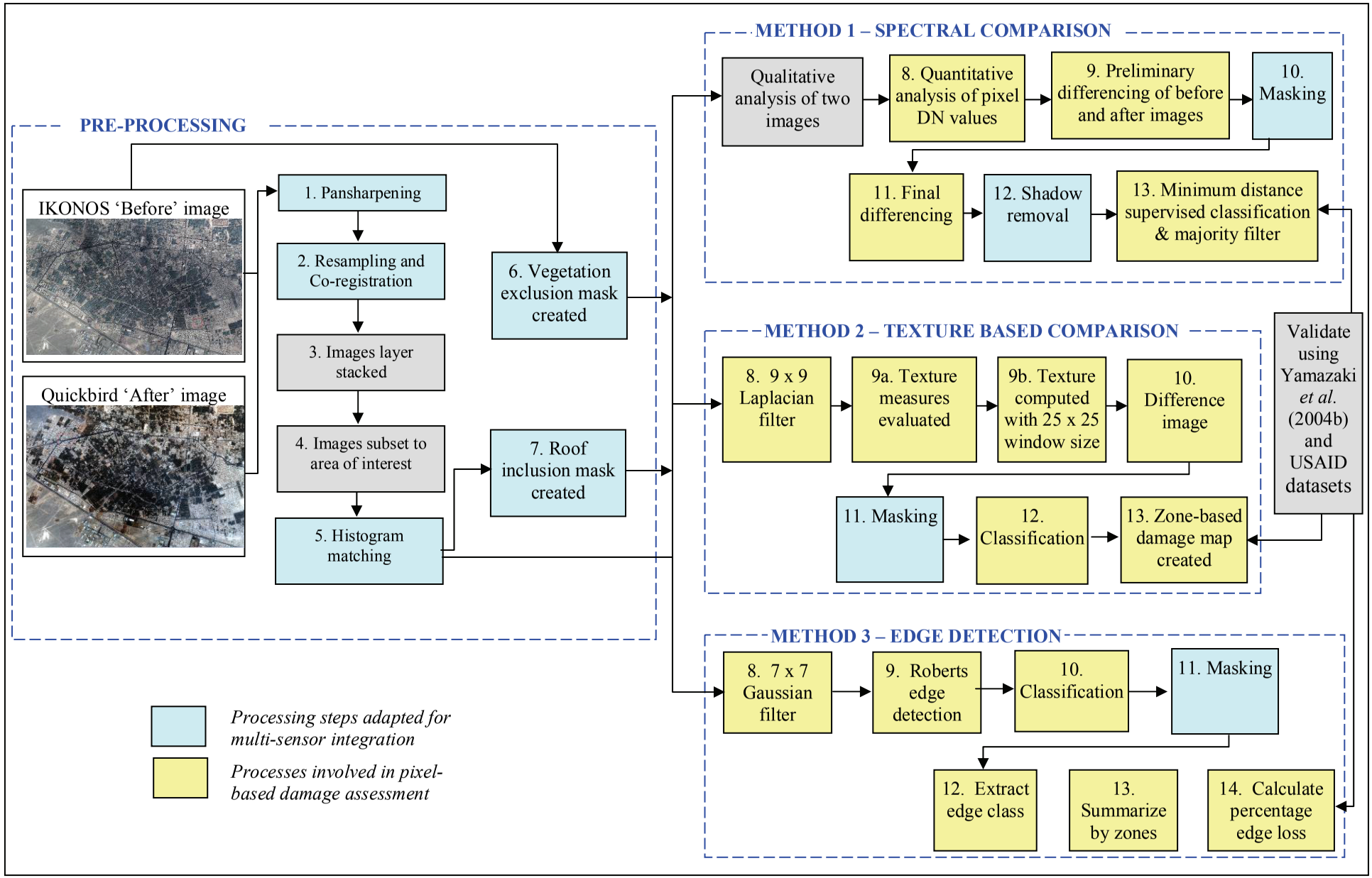

Figure 1-2 Methodology Flow Diagram Illustrating the Three Different Pixel-Based Processing Algorithms Investigated for Assessing Damage Severity and Extent at a Neighborhood Scale: (a) Spectral Comparison; (b) Texture-Based Comparison; and (c) Edge-Detection

The imagery specifications are shown in table 1-3a and table 1-3b. The 'before' dataset was delivered by DigitalGlobe as separate RGB multispectral and panchromatic bands. The panchromatic band has a pixel resolution of 61cm at nadir, and the multispectral band a resolution of 2.44m. The IKONOS image was delivered in pre-pansharpened format, and was therefore subject to the in-house pansharpening regime employed by Geoeye. The algorithm for this operation is unfortunately not available leading to a black box situation in terms of input. The pan-sharpened image has a 1m spatial resolution, integrating 1m panchromatic and 4m multispectral bands. Both images were subject to pre-delivery processing steps conducted by the data provider, including proprietary geometric correction to projection and datum UTM zone 40N WGS84 and radiometric correction to 8 bit range for Quickbird and an 11 bit range for IKONOS.

From preliminary visual assessment, a number of differences are evident between urbanized regions of the 'before' and 'after' scenes. When studied in more detail these are due to a range of sources. Damage to buildings is evident, through changes in the color and configuration of individual structures. However there is, in addition, considerable variability between the general brightness and colors of ground surface features throughout the two scenes. This variability may be distinguished in figure 1-3a and figure 1-3b from, for example, the general increase in brightness across the 'after' image, and the more pronounced visual distinction between vegetated and built environments. As noted in Section 1.1, variability between these datasets emanates from three main sources:

a.) Multi-sensor: different spatial, spectral, system and platform specifications of the sensors

b.) Multi-temporal: temporal effects such as seasonal differences in vegetation cover, as well as acquisition characteristics such as different viewing angle, different illumination angle, different overpass time

c.) Disaster-related: a special case of temporal effects, capturing disaster impacts within the urban environment such as building collapse.

Table 1-3 is color coded to show the relationship between aspects of the imagery specification and their potential importance as a source of multi-temporal or multi-sensor variability. Disaster-related differences are a special case of temporal effects, present due in this case to the use of pre- and post-earthquake datasets.

The present study explores whether a new comparative methodology can be devised using pre- and post-disaster images of Bam that addresses multi-sensor differences, with the overarching goal of developing a truly flexible and rapid approach to earthquake damage detection. The hypothesis is tested that significant non-damage-related changes between the IKONOS and Quickbird imagery are systematic and scene wide, and can therefore be negated out of the analysis.

Before the damage detection analysis can be undertaken, pre-processing of the available datasets is required. As shown in table 1-4, pre-processing by the data provider has already taken place prior to imagery delivery. These processes, however, together with fundamental differences between the sensors, are responsible for a number of multi-sensor variations between the Bam images.

Table 1-3a Quickbird Pre-Earthquake Image Specifications and Pre-Processing Conducted by Data Provider. Potential Sources of Multi-Sensor Difference Addressed in this Research are Highlighted in Blue, and Multi-Temporal Differences in Yellow.

Quickbird Before Earthquake image	Panchromatic	Multispectral
Product level	LV2A (Standard 2A)	LV2A (Standard 2A)
Date of image	03/09/2003	03/09/2003
Pixel size	0.6m	2.4m
numRows	9896	2474
numColumns	15024	3756
Projection and datum	UTM zone 40N WGS84	UTM zone 40N WGS84
Pan-sharpening by data provider	No	No
Radiometric level corrected by data provider	Yes	Yes
Multispectral bands used and wavelength range	-	Red = 630-690 Green = 520-600 Blue = 450-520
Bits per pixel	8	8
Sun angle azimuth	145.3	145.3
Sun angle elevation	53.0	53.0
Satellite azimuth	188.1	188.1
Satellite elevation	79.3	79.3
In-track view angle	-9.8	-9.8
Cross-track view angle	-0.0	-0.0
Off Nadir view angle	10.2	10.2
% Cloud cover	0	0

Table 1-3b IKONOS Post-Earthquake Image Specifications and Pre-Processing Conducted by Data Provider

IKONOS After Earthquake image	Pansharpened
Product level	Standard geometrically corrected
Date of image	27/12/2003 07.01 GMT
Pixel size	1m
numRows	1004
numColumns	1004
Projection and datum	UTM zone 40N WGS84
Pan-sharpening by data provider	Yes
Interpolation level	Cubic convolution
Radiometric level corrected by data provider	Yes
Multispectral bands used and wavelength range	Red = 632-698 Green = 506-595 Blue = 445-516
Bits per pixel	11
Sun angle Azimuth	161.1391
Sun angle elevation	35.29197
Satellite azimuth	177.3888
Satellite elevation	67.21973
Scan Azimuth	359.97
% Cloud cover	43%
% component cloud cover	9%

Table 1-4 Specific Multi-Sensor Variations Between Quickbird and IKONOS Identified for the Pre- and Post-Earthquake Imagery of Bam, Together with Implications for the Methodological Approach Used in this Study

Quickbird 'before'	IKONOS 'After'	Implications for present analysis
No pan-sharpening	Pan-sharpened	• IKONOS combines detailed spatial and spectral information within a single image. For Quickbird the spatial and spectral information is split between separate panchromatic and multispectral images. • Pan-sharpening prior to data delivery precludes use of detailed radiometric adjustment. • Use of different pan-sharpening algorithms creates fundamental spectral variations.
60cm pixels	1m pixels	• Each pixel covers a slightly different area of the ground surface.
8 bit data	11 bit data	• The IKONOS image shows differences between the brightness and colors of each pixel in greater detail.
Proprietary radiometric correction	Proprietary radiometric correction	• Differences not known because technical details of the algorithms used are unavailable.
Red, green, blue Band wavelengths	Red, green, blue Band wavelengths	• The recorded colors of ground surface features are slightly different due to subtle variations between red, green and blue wavelengths.

1.3.2 Pre-Processing

The methodology flow diagram in figure 1-2 shows the full pre-processing sequence employed here, comprising:

1. Pansharpening
2. Co-registration and resampling
3. Image layer stacked
4. Images subset to area of interest
5. Histogram matching
6. Vegetation exclusion mask
7. Roof inclusion mask

Specific pre-processing steps of pan-sharpening, co-registration and resampling and histogram matching are highlighted because they accommodate differences arising from the use of multi-sensor data. The vegetation exclusion and roof\ inclusion masks are also highlighted, as they counteract both multi-sensor and non-disaster multi-temporal differences.

Step 1 Pan-sharpening: The image-fusion pan-sharpening technique offered by PCI Geomatica software was applied to the Quickbird 'before' image. This was used in order to improve multi-sensor compatibility with the IKONOS 'after' image that was delivered in pan-sharpened format. This process also optimizes visual interpretation by combining the detail of the higher resolution panchromatic band with the information content of the red, green and blue spectral bands.

For optimum visualization, a 2% linear contrast stretch was applied to the pansharpening results in figure 1-3. Across the scene, general patterns of spectral response a similar, with the vegetated regions standing out against urban development and open space. However, obvious differences remain between the IKONOS and Quickbird images, in terms of the brightness of the landsurface cover and degree of contrast between vegetation and other landuses. These variations are important sources of non-disaster related difference between images, and as such, affect the ability of change detection methodologies to identify earthquake-related damage. Consequently, subsequent pre-processing steps see to moderate the effects.

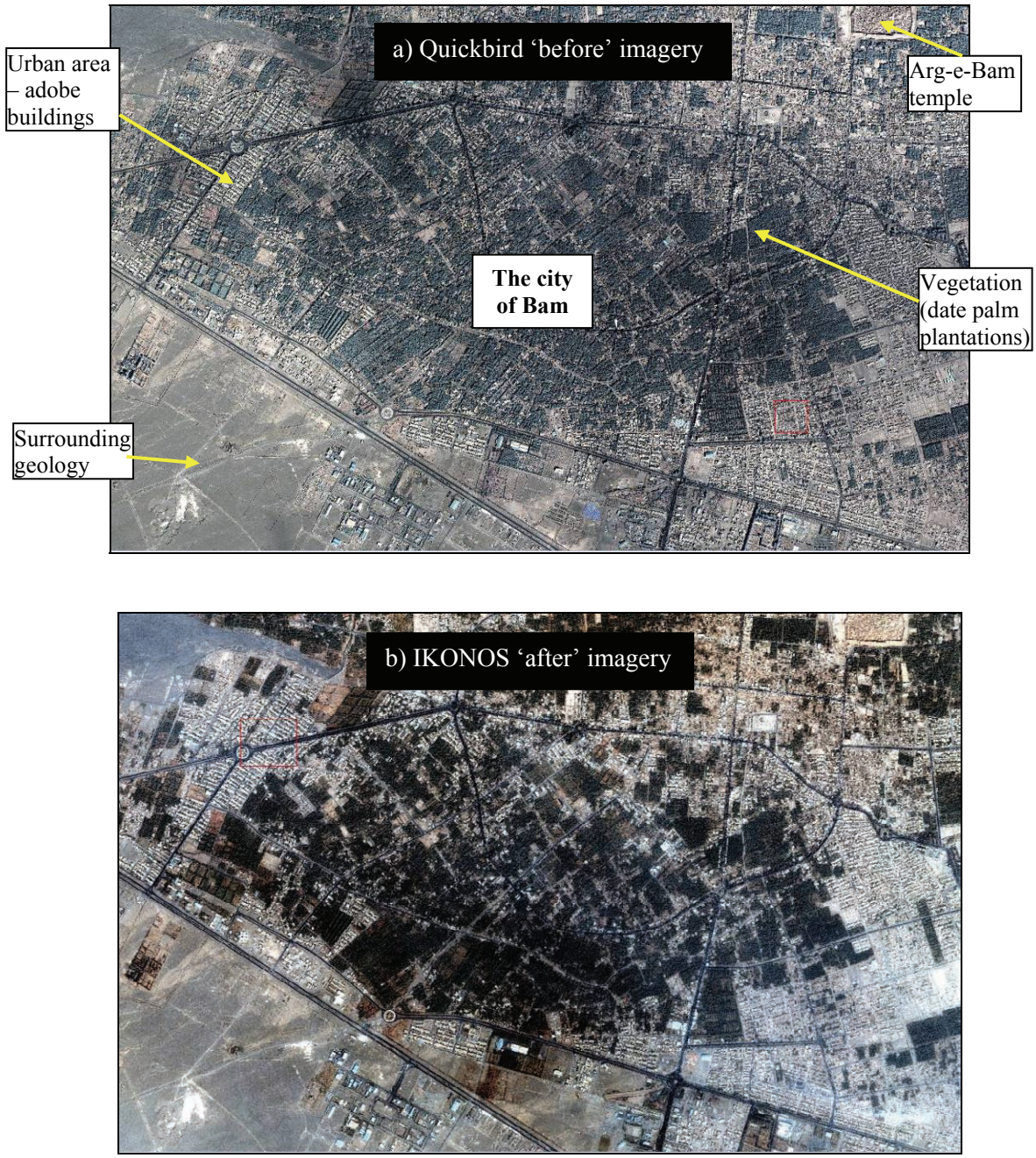

Figure 1-3 (a) Pre-Earthquake Quickbird and (b) Post-Earthquake IKONOS Imagery Delivered in Pan Sharpened Format, with Linear 2% Stretch

Step 2 Resampling and co-registration: One of the most important aspects of a remote sensing-based change detection methodology is the ability to compare 'like with like' in terms of the geographic location of ground surface features. There are several potential sources of differences between the position of ground surface features in this multi-sensor image pair. First, the spatial resolution of the images is different (60cm versus 1m). Second, there may be a spatial offset due to error margins surrounding the georeferencing process. Thirdly, the difference between look angles means that building roofs do not correlate exactly with each other. Steps were taken to address these multi-sensor differences.

A resampling process was undertaken in ENVI to match the pixel size within the pan-sharpened pre- and post-event scenes. A resize function with a nearest neighbor algorithm was applied to the IKONOS image, achieving an output pixel dimension of 60cm. It should be noted that no more information content was achieved by this procedure, only a comparable pixel size.

Accurate registration and georeferencing are critical as 'misregistration causes artificial colors or features in multi-sensor data sets which falsify the interpretation later on' (Pohl and van Genderen, 1998). Geometric corrections have already been carried out prior to the receipt of standard level Quickbird and IKONOS products used here. These include correction of spatial distortions due to systematic sensor and platform-induced effects. Theoretically, geographic locations within the two Bam images should correspond, since they have been geometrically corrected and georeferenced to a common projection and datum. However, initial testing indicated that ground surface features remain slightly offset.

Part of this offset may be due to topographic effects, and should in theory be counteracted by ortho-rectification. The purchase of pre-orthorecified imagery is costly and often delays delivery time, which is unacceptable in a post-disaster situation. In the case of Bam, a trial orthorectification was instead conducted following imagery delivery, using the only readily available DEM (Digital Elevation Model). Application of a 90m SRTM DEM to this relatively flat and homogenous landscape produced only a minor improvement in spatial correspondence. Given the cost of purchasing orthorectified imagery from the satellite provider, the limited success using 90m DEM data, the increase in processing time, and the lack of more detailed and publicly available elevation models for locations around the World, ortho-rectification is not included here as a key processing step.

Instead, to mitigate the offset between the 'before' and 'after' images, a general co-registration process was undertaken. This performs a scene-wide transformation on the images, to ameliorate geographic offset. The Quickbird image was used as a base image as it originally had higher spatial resolution. The IKONOS image was warped using 12 well-spaced ground control points (GCPs). Control points were found that were strong candidates, such as road junctions and building points. Roof points could be matched as the imagery was fairly nadir looking (i.e. the base of the building was indistinguishable from the top of the roof). However, it is noted that small error margins may have been introduced here because of the slight difference in viewing angle between the two acquisitions. This was deemed an important procedure since building roofs are the areas that will be compared by change detection.

Although the resulting RMS error was acceptable at 1.09, there remains, on average, a ground displacement of ~60cm (<1 pixel) between the 'before' and 'after' images.

Step 3 Image layers stacked: The 'before' and 'after' images were subsequently incorporated into a single layer stack for Bam. The purpose of doing this was to ensure the two datasets were aligned and accelerate further processing by analyzing on both images at once rather than separately.

Step 4 Images subset to area of interest: The original images obtained for Bam covered a relatively wide geographic extent, including the foothills of surrounding mountainous regions and the south-eastern satellite settlement of Baravat. Eliminating areas of secondary importance from around the periphery of the image increases the interpretability of the primary area of interest, by minimizing extraneous differences between their spectral characteristics. The full extent of the layer stack was reduced to the area of interest in figure 1-3, with the additional benefit that the efficiency of subsequent image processing steps is optimized.

Step 5 Histogram matching: Following the subsetting process, some spectral variations remain between the Quickbird and IKONOS scenes, as shown in figure 1-4a and figure 1-4b. There are a number of sources of radiometric difference, arising from the subtle variation in wavelength of the red, green and blue bands, the atmospheric conditions on the day/time of imaging, and the proprietary radiometric algorithms applied to standard imagery by the data provider.

Theoretically, a more detailed atmospheric correction may be completed (Pohl and van Genderen, 1998) or a conversion to a Top-of-Atmosphere (TOA) radiance conducted. However, each of these processes adds time to the damage detection process. Moreover, for the present study, detailed correction is precluded due to preprocessing procedures conducted prior to data delivery. The data was delivered in standard format (rather than basic) to which a different black-box correction had been applied by the respective providers.

Furthermore, prior pan-sharpening of the IKONOS scene precludes the use of other potentially useful pre-processing steps such as scene-specific radiometric normalization routines. Since the implementation of a detailed correction routine is precluded, for the present study, a histogram matching process was undertaken instead. Histogram matching automatically matches the histogram of one displayed image to another displayed image, making the brightness distribution of the two images as close as possible. This helps to balance the universal spectral characteristics of the images on a scene-wide basis, and thus encompasses the above sources of variation.

To help facilitate the detection of collapsed buildings, non-collapsed roof signatures needed to be as similar as possible between the two images. Therefore the histogram matching focused on an area of the image where only non-collapsed buildings were found, utilizing the input histogram from a subset of the image where little change was thought to occur. As shown in figure 1-4c, after histogram matching this area of the IKONOS image bears a much closer resemblance to the Quickbird scene.

Step 6 Vegetation exclusion mask: A mask to eliminate ground surface vegetation was created using the 'before' Quickbird image. This was used within the multi-sensor analysis to minimize the effects of vegetation as a source of multi-temporal change between the 'before' and 'after' images. Otherwise, this source of change could override important patterns of disaster-related variation due to building collapse.

(a) Quickbird after PCI pan-sharpening

(b) IKONOS image as delivered, before resampling and histogram matching

(c) IKONOS after resampling and histogram matching

Figure 1-4 Original (a) Quickbird and (b) IKONOS Images, Subject to Different Radiometric Pre- Processing. (c) IKONOS Image After Resampling and Histogram Matching with the Quickbird Scene

An NDVI analysis was performed using the Quickbird multispectral image. From Equation 1-1, NDVI computes the ratio between red (RED) and near-infrared (NIR) bands. Since vegetation has a particularly strong response in the NIR, NDVI values are markedly higher for vegetation compared with other ground surface features. A two class (binary) unsupervised ISODATA classification was undertaken, which thresholded the NDVI image at 0.11. This was then applied to the NDVI result. From figure 1-5a, this successfully separated vegetated from non-vegetated regions, with vegetation assigned a value of zero and non-vegetated areas a value of unity.

$$NDVI = \frac{NIR-RED}{NIR+RED} \tag{1-1}$$

Step 7 Roof inclusion mask: An urban mask retaining building roofs, and suppressing other land surface features such as roads and large areas of geology, was created using the pan-sharpened Quickbird image. Two characteristic classes of building roof are evident within Bam: (1) the scene is dominated by the bright white response of residential adobe structures; and (2) there is limited occurrence of blue-roofed buildings, predominantly in industrial /commercial regions. These roof spectral signatures are relatively constant throughout the Quickbird image, enabling a range of DN values for adobe roofs, and commercial/industrial to be employed as a roof inclusion mask. The mask was created by using a three class supervised classification.

Visual inspection of the mask (figure 1-5b) suggests that the roofs exhibit similar DN values to selected areas of the surrounding geology. Although some non-structural features were retained, the mask is still useful for expelling other areas of the Quickbird image that could hamper analysis, such as roads. The mask does not account for urban features unique to the post-earthquake IKONOS scene, such as shadowing around the margins of intact structures.

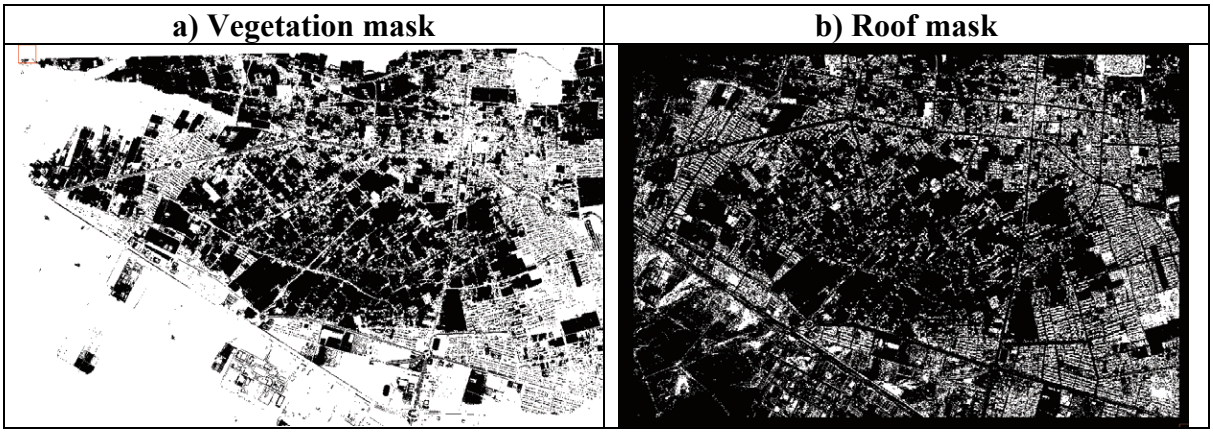

Figure 1-5 Masks Developed for (a) Vegetation Exclusion; and (b) Roof Inclusion

1.3.3 Validation Data

This study explores a series of different neighborhood-scale validation techniques, using damage readings sampled into spatially varied grids that follow street patterns, and a standard grid of regular dimensions. Two datasets were available for validating the results obtained:

1. Percentage building collapse by zone- from USAID (2004)
2. Per building EMS98 damage level – from Yamazaki *et al.* (2004b)

The first validation dataset was published by USAID. This ranks the damage in Bam by percent destroyed buildings within a given city region, as shown in figure 1-6. This was created by a United Nations Disaster Assessment and Coordination (UNDAC) team, undertaking a joint aerial assessment with a team from the United Kingdom. Damage severity was estimated by low-flying over all six search and rescue (SAR) operational zones in 21 districts in Bam and estimating the percentage of collapsed structures. It was noted that areas near the historic Old Fort of Arg-e-Bam, the old city, and the football stadium are particularly badly damaged.

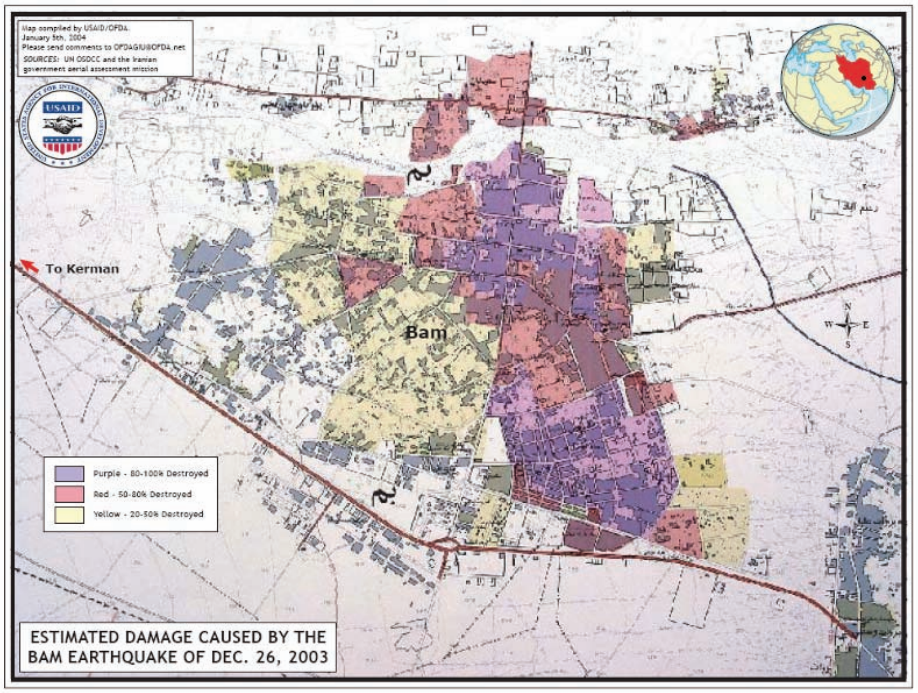

Figure 1-6 USAID Damage Map Showing Three Categories if Building Collapse: 80-100%, 50-80% and 25-50%

The second validation dataset comprises a visually-based per-building damage assessment of ~10,000 buildings within the remote sensing imagery, conducted according to the EMS98 scale (see figure 1-7):

- EMS grade 5, destroyed buildings;
  Total number of buildings counted = 4,097

- EMS grade 4, damaged buildings (Partially collapsed building);
  Total number of buildings counted = 1,436

- EMS grade 3, damaged building (Buildings surrounded by debris);
  Total number of buildings counted = 3,222

- EMS grade <2, undamaged buildings
  Total number of buildings counted = 1,349

For analytical purposes, two validation layers were available from Yamazaki *et al.* (2004b): (a) a layer of points showing individual buildings categorized by their EMS98 damage state post-earthquake (see figure 1-8a); and (b) a percent building destruction map (figure 1-8c) produced by summarizing the count of building points within EMS98 categories 4 & 5 (destruction and very heavy damage) into a polygon file of city zones (figure 1-8b).

Classification of damage to masonry buildings	
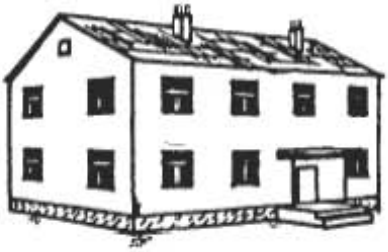	**Grade 1: Negligible to slight damage** **(no structural damage,** **slight non-structural damage)** Hair-line cracks in very few walls. Fall of small pieces of plaster only. Fall of loose stones from upper parts of buildings in very few cases.
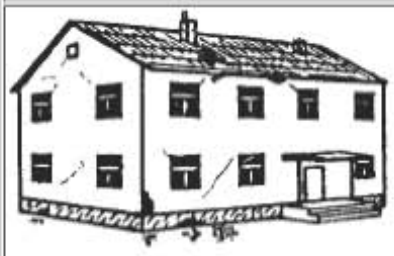	**Grade 2: Moderate damage** **(slight structural damage, moderate** **non-structural damage)** Cracks in many walls. Fall of fairly large pieces of plaster. Partial collapse of chimneys.
	**Grade 3: Substantial to heavy damage** **(moderate structural damage,** **heavy non-structural damage)** Large and extensive cracks in most walls. Roof tiles detach. Chimneys fracture at the roof line; failure of individual non-structural elements (partitions, gable walls).
	**Grade 4: Very heavy damage** **(heavy structural damage,** **very heavy non-structural damage)** Serious failure of walls; partial structural failure of roofs and floors.
	**Grade 5: Destruction** **(very heavy structural damage)** Total or near total collapse.

Figure 1-7 EMS 98 Earthquake Building Damage Scale for Masonry Structures (Grünthal, G., 1998)

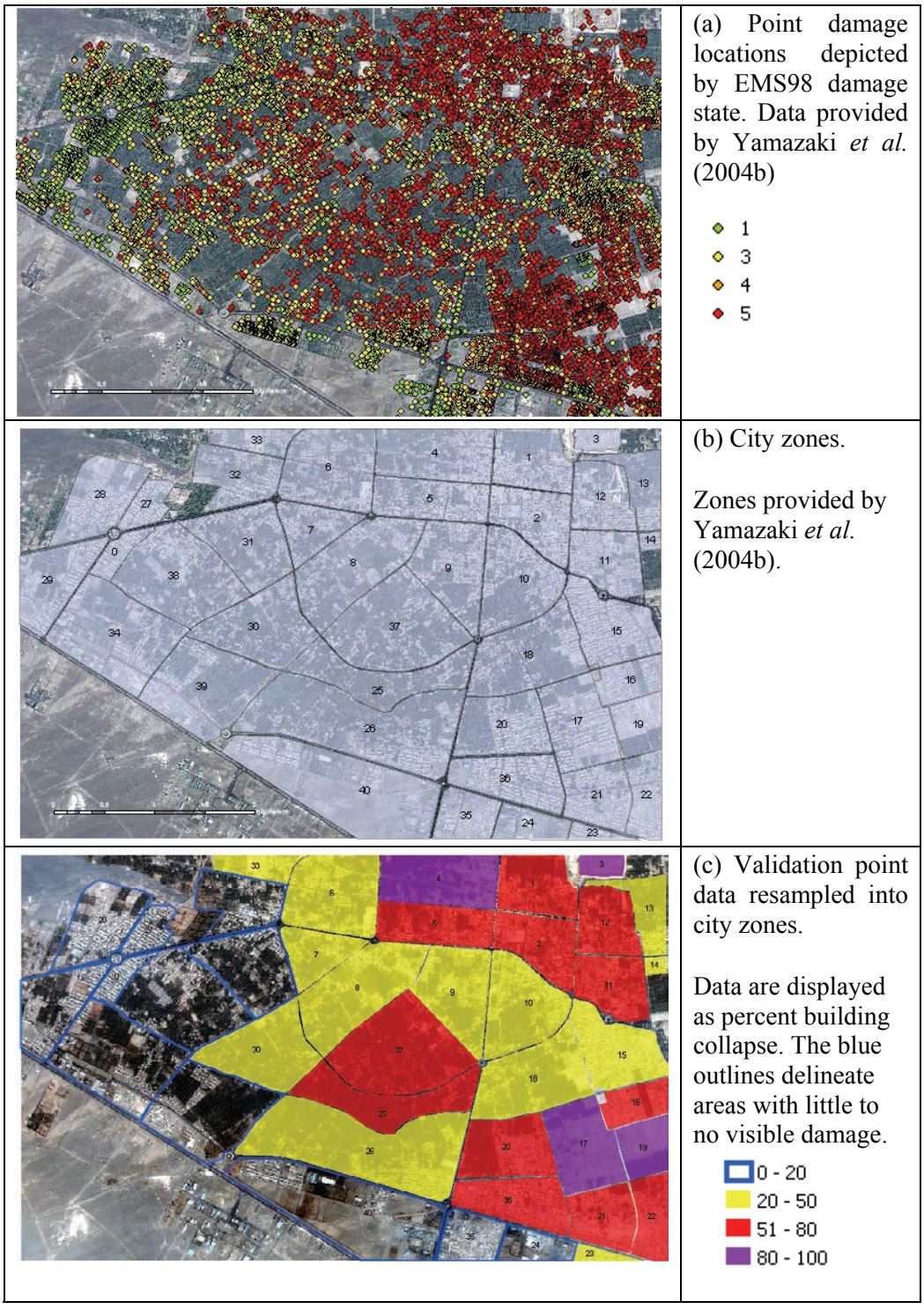

Figure 1-8 Validation Datasets: a) Visually Assessed Building Points Categorized by EMS98 Damage State (Yamazaki et al. 2004b); b) City Zones (Yamazaki et al. 2004b); and c) Points Expressed as Percent Building Collapse within these Zones

SECTION 2
METHOD 1: SPECTRAL COMPARISON

2.1 Qualitative Analysis

The flow diagram in figure 1-2 outlines Method 1: spectral comparison, for detecting the extent and severity of urban damage in Bam at a pixel-scale. The working hypothesis is that building collapse in Bam creates a reduction in reflectance within optical bands of the spectrum, where bright roofs of intact buildings are replaced by darker piles of rubble comprising the constituent materials.

An initial qualitative evaluation was undertaken to identify focus areas within the city for assessing the performance of the damage assessment methodology. Visually inspecting the pre- and post-earthquake images it was apparent that the urban analysis could be split into three main geographic areas as shown in figure 2-1, and depicted in detail within table 2-1.

Area 1 is characterized by mainly non-collapsed buildings within the IKONOS post-earthquake image. Area 2 is characterized by near-total collapse of most buildings, with a red tinged sandy soil underlying the structures. Area 3 is characterized by heavy structural collapse of buildings. The ground underlying these buildings however is less red, and more grey/blue in hue. This distinctive hue may also in part be due to atmospheric effects. Figure 2-2 shows a part of this area in more detail, where the general contrast on the ground is seen to be visibly lower. Although the imagery header information (see table 1-3) indicates that this image has 9% cloud cover, at this stage it is not possible to ascertain if haze in this particular area is due to cloud, or smoke linked to destruction after the earthquake.

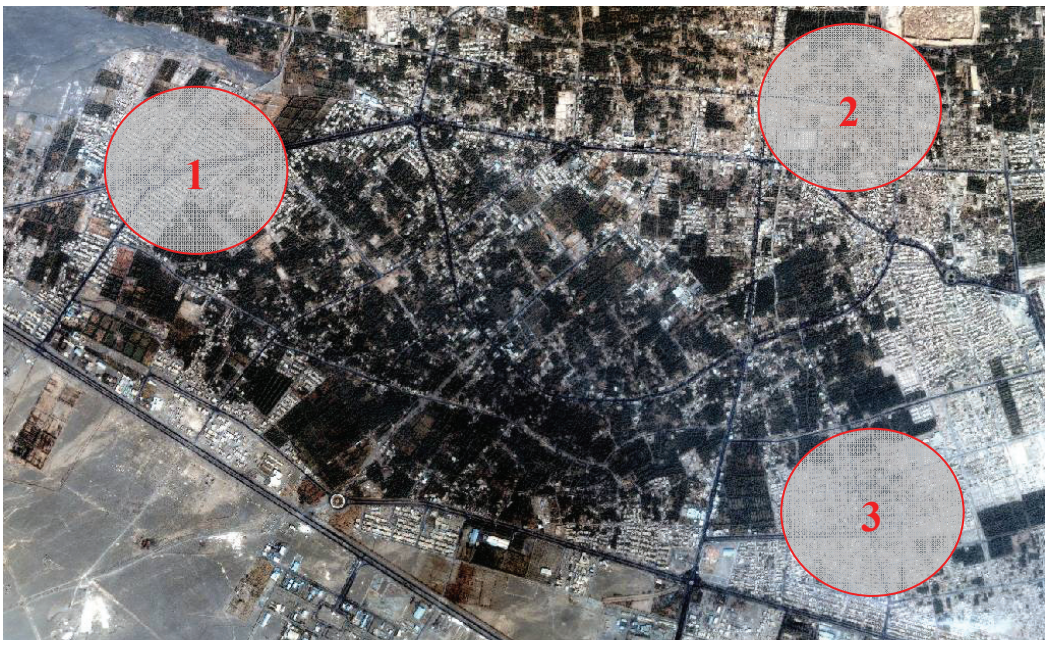

Figure 2-1 Areas of Interest within Bam, Overlaid on the Post-Earthquake IKONOS Image. (1) Area 1: Predominantly Non-Collapsed Buildings; (2) Area 2: Concentrated Building Collapse Overlaying Red Sandy Soil; and (3) Area 3: Concentrated Building Collapse Overlaying Grey/Blue Sandy Soil

Table 2-1 Detailed Visual Comparison of IKONOS and Quickbird Images in Bam Study Areas

QUICKBIRD 'Before'	IKONOS 'After'
	
Area 1: Non-collapsed buildings in the West	**Area 1: Non-collapsed buildings in the West**
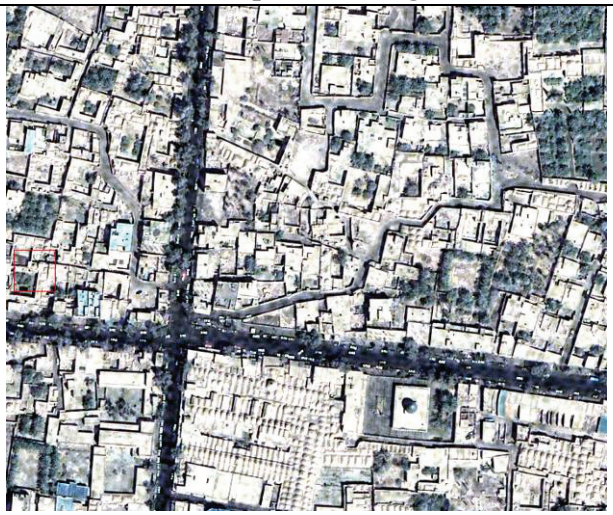	
Area 2: Buildings in the North	**Area 2: Collapsed buildings in the North**
	
Area 3: Buildings in the South.	**Area 3: Collapsed buildings in the South.**

Figure 2-2 Cloud or Smoke Seen in the South East Area of the IKONOS Image, Reducing Ground Contrast Over the Area

Following the initial qualitative evaluation, a quantitative spectrally-based damage assessment methodology was explored, comprising the following analytical steps. These are numbered in sequence, continuing on from the pre-processing procedures described in Section 1.3:

(8) Quantitative analysis of pixel DN values within key areas of the city to identify the characteristic response of intact versus collapsed roofs within the pre- and post-disaster imagery;

(9) Preliminary differencing between the 'before' and 'after' pan-sharpened images to highlight areas of change and investigate the potential for distinguishing a distinct pattern of spectral response for building damage;

(10) Masking the difference image to focus on roof structures and remove non-disaster related sources of change, such as vegetation and roads. This uses the masks created during pre-processing Step 6 and Step 7;

(11) Final differencing between the 'before' and 'after' pan-sharpened images, following application of the cumulative vegetation exclusion and roof inclusion mask;

(12) Shadow removal reduces the occurrence of artifacts within the final difference image, caused by residual shadowing around the edge of buildings within the IKONOS scene that was not removed using the Quickbird of inclusion mask;

(13) Classification of the difference image using a supervised classifier to identify and distinguish between damaged versus non damaged areas.

Validation: After processing was completed, results were validated against the area-based dataset in figure 1-8c, developed using data from Yamazaki *et al.* (2004b).

2.2 Quantitative Analysis of DN values

From the detailed visual comparison in table 2-1, spectral differences between IKONOS and Quickbird are manifold. To further examine these differences, a randomly distributed set of regions of interest (ROIs) was created for building roofs in Area 1, Area 2 and Area 3, using the pre-earthquake image as a guide. Statistics were subsequently calculated for the roofs in the Quickbird and IKONOS image, for each spectral band.

2.3 Preliminary Differencing

To further examine the changes between pre- and post-disaster roof spectral characteristics identified through the quantitative assessment of DN values, a preliminary difference image was computed. A b1-b2 band math operation was conducted for each of the image colour bands. To save processing time, one colour channel was differenced only. The green band was utilized for further analysis as it provided a consistent representation of damage-related change, while minimizing extraneous effects such as differences in soil type.

The green band difference image in figure 2-3 shows that certain land cover types dominate the result. The main areas include vegetated areas (date palm plantations), roads, and to a lesser extent the surrounding geology. Differences in viewing angle and shadow at the respective times of image acquisition are also apparent. Together, these temporal changes complicate the identification of earthquake-related differences between the spectral characteristics of collapsed versus intact roofs. Thus, further processing is employed to minimize these non-disaster related signatures, and emphasize changes caused by building damage.

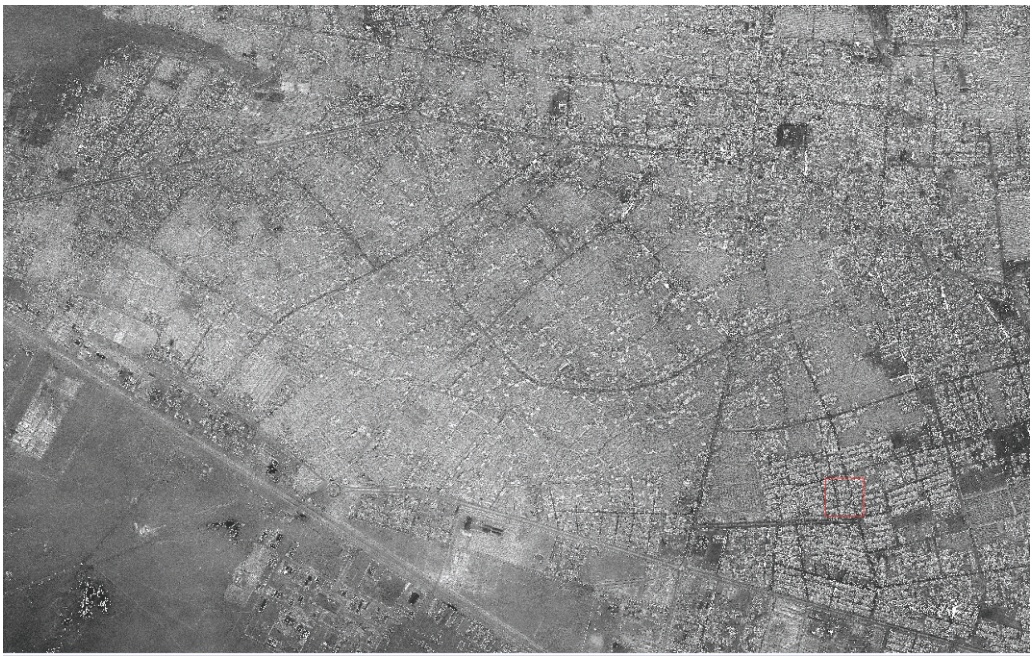

Figure 2-3 Quickbird Minus IKONOS Difference Image (Green Band)

2.4 Masking

In order to minimize these non-disaster related sources of temporal change, the pre- and post-earthquake images were masked using the vegetation exclusion and roof inclusion operators. Figure 2-4 shows the cumulative mask developed for Bam, which in one step excludes vegetation, roads and many areas of surrounding geology, while retaining building roofs. This was computed using a simple multiplication function. The cumulative mask was applied to the image using a simple binary operation. For areas of interest spanning building roofs, the DN value is multiplied by unity to retain the original reading. Other regions are assigned a value of zero.

Figure 2-4 Cumulative Mask Applied to All Images to Dispel Many False Areas of Analysis Such as Vegetation and Roads

2.5 Final Differencing

Having applied the cumulative mask to the Quickbird and IKONOS inputs, a final difference image (before-after) was created to distinguish between collapsed and non-collapsed roof structures.

From a quick-look examination of the scene-wide results, there is a subtle, but definite change of pixel values between areas where building collapse had occurred, opposed to non-collapsed areas. However, in addition to this damage signature, from figure 2-5a some artifacts clearly remain, corresponding with shadows around the margins of the building. They are characterized by exceptionally high DN values. These are likely due to temporal multi-sensor variations in viewing parameters, such as time of day and look angle, and residual errors following co-registration during pre-processing. To minimize these potential sources of error in the change detection process, a shadow removal process was conducted.

(a) Shadows produce a high-value return **(b) Shadow occurrence reduced by masking**

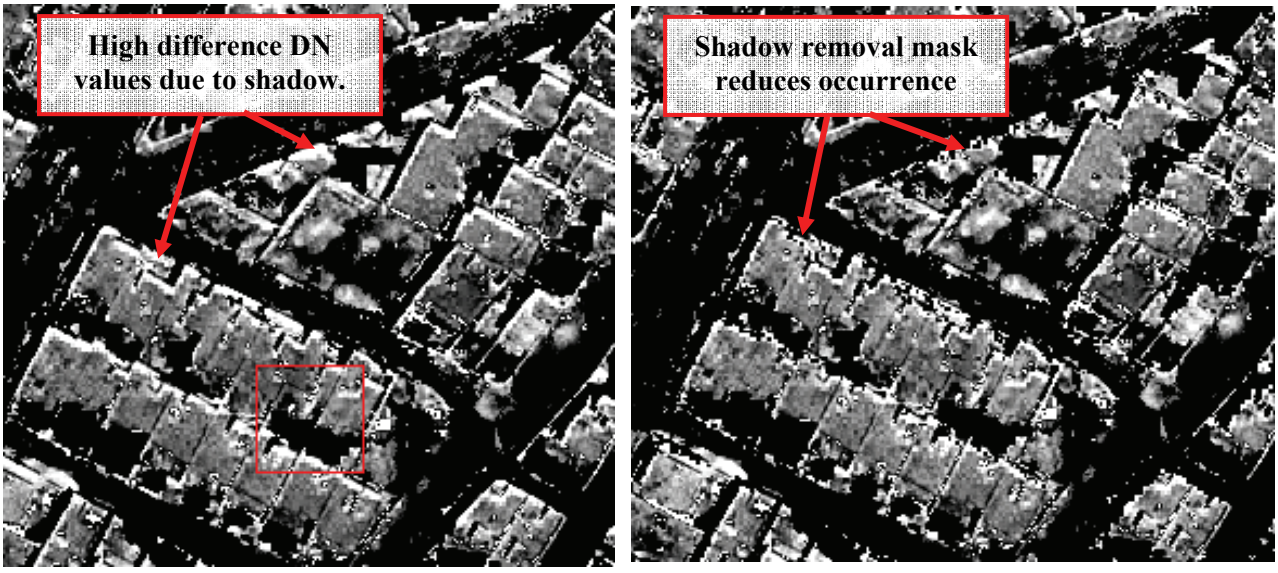

Figure 2-5 Difference Image Showing (a) Exceptionally High DN (Bright) Values Due to Shadow Around Building Margins; and (b) Reduction in Shadow Occurrence Following Masking

2.6 Shadow Removal

For accurate change detection it is important to identify and remove as many non-disaster related sources of variation as possible. Accordingly, methods were explored for eliminating the high-value artifacts caused by shadow and residual spatial offset remaining from co-registration during pre-processing.

Further visual inspection of the original images and the difference statistics indicates that the shadows emanate from the IKONOS scene; shadows sourced from the Quickbird image would have been eliminated by the roof mask. The shadows have a mean spectral value of ~54DN with a standard deviation of 12DN. These statistics provided a basis for artifact removal. A band thresholding technique was used to create an adjusted shadow removal mask, which was in turn applied to the difference image. Figure 2-5b shows the output, with most of the shadow edges removed. This composite mask is the final mask used in other analyses throughout this study.

2.7 Classification and Majority Filter

The preceding processing steps aimed to remove as many potential multi-sensor and multi-temporal sources of error as possible, prior to the final damage detection process. The spectral distinction between areas dominated by collapsed and non-collapsed buildings was achieved using supervised classification. This has been successfully employed by several other studies (see for example, Rathje *et al.* 2005, Woo *et al.* 2005). Huyck *et al.* 2005 employ a more basic form of threshold-based classification.

To perform the classification, two training sets were created from ROIs of roof areas, which from visual inspection were evidently collapsed and non-collapsed buildings within the IKONOS image. A minimum distance supervised classification was then applied to the masked difference image in order to identify classes of extreme versus limited urban collapse.

Preliminary inspection of the classification output (figure 2-6) indicated the persistent occurrence of a small area of change/damage around building margins in Area 1, which are known to be non-collapsed. This artifact from the co-registration and shadow removal processes appears to be causing misclassification. From figure 2-6b, a 13 x 13 majority filter was utilized to negate these small artifacts, leaving only the main areas of damage.

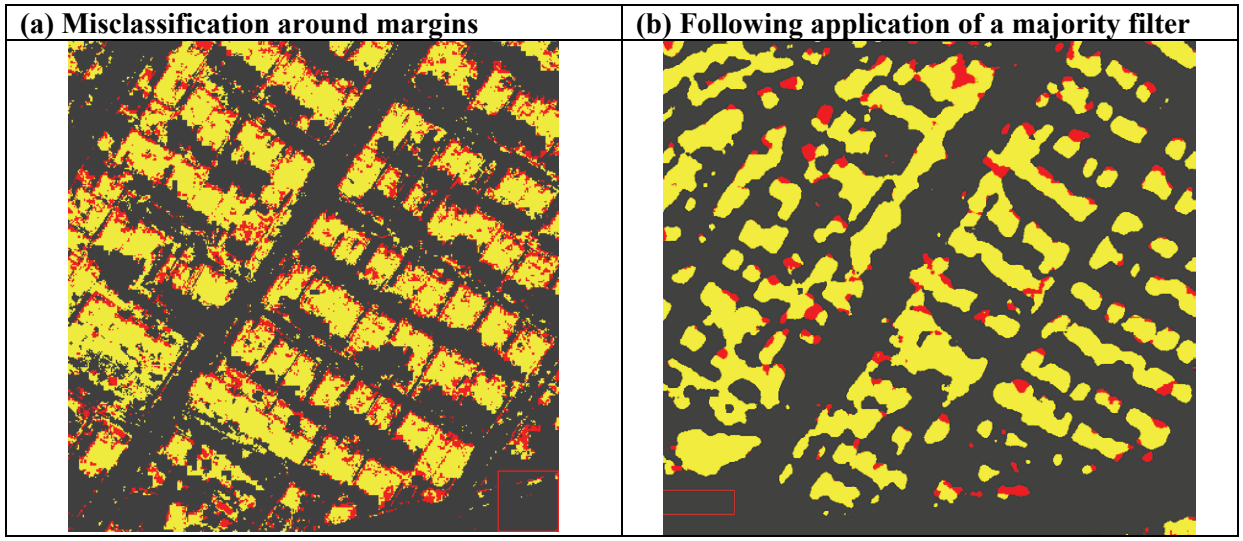

Figure 2-6 Classification Result for a Sample of Buildings in Study Area 1 (Western Bam). (a) Small Areas around the Building Margin have been Misclassified as Damaged, although the Structures Themselves were Non-Damaged; (b) the Same Area Following Application of a Majority Filter

The resulting classification images provide a useful visual representation of the city-wide distribution of pixels denoting 'collapsed' versus 'non-collapsed structures. However, it is often useful for disaster managers to be able to disseminate information about the general distribution and severity of damage. Therefore, some measures of the destruction per city zone were calculated to provide a quick estimate of the most damaged parts of the city. This is also in line with the neighborhood damage assessment of this study's aim. Accordingly, the classification results were summarized into the city zones as defined by Yamazaki *et al.* (2004b). A series of measures of damage were computed using the classification information, including: (1) frequency of damaged pixels per zone; (2) the percentage of destroyed urban structures; and (3) the percentage of damaged pixels per city zone.

2.8 Validation

The supervised classification result was validated against the data from (Yamazaki *et al.* 2004b) using two methods:

a) an intersection analysis between the classification output and validation points
b) an area-based analysis of the percentage of classified damage within a given city zone

For the intersection analysis, to facilitate a comparison between the two level classification result and five level validation dataset, the damage point dataset (see figure 1-8a) was reclassified into two points classes: (1) damage state 1-3; and (2) damage state 4 and 5. The two classified damage classes of (a) damage and (b) no-damage were then extracted into different layers, and converted to polygons, for further GIS analysis. The frequency of damage state 1-3 and 4-5 points occurring within the no-damage and damage polygon classes were calculated.

For the area-based analysis, the percentage damage dataset (figure 1-8c) was employed, which records the percentage of extreme building damage within each EMS damage state. The two most heavily damaged classes (EMS98 damage level 4 and 5) within a given city zone (see figure 1-7) were utilized. This is deemed comparable to the remote sensing classification result, which divides individual pixels into classes of extreme versus non-damaged.

SECTION 3
RESULTS 1: SPECTRAL COMPARISON

3.1 Quantitative Analysis of DN Values

Table 3-1 summarizes the statistical characteristics of structures exhibiting collapsed versus non-collapsed damage states in Area 1 (residential non-collapsed structures in western Bam), Area 2 (residential collapsed structures in northern Bam), and Area 3 (residential structures in southern Bam with cloud/smoke imagery effects). The graphical representations in figure 3-1 show the mean values of the 'before' and 'after' scenes and the difference between them (before-after).

Examining the statistics in figure 3-1a reveals a number of interesting characteristics. Following the visually determined differences between the brightness and contrast of the pre- and post-disaster images, the spectral signature of roofs in Area 1, Area, 2 and Area 3 of the 'after' IKONOS image consistently exhibit a lower mean pixel DN (digital number) value of approximately 150 DN compared with the Quickbird 'before' image of 225DN. This fundamental offset between the sensors may be due to a number of the multi-sensor variables described in Section 1.3, such as differences in the spectral wavelength ranges spanned by the two sensors, the use of different pan-sharpening and atmospheric correction routines, and different radiometric calibration across 8 bit versus 11 bit ranges. To achieve closer spectral comparability between the datasets, one would in theory, need to start with basic level images and process them in a similar fashion.

Table 3-1 Roof Spectral Properties in Bam Study Regions Area 1: Limited Collapse, Area 2: Collapse with Red Soils; and Area 3: Collapse with Grey/Blue Soils

AREA 1: Limited collapse		AREA 2: Frequent Collapse		AREA 3: Frequent collapse	
1. Quickbird	**1. IKONOS**	**2. Quickbird**	**2. IKONOS**	**3. Quickbird**	**3. IKONOS**
Red band	**Red band**	**Red band**	**Red band**	**Red band**	**Red band**
Min = 39 Max = 255 Mean = 233 SD = 37	Min = 8 Max = 255 Mean = 151 SD = 33	Min = 56 Max = 255 Mean = 234 SD = 23	Min =49 Max = 255 Mean = 151 SD = 32	Min = 25 Max = 255 Mean = 237 SD = 31	Min = 43 Max = 206 Mean = 111 SD = 23
Green band	**Green band**	**Green band**	**Green band**	**Green band**	**Green band**
Min = 47 Max = 255 Mean = 233 SD = 32	Min = 4 Max = 255 Mean = 150 SD = 38	Min = 63 Max = 255 Mean = 235 SD = 22	Min = 38 Max = 255 Mean = 136 SD = 31	Min = 38 Max = 255 Mean = 237 SD = 29	Min = 41 Max = 215 Mean = 117 SD = 23
Blue band	**Blue band**	**Blue band**	**Blue band**	**Blue band**	**Blue band**
Min = 49 Max = 255 Mean = 230 SD = 31	Min = 15 Max = 255 Mean = 151 SD = 38	Min = 61 Max = 255 Mean = 233 SD = 22	Min = 16 Max = 255 Mean = 127 SD = 31	Min = 34 Max = 255 Mean = 235 SD = 29	Min = 55 Max = 239 Mean = 129 SD = 24

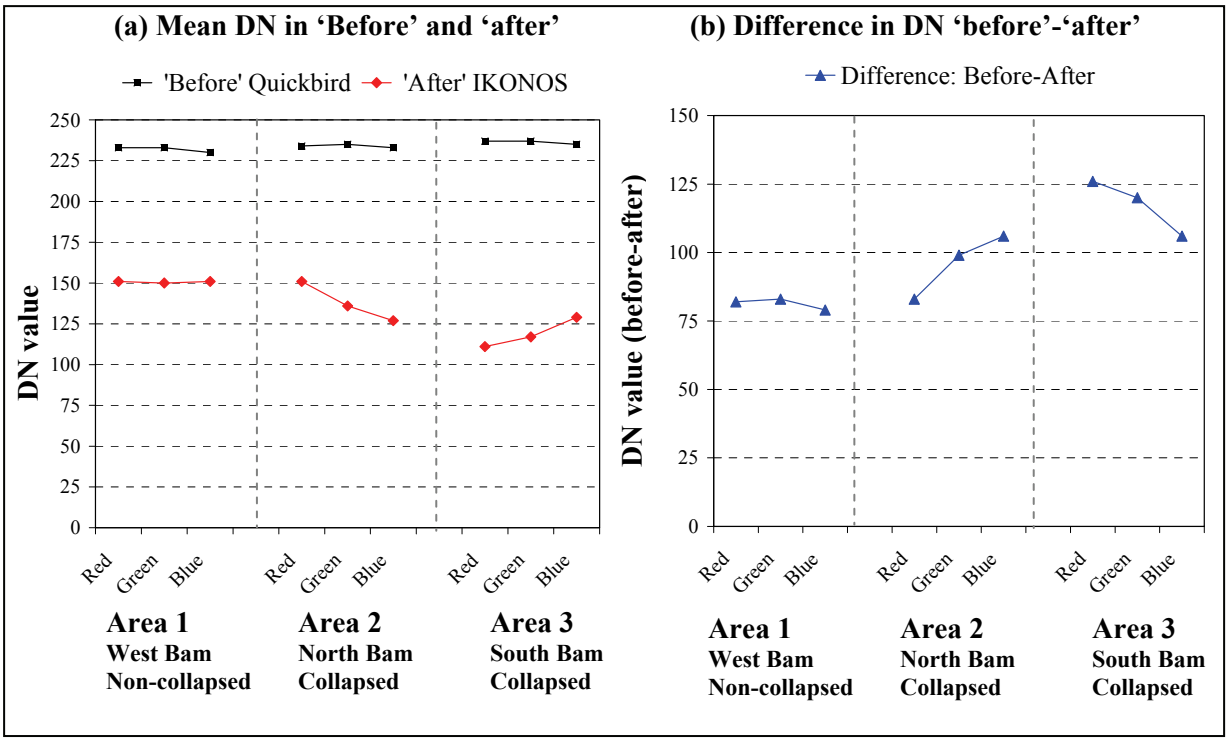

Figure 3-1 Graphical Representation of Mean DN Values of Building Roofs within Study Areas Exhibiting Limited Post-Earthquake Collapse (Area 1), Severe Collapse (Area 2) and Severe Collapse in Conjunction with Atmospheric Haze (Area 3)

The qualitative visual and quantitative DN value analysis also suggests that the 'before' Quickbird scene exhibits a similar response throughout Area 1, Area 2 and Area 3, which was to be expected, given the homogenous nature of building stock within these regions, coupled with the absence of significant sources of intra-scene variability such as cloud cover or haze. The IKONOS 'after' image has a wider spread of color values within the roof ROIs. The non-collapsed buildings of western Bam in Area 1 exhibit a consistent response throughout all bands. The collapsed buildings of northern Bam in Area 2 are instead characterized by a *reduction* in return within green and blue bands compared with Area 1. This is consistent with a lower spectral response from the debris of collapsed structures versus the homogenous roofs of non-damage buildings. The red band still shows a relatively high response. This is likely due to the sand colour underneath the collapsed buildings, and suggests that the red band is not so useful for distinguishing damage in this area.

Collapsed structures in southern Bam (Area 3) exhibit the lowest return across all IKONOS bands. This may be due to a combination of damage coupled with a general subduing of spectral contrast due to haze. In terms of inter-band differences for the 'after' scene, collapsed buildings do not display a constant signature through the image. Collapsed buildings in the south have a higher blue DN component, whereas the North is characterized by a stronger red signal. This seems to be due to the sandy foundations of this area. Therefore the most useful band for showing a consistent lowering of response due to building collapse in Bam is seen to be the green band.

Difference values between the Quickbird and IKONOS images in figure 3-1b provide a sense of the spectral change detection signature accompanying building collapse in Bam. Since the Quickbird values are fairly constant, the difference values largely mirror the pattern of variation exhibited by the IKONOS bands. The non-collapsed structures in western Bam Area 1 exhibit a difference of ~75DN, which as discussed above is probably due to fundamental radiometric differences between the scene acquisition and processing specifications. The margin of difference increases where collapsed buildings are present. Difference values for the collapsed structures in northern Bam Area 2 are considerably higher, achieving >100DN within the blue and green bands. The highest differences of >100DN for all bands accompany collapsed buildings in southern Bam Area 3. While collapse was prevalent throughout both Area 2 and Area 3, the latter region is also subject to contrast suppression effects due to haze. Importantly, these pronounced changes in DN values within building collapse areas, provides a compelling theoretical basis for extracting collapsed and non-collapsed buildings on a spectral basis.

3.2 Final Differencing

From the overview and detailed difference images in figure 3-2, on a city-wide basis, the spectral difference where non-collapse prevails (for example, the western community) is lower compared with a predominance of collapse (the south eastern community). Returning to the difference statistics in table 3-1, this is consistent with the finding that values are generally higher in the Southern and Northern areas, where damage has occurred, than the non-damaged Western area of Bam.

3.3 Classification

Figure 3-3 shows results from the minimum distance supervised classification before application of the majority filter. The image is split into classes of non-collapsed (yellow), and areas of high change inferred to be collapsed areas (red).

The main areas of collapse are located in the south-eastern part and the north-eastern regions of Bam. These areas are also characterized by dense building stock. The central area of Bam is also classified as having heavily damaged areas. However, this region is characterized by lower density building stock, as this is a palm plantation area. The classification shows that generally the easternmost and westernmost fringes of Bam, characterized by dense urban development do not exhibit high levels of damage from the earthquake. Further, surrounding geology which was not completely masked out, was correctly classified as no-change.

a) Final difference image (before-after) with cumulative mask

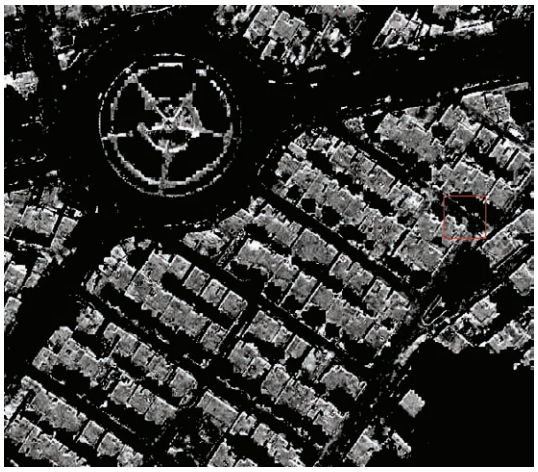

b) Western community – Non-collapsed buildings look darker due to a lower difference in DN values

c) South eastern community - collapsed buildings, look brighter due to a higher difference in DN values

Figure 3-2 Masked Difference Image, Showing Increased Detail for Key Areas to Demonstrate Higher (and Brighter) Difference Values within a South Eastern Community that Sustained Widespread Building Collapse, Compared with Lower (and Darker) Values within a Western Community that Recorded Little Damage

Figure 3-3 Minimum Distance Supervised Classification with Majority Analysis. The White Circles Depict the Magnified Areas Examined in Further Detail.

Having provided a general overview of the change detection results, three key areas of damage were examined in more detail, and compared with the validation dataset of Yamazaki *et al.* (2004b). From figure 3-3, Area 2 is high density housing with complete collapse, Area 3 is also dominated by collapse, with the complicating presence of haze, and Area 4 is lower density housing surrounded by date palm plantations, which sustained heavy damage.

3.4 Validation of Classification Results

Validation was undertaken using datasets obtained from Yamazaki *et al.* (2004b). Three approaches were employed: (1) a qualitative comparison between the classification results for Area 2, Area 3, and Area 4 and per-building damage levels; (2) a quantitative comparison using an intersection analysis; and (3) a quantitative area-based comparison.

For the *qualitative* assessment, figure 3-4 depicts the classification results overlaid with the per-building validation points for Area 2. The majority of building damage within this area is correctly classified, with large classified differences between the pre- and post-disaster imagery coinciding with very heavy structural damage, and smaller differences with limited structural damage. Considering this, it is thought that this spectral classification gives a reasonable indication of building collapse areas around adobe and clay buildings, suitable for a Tier 2 neighborhood scale damage analysis.

However, several areas are highlighted where the classification and validation results disagree. For annotated regions of interest A and B, the classification result suggests limited change within the imagery, whereas the validation dataset records collapse. From visually inspecting the images in figure 3-4a and figure 3-4b, the structures appear to be intact. Accordingly the disagreement could be due to an error in the validation dataset, which was produced through visual classification of damage levels rather than in-field inspection, and thus is subject to human error. For region of interest C, the supervised classification experienced difficulties identifying a standing blue roofed building as collapsed. Again, examining the pre- and post-earthquake images, this is probably due to multi-sensor differences, where the fundamental spectral offset between the Quickbird and IKONOS scenes is of a similar order of magnitude to the collapse of adobe and clay roofed structures.

Within Area 3 to the south of the city (figure 3-5), there is general agreement between the classification result and validation dataset. In several neighborhoods, the classification underestimates damage, identifying low levels of change compared with the EMS 4-5 damage state identified by Yamazaki *et al.* (2004b). Examining the pre- and post-earthquake images, building collapse in these communities exhibits an uncharacteristically bright appearance, which is similar to intact roofs. However, despite this misleading spectral response, visually they appear to have collapsed because the distinctive edges associated with building walls are no longer in evidence. The bright response of collapsed structures may be a function of the construction materials, or the distorting effect of cloud/haze that is present in this area. In these cases, an alternative method of damage classification that draws on the occurrence of edges rather than spectral signatures may perform better.

For the neighborhood in Area 4 where date palm trees are prevalent, in general the classification and validation results correspond relatively well. The classification overstates damage in certain areas (highlighted in figure 3-6). This may in part be due to different illumination conditions between the dates, as buildings surrounded by tall trees are subject to significant shadowing. From visually examining the pre- and post-earthquake images, however, it appears that most of the structures remain standing since their signature is still relatively bright and homogenous. This misclassification is therefore likely due to the supervised method not being flexible enough to fully encompass the full range of variability in building roof signatures between the two dates, and between the two sensors.

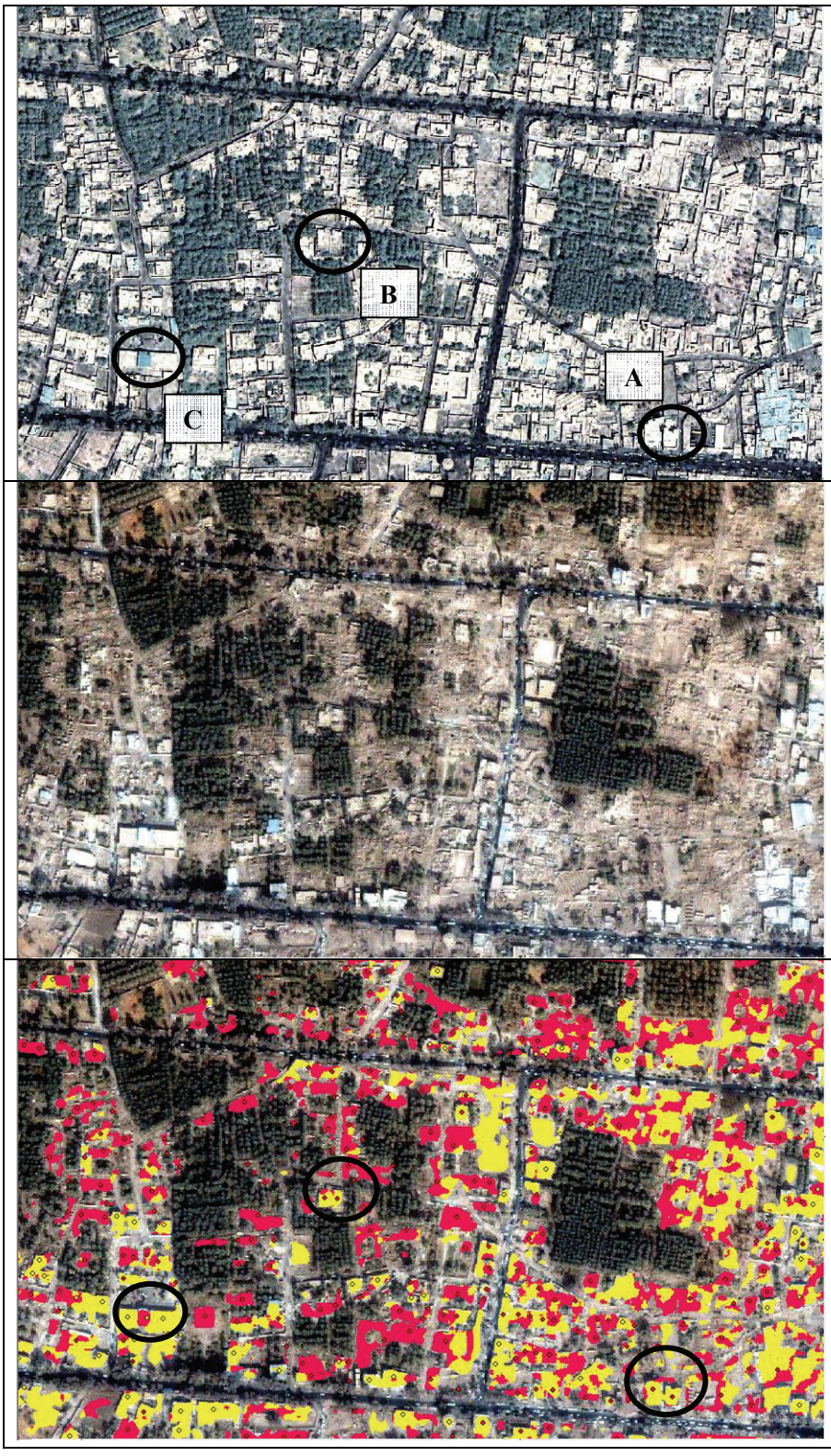

(a) Quickbird Pre-earthquake image

(b) IKONOS Post-earthquake image

(c) Supervised classification image, and Yamazaki *et al.* (2004b) point layer

Large classified change

Very heavy damage (EMS levels 4 or 5).

Small classified change

Limited structural damage (EMS levels 1-3)

Figure 3-4 Magnified Sample Region Bordering Area 2 (Northern Bam), Used to Examine the Supervised Classification Signal of Change/Damage. Discrepancies Between the Classification Result and Validation Dataset are Highlighted.

(a) Quickbird Pre-earthquake image

(b) IKONOS Post-earthquake image

(c) Supervised classification image, and Yamazaki *et al.* (2004b) point layer

Large classified change

Very heavy damage (EMS levels 4 or 5).

Small classified change

Limited structural damage (EMS levels 1-3)

Figure 3-5 Magnified Sample Region Bordering Area 3 (Southern Bam), Used to Examine the Supervised Classification Signal of Change/Damage. Discrepancies Between the Classification Result and Validation Dataset are Highlighted.

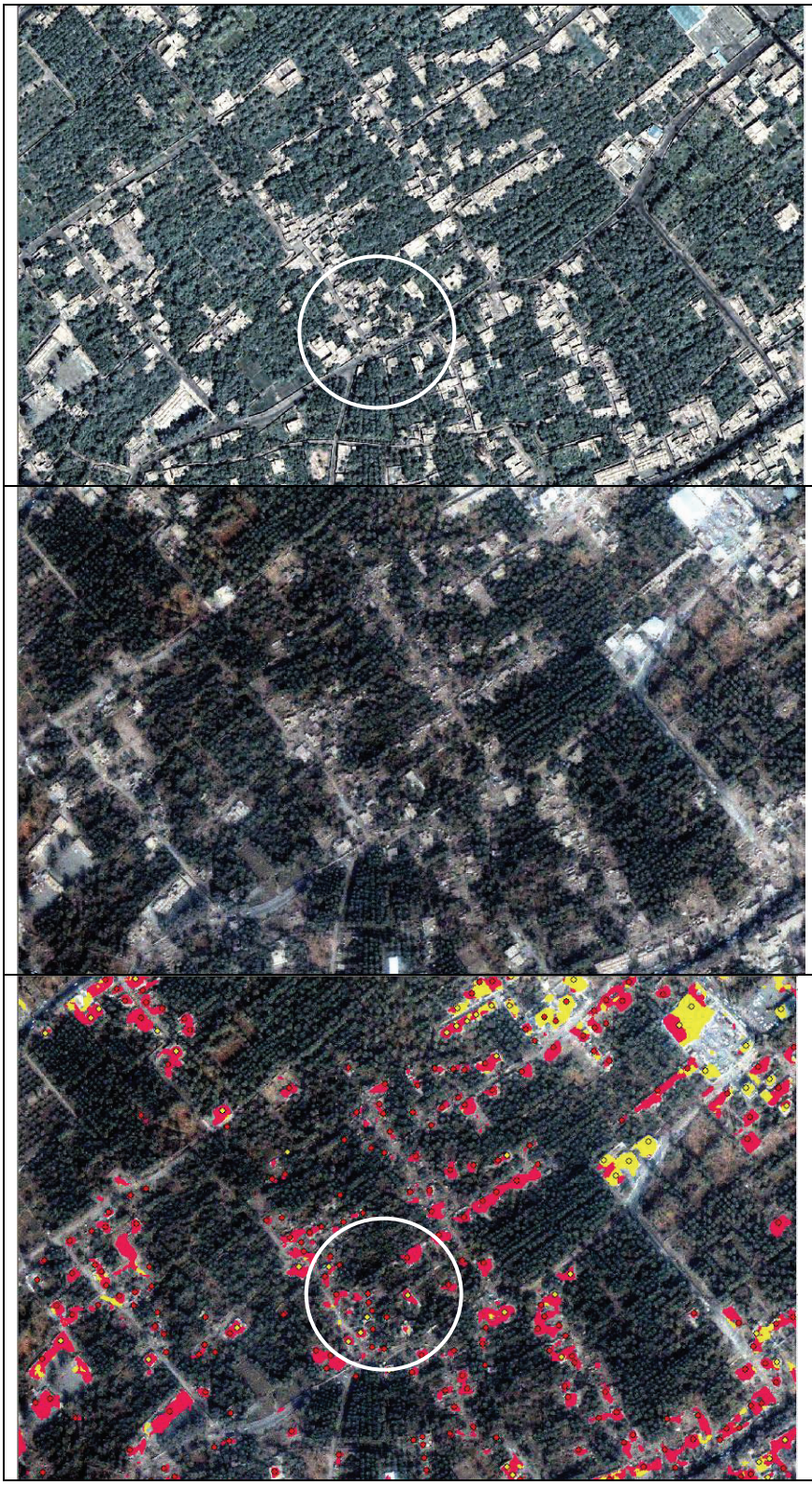

(a) Quickbird Pre-earthquake image

(b) IKONOS Post-earthquake image

(c) Supervised classification image, and Yamazaki *et al.* (2004b) point layer

Large classified change

Very heavy damage (EMS levels 4 or 50.

Small classified change

Limited structural damage (EMS levels 1-3)

Figure 3-6 Magnified Sample Region Bordering Area 4 (Central Bam), Used to Examine the Supervised Classification Signal of Change/Damage. Overestimation of Damage by the Spectral Classification is Highlighted.

To *quantitatively* examine the relationship between the classified output and the point- and derived areas-based validation datasets from Yamazaki *et al.* (2004b) (see figure 1-8), two methods were employed, comprising an intersection analysis and a zone-based comparison. Table 3-2 provides a visual representation of the steps involved and results obtained for the intersection analysis. The percentage of validation points falling within each classification level are shown in table 3-3.

Table 3-2 Intersection Analysis Between Classification Results and Point Validation Data

1) Yamazaki *et al.* (2004b) Building point dataset 	2) Yamazaki *et al.* (2004b) building class levels 1-5 Reclassified to 1-3 and 4-5 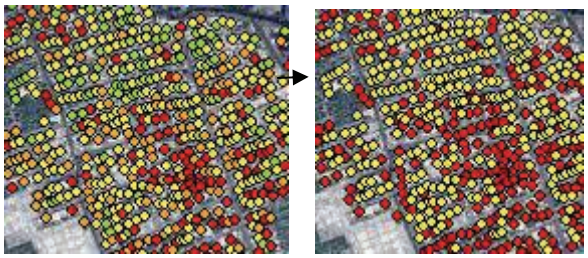
3) Reclassified point data set 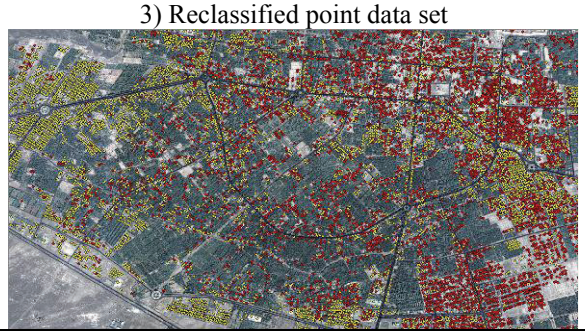	4) Supervised classification 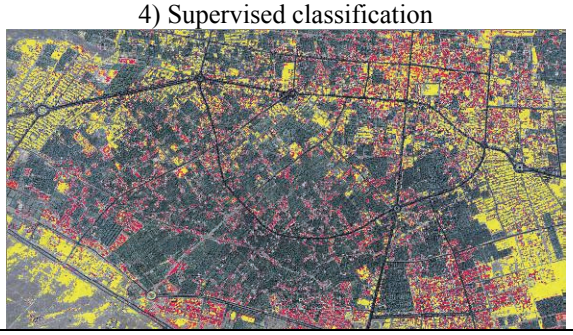
Extracted damage polygons 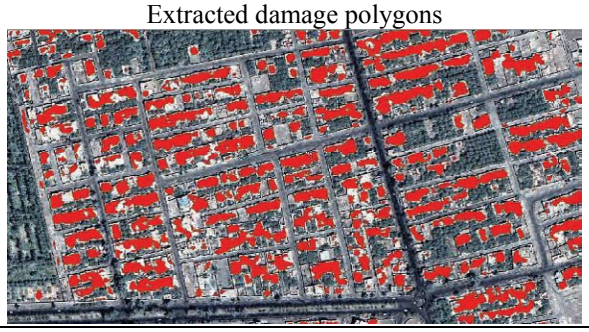	Extracted no damage polygons 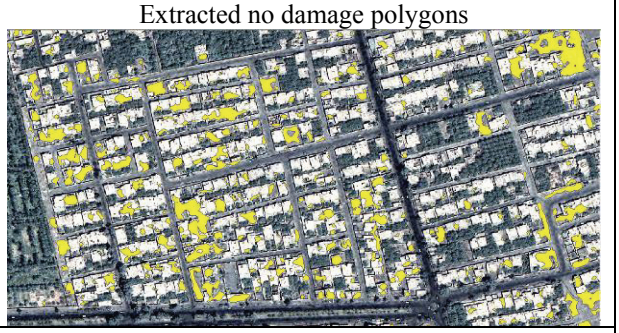
Intersection analysis between damage polygons and points 	Intersection analysis between no-damage polygons and points 

Table 3-3 Results of the Intersection-Based Validation, Showing Correspondence Between the Classification Result and Compressed Validation Classes

	Damage Polygon	Non damage polygon	Total	% accuracy
No Damage points	1865	4495	6360	71
Damage points	3929	1516	5445	72
Total	5794	6011		
% accuracy	68	75		

The results are promising, with the point-based validation producing high accuracy levels for both the damage and non-damaged classes. Within the polygons classified as damaged, 68% of the validation points were also damaged. 75% of points falling within the no-damage polygon are no-damage points. Of all the validation points available, 72 % of damage points fell within damage polygons, and 71% of no-damage points fell within non damaged polygons.

For the zone-based comparison, the percentage damage validation layer (figure 1-8c) developed from data provided by Yamazaki *et al.* (2004b) was used to assess the accuracy of supervised classification results resampled into corresponding city zones. Figure 3-7 shows the classification results resampled into the city zones using a range of different summarizations. Unless a specific class break is required, results are shown by Jenks' natural breaks classification (see equation 3-1). This determines the best arrangement of values into classes by comparing the sum of squared differences of values from the means of their classes (Terraseer, 2007).

$$SSD_{i\ldots j} = \sum_{n=i}^{j} A[n]^2 - \frac{\left(\sum_{n=1}^{j} A[n]\right)^2}{j-i+1} \qquad (3\text{-}1)$$

A is the set of values that have been ordered from 1 to N.

$1 \leq i < j < \mathrm{N}$

$\mathrm{Mean}_{i..j}$ is the mean of the class bounded by i and j.

First, the frequency of classified damage pixels was computed per city zone. These counts per zone were classified into four different levels of damage using Jenk's natural breaks statistics. From the classification result in figure 3-7a, the South records the highest frequency of damage pixels (zones 26 and 40), followed by areas in the North East, South East, Centre and West (zones 1,2,4,5, 17,20,34, 36,37, 38). Comparing this with the validation percentage building collapse from Yamazaki *et al.* (2004b) (figure 3-7b), zones in the North East, South East and centre are also identified as heavily damaged. However, areas 26 and 40 record <50% collapse, while the West is not heavily damaged.

(a) Damage classification result resampled within zones

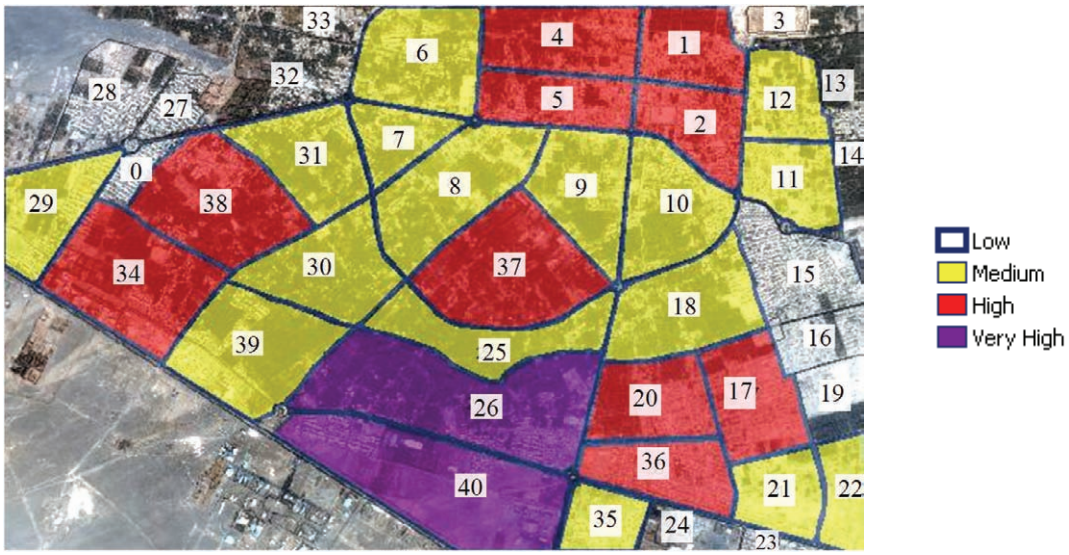

(b) Validation data

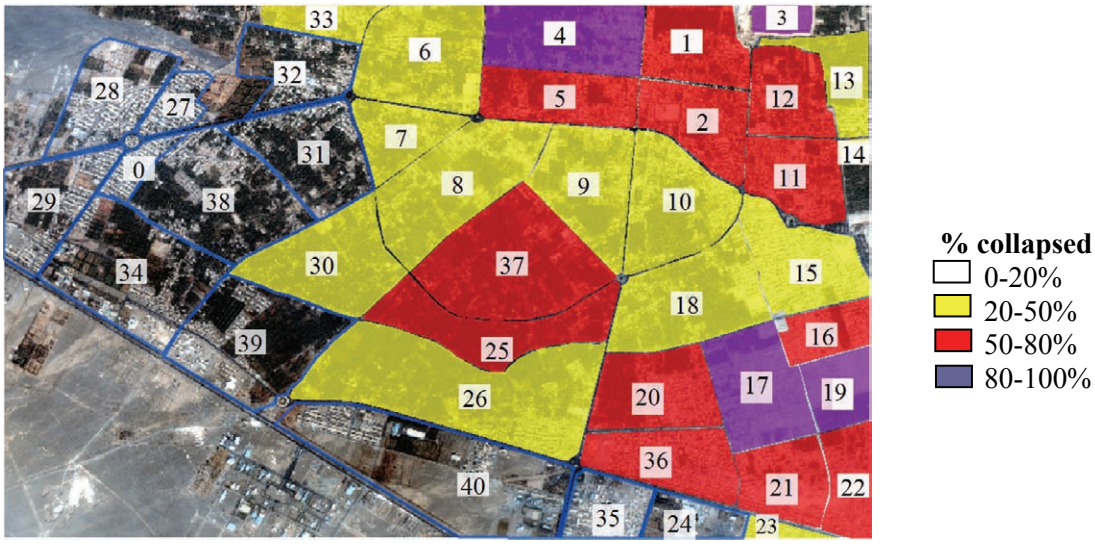

Figure 3-7 (a) Supervised Classification Output of Damage Pixel Frequency, Summarized by Zone and Visualized by Natural Breaks. (b) Yamazaki et al. (2004b) Validation Dataset Summarized by Zone.

These differences in zone-based damage level may be attributable to a number of effects. Firstly, scaling is an issue. The frequency of damage is correlated to the size of the zone, as shown in figure 3-8, indicating that larger zones are more likely to have more classified damage pixels in them. As the Yamazaki *et al.* (2004b) dataset is a percentage damage, this is not an issue with that dataset. Secondly, the frequency of classified damage pixels does not account for the amount of buildings in each zone, and so for a similar sized zone, one with a small number of buildings which are all destroyed, would produce less of a response than a zone with many buildings only a few of which collapsed. Thirdly, are misclassification effects which are described in further detail below.

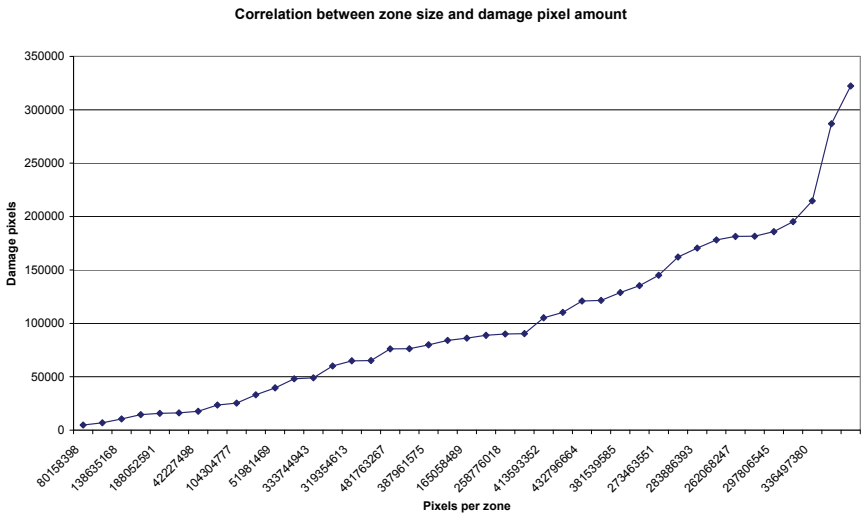

Figure 3-8 Correlation of Frequency of Classified Damage Pixels and Zone Size

The second zone-based measure records the percentage of urban structures that were classified as destroyed, disregarding the zone size. It was anticipated that this would be more comparable to the percentage building collapse, since steps were taken to focus on pixels corresponding with buildings rather than other features within the urban landscape. The damaged and non-damaged building classes were combined to quantify the frequency of urban landcover; the majority of other land cover classes (including roads) were masked out. The percentage of the urban structure pixels classified as damaged was mapped for each zone in figure 3-9.

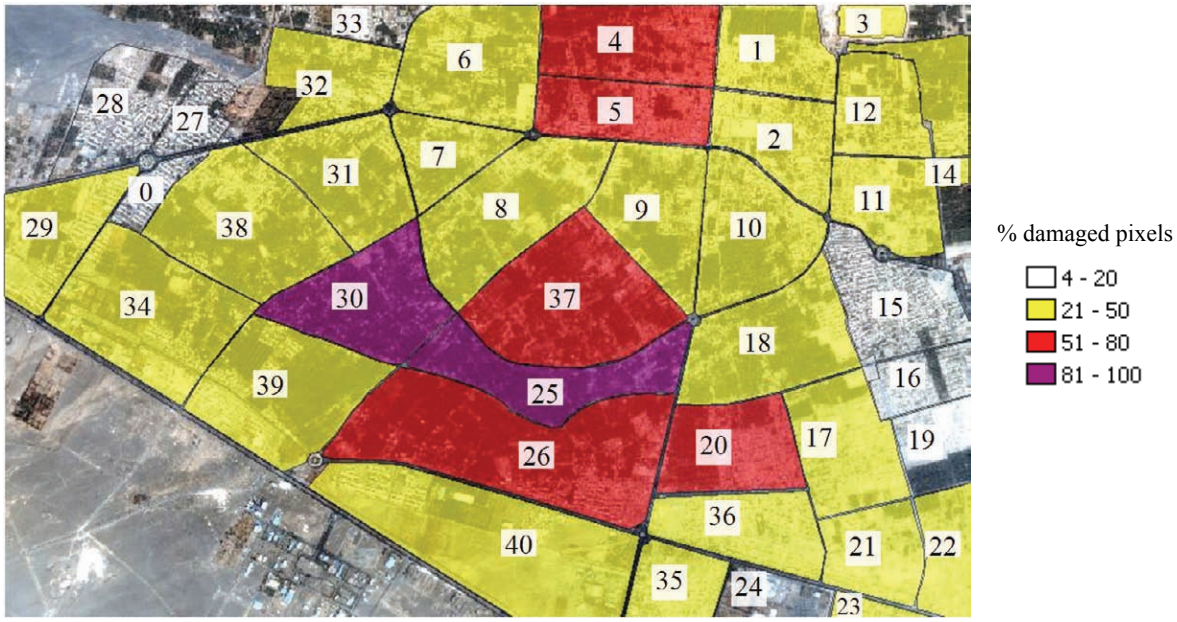

Figure 3-9 Supervised Classification Visualized as Percentage of Urban Pixels Marked as Damage, Broken Out into 4 Damage Classes as Specified by Yamazaki et al. (2004b)

Zones recording the highest concentration of classified urban collapse are located in central and northern Bam (zones 4,5,20,25,26,27,30). Compared with the validation dataset (figure 3-7a), the

damage level is underestimated in the north-east and south-east. Magnifying the north-east area in figure 3-10, the difference may be attributable to several factors. There is an issue of comparability between a single damage point on a building, and a measure of the area of damage or non-damage in pixels. Large buildings (or buildings with courtyards within them) can bias results either way (see annotated structures). Also, some small areas where the ground and roof spectral signature were similar were not removed using the urban mask – allowing areas of ground to bias the non-damaged statistics. Further, due to the manner of building collapse some walls may still remain, and would give a non-damaged response, whereas the rest of the building would give a damaged response. In the Yamazaki *et al.* (2004b) validation point data, this would simply be noted as a single damaged structure.

(a) Validation map, showing occurrence of collapsed (red) and non-collapsed (yellow) buildings

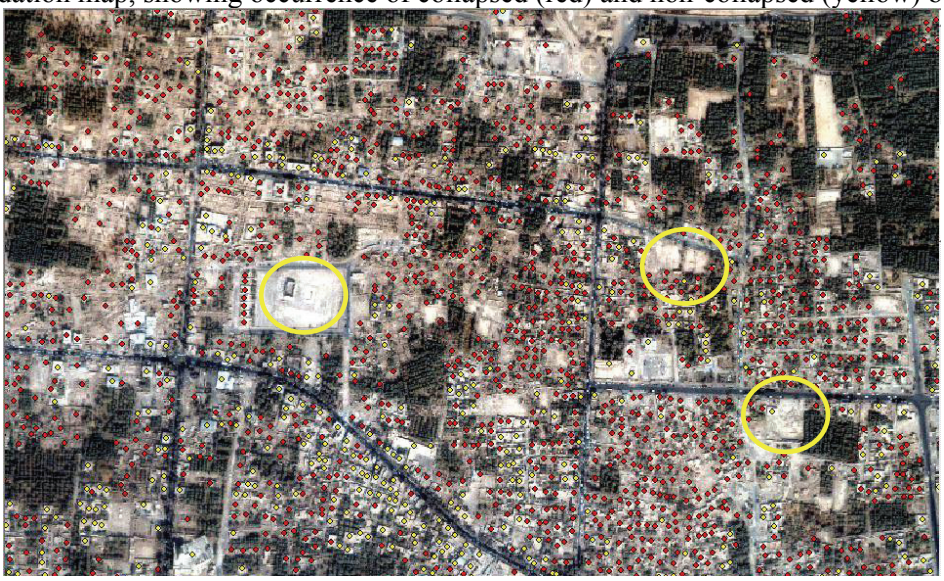

(b) Classification result showing collapses (red) and non-damaged (yellow) urban pixels

Figure 3-10 Underestimation of the Frequency of Building Collapse in this Area of North-East Bam May be Due to an Issue of Comparability Between a Single Damage Point in the Validation Dataset (a), and a Percentage of Damaged Urban Pixels (b).

These two sets of results highlight the limitations of a pixel-based estimate urban damage. However, as stated in the aim of this chapter, this study seeks to create a *neighborhood* damage assessment, as opposed to a per-building level (see Volume II). Due to these pixel-based limitations a third result was computed, visualizing the damage pixels as a percentage of damage per city zone (figure 3-11).

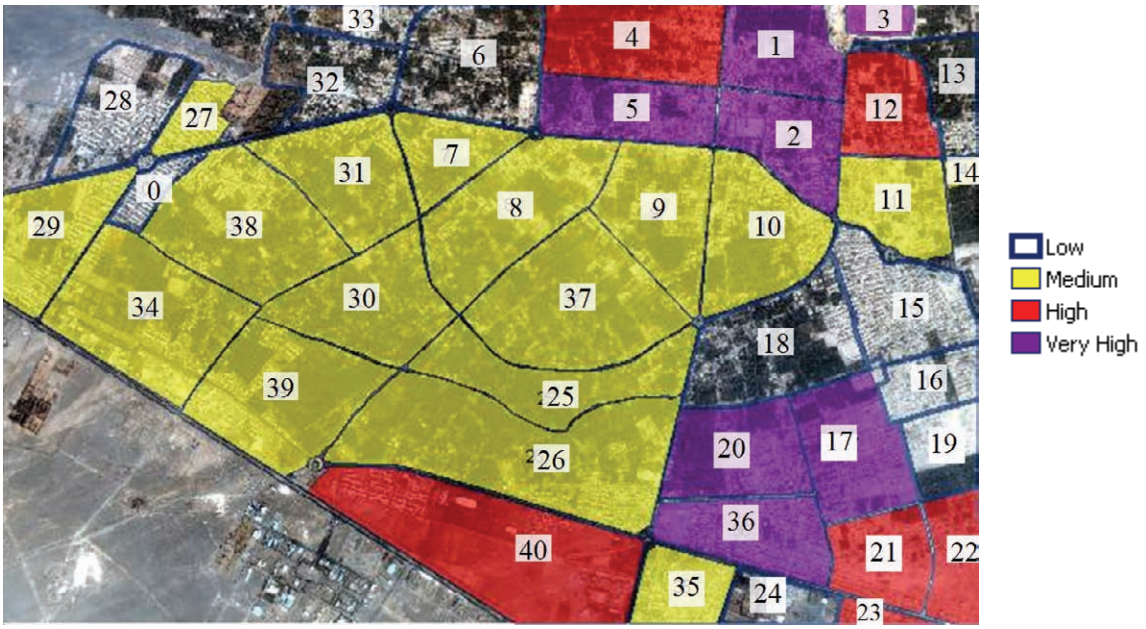

Figure 3-11 Supervised Classification Output Mapped as the Ratio of Damage Per City Area, Displayed as Natural Breaks

Again, this method has the disadvantage of not knowing the frequency of buildings per zone, and so although normalizing for the area ameliorates some of the scale related issues seen previously, it does not account for all of them. Nevertheless, the percentage of damage per city zone produces a reasonable indication of the hardest hit areas. In particular, it helps to emphasize the smaller zones where urban development is more concentrated. There is a general similarity with the validation result in figure 3-7b. The north-east and south-east were identified in both datasets as the most severely damaged areas. However, the central area of Bam was not identified as sustaining high levels of building collapse. This pattern of agreement is reaffirmed by the correlation statistics in table 3-4, which compare the validation data with results obtained using the three different measures (damage frequency, percentage urban damage, and percentage damage per zone). Neither the frequency of damage pixels per zone, nor the percentage of urban damage were not found to be statistically significant when compared to the validation classes. However, for the 40 sample zones, damage as a percent of the city zone area was found to be statistically significant at $p < 0.05$.

Table 3-4 Correlation Coefficients Expressing Agreement Between the Zone-Based Measures of Classified Damage and Validation Results. The Statistically Significant Relationship for the Percentage of Damaged Land is Highlighted.

	Damage frequency	Percent of urban damage	Percent of damaged land
Cor. coefficient	0.17	0.26	**0.52**

To further explore the pattern of agreement between the percentage damage per zone and validation data, a zone-based correspondence chart was produced. Figure 3-12 shows that although 15 zones are correctly classified, a large number of zones are also classified 1 class away from the validation. From the widespread distribution of these cases among the zones (figure 3-13), there does not seem to be a systematic geographic bias.

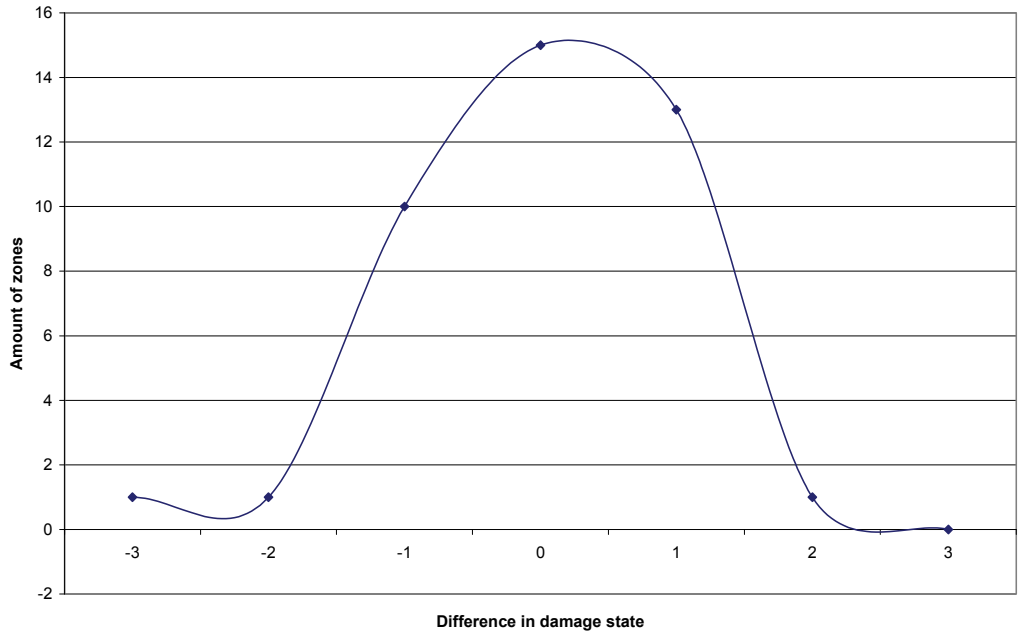

Figure 3-12 Relationship Between Percentage Damaged Land Per Zone and the Percentage Collapsed Structures from the Validation Dataset (Yamazaki et al. 2004b).

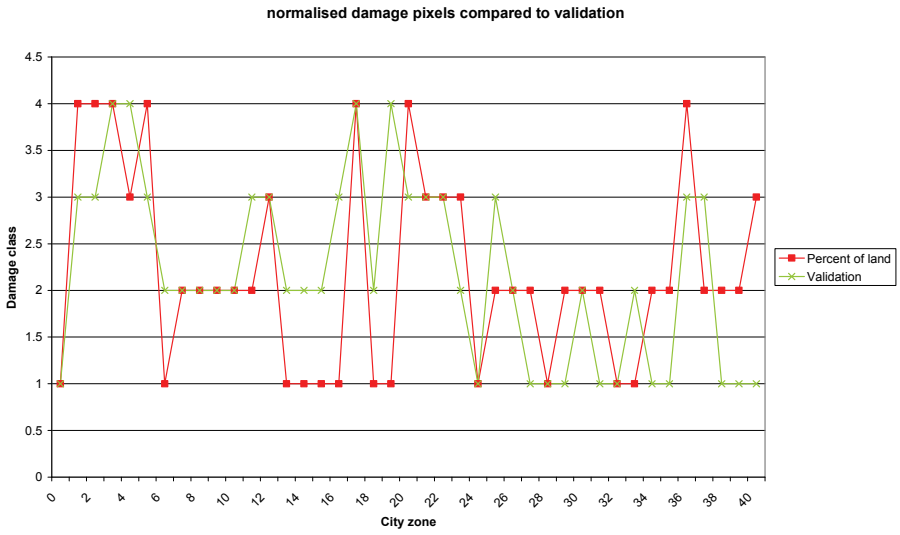

Figure 3-13 Correspondence Chart Denoting the Pattern of Agreement Between the Damage Level Classification Expressed as Four Classes (Very High, High, Medium, Low) and the Validation Percentage of Damaged Buildings

Further assessing the geographic distribution of correspondence between the classification and validation results, figure 3-14 shows that there are three main areas of disagreement, marked A, B and C. Area A is subject to misclassification as a high-damage zone, and significantly overestimates damage. Examining the pre- and post-earthquake imagery and classification result (figure 3-15), most of the building roofs in this area are not collapsed. The spectral properties between the Quickbird pre-earthquake image and the IKONOS 'after' image are very different. Taking a sample of DN values for the building roofs, the difference between the layers is ~106DN, which means that despite histogram matching efforts, the difference in color of the roofs is very close to the difference in colour between an intact roof, rubble and the surrounding bare earth. Therefore due to this multi-sensor sensor effect it cannot be reliably distinguished from building collapse. It is useful to note that the larger industrial buildings are not misclassified, as their roof colour is brighter.

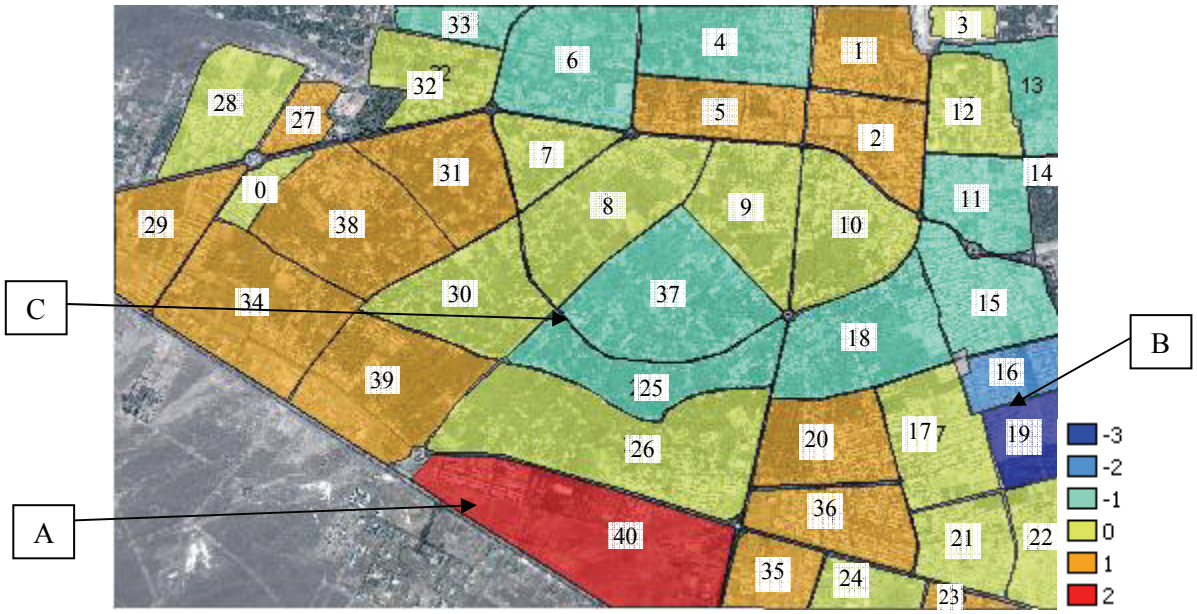

Figure 3-14 Difference in Classification Zone Between Derived Output and Validation Layer for Percent Damage Per City Zone

In area B (figure 3.16), although the classification has correctly classified most buildings as collapsed, due to the inclusion of large areas of ground cover that are spectrally similar to buildings, the damage percent per zone is underestimated. Area C is also prominent in figure 3-14. Figure 3-17 shows that here, many of the collapsed buildings are correctly marked as damaged. However, because there are only a few buildings in this area and lots of date palm trees, as a percentage of the total area, it is not marked as heavily damaged.

Overall, the inaccuracies in results obtained for area-based damage assessments all relate back to scale-based issues and point to the need for a scale-independent measure of damage.

a) Quickbird before image

b) IKONOS after image

c) Classification result Red = high change Yellow = low change.

Figure 3-15 Area A (Zone 40) Where Urban Damage was Substantially Overestimated by the Classification Result

a) Quickbird before image

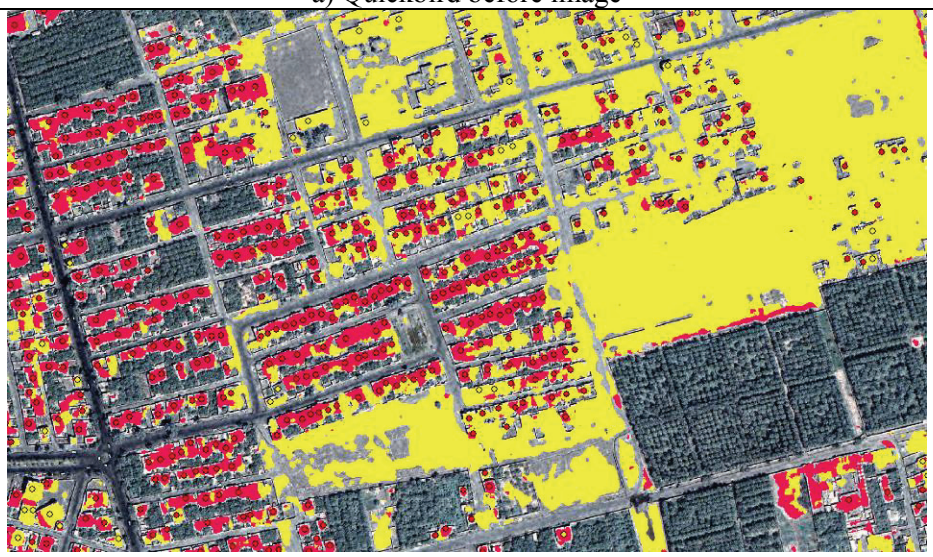

c) Classification result Red = high change Yellow = low change.

Figure 3-16 Area B (Zone 19) Where Urban Damage was Underestimated by the Classification Result

a) Quickbird before image

b) IKONOS after image

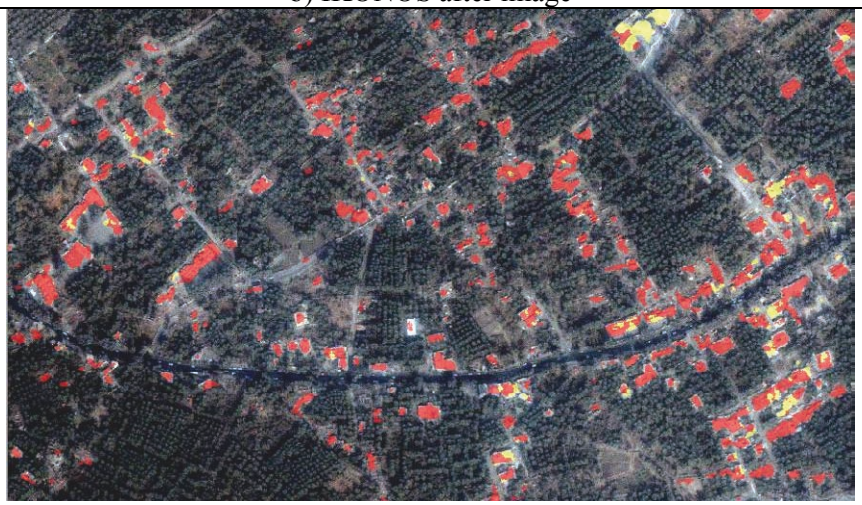

c) Classification result Red = high change Yellow = low change.

Figure 3-17 Area C (Zone 37) Where Urban Damage was Underestimated by the Classification Result

SECTION 4
METHOD 2: TEXTURE-BASED COMPARISON

The flow diagram in figure 1-2 outlines Method 2: Texture-based Comparison, for detecting the extent and severity of urban damage in Bam at a pixel-scale. It differs from Method 1: Spectral Comparison because damage is assessed in terms of neighborhood-scale textural changes between the two input images. The working hypothesis is that the chaotic piles of rubble associated with collapsed buildings will exhibit poorly-defined edge structures and high textural variability, which produces a statistically measurable difference in textural indicators.

Again, the use of Quickbird pre-earthquake imagery with the IKONOS post-earthquake data will accentuate non-disaster-related sources of difference between the images. This method also provides scope for investigating if the use of textural measures reduces inter-sensor differences between the images that affect the performance of spectrally-based methodologies. Processing steps taken to minimize these effects are highlighted in figure 1-2.

This methodology follows the general approach employed by Adams *et al.* (2004a), who examined building collapse in Bam using pre- and post-event Quickbird imagery. This exploratory study found that by comparing two Quickbird images, differences due to damage could be detected using textural methods, and in particular that a dissimilarity measure was found to be altered enough between collapsed and non-collapsed buildings to detect extreme changes across the city.

A quantitative texture-based damage assessment methodology was explored, comprising the following analytical steps. These are numbered in sequence, continuing on from the pre-processing procedures described in Section 1.3:

(8) Laplacian filtering to highlight the chaotic pattern of edges associated with intact versus collapsed roofs within the pre- and post-disaster imagery;

(9) Textural measures were evaluated and based on exploratory research findings, the best performing dissimilarity filter carried forward to subsequent steps of the analysis;

(10) Differencing between the ‘before’ and ‘after’ dissimilarity images;

(11) Masking the difference image to focus on roof structures and remove non-disaster related sources of change, such as vegetation and roads;

(12) Classification of the difference image using an supervised and interactive classifier to distinguish between damaged versus non damaged areas;

(13) A grid-based damage map was created, statistically expressing the pattern of ‘collapsed’ pixels within a regular grid system spanning the city;

Validation of the classification results was conducted using area-based damage observations made by Yamazaki *et al.* (2004b).

4.1 Laplacian Filtering

Filtering accentuates roofs, vegetation, cars, and other areas with a well defined change in pixel gradient To accentuate textural properties of the scene, a 9 x 9 Laplacian filter was run over the red band of the pansharpened 'before' and 'after' images. A single band was used (oppose to the three optical red, green and blue bands), because visual inspection suggested that all three bands correspond closely in terms of information content, yet the use of a single channel significantly reduces processing time. .

The Laplacian is a 2-D isotropic measure of the 2nd spatial derivative of an image. The Laplacian of an image highlights regions of rapid intensity change and is therefore often used for edge detection (Fisher *et al.* 2003). A 9 x 9 filter was found to be the optimum window size from exploratory research focusing on Bam (Adams *et al.* 2004a; Huyck *et al.*, 2005). This filter size was deemed large enough to pick out the main walls of adobe structures, without capturing unnecessary detail.

A sample of the edge-accentuated output from this operation is shown in figure 4-1. Comparing the pre- and post-earthquake images for the area of building collapse (see Area 3 in figure 3-3), there are pronounced differences between the scenes. Distinct areas of homogeneity are evident within the 'before' image, whereas features are indistinct and fuzzy within the 'after' image. This distinctive qualitative signature associated with building damage suggests that texture may be a useful quantitative indicator for quantifying damaged areas. From a multi-sensor standpoint, within a non-damaged neighborhood (see Area 1 in figure 2-1), the difference between Quickbird and IKONOS is visually recognizable. The Quickbird product exhibits sharper walls, and in line with the higher spatial resolution, is less 'fuzzy' than the IKONOS product.

4.2 Textural Analysis

A range of different texture-based image processing algorithms are documented in the literature, including: dissimilarity; contrast; entropy; second moment; mean; variance; and correlation (e.g. Sonka *et al.*1998). Algorithms for applying these techniques are available in the ENVI image processing environment (RSI 2007), and were therefore considered for analysis.

From a theoretical standpoint, a grey level co-occurrence matrix (GLCM) routine, uses a window to examine pixel values and their neighborhood relations within a certain i x j matrix (normally square). This type of analysis is a second order texture calculation. Considering a shift of 1X and 1Y, and assuming a symmetrical, normalized co-occurrence matrix, the diagonal values relate to identical pixels. Moving progressively diagonally away in each direction gives pixel values 1 DN apart, 2 DN apart, and so on. Performing weighting operations on these diagonals accentuates spectral variations, such as those highlighted by application of a Laplacian filter. Examples of these operators are dissimilarity and contrast. Weighting depending on the commonness of the relationship between neighboring pixels gives measures of orderliness. Examples of these are entropy and second moment. Other texture measures exist, which examine the statistical relationship of the data. These include mean, variance and correlation.

Previous research indicates that many of the texture measures are correlated (Hall-Bey 2007). Accordingly, the present study evaluated performance of a subset of one contrast, one orderliness and one statistical texture measure:

- Dissimilarity (contrast measure)
- Entropy (orderliness measure)
- Correlation (statistical measure)

Quickbird	IKONOS
a) Damaged area - before earthquake (SE Bam)  **Result of 9 x 9 laplacian filter on Quickbird pre-earthquake image**	b) Damaged area - after earthquake (SE Bam) 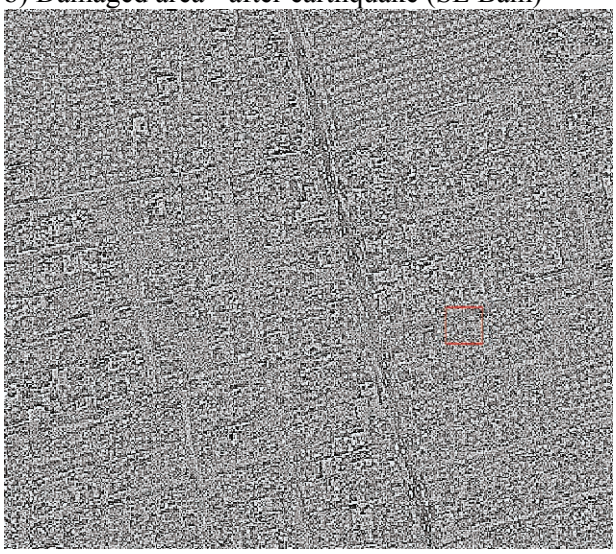 **Result of 9 x 9 laplacian filter on IKONOS post-earthquake image**
c) Non-damaged area (West Bam) 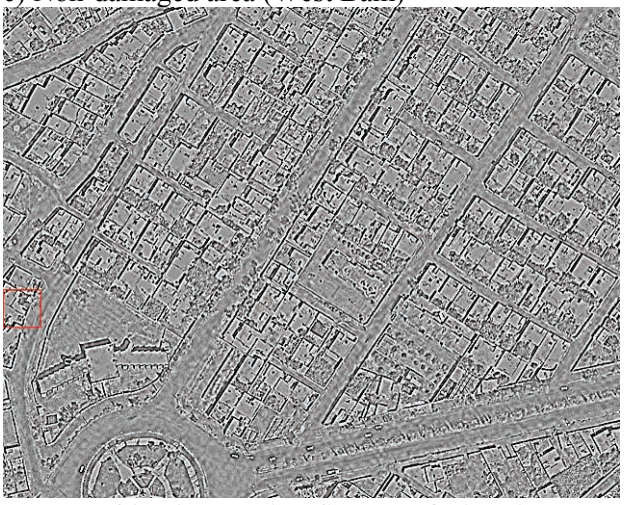 **Result of 9 x 9 laplacian filter on Quickbird pre-earthquake image**	d) Non-damaged area (West Bam)  **Result of 9 x 9 laplacian filter on IKONOS post-earthquake image**

Figure 4-1 Quickbird and IKONOS Scenes After Laplacian Filtering in Damaged and Non-Damaged Areas. Pronounced Textural Differences are Evident within the Neighborhood that Sustained Building Damage.

Dissimilarity was chosen to examine the relationship between the colour of neighboring pixels in a pre-disaster and post-disaster scenario. Equation 4-1 presents the dissimilarity texture measure. This weights the co-occurrence matrix linearly outwards from the diagonal, meaning that 'a larger number will be seen for windows with little contrast' (Hall-Bey 2007). This measure was chosen as it would be useful to compare with previous research undertaken by Adams *et al.* (2004a; Huyck *et al.*, 2005). It is a contrast measure, where weights in the GLCM matrix increase linearly away from the diagonal. Other measures such as contrast and homogeneity are thought to give similar information (respectively with an exponential set of weights from the matrix diagonal, and the inverse of this) and so were not examined.

$$\sum_{i,j=0}^{N-1} P_{i,j} \, |i-j| \tag{4-1}$$

Entropy was the second texture measure examined (Equation 4-2). It describes chaos in a system, and is therefore the opposite of an orderliness measure. This was selected to examine whether the post-earthquake rubble created a more chaotic arrangement of pixel values than non-collapsed roof areas. Texture measures such as the angular second moment and energy were not utilized as these give similar measurements.

$$\sum_{i,j=0}^{N-1} P_{i,j} \, (-\ln P_{i,j}) \tag{4-2}$$

The third texture measure examined was correlation (Equation 4-3). Correlation measures the 'linear dependency of grey levels on those of neighboring pixels' (Hall-Bey, 2007) and is a descriptive statistics measure. This measure was chosen to explore whether destroyed roof structures had an increased occurrence of certain pixel combinations, or a decreased occurrence. It is generally the case that areas with homogenous texture such as bare ground have high correlation, while textured areas where a lot of different structures occur, such as in an urban area, records lower correlation.

$$\sum_{i,j=0}^{N-1} P_{i,j} \left[\frac{(i-\mu_i)(j-\mu_i)}{\sqrt{(\sigma_i^2)(\sigma_i^2)}} \right] \tag{4-3}$$

When employing texture measures, the relationship between processing window size and ground surface objects is an important consideration. Table 4-1 illustrates variation in textural response with window size. For all three measures, as the window size increases the amount of detail decreases and edge features appear blurred. When looking at damaged buildings, a window size smaller than the roof would not pick up edges. A window size that was too large would not pick up an appropriate level of detail for a neighborhood scale analysis. For the present study, a 25 x 25 window size was chosen for the above measures based on the work by Adams *et al.* (2004a). Given the high-resolution imagery, this window encapsulates several buildings.

Table 4-1 Texture Measures of Varying Window Size Applied to Quickbird Pre- and IKONOS Post-Earthquake Images for a Damaged Area of SE Bam

	Dissimilarity	Entropy	Correlation
3 x 3 Quickbird		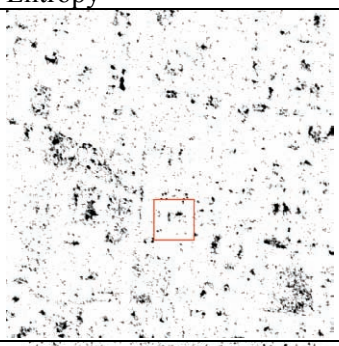	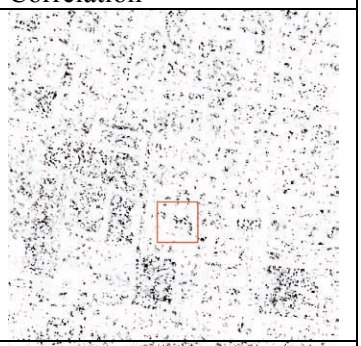
3 x 3 IKONOS	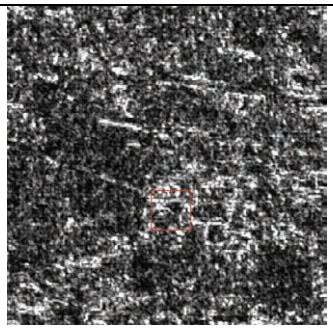	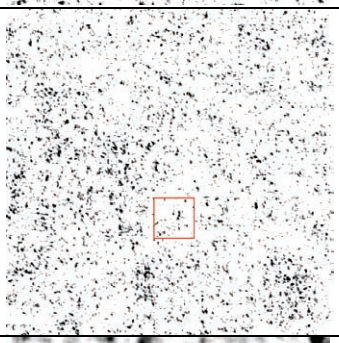	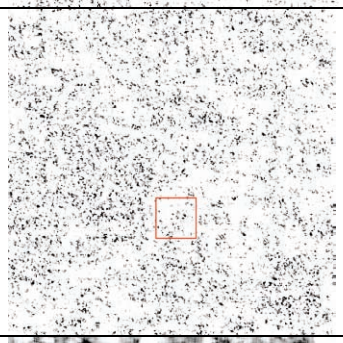
9 x 9 Quickbird	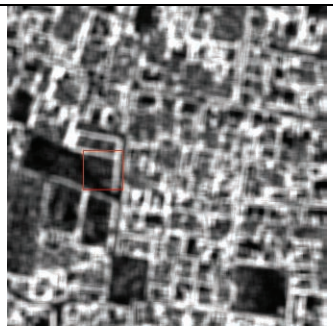	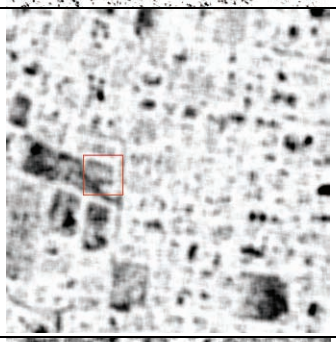	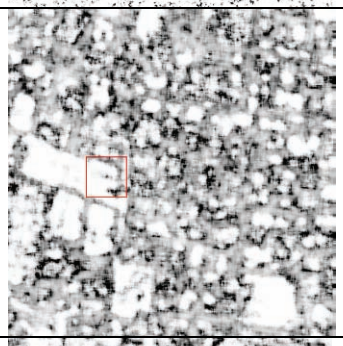
9 x 9 IKONOS	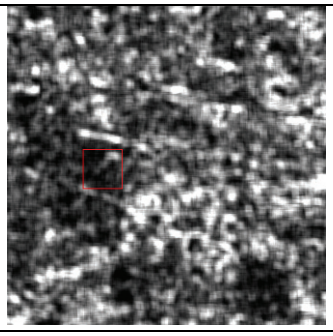	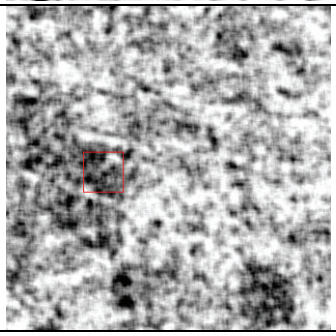	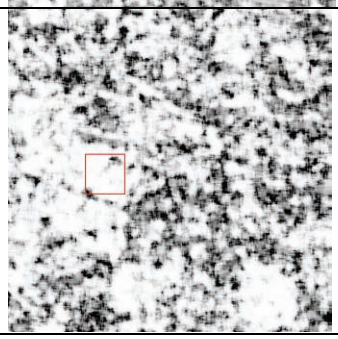

Table 4-1 (cont) Texture Measures of Varying Window Size Applied to Quickbird Pre- and IKONOS Post-Earthquake Images for a Damaged Area of SE Bam

	Dissimilarity	Entropy	Correlation
15 x15 Quickbird	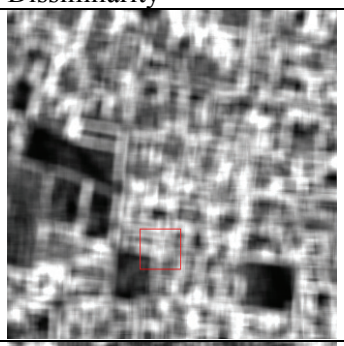	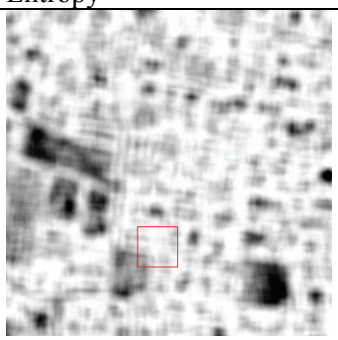	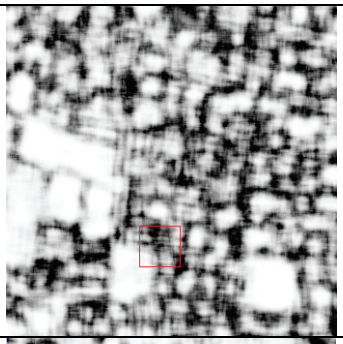
15 x 15 IKONOS	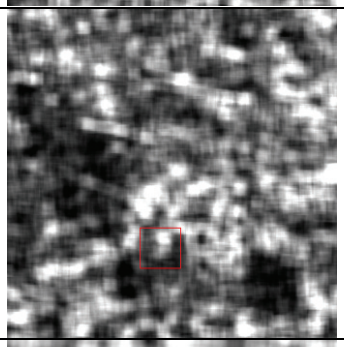	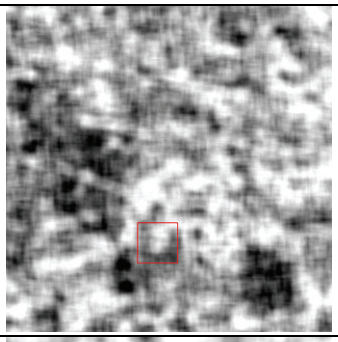	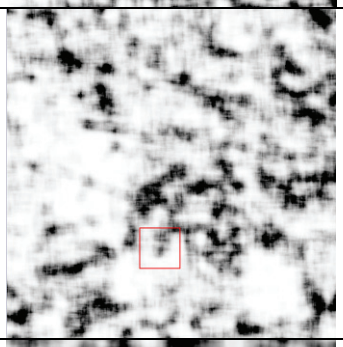
25 x 25 Quickbird	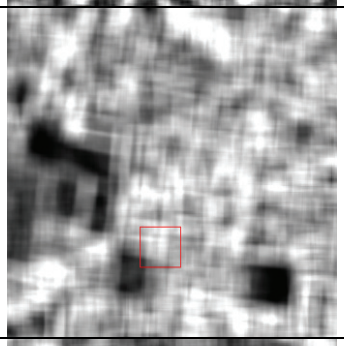	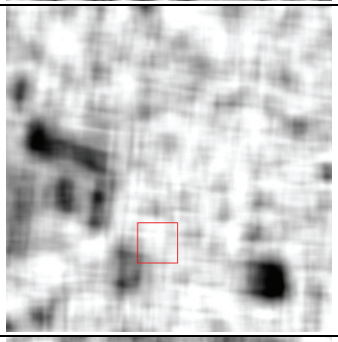	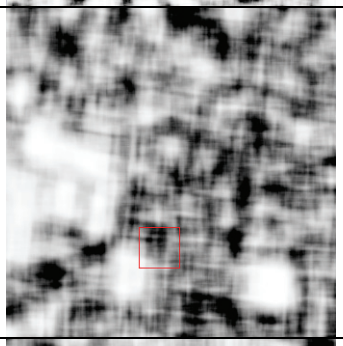
25 x 25 IKONOS	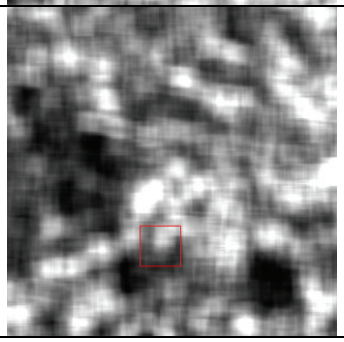	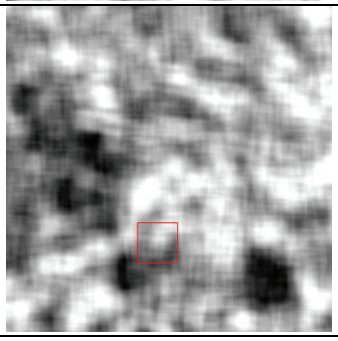	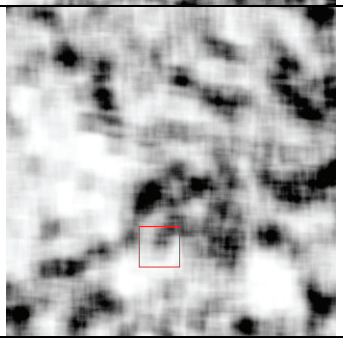

4.3 Masking

In order to highlight urban areas of interest within the image, and reduce the influence of non-disaster-related changes, the images for dissimilarity, entropy and correlation were masked using the cumulative masks employed during Method 1. Described in Section 1.3.2 and Section 1.3.5, the masks comprise:

- Vegetation exclusion mask
- Roof inclusion mask
- Shadow removal mask

Statistical characteristics of structures within the change scene were examined, to establish if distinctive patterns of variation accompany building collapse. Regions of interest were created which examined the texture measures on a neighborhood scale.

4.4 Differencing

The pre- and post-earthquake textural images for dissimilarity, entropy and correlation were respectively differenced on a pixel by pixel level, to create a textural change product. The difference image was also visualized using ArcGIS software, converting the change values to an 8-bit range in order to highlight areas of maximum change.

4.5 Classification

The 8-bit difference images for dissimilarity, entropy and correlation were classified using a natural breaks algorithm within the ArcGIS environment. This straightforward method towards classification was employed, oppose to supervised and unsupervised methodologies typical of image processing systems, since it is more interactive for the operator. As such, intra-class statistical characteristics and inter-class boundaries can be explored in detail, varying the boundaries to achieve an optimal result.

The damage class identified within each of the three texture measures was then extracted from the rest of the classification results, in preparation for creating a damage map. A reclassification processing routine was used to create classes of damage versus no-data.

4.6 Damage Map and Validation

The classification results were grouped using a neighborhood grid system (see, for example, Huyck *et al.*, 2005). A range of different grid spacing intervals were explored, ranging from 60 to 240. A 120m grid interval was deemed useful to show damage at a neighborhood scale, because it was a good compromise between a quick visual assessment of the area, and relatively detailed area by area coverage. The grid employed is shown in figure 4-2.

A summarize zone procedure was utilized from a proprietary ‘Hawks Analysis Tool’ within the ArcGIS environment. This calculated the frequency of damaged pixels within each zone and generated associated statistics including: mean; median; minimum; maximum; sum; and count.

The output from the summarize zones was joined to the newly created grid to visualize statistics by grid square. This showed the damage class count per zone.

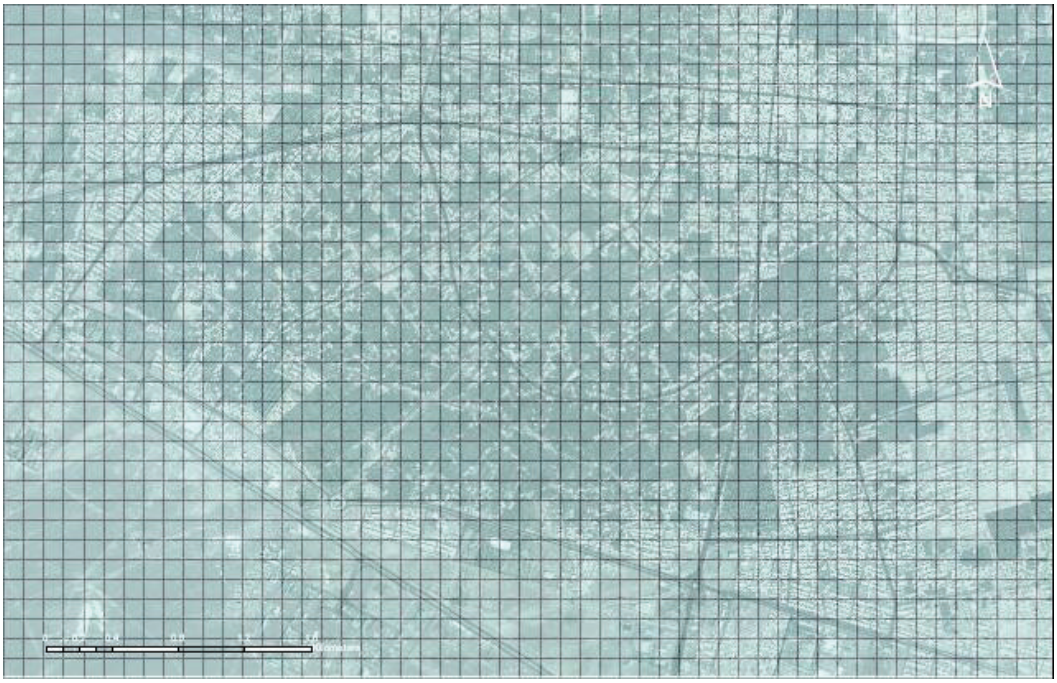

Figure 4-2 120m Grid Layout Used to Examine and Identify Generalizations in Damage Statistics for the Masked Difference Image and Validation Data

To support subsequent validation steps, the point sample dataset from Yamazaki *et al.* (2004b) in figure 1-8a was summarized into an equivalent 120m interval grid. The top two point classes pertaining to category 4 and 5 damage were summed, to show heavy damage per cell.

SECTION 5
RESULTS 2: TEXTURE-BASED COMPARISON

5.1 Dissimilarity Analysis

Figure 5-1 shows the *dissimilarity* results produced from the Quickbird and IKONOS imagery at the city wide scale. In the pre-earthquake Quickbird image using the 25 x 25 window size, large dissimilarity (represented by high pixel values and a bright return of ~7-9), is evident around urban neighborhoods where there is considerable variability in land surface cover. Medium-low dissimilarity is apparent amongst vegetated areas (around 4-6), and low dissimilarity around homogenous bare geological areas (0-3).

On a scene-wide basis, the IKONOS data has a lower dissimilarity range. This global difference may be a function of multi-sensor variability, caused by the difference in resolution of the two sensors, differences in wavelength, atmospheric effects etc. Within the IKONOS image, specific areas of the city have a more accentuated difference. For urban landcover, non-damaged areas in the west (see Area 1 in figure 2-1) exhibit a similar level of brightness. However, values the heavily damaged South East (Area 3 in figure 3-3) are lower and the scene darker, suggesting that a high concentration of collapse suppresses dissimilarity. The vegetated central urban areas (Area 4 in figure 3-3) are also considerably darker, which could be due to seasonal effects.

Returning to the texture values in the south-east where a proportion of buildings are known to have collapsed, from visual inspection of figure 5-2a there is a substantial *decrease* in dissimilarity, with Area 3 appearing considerably darker in the 'after' scene. This may at first seem counter-intuitive, given the working hypothesis that more chaos is produced on the ground after the earthquake. From these results it appears that standing buildings create more dissimilarity with their surroundings, especially after Laplacian filtering, with sharp gradient changes associated with building edges, vegetation to road boundaries between walls, shadows, roof structure and surrounding ground. Once buildings have fallen, there are no sharp differences such as those in the non-damaged neighborhood (figure 5-2b), just a jumbled, relatively homogenous pile of rubble, or sand, which blends in with surrounding bare earth.

The quantitative characteristics of dissimilarity accompanying different levels of building damage were examined within the collapsed and non-damaged neighborhoods in figure 5-3. Statistics were derived for these particular areas within the 'before' and 'after' images (table 5-1), and used to develop the histograms in figure 5-4.

From the summary statistics in table 5-1, heavily damaged areas of Bam generally exhibit a more pronounced difference in dissimilarity compared with lesser damaged regions. Within Area 3 and Area 4, dissimilarity difference >1, while for Area 1 and Area 5 dissimilarity difference <0.6. The decrease in dissimilarity within heavily damaged regions is also apparent from the histograms. The mean values for the pre-earthquake Quickbird and post-earthquake IKONOS images are similar within Area 1 and Area 5, while in Area 3 and Area 4 the post-event histogram peaks at a markedly lower value. As such, dissimilarity appears to be an effective textural measure for distinguishing between collapsed versus non-damaged neighborhoods.

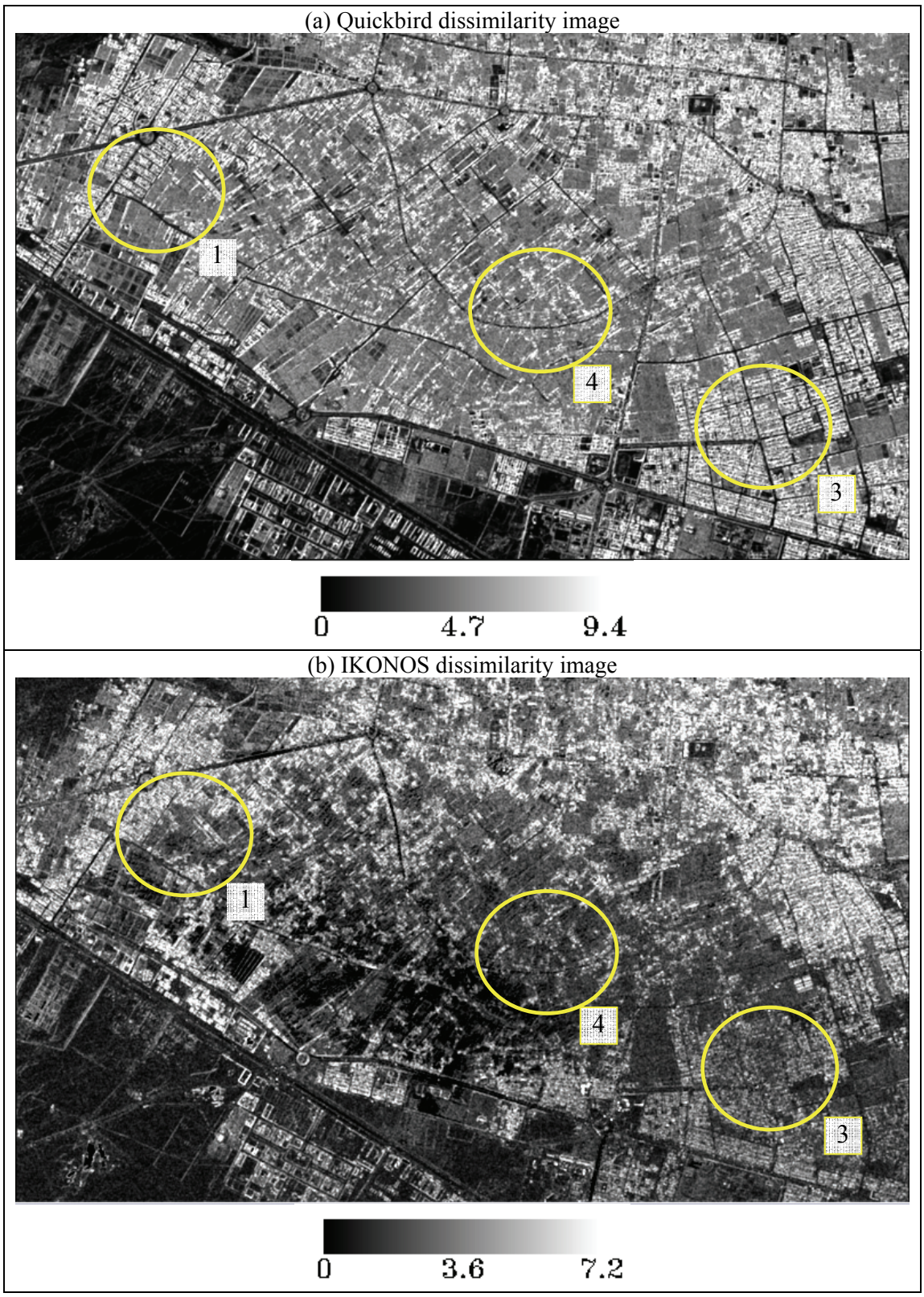

Figure 5-1 City-Wide (a) Pre-Earthquake and (b) Post-Earthquake Dissimilarity Images

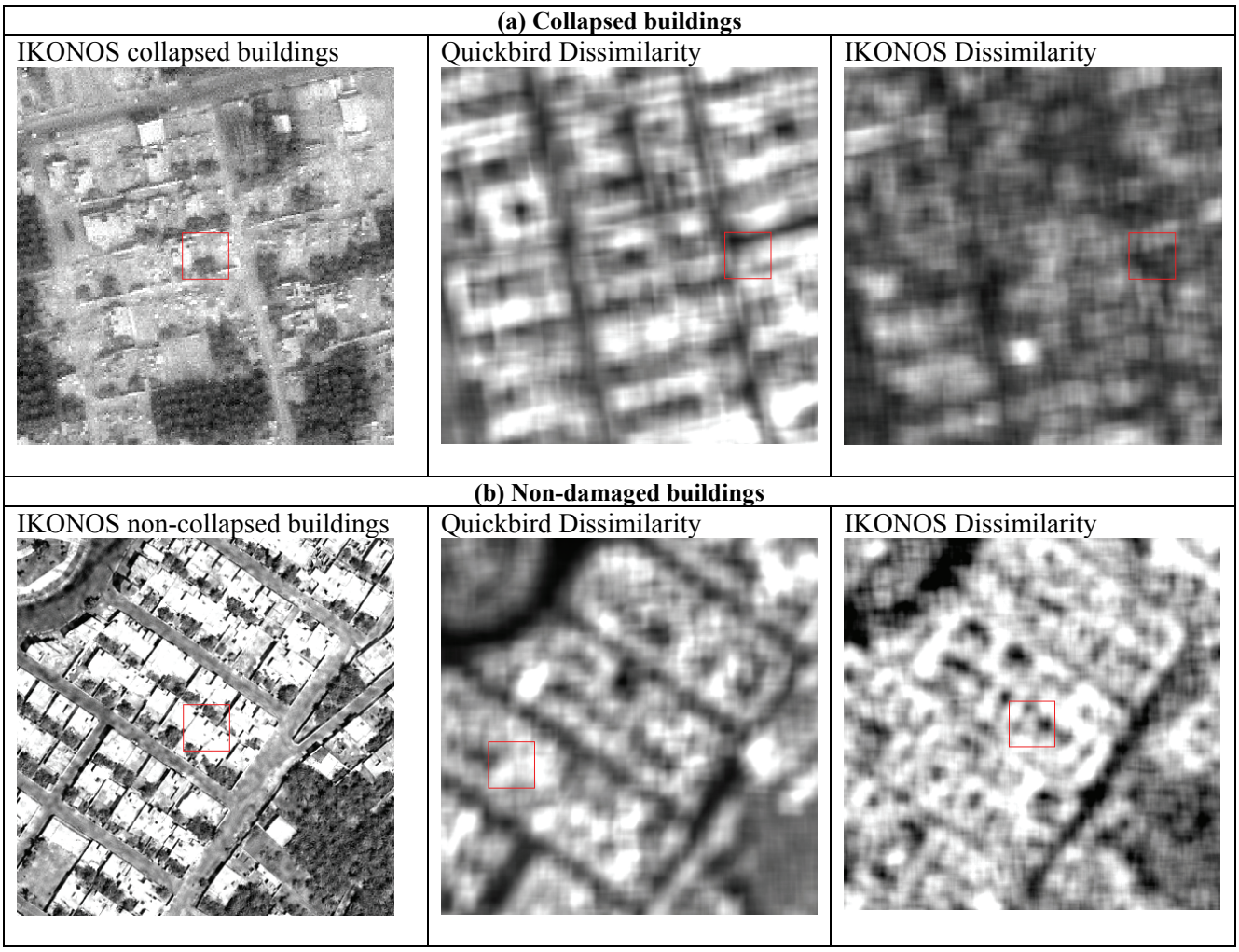

Figure 5-2 Visual Comparison Between Dissimilarity Results in Pre- and Post-Earthquake Imagery Obtained for Neighborhoods with (a) Extreme Building Collapse and (b) (a) Non-Damaged Buildings

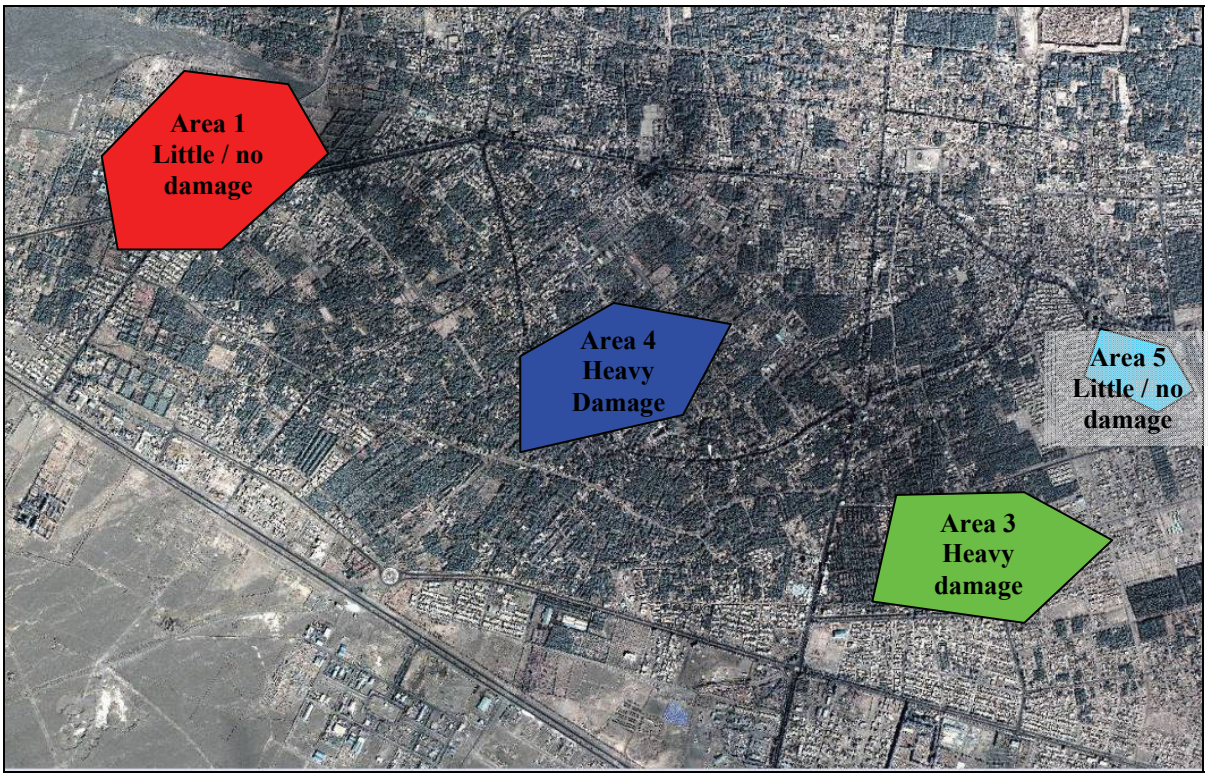

Figure 5-3 Neighborhoods within Bam for which Histograms were Developed to Illustrate the Quantitative Textural Characteristics Accompanying Collapsed versus Non-Collapsed Buildings

Table 5-1 Dissimilarity Measures in Key Areas. In Bold are Known Heavily Damaged Areas.

	Area 1	**Area 3**	**Area 4**	**Area 5**
Damage	Non-collapsed	**Heavy damage**	**Heavy damage**	Non-collapsed
Quickbird 'before'	3.34 +/- 0.97	**3.25 +/- 0.93**	**3.43 +/- 0.91**	3.26 +/- 0.77
Ikonos 'after'	2.81 +/- 0.51	**2.18 +/- 0.33**	**2.35 +/- 0.44**	2.96 +/- 0.43
Difference	0.5	**1.1**	**1.1**	**0.3**

5.2 Entropy Analysis

Figure 5-5 shows the results obtained using an *entropy* texture measure. On a city-wide scale, the pre-earthquake Quickbird imagery has a relatively high level of entropy throughout the imagery, appearing as bright DN values. The highest entropy levels occur in urban areas, at around values of ~5-6. Vegetation records a lower entropy value of ~3-4, while the geology is lower still, at ~0-3.

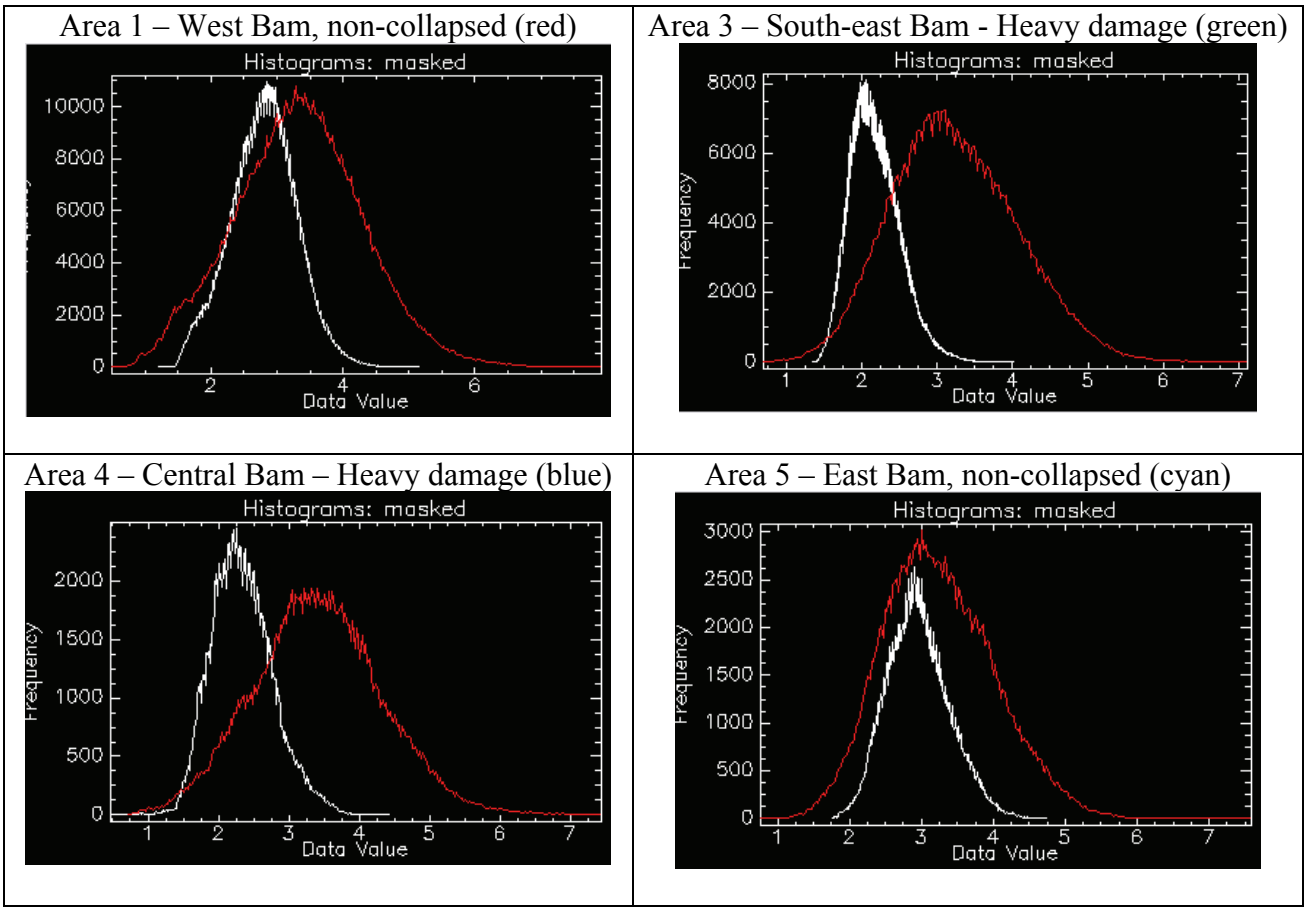

Figure 5-4 Quickbird (Red) Pre-Event and IKONOS (White) Post-Event Dissimilarity Histograms for Selected Areas of Bam Exhibiting Collapse and Non-Collapsed Buildings

Within the post-earthquake IKONOS imagery, a generally lower range of entropy values is observed. As was the case for the dissimilarity textural result, relatively high entropy levels remain around lesser damaged urban neighborhoods such as Area 1 (values ~5-6), where the rapidly changing roof, shadow, vegetation, and road configurations create a more chaotic pattern at the 25 x 25 window size. Damaged regions in the south-east (Area 3) appear darker, indicating that values are lower. Vegetated regions in the central regions of Bam (Area 4) are also substantially darker, signifying a reduction in values.

Examining this difference in more detail within non-damaged areas (see figure 5-6), high entropy with a bright pixel return is seen around building edges in both the Quickbird and IKONOS images. Lower entropy characterized by darker pixels is evident in the middle of building roofs and on homogenous roads. Where the buildings have collapsed (figure 5-5b), in IKONOS image a marked decrease in entropy is apparent.

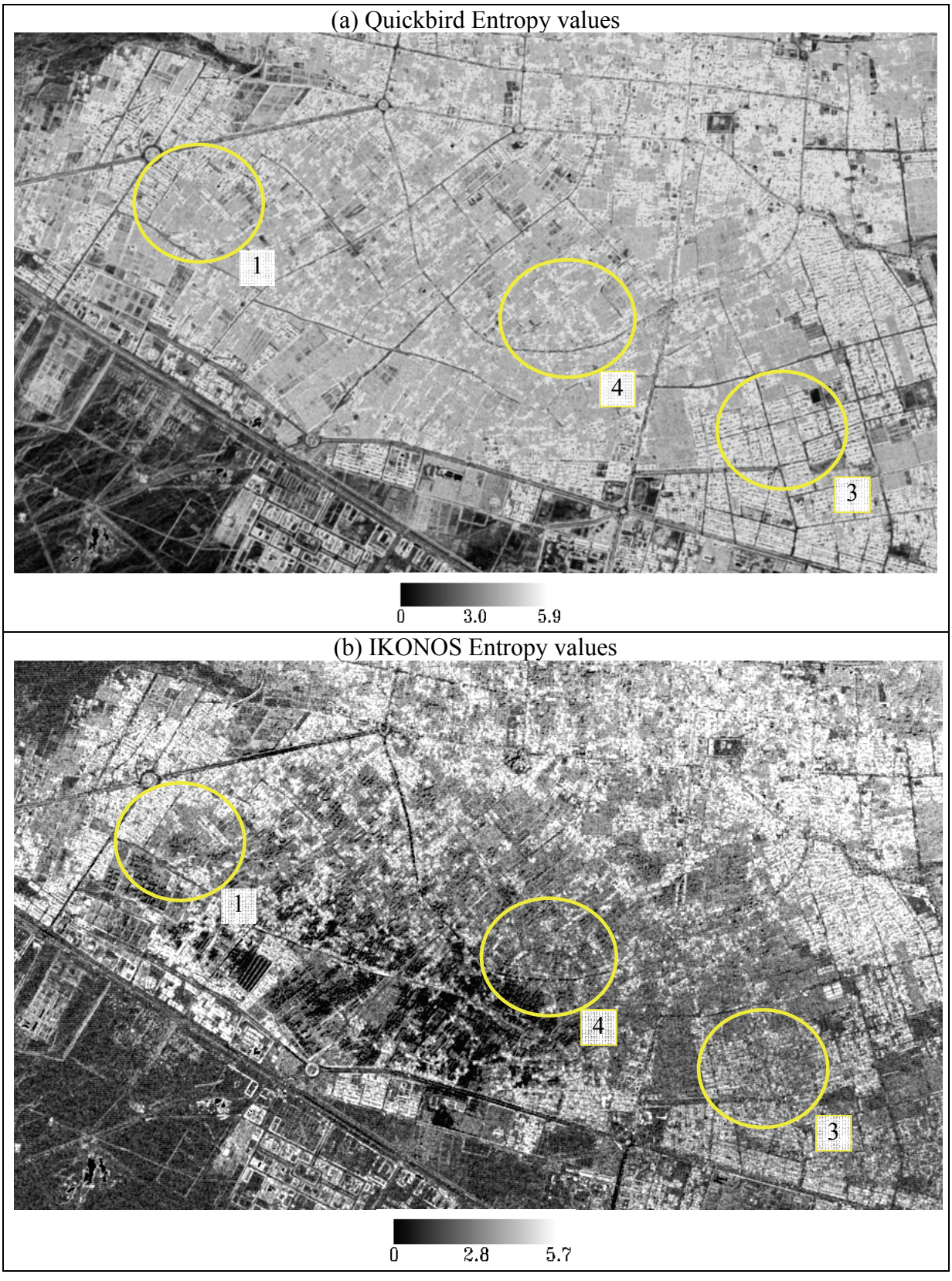

Figure 5-5 City-Wide Entropy Values in (a) Quickbird and (b) IKONOS Imagery

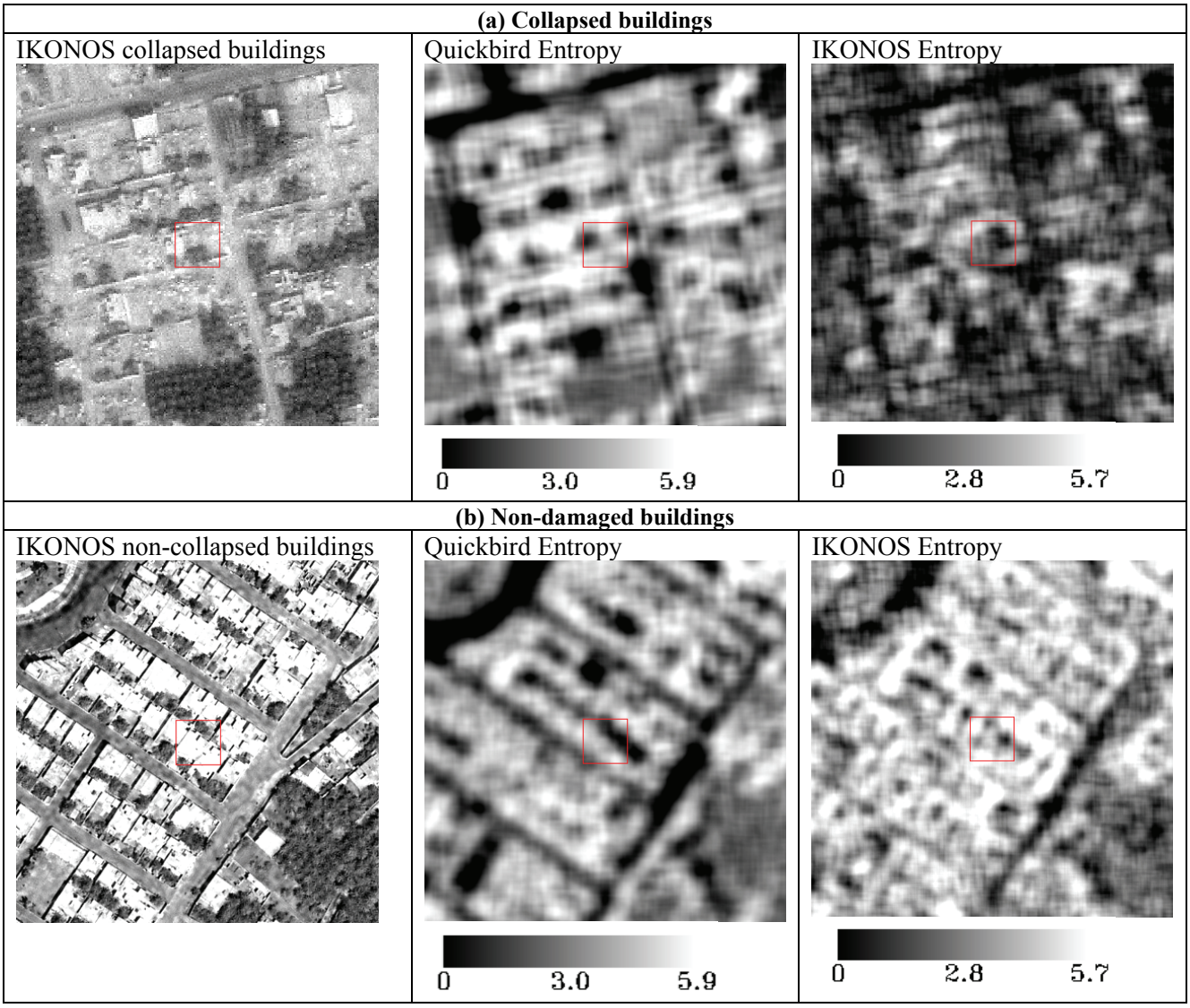

Figure 5-6 Visual Comparison Between Entropy Results in Pre- and Post-Earthquake Imagery Obtained for Neighborhoods with (a) Extreme Building Collapse and (b) Non-Damaged Buildings

Examining the histograms and statistics for damaged and non-damaged Areas 1, 3, 4 and 5 (for locations see figure 5-3) in table 5-2 and figure 5-7, there is a distinction in mean entropy value between the Quickbird and IKONOS imagery, particularly in heavily damaged areas. For the non-damaged case, entropy difference ~ 0.2, whereas in neighborhoods where buildings collapsed entropy difference ~0.65. Although a relatively large standard deviation means that the distributions are not totally separate from one another, a substantial shift in histogram peaks is evident in Areas 2, 3 and 4. This result suggests that entropy may also be a useful measure for distinguishing between neighborhoods dominated by collapsed versus non-damaged buildings.

Table 5-2 Entropy Measures in Key Areas. In Bold are Known Heavily Damaged Areas.

	Entropy Mean and SD			
	Area 1	**Area 3**	**Area 4**	Area 5
Damage	Non-collapsed	**Heavy damage**	**Heavy damage**	Non-collapsed
Quickbird 'before'	4.61 +/- 0.49	**4.62 +/- 0.47**	**4.78 +/- 0.41**	4.67 +/- 0.40
Ikonos 'after'	4.37 +/- 0.35	**3.99 +/- 0.27**	**4.10 +/- 0.33**	4.45 +/- 0.27
Difference	0.2	**0.6**	**0.7**	0.2

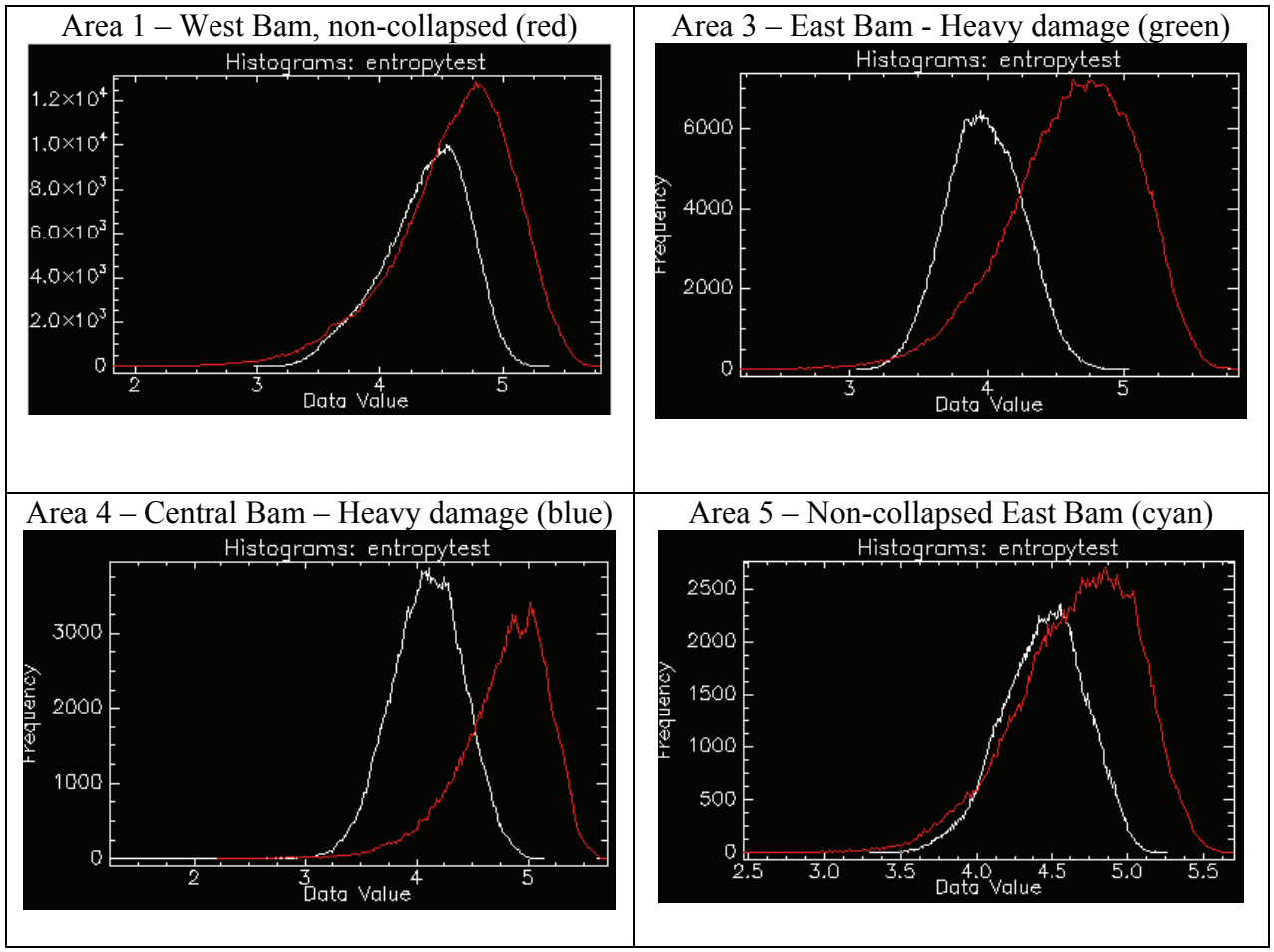

Figure 5-7 Quickbird (Red) Pre-Event and IKONOS (White) Post-Event Entropy Histograms for Selected Areas of Bam Exhibiting Collapse and Non-Collapsed Buildings

5.3 Correlation Analysis

Figure 5-8 shows the results obtained for *correlation*, which measures the 'linear dependency of grey levels on those of neighboring pixels' (Hall-Bey, 2007). On a city-wide scale, for the non-damaged case, areas of Bam with homogenous texture, such as bare ground, have high (bright) correlation values. In general, areas with dense urban development record lower (darker) correlation values. Within these neighborhoods (figure 5-9), higher values of correlation occur along roads and in the centre of buildings.

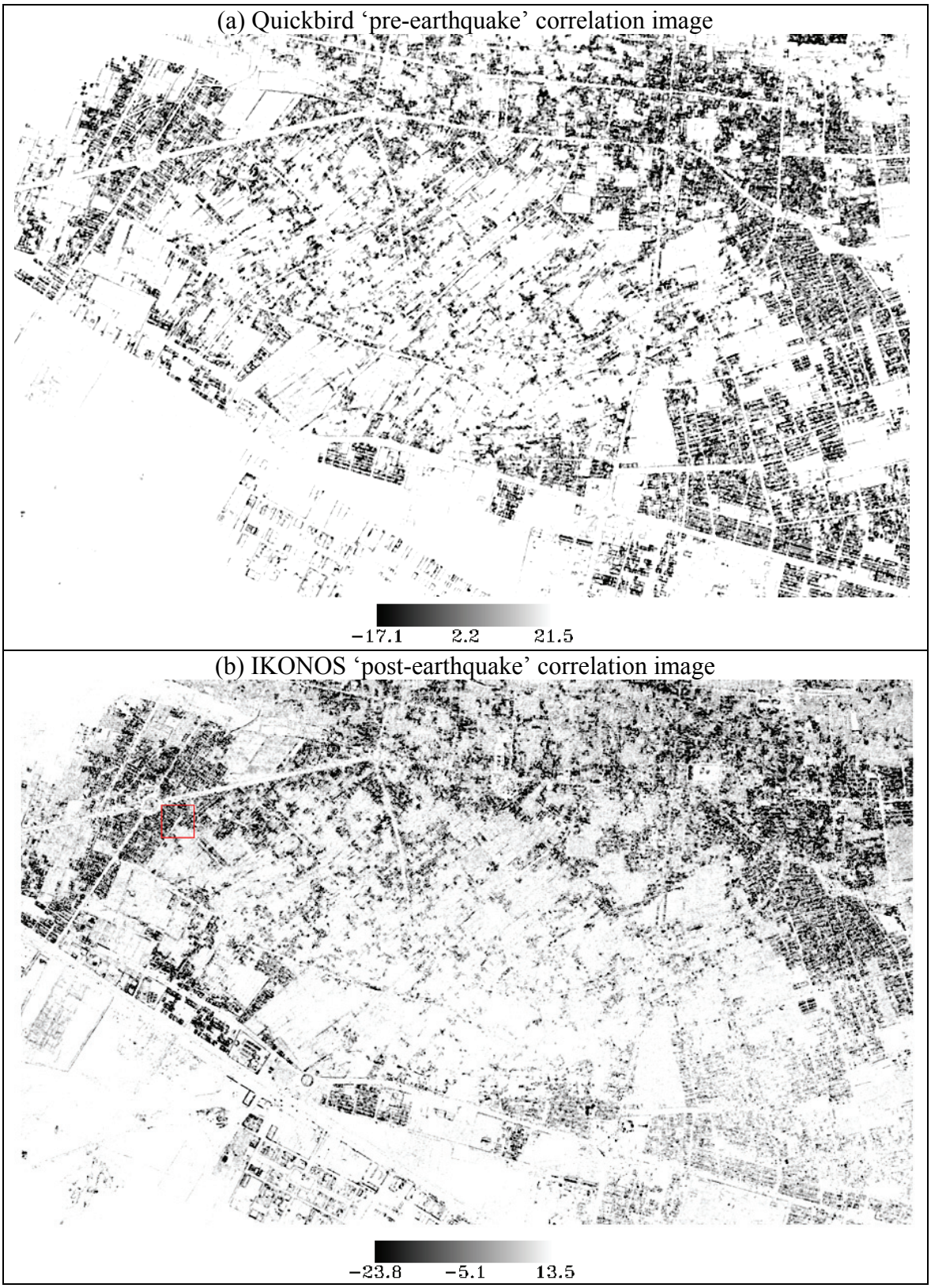

Figure 5-8 City-Wide (a) Pre-Earthquake and (b) Post-Earthquake Correlation Images

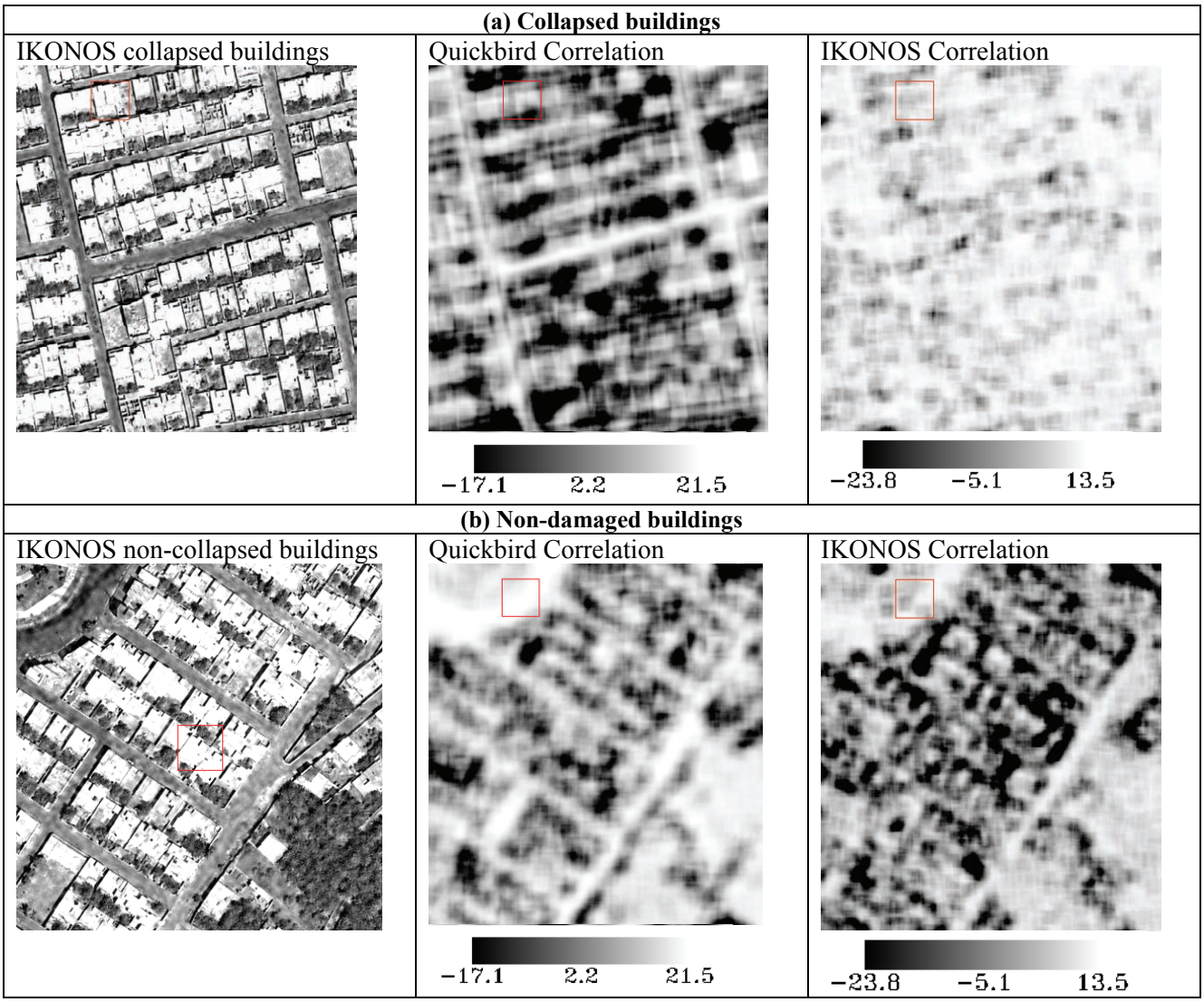

Figure 5-9 Visual Comparison Between Correlation Results in Pre- and Post-Earthquake Imagery Obtained for Neighborhoods with (a) Extreme Building Collapse and (b) Non-Damaged Buildings

The IKONOS 'after' image (figure 5-8b) exhibits the same general pattern. Areas of geology have the highest correlation. From the accompanying legends, these are represented by values of correlation >21 for Quickbird and correlation >13 for IKONOS. Non-damaged Urban areas have the lowest correlation within the IKONOS scene. However, heavily damaged south-eastern areas of the city, as well as parts of central and northern Bam exhibit considerably higher correlation values >0. From figure 5-9b, this positive correlation occurs where buildings edges have been replaced by a pile of rubble, suggesting that building collapse *reduces* neighborhood scale variations in pixel greyscale values. As was the case for the dissimilarity and entropy results, this finding for a 25x25 filter is contrary to the original hypothesis that building collapse produces a more highly textured and 'decorrelated' optical signature.

Considering the summary statistics and histograms in table 5-3 and figure 5-10, within damaged neighborhoods, correlation values in the 'after' image are generally higher than in the 'before'. Compared with the dissimilarity and entropy results, correlation records positive rather than negative difference values. In non-damaged areas, values in the two histograms are similar. Damaged Areas 3 and 4 have the largest difference in mean correlation values of >0.7. Areas 1 and 5 record a smaller difference of <0.2. These results correlate to areas of heavy and light damage respectively. Overall, these results suggest that a correlation texture measure is able to distinguish between neighborhoods dominated by collapsed versus non-collapsed buildings.

Table 5-3 Correlation Measures in Key Areas. In Bold are Known Heavily Damaged Areas

	Correlation Mean and SD			
	Area 1	**Area 3**	**Area 4**	Area 5
Damage	Non-collapsed	**Heavy damage**	**Heavy damage**	Non-collapsed
Quickbird 'before'	-1.10 +/- 0.77	**-1.12 +/- 0.78**	**-1.12 +/- 0.71**	-1.06 +/- 0.62
Ikonos 'after'	-0.91 +/- 069	**-0.34 +/- 0.21**	**-0.46 +/- 0.32**	-0.94 +/- 0.61
Difference	0.2	**0.8**	**0.7**	0.1

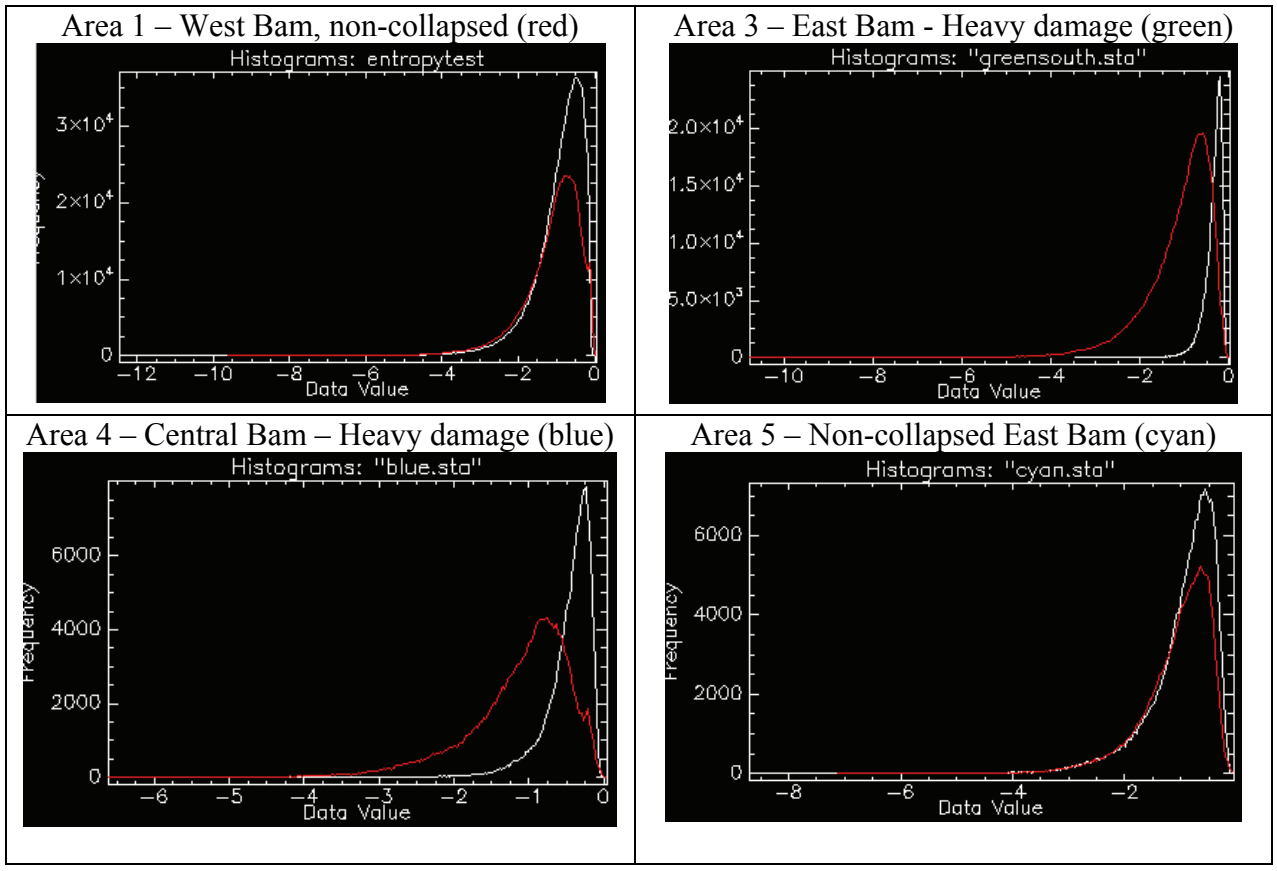

Figure 5-10 Quickbird (Red) Pre-Event and IKONOS (White) Post-Event Correlation Histograms for Selected Areas of Bam Exhibiting Collapse and Non-Collapsed Buildings

5.4 Classified Differencing

Figure 5-11 shows classified difference images produced from the 'before' and 'after' dissimilarity, entropy and correlation scenes. In order to effectively visualize dissimilarity characteristics, for ease of interpretation texture values are grouped into categories of high, moderate and low return, and color coded. Figure 5-11 shows the results from masking and classifying the difference images using a natural breaks classifier. High levels of change are denoted in red, whereas consistency between the pre- and post-earthquake images appears in blue.

Classifying the *dissimilarity* output helps to accentuate particular areas that show the most change. Red corresponds with areas of high dissimilarity difference, inferring building collapse at the 25 x 25 window size. Green is areas of medium dissimilarity difference and blue is the lowest difference. It is a compelling result that most red areas are concentrated in the south east and north east of Bam. Arg-E-Bam is also accentuated as a collapsed building by this classification. Limited difference is seen in many parts of the urban area, with this localized variability likely due to viewing angle differences, shadow differences etc. as well as building collapse.

Figure 5-12 highlights patterns of variation within three neighborhoods that recorded extreme, limited and no damage (for locations see figure 5-3). Within non-damaged neighborhoods in Area 1 to the west (figure 5-12a), textural variation in the Quickbird 'before' dissimilarity image is pronounced around buildings, due to a sharp gradient of change from walls to shadows between structures. On the homogenous rooftops and roads and vegetated swaths the dissimilarity is lower. The pattern of response in the IKONOS image is remarkably similar, resulting in minimal differences. Those present are likely due to differences in viewing angle, suggesting that dissimilarity is a suitable measure for comparing textural changes between scenes acquired by different satellite platforms.

Within areas of the south east (Area 3) that endured heavy building destruction (figure 5-12b), the patterns of response in Quickbird and IKONOS data are markedly different. The dissimilarity measure abruptly decreases between the Quickbird 'before' scene where dissimilarity is once again high, and the 'after' IKONOS image, where values are universally lower. This is confirms that the hypothesis of increasing chaos and high dissimilarity in the textural response in severely damage urban areas may be rejected. Instead, using a 25x25 pixel filter after Laplacian filtering, standing buildings create a highly varied textural response within their surroundings, due to pronounced differences between walls, shadows, roof structure and surrounding ground. Once buildings have fallen, sharp differences are replaced by a jumbled, relatively homogenous pile of rubble, or sand, which blends in with the surrounding bare earth and records a low dissimilarity. *An alternative hypothesis is therefore proposed of reduced chaos and lower dissimilarity within neighborhoods sustaining extreme building damage*.

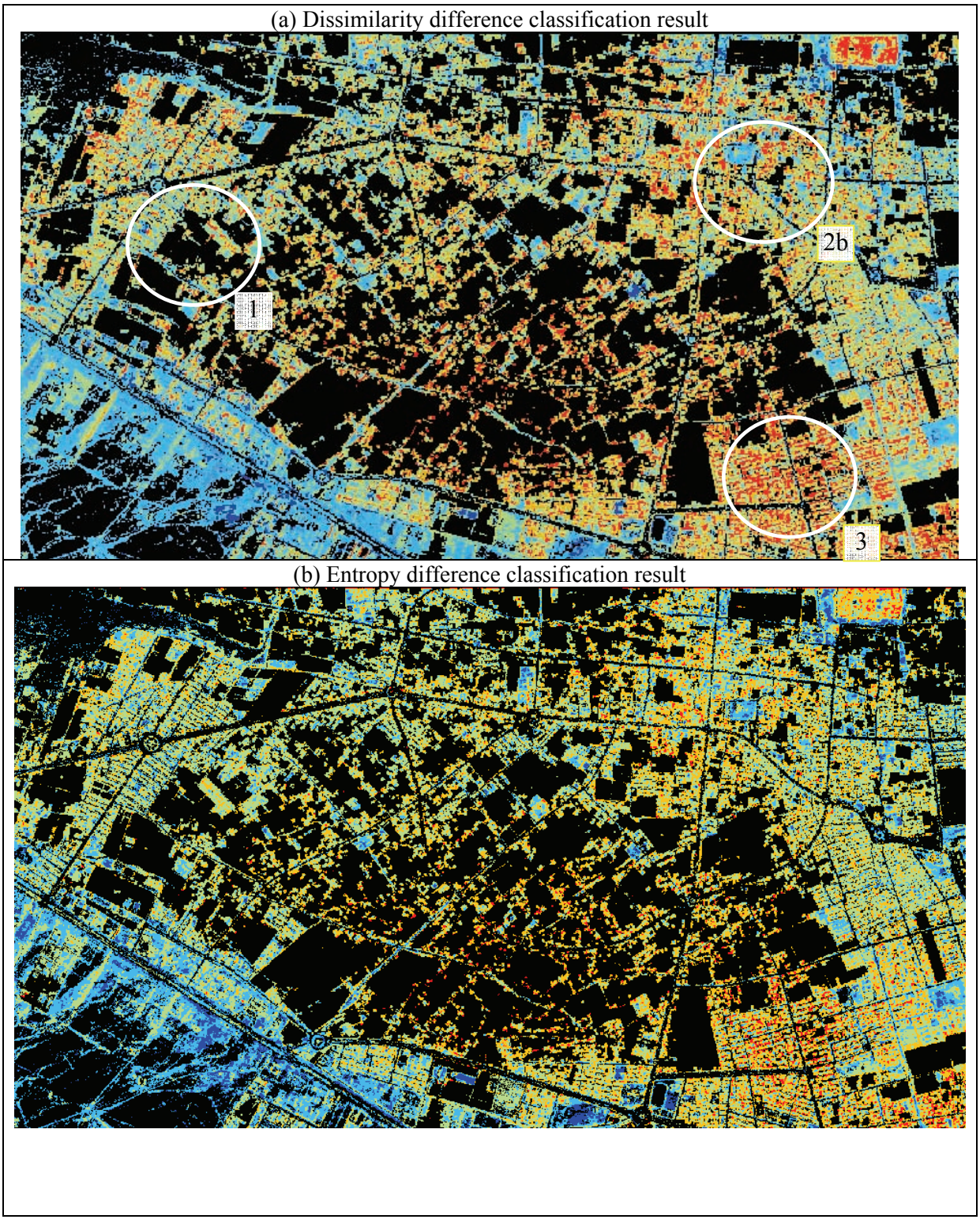

Figure 5-11 Classification of Difference Results, Produced from (a) Dissimilarity; (b) Entropy; and (c) Correlation Textural Analysis. Masked Areas Appear in Black. Area 1 Sustained Non Damage, Area 2b Partial Damage and Area 3 Extreme Damage.

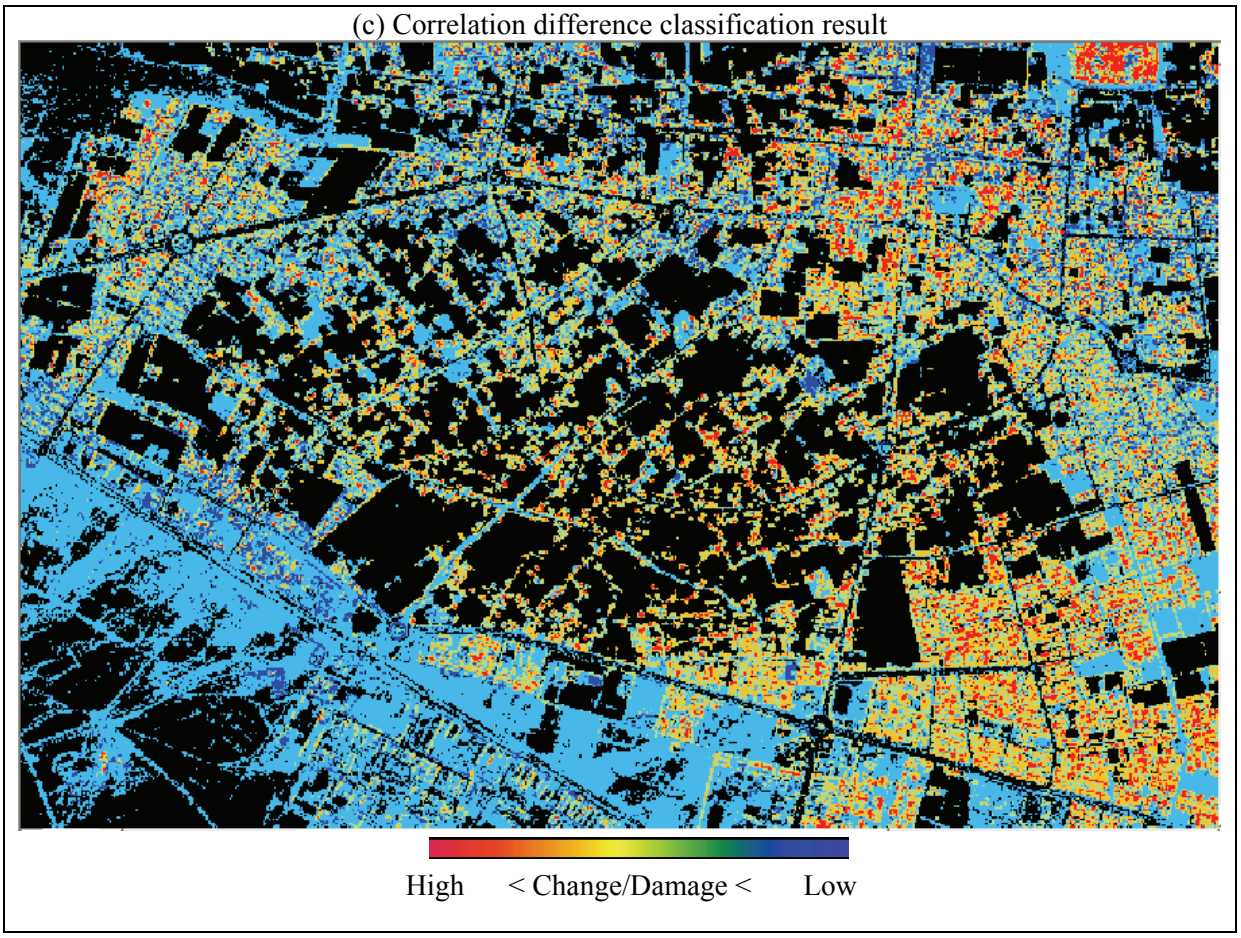

Figure 5-11 (cont.) Classification of Difference Results, Produced from (a) Dissimilarity; (b) Entropy; and (c) Correlation Textural Analysis. Masked Areas Appear in Black

Figure 5-12c illustrates the more complex case of a neighborhood in north-east Bam (Area 2b) where buildings and walls sustained partial damage and some are still standing. The pre- and post-earthquake outputs exhibit a complex mixture of high and low classified difference. Given the indistinct damage signal on a neighborhood scale, these 'mixed' areas may prove to be more difficult to identify using pixel-based change detection techniques. An object-oriented approach, which treats each building as an individual sample unit (see Volume II of this report series) may perform better in these areas.

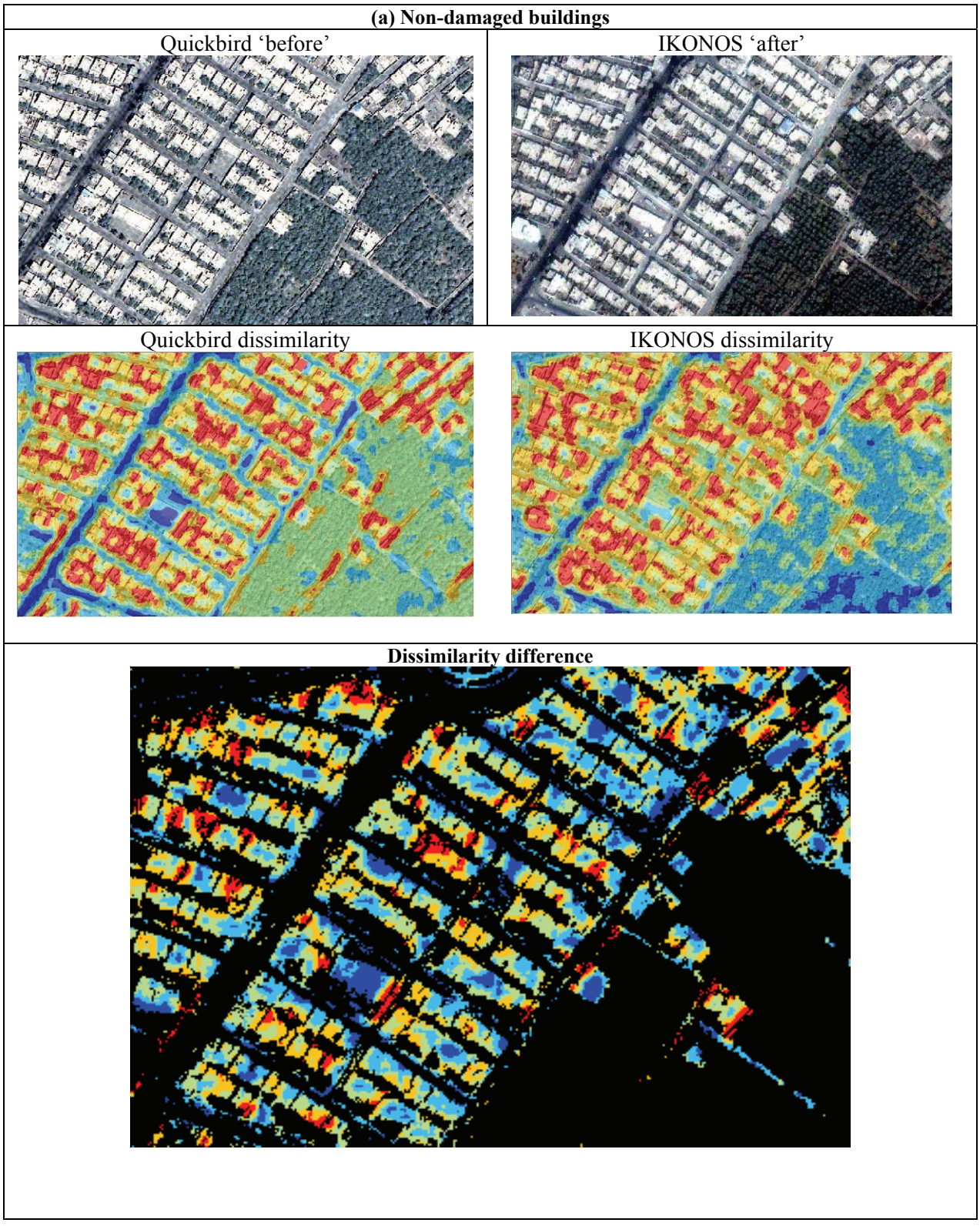

Figure 5-12 Visual Comparison Between Classified Dissimilarity and Difference Values for Neighborhoods with (a) No Damage, (b) Extreme Damage and (c) Limited Damage

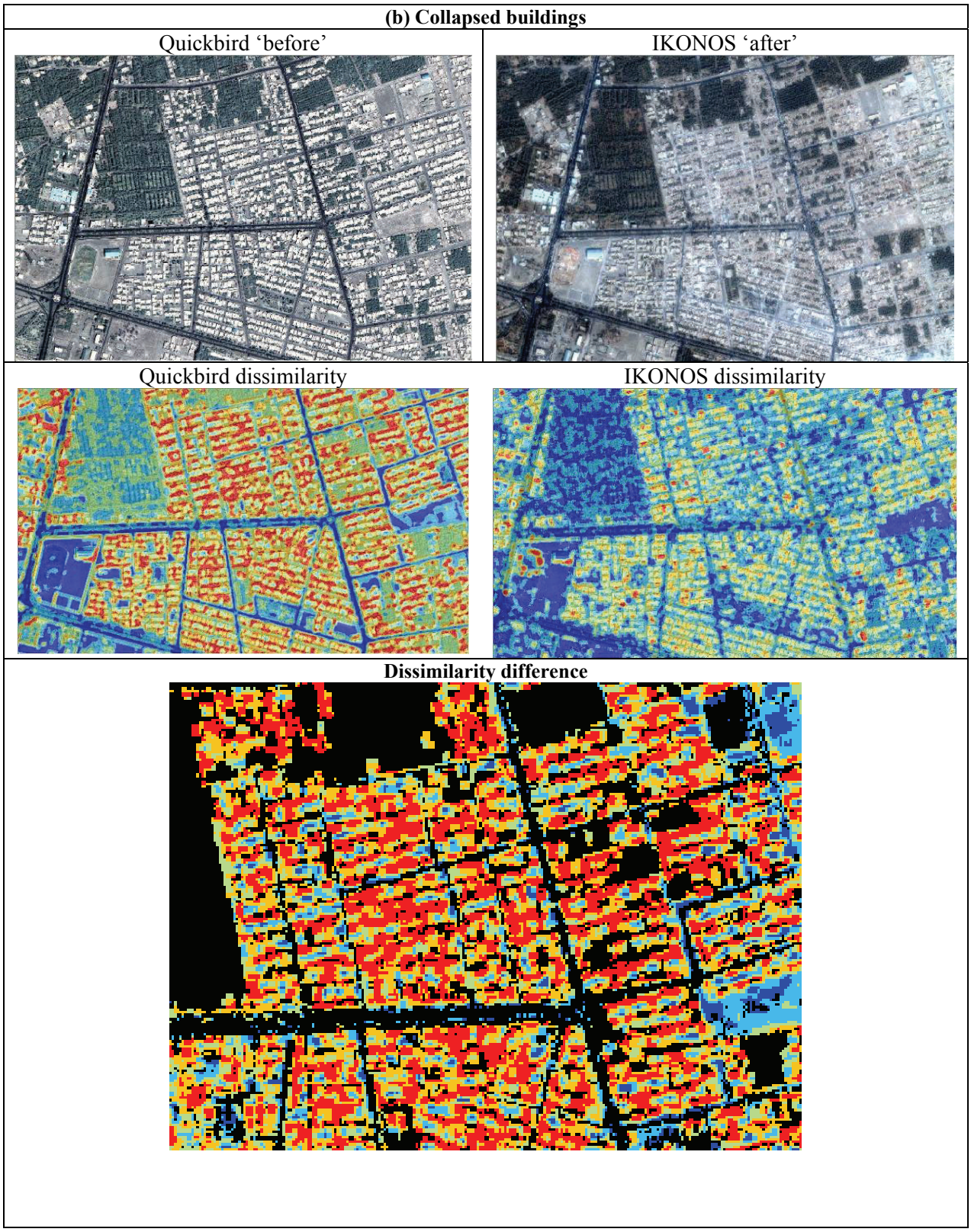

Figure 5-12 (cont.) Visual Comparison Between Classified Dissimilarity and Difference Values for Neighborhoods with (a) No Damage, (b) Extreme Damage and (c) Limited Damage

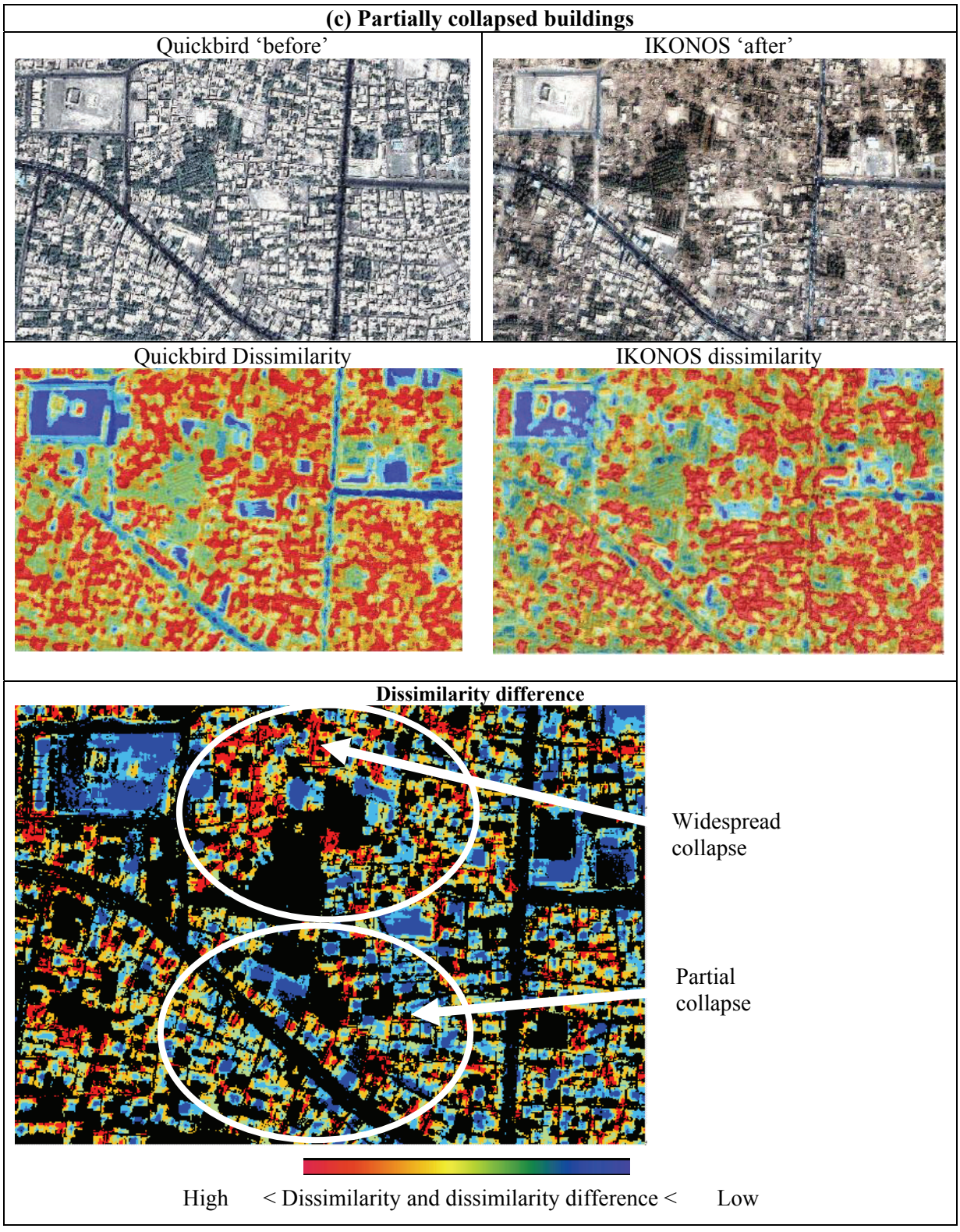

Figure 5-12 (cont.) Visual Comparison Between Classified Dissimilarity and Difference Values for Neighborhoods with (a) No Damage, (b) Extreme Damage and (c) Limited Damage

From the city-wide overview in figure 5-11b, within the classified *entropy* output, areas associated with heavy damage of buildings recording high entropy difference values (around 4-5) appear in red. Non-damaged areas are distinguished by low difference values in blue. Examining the city-wide classification of values the spatial distribution of these respective areas is apparent. High difference relating to a sizeable decrease in entropy occurs in the south-east of Bam and also in the north around Arg-E-Bam. Areas in the west generally have less entropy difference. As with the dissimilarity measure, using a filter of 25x25, the amplified difference within damaged neighborhoods is likely due to the variation between homogenous textured rubble and textural gradients between roofs, vegetation, roads etc.

Examining areas with extreme versus non-damage in more detail (figure 5-13), where buildings remain standing the entropy response is similar in the Quickbird and IKONOS scenes. However, there is a marked reduction in entropy within the 'after' IKONOS data where a prevalence of buildings collapsed.

The *correlation* results exhibit a similar pattern of response with an abrupt difference associated with building collapse (figure 5-11c). Urban areas generally show lower values of correlation compared with geology and vegetation. However, in the post-earthquake IKONOS scene (figure 5-14), the direction of change is opposite to the dissimilarity and entropy measures, with extreme damage recording higher correlation. Of the three texture measures, a visual comparison between damaged versus non-damaged correlation maps shows the most obvious distinction between heavily and lesser damaged neighborhoods. The *increase* in correlation accompanying collapse leads to *positive changes* in difference figures. For ease of comparison with the other texture measures, these areas of high positive difference were colored red in figure 5-14. Extreme damage is evident thought the south of Bam.

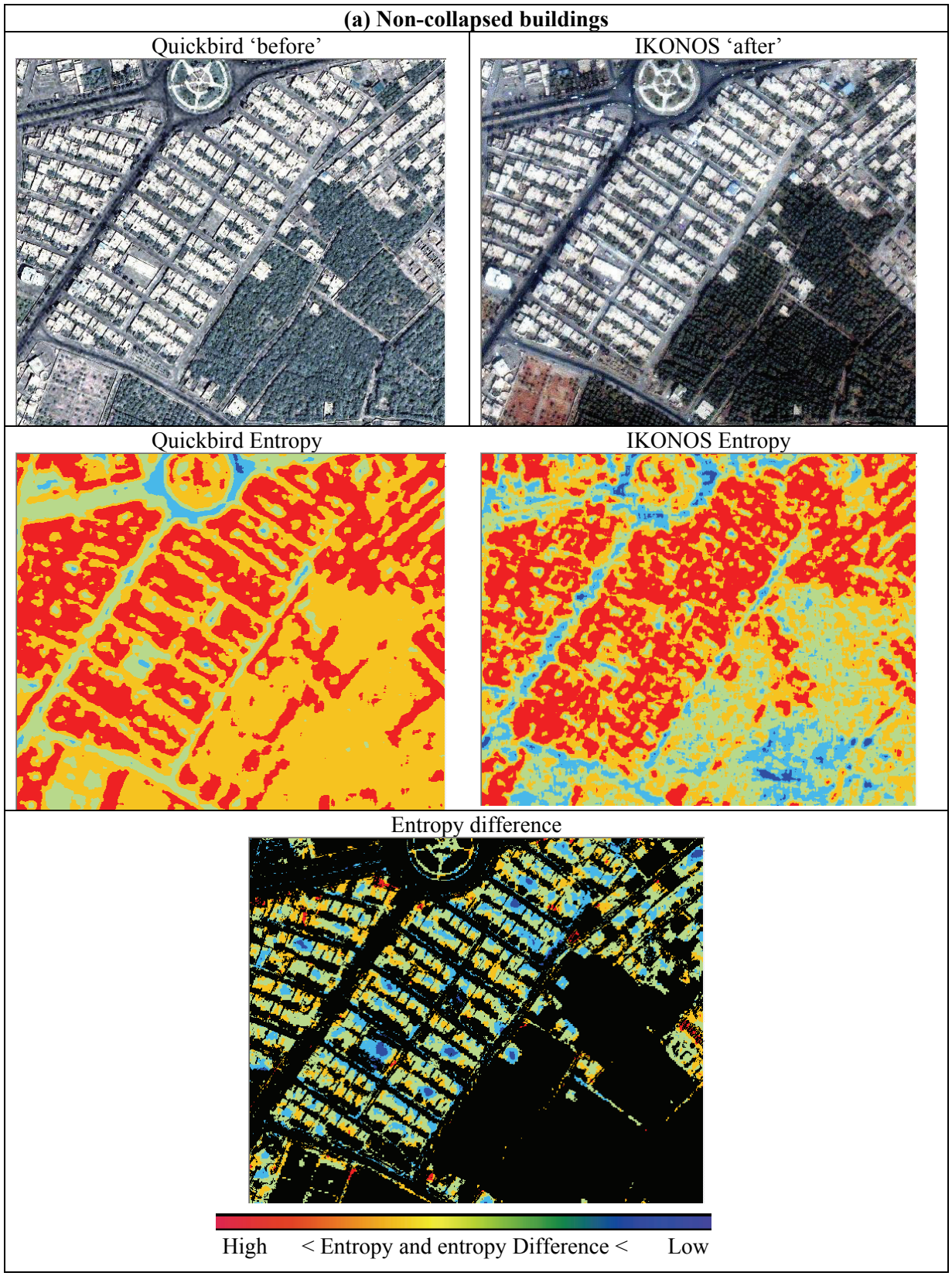

Figure 5-13 Visual Comparison Between Classified Entropy and Difference Values for Neighborhoods Recording (a) No Damage, and (b) Extreme Damage

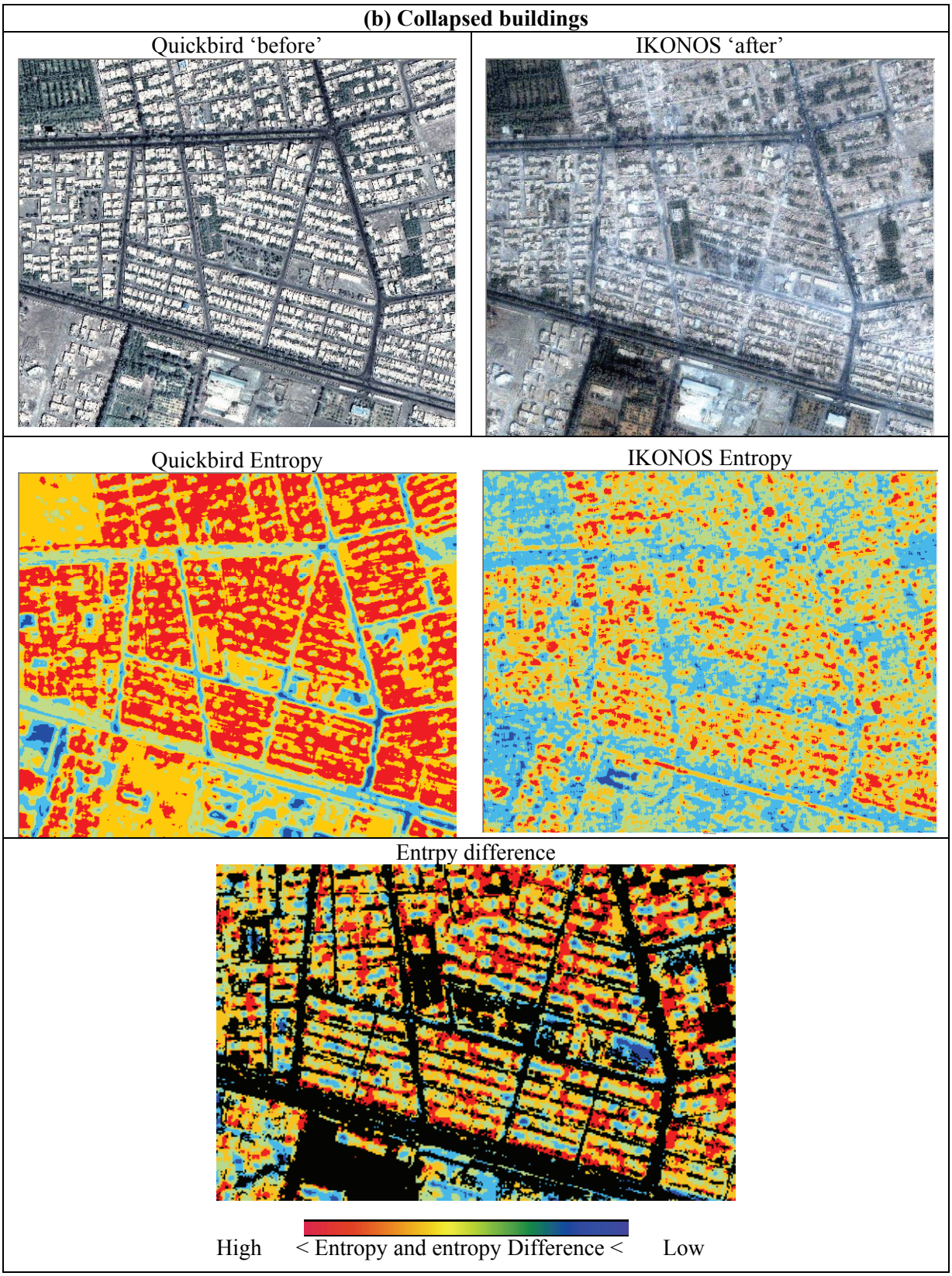

Figure 5-13 (cont.) Visual Comparison Between Classified Dissimilarity and Difference Values for Neighborhoods with (a) No Damage, (b) Extreme Damage and (c) Limited Damage

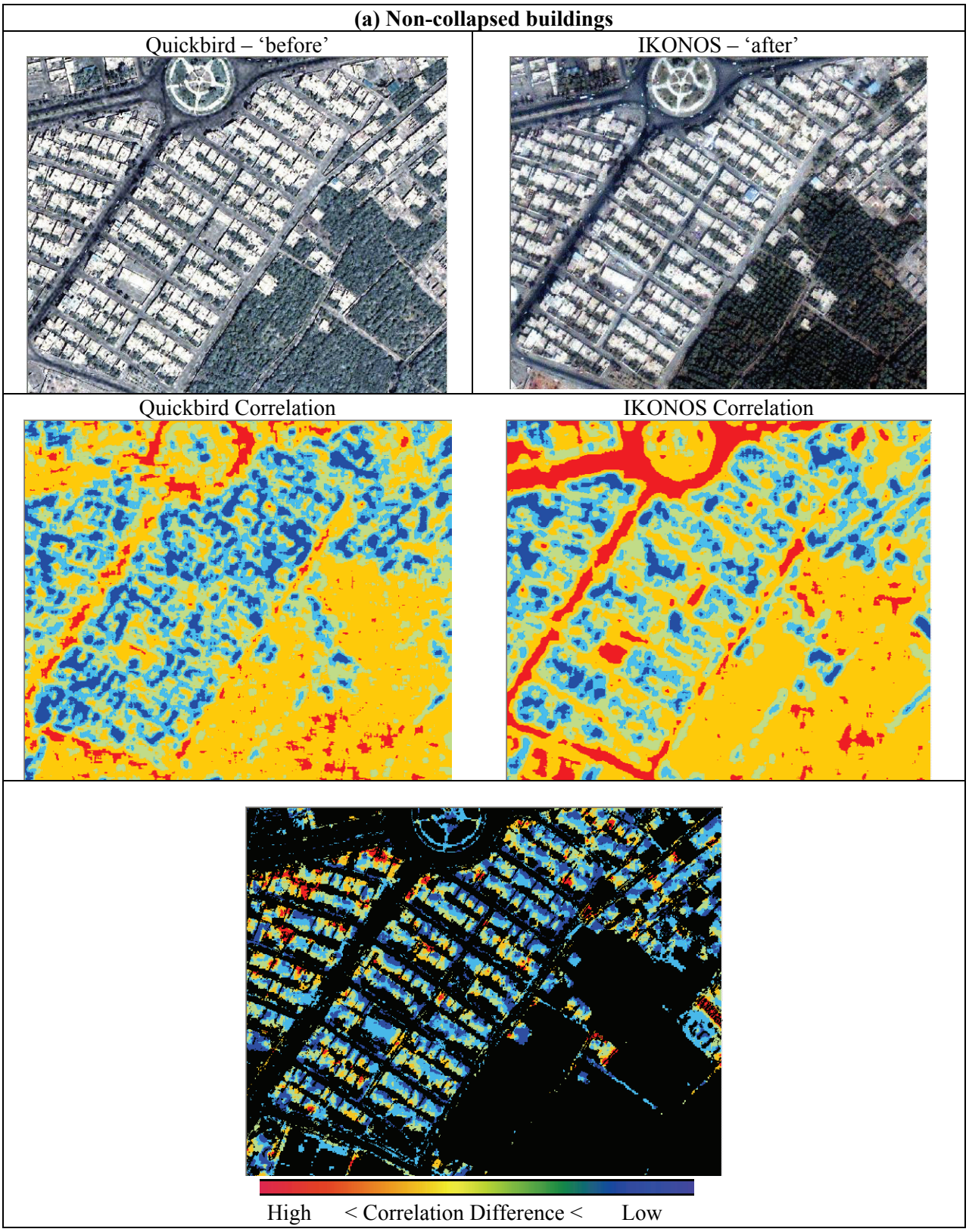

Figure 5-14 Difference in Correlation Measures Between Quickbird and IKONOS, in Areas Exhibiting a Concentration of (a) Collapsed versus (b) Non-Collapsed Buildings

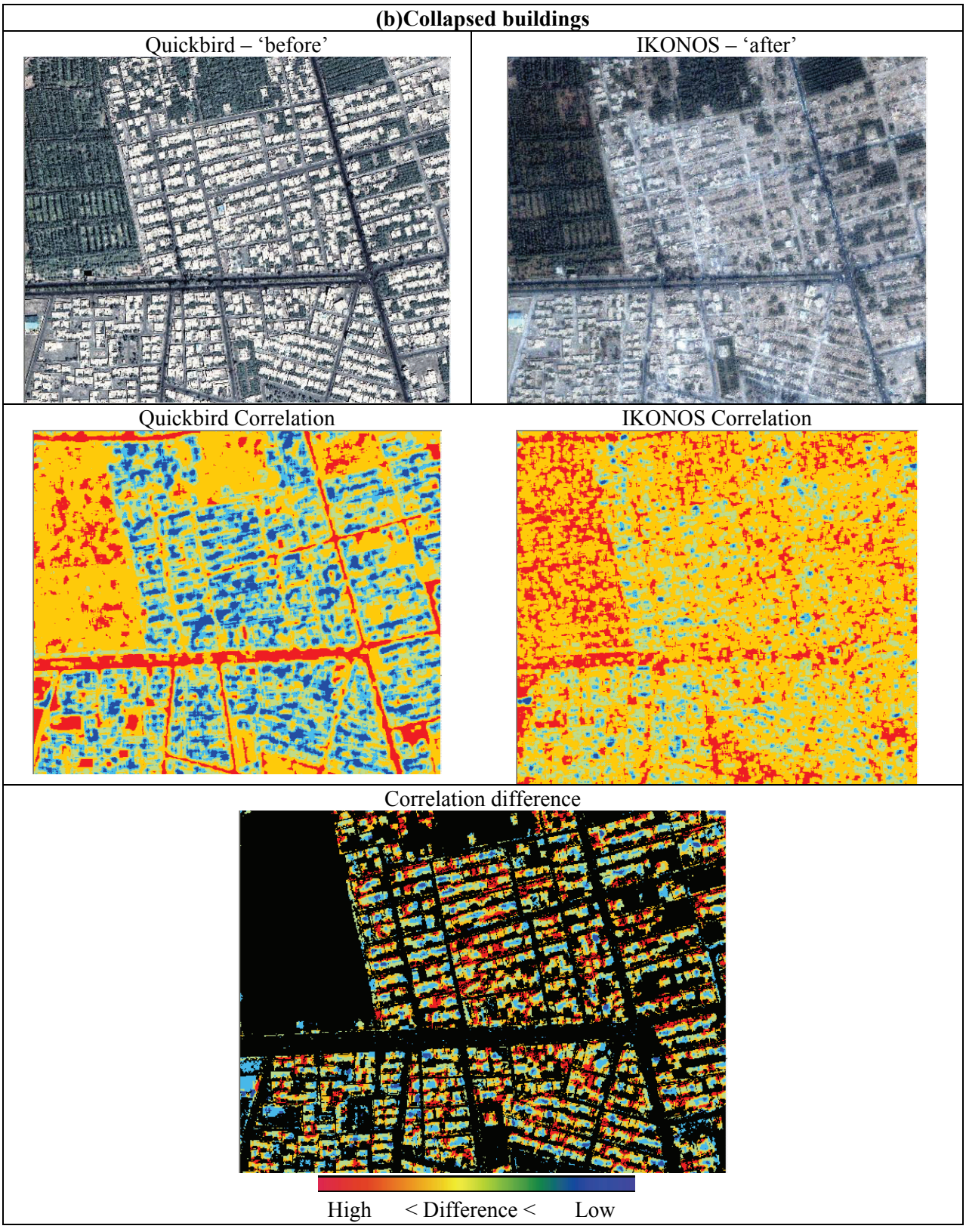

Figure 5-14 (cont) Difference in Correlation Measures Between Quickbird and IKONOS, in Areas Exhibiting a Concentration of (a) Collapsed versus (b) Non-Collapsed Buildings

From these visualizations it is possible to suggest that damaged buildings can be detected using each of the three texture measures. Table 5-4 summarizes the pattern of responses seen for dissimilarity, entropy and correlation.

Table 5-4 General Characteristics of Textural Measures Associated with Different Levels of Neighborhood-Scale Building Damage in Bam

Imagery	Neighborhoods with severe building damage	Neighborhoods with some building damage	Neighborhoods with limited/no building damage
(a) Dissimilarity			
'Before' value	Bright	Bright	Bright
'After value	Dark	Mid	Bright
Difference value	Large negative	Medium negative	Small negative
Classification color	Red	Mixed	Blue
(b) Entropy			
'Before' value	Bright	Bright	Bright
'After value	Dark	Bright	Bright
Difference value	Large negative	Medium/large negative	Small negative
Classification color	Red	Mixed	Blue
(c) Correlation			
'Before' value	Dark	Dark	Dark
'After value	Bright	Mid	Dark
Difference value	Large positive	Medium positive	Small positive
Classification color	Red	Mixed	Blue

5.5 Damage Map and Validation

At this time it is difficult to ascertain which texture measure is the most useful for damage detection as they all give relatively similar outputs. To examine performance further, a validation dataset was employed. From the results above, the hypothesis is proposed that the chaotic piles of rubble associated with collapsed buildings will exhibit poorly-defined edge structures and less defined textural variability, which in turn produce a statistically measurable difference in textural

indicators. To test this hypothesis, a quantitative validation was completed using the dataset compiled by Yamazaki *et al.* (2004b).

The classes pertaining to heavy damage difference were extracted for each of the texture measures. The frequency occurrence of damaged pixels (i.e. the positive change difference classes) was summarized into 120m interval grids, and visualized in categories of standard deviation about the image-wide mean to emphasize the most concentrated areas of damage. For comparison, the damage validation data from Yamazaki *et al.* (2004) was defined in the same way.

In figure 5-15, the highest areas of damage recorded by the texture measures and validation dataset are shown in red, followed by heavy damage in orange, and moderate damage in yellow. All three texture measures generally perform well when identifying extreme damage, locating hard-hit neighborhoods in south eastern and northern Bam. However, some differences can be seen between the texture measures. For instance, the entropy map records few false positives in western of Bam, whereas dissimilarity and correlation map limited damage here. The output was also compared visually with the USAID damage map, although it was not possible to summarize the USAID information using the grid squares. The similarity in damage concentration within the north east and south east of Bam is apparent.

For the three texture measures, calculating the offset between the damage map and validation results produces a similar pattern of agreement. Class values were assigned to the standard deviation measures from figure 5-16, where class 1 = yellow, class 2 = orange and class 3 = red. The difference was calculated between these classes for the texture and validation results. The most misclassification is seen to occur in the north-east of the city, underestimating the amount of damage by up to three classes. This is likely due to the mixture of damaged versus standing structures, which may be better classified at a per-pixel rather than neighborhood scale. Also the damage state at Arg-E-Bam has been overestimated. This is because this is treated as a single building by Yamazaki *et al.* (2004b). Some overestimation of damage is also seen in the South East of Bam, which may be linked to the increased difference due to haze/cloud.

Overall, it is difficult to identify the best performing textural measure from *visual* inspection. Comparatively, the entropy measure appears to have the least misclassification in the West, but has enhanced misclassification in the East. Dissimilarity has misclassification both in the West and the East. The correlation measure has less extreme misclassification in the East. To formalize the relative performance of the respective measures a *statistical* and *graphical* comparison between the texture and validation datasets was conducted.

Considering the frequency plot in figure 5-17, generally, the three measures produce similar results, with a high concentration of correctly classified zones in all cases. The dissimilarity measure has a slightly higher frequency correctly classified zones. However if the statistics are weighted so that the more serious the misclassification the higher the penalty (table 5-5), the correlation measure performs best.

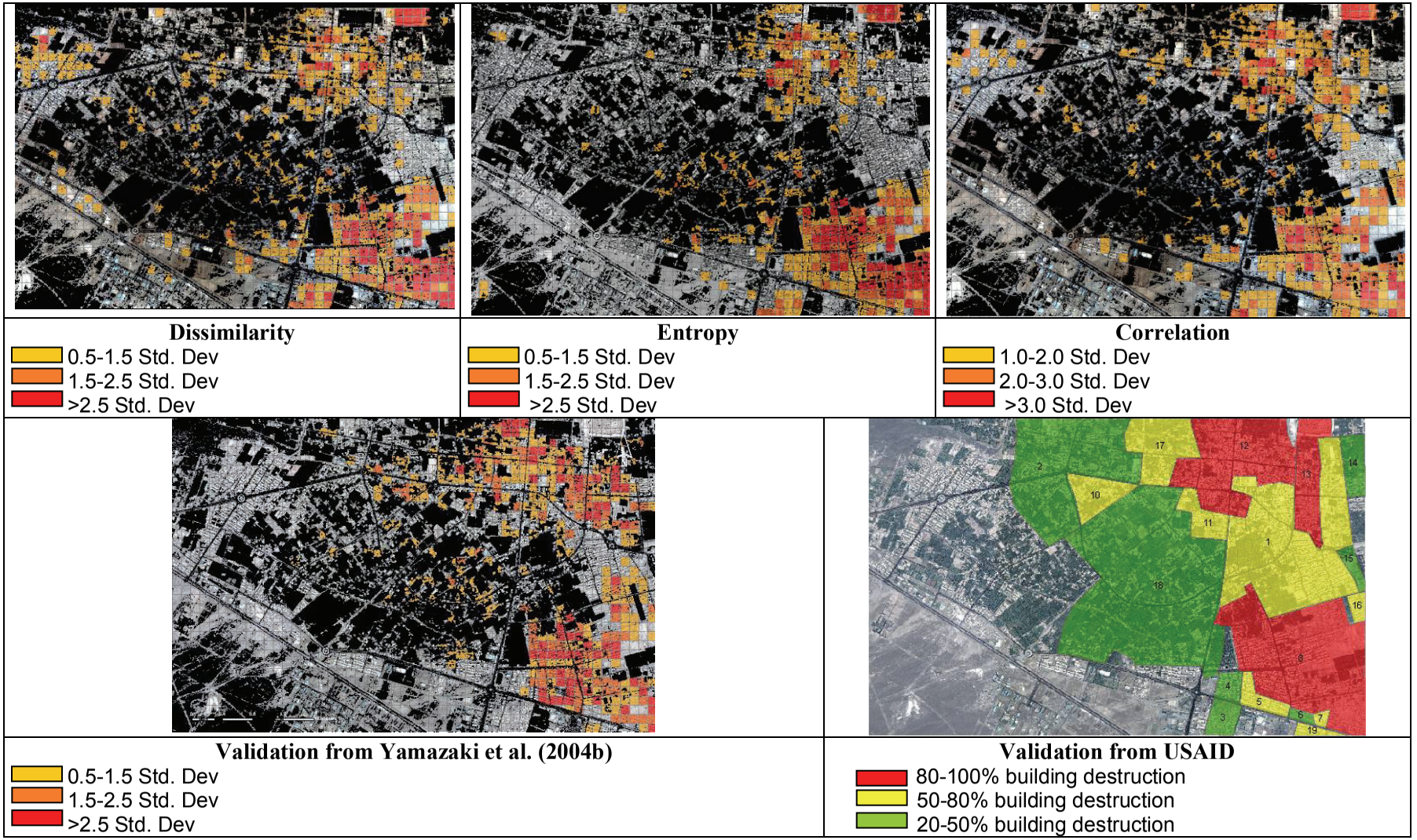

Figure 5-15 Classified Difference in Correlation Texture Measures, with the Frequency of Damage Pixels Summarized into 120m Zones and Visualized by Standard Deviation for (a) Dissimilarity; (b) Entropy and (c) Correlation. Validation Datasets are shown for (d) Yamazaki et al. (2004b) Resampled into the 120m Grids and (e) USAID

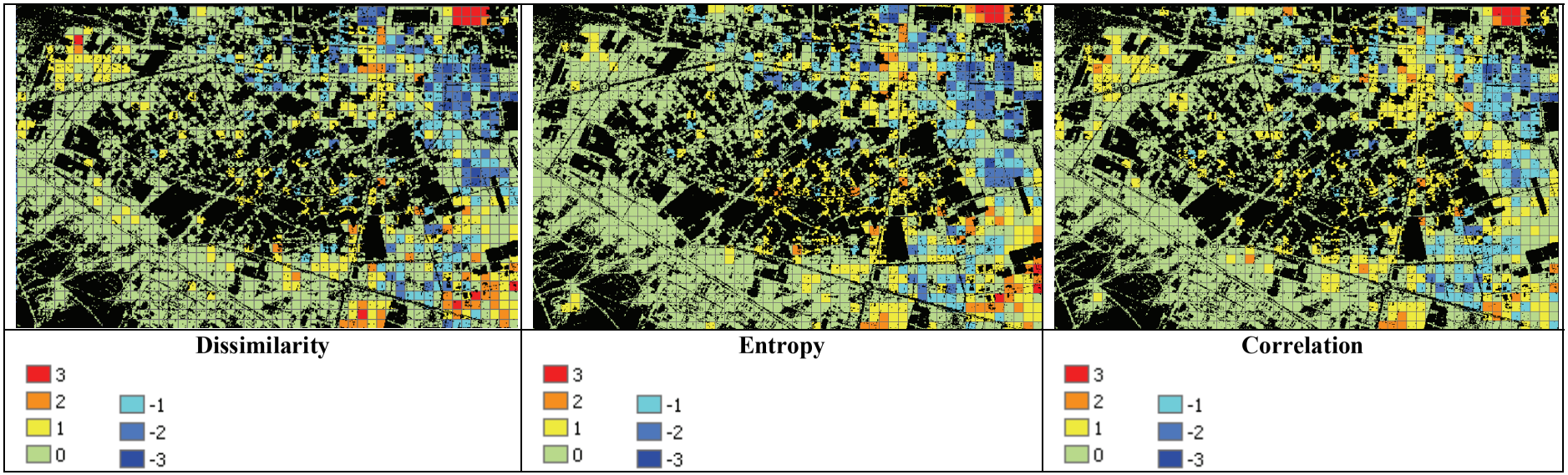

Figure 5-16 Difference in Damage Classes Between Texture Measures and Validation Dataset from Yamazaki et al. (2004b). Class Values were Assigned to the Standard Deviation Measures from Figure 5-15, Where Class 1 = Yellow, Class 2 = Orange and Class 3 = Red. The Difference was then Calculated Between these Classes for the Texture and Validation Datasets, with Results Falling in the Range -3 < Difference < 3.

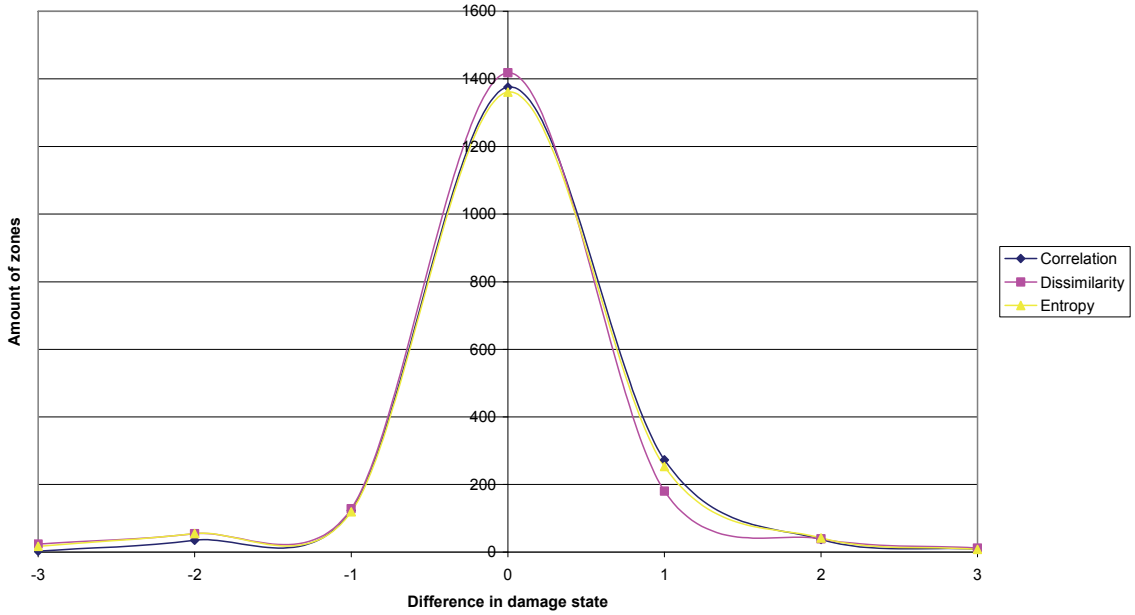

Figure 5-17 Frequency of Difference Between Texture and Validation Results, Where Class Values were Assigned to the Standard Deviation Measures from Figure 5-15, with Class 1 = Yellow, Class 2 = Orange and Class 3 = Red.

Table 5-5a Statistical Difference Between Texture and Validation Results

	Difference in SD class between texture value and validation datasets						
	-3	**-2**	**-1**	**0**	**1**	**2**	**3**
Correlation	3	35	123	1376	273	37	8
Dissimilarity	24	54	128	**1418**	180	39	12
Entropy	17	55	119	1361	253	42	8

Table 5-5b Weighted Difference Between Texture and Validation Results

	Weighted sum							
	-3 (x 3)	**-2 (x 2)**	**-1 (x 1)**	**0 (x 0)**	**1 (x 1)**	**2 (x 2)**	**3 (x 3)**	**Sum**
Correlation	9	70	123	0	273	74	24	**573**
Dissimilarity	72	108	128	0	180	78	36	602
Entropy	51	110	119	0	253	84	24	641

SECTION 6:
METHOD 3: EDGE DETECTION

The flow diagram in figure 1-2 outlines Method 3: edge detection-based comparison, for detecting the extent and severity of urban damage in Bam at a pixel-scale. It differs from Method 1: Spectral comparison and Method 2: textural comparison, because damage is assessed in terms of neighborhood-scale changes in the density of *edge features* between the two input images. The working hypothesis is that that collapsed buildings show fewer edges in the post-earthquake image, as distinct building boundaries are replaced by an indistinct and chaotic pattern of debris. Again, the comparison of Quickbird pre-earthquake imagery with the IKONOS post-earthquake data will accentuate non-disaster-related sources of difference between the images. This method also provides scope for investigating if the use of edge-based measures reduces inter-sensor differences between the images that affect the performance of spectrally-based methodologies. Processing steps taken to minimize these effects are highlighted in figure 1-2.

A quantitative edge-based damage assessment methodology was explored, comprising the following analytical steps. These are numbered in sequence, continuing on from step 7, the last of the pre-processing procedures described in Section 1.3.2:

(8) Gaussian filtering to remove noise from the input images;

(9) Edge detection filtering was applied to retrieve sharp gradient information such as building edges. It is hypothesized that the frequency of these edge pixels will change after an earthquake event and building collapse. Several different filters were examined to identify the optimum operator

(10) Classification of the edge images using a thresholding technique, to highlight damaged versus non damaged regions;

(11) Masking the classified images to focus on roof structures and remove non-disaster related sources of change, such as vegetation and roads;

(12) Extraction of edges was performed

(13) The frequency of edges within neighborhood scale zones was summarized using statistical measures;

(14) The difference and percentage edge change were calculated between the 'before' and 'after' results, as measures of damage within each of the zones employed for validation;

Validation of the classification results was conducted using area-based damage observations made by Yamazaki *et al.* (2004b) and USAID.

6.1 Gaussian Filtering

A Gaussian low pass filter was applied to the input pre- and post-earthquake images, in order to smooth out unwanted noise as a potential source of error. The Gaussian filter is a 2-D smoothing operator. It outputs a `weighted average' of each pixel's neighborhood, with the average weighted more towards the value of the central pixels, preserving edges better than a similarly sized mean filter (HIPR 2003). A range of different filter sizes were considered, with a 7x7 operator

achieving the selected because this is seen to smooth the IKONOS image but still keep enough detail in the Quickbird image (figure 6-1).

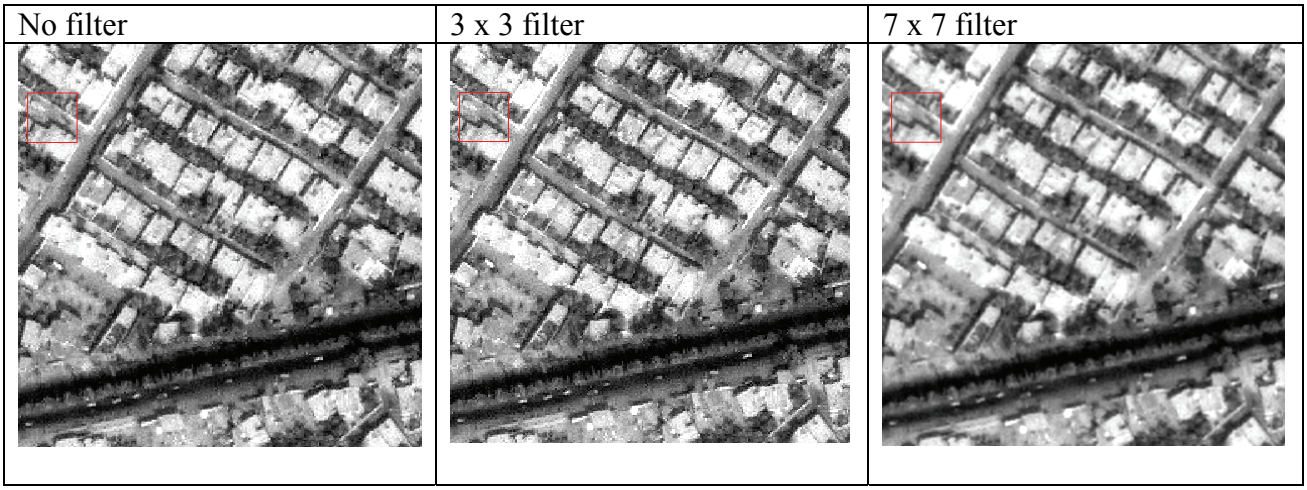

Figure 6-1 Comparison of Gaussian Filter Sizes Using a Non-Damaged Neighborhood in the IKONOS 'After' Image. A 7x7 Filter Size was Selected for the Analysis.

6.2 Edge Detection Filtering

Several different edge detection routines were examined in order to identify the optimum operator for distinguishing building collapse. Sobel and Roberts edge detection filters were investigated. As illustrated in figure 6-2, the Roberts filter is a simple set of 2 x 2 convolution filters (90º apart) which detects high spatial frequency shifts, pertaining to edges that run 45º.

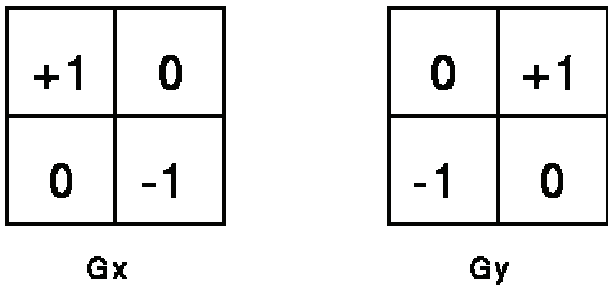

Figure 6-2 Roberts Filters (after HIPR 2003)

The Sobel filter is similar to the Roberts filter. However, it has a larger convolution filter. It is again an edge detection procedure which uses two convolution filters shifted 90 º from each other. This helps to pick up vertical and horizontally running edges. The Sobel operator performs a 2-D spatial gradient measurement on an image and so emphasizes regions of high spatial frequency that correspond to edges. Typically it is used to find the approximate absolute gradient magnitude at each point in an input grayscale image (HIPR 2003).

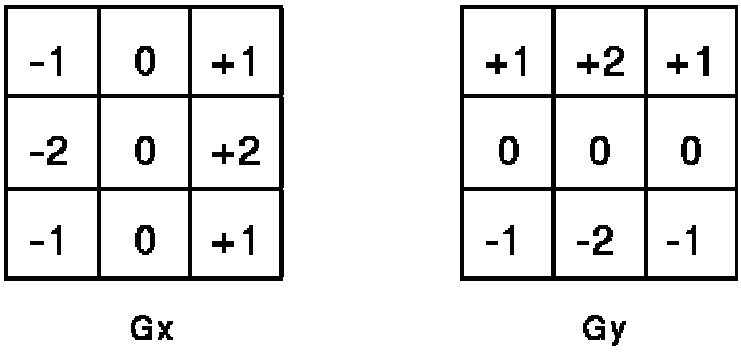

Figure 6-3 Sobel Convolution Filters (after HIPR 2003)

The Sobel operator (figure 6-3) is slower to compute than the Roberts Cross operator, but its larger convolution kernel smoothes the input image to a greater extent and so makes the operator less sensitive to noise. However, Gaussian smoothing operation has already been undertaken on the image, which may negate this process.

In order to select the preferred operator, the outputs from both of these edge detection filters were examined visually. Their performance on each color band within the pan-sharpened image was examined in turn, but since there was no major difference in the responses obtained, only the red band of each image was carried forwards to subsequent stages of the methodology.

Visually inspecting the outputs in figure 6-4, the output from the two operators are fairly similar, although Roberts output is characterized by thinner lines than for Sobel. For both Roberts and Sobel, the inclusion of a Gaussian filter influences the distinctiveness of edges, which appear considerably brighter in the output. As the Roberts filter is also faster, this was taken to be the preferred edge detection filter. Accordingly, a processing sequence of the Gaussian followed by the Roberts filter was implemented on red bands of the pre- and post-earthquake scenes.

6.3 Classification

A manually-based classification was used to extract edge pixels from the filtered images. Examining statistical characteristics of the edge pixels, they generally recorded values >40DN in the case of Quickbird, and >30DN in the case of IKONOS. A band threshold was initiated on the two images, leading to the binary classification illustrated in figure 6-5.

Figure 6-5a shows the ‘before and ‘after’ classification output for the neighborhood in western Bam that sustained minimal damage. The responses from buildings and the roundabout in the area are seen to be reasonably similar, although both have slightly different responses due to car positions on the road. Comparing these outputs with a severely damaged neighborhood in southern Bam (figure 6-5b), a significantly different pattern of response is noted. While edged are prevalent in the ‘before; image, few edge pixels are evident in the IKONOS ‘after’ image. Many of the large walls of the neighborhood have collapsed, leaving only small parts of wall and well defined rubble pieces to be picked up by the filter.

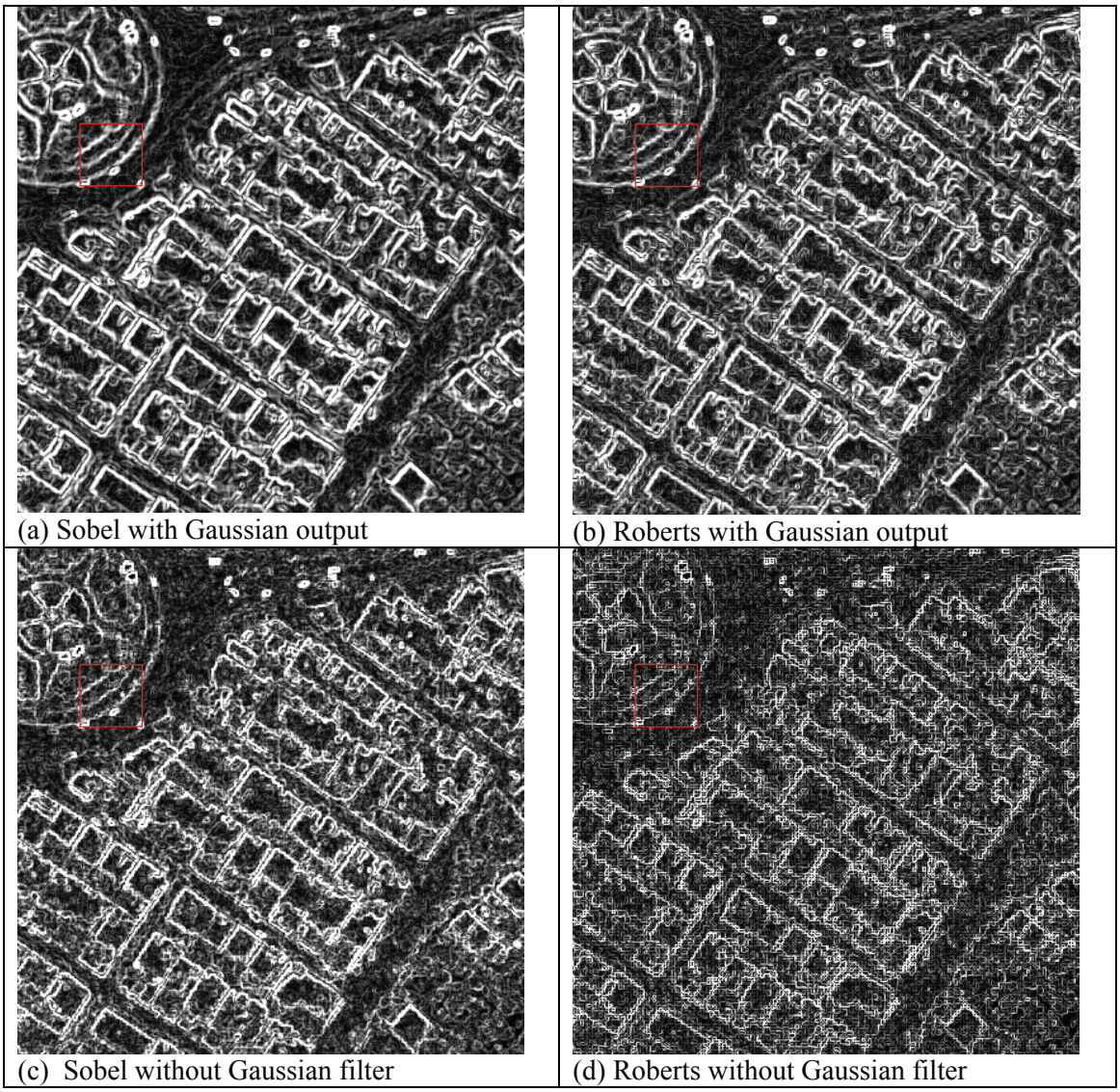

Figure 6-4 Comparison of Edge-Detection Outputs for A Non-Damaged Neighborhood in West Bam within the Post-Earthquake IKONOS Image of Bam. a) Sobel Filter with Gaussian Filtered Image; b) Roberts Filter with Gaussian Filtered Image; c) Sobel Output Without Gaussian Filter; and D) Roberts Output Without Gaussian Filter

6.4 Masking

The classification outputs were masked using the urban mask developed from Methodology 1. This mask is designed to highlight the urban built environment by eliminating non-urban regions including vegetation and roads, and mitigating the effects of non-damage-related sources of change between the Quickbird and IKONOS images, such as shadows.

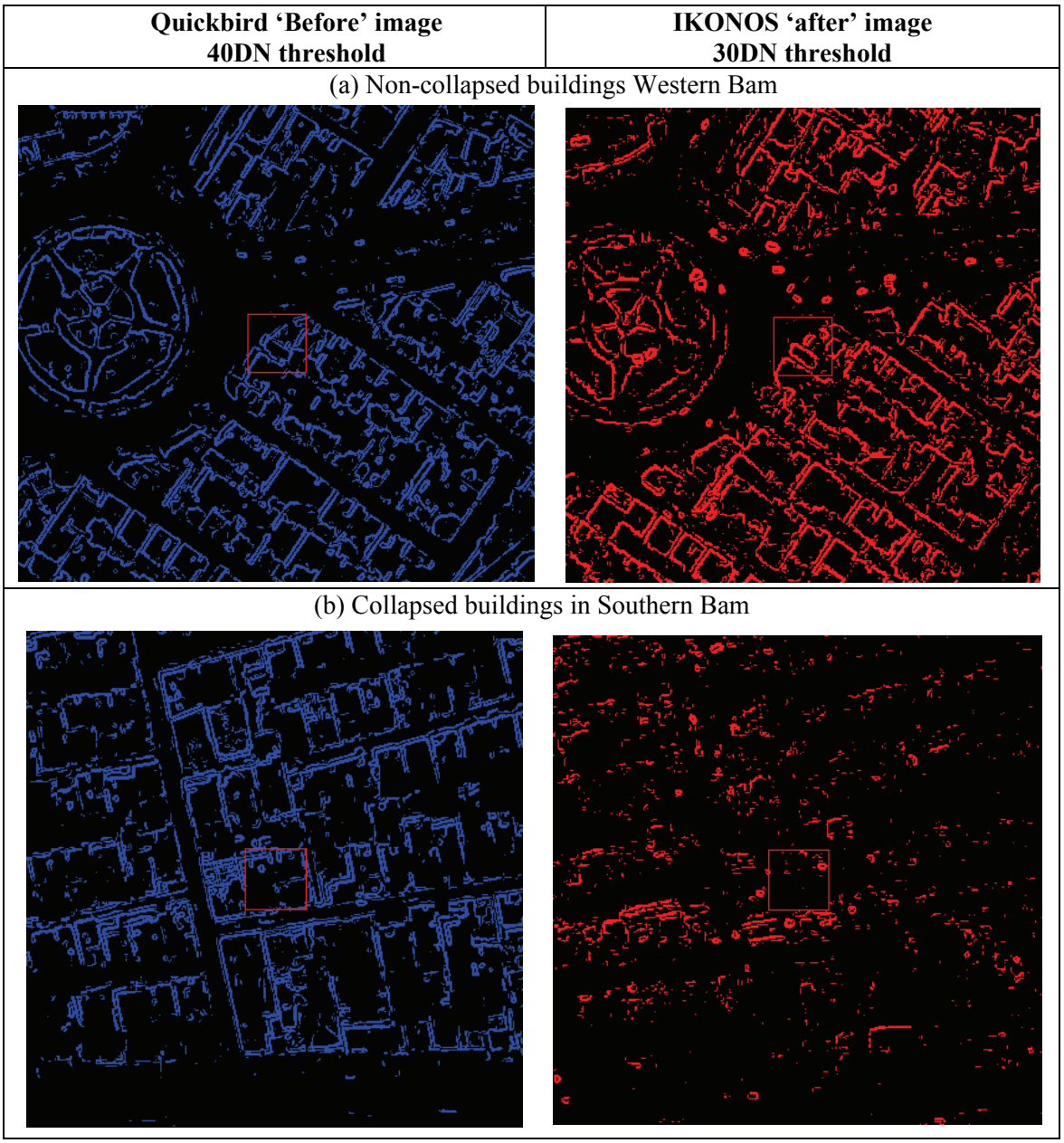

Figure 6-5 Comparison of Gaussian/Roberts Edge Detection Output within (a) Western Neighborhoods of Bam that Experienced Minimal Damage, and (b) Concentrated Damage in Southern Bam

6.5 Edge Class Extraction and Frequency Calculation

The images were reclassified into a layer of edge pixels only, with background values appearing as No-Data. The pixels were then summarized by zones using the city-wide GIS validation zones from Yamazaki *et al.* (2004b). The frequency of edge pixels was computed per city zone in the IKONOS and Quickbird images.

6.6 Difference and Percentage Edge Change

To examine the change in edge pixel frequency between the pre- and post-earthquake images, attribute tables recording the frequency per zone were used to compute the difference (before-after). As an absolute measure of the number of edge pixels, this index is subject to scale effects, whereby edge pixel frequency is correlated with the size of the city zone over which the count is being performed (see also Section 3). To minimize scale issues, a standardized measure of the percent change in edge pixels within the urban areas of each city zone was also calculated. A damage map was prepared, expressing the percentage building collapse as four natural breaks classes.

To assess methodology performance, the damage map was compared with zone-based validation data from Yamazaki *et al.* (2004b) and USAID (2004).

SECTION 7:
RESULTS 3: EDGE DETECTION

7.1 Edge Frequency Calculation

Figure 7-1 shows the city-wide occurrence of edges within the before and after imagery. There is a visible reduction in the amount of edge pixels visible in heavily damaged neighborhoods within south-east, central and northern Bam. This preliminary result reinforces the hypothesis that damage may be able to be mapped by the difference in edge pixels between the two inputs.

7.2 Difference and Percentage Edge Change

Having extracted the frequency of edge pixels within each image, the number of edges per city zone was calculated, and the difference in edge pixels between the 'before' and 'after' images computed. Table 7-1 shows the minimum, maximum and mean frequency of edge pixels found within urban areas of the two images. Overall, the IKONOS post-earthquake image is found to have considerably fewer edge pixels than the Quickbird pre-earthquake image.

From figure 7-2, this general trend is mirrored across all zones. However, importantly the margin of difference between the frequency of edge pixels varies considerably, with some zones recording similar magnitudes and others widely differing amounts. There is no obvious relationship between this margin of difference and the overarching size of the zone, since the offset (y-axis) between the IKONOS and Quickbird data series varies widely as the zone size (x-axis) increases.

These difference statistics were mapped to show the spatial distribution of occurrence and percentage occurrence per city zone. The zones were classified into 4 classes using Jenks' natural breaks (for details, see Section 3).

Examining figure 7-3a the greatest difference in frequency of edges is seen in the south-east of Bam, around zones 17, 20, 21, 26 and 36. Substantial changes in edge frequency are also recorded in the north of Bam, around zone 2. Negligible change was detected in the north-west and the west of the city. Visually, this general pattern of occurrence is consistent with the validation dataset (figure 7-3c), although the frequency/damage is markedly higher in central regions such as zones 10, 15 and 18, and lower in zones 25 and 37.

Table 7-1 Minimum, Max and Mean Amount of Edge Pixels within Bam City Zones

	QB	IKONOS	Difference
min	17,076	4,972	7,007
max	231,064	127,886	133,445
mean	107,342	52,686	54,656

a) Quickbird pre-earthquake edge detection image

b) IKONOS post-earthquake edge detection image

Figure 7-1 Scene Wide Edge Detection Image Derived from A) Quickbird and B) IKONOS Images. Areas with a Clear Reduction in Edge Frequency are Annotated.

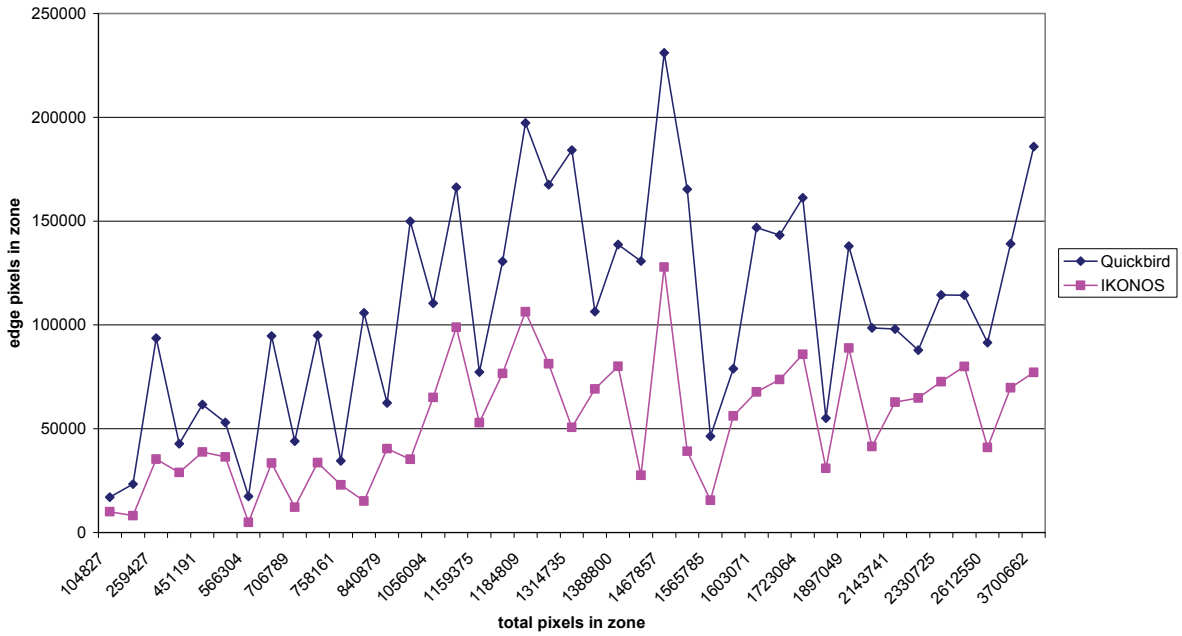

Figure 7-2 Graphical Representation of the Relationship Between Edge Pixel Frequency and the Total Number of Pixels in Each Zone within the IKONOS and Quickbird Images

Figure 7-3b shows the percentage reduction in edge pixels per urban zone. Compared with the frequency results, a major reduction in edge pixels is once again identified within the south east, with up to 86% reduction in edge pixels within the urban area, inferring very heavy building collapse. The distribution of damage is seen to differ somewhat in other areas, once zone size is taken into consideration. For example, central Bam is now also shown to record a major reduction in edge pixel occurrence. In the heavily damaged north, the percentage reduction is considerably lower.

7.3 Validation

From visual comparison with the validation data (figure 7-3c), the percentage results appear to perform better than the frequency data in terms of absolute agreement between the zones and degree of disagreement. As such, these are carried forwards for further evaluation.

In order to understand the occurrence of high and limited agreement, the graphical representation in figure 7-4 quantifies the offset between zones-based damage determined from the validation data and edge pixel percentages. 17 zones agree. Most misclassifications are one class away from the actual result, with positive and negative disagreement distributed fairly evenly. There are very few cases where disagreement >1.

Figure 7-5 shows the spatial distribution of agreement. Southern Bam has the most positive misclassifications where change is overestimated. The north of Bam has the most negative misclassification where the edge-based approach underestimates change.

(a) Edge difference frequency

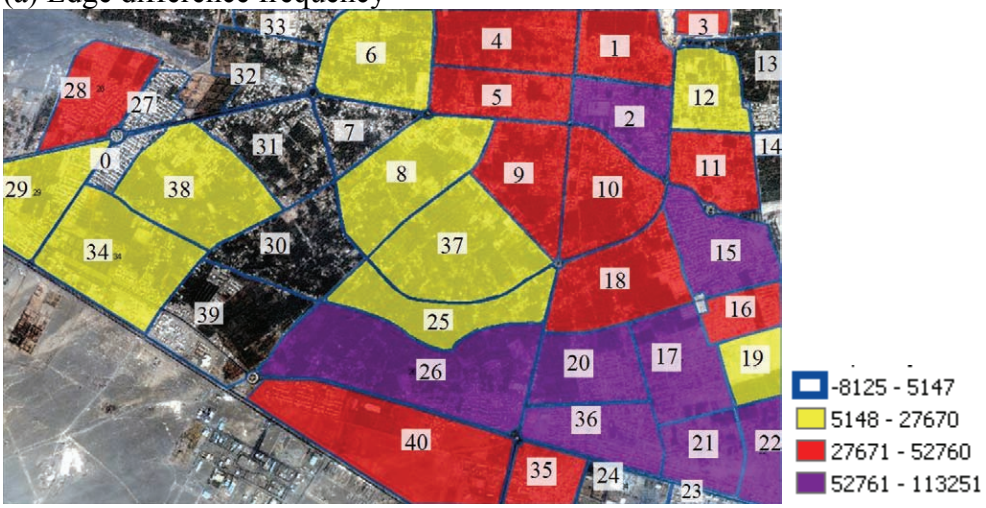

(b) Percentage change in urban edges within each zone

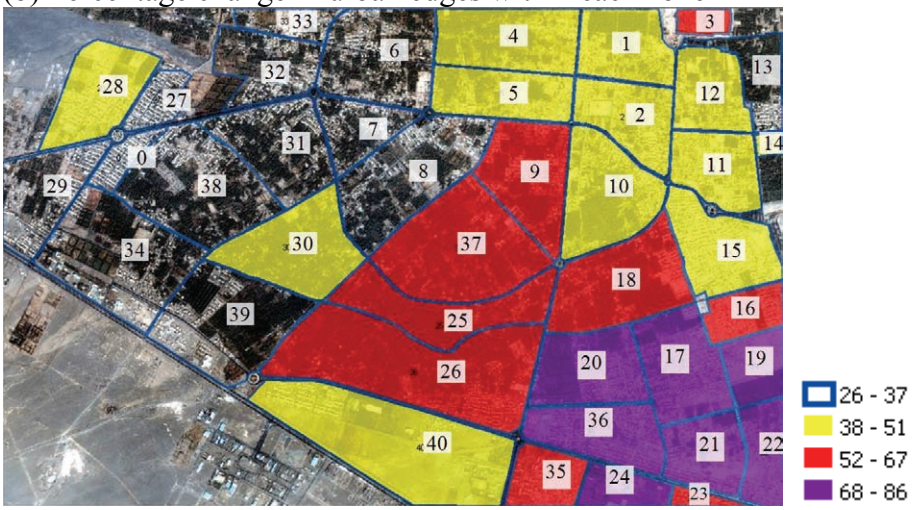

(c) Validation data

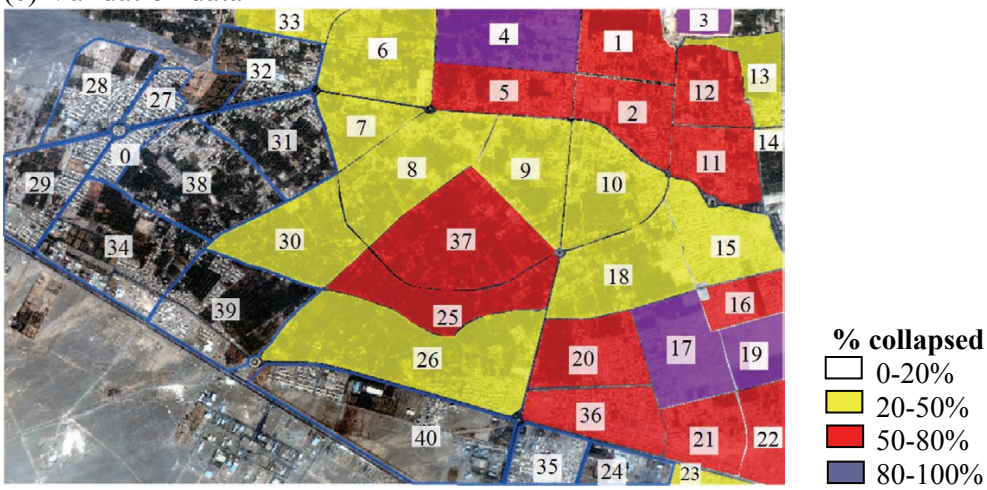

Figure 7-3 Zone-Based Difference in Edge Pixel Occurrence Between the Quickbird and IKONOS Displayed as Natural Breaks, Expressed as (a) Frequency and (b) Percentage of Urban Zone Area. (c) Shows the Validation Dataset Developed by Yamazaki et al. (2004b).

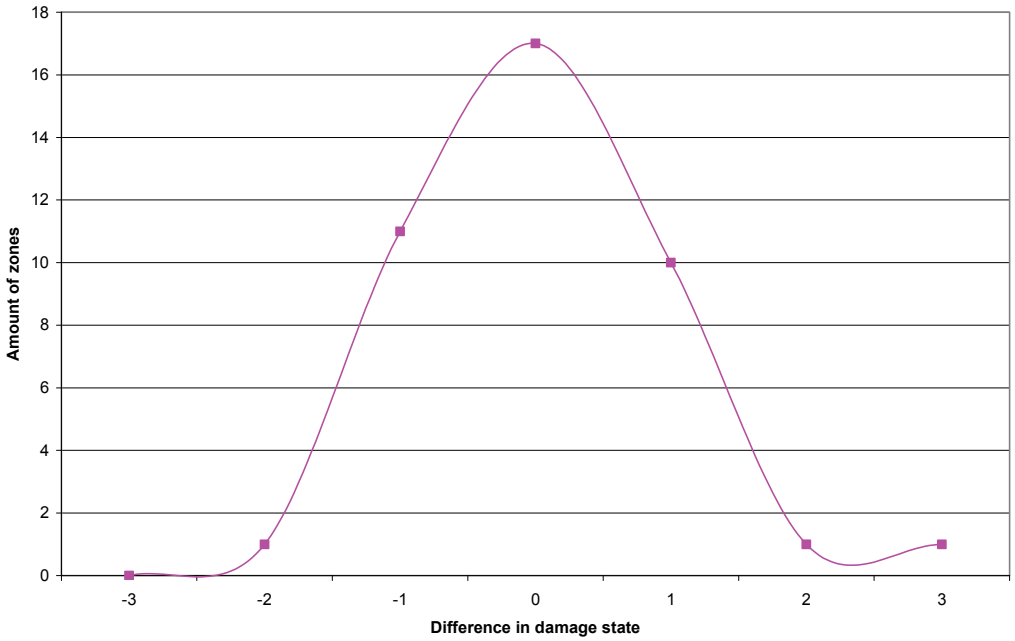

Figure 7-4 Difference in Zone Classification Between the Percentage Reduction in Edges and Validation Datasets

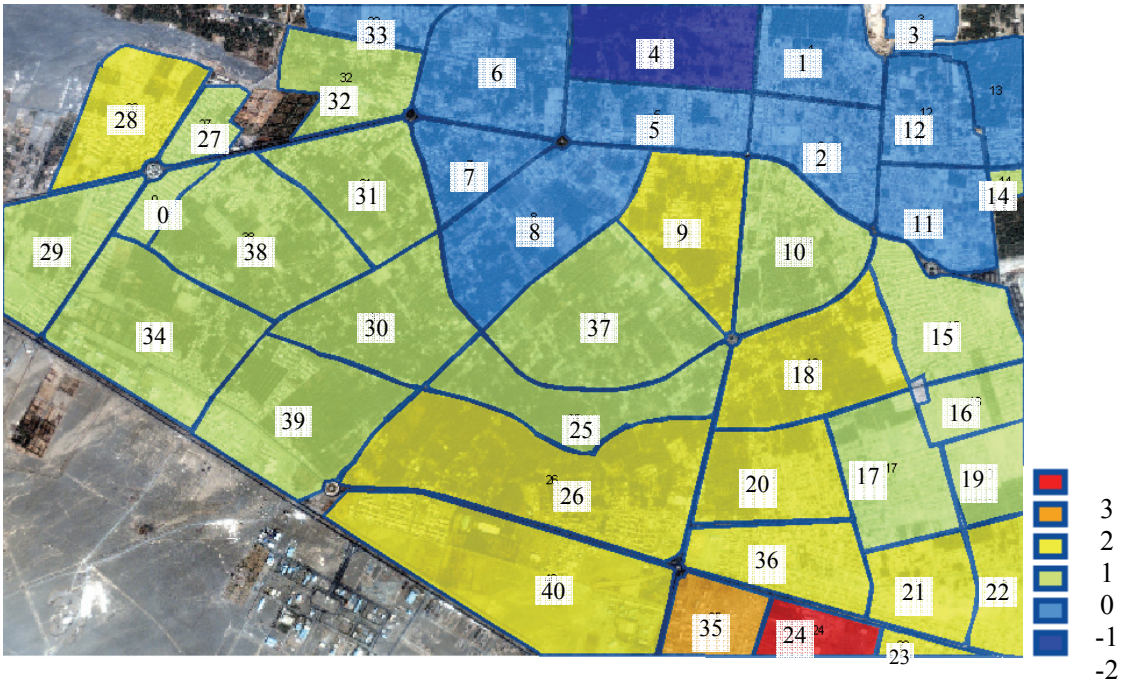

Figure 7-5 Difference in Zone Classification Between Edge Detection Classification and Validation Datasets

Magnifying the pattern of change observed in South of Bam (figure 7-6), where the edge-based approach tends to overestimate change, the decrease in edge pixels due to building collapse is

very evident. Remaining edge pixels correspond with remaining buildings, and also standing walls which have a sharp gradient change with the surrounding land. However, the reduced occurrence of edges in the IKONOS image does not seem to be purely a function of building collapse. From figure 7-6c, the spectral contrast in this area of the IKONOS image is affected by atmospheric haze. In order to understand the degree of influence that this exerts, further work is needed to investigate if an alternative haze-free IKONOS image records a similar response.

a) Quickbird pre-earthquake image overlaid with edge detection output (in red)

b) IKONOS post-earthquake image overlaid with edge detection output (in red)

(c) Potential haze-effects in southern neighborhoods affecting the 'after' imagery

Figure 7-6 Overestimation of Damage in Southern Bam Using the Edge Detection Methodology. This may be Due to Haze Effects within the IKONOS 'After' Imagery Suppressing Edges.

Within northern Bam, damage is underestimated in some zones. For instance, Area 1 is one of most under-classified areas of damage. Visual inspection of the detailed edge map of Zone 1 in figure 7-7 suggests that most of the buildings completely collapsed, affirming a category of very heavy damage. However, there was only a 12% reduction in edge pixels. A lot of edges are still being picked up after the earthquake, although not as coherently. Without knowing conclusively from ground observations, it appears that this is due to small segments of wall structure remaining standing, which produce a distinctive white colour against the red-brown earth. Thus anything that creates shadows in this area, such as wall remnants, continue to produce an edge response even if the roofs of the buildings have collapsed, leading to a decreased estimate of building destruction. We can see from that although many of the buildings show near or total collapse, this is not reflected so acutely in edge pixels.

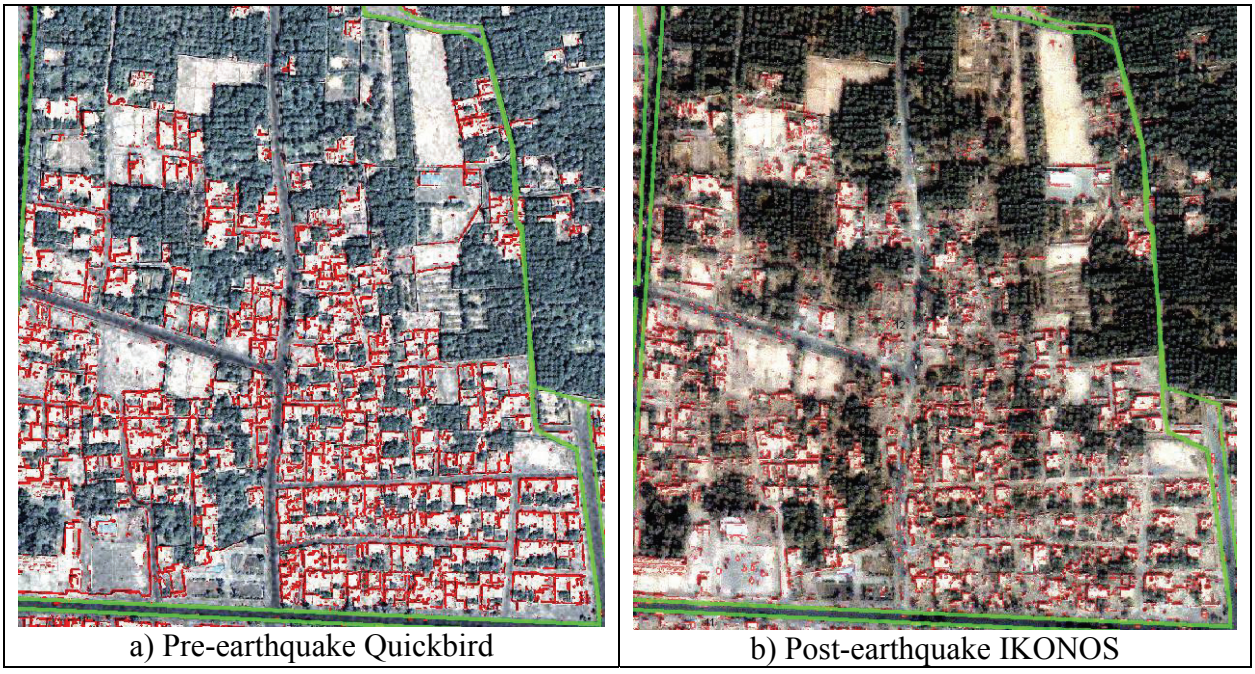

a) Pre-earthquake Quickbird b) Post-earthquake IKONOS

Figure 7-7 Area 1 in Northern Bam Where Heavy Damage was Recorded by Yamazaki et al. (2004b). (a) 'Before' Quickbird Image with Overlaid Edge Pixels (b) IKONOS 'After' Image Where an Exceptionally High Frequency of Edge Pixels Remain.

Within area 24, the remote sensing analysis identifies a major reduction in edge occurrence, whereas the validation dataset records negligible damage. In this case, figure 7-8 indicates that the occurrence of edges within the 'before' image was uncharacteristically high. Erroneous edges were detected that do not appear to correspond with the buildings. Combined with the reduction in resolution of the IKONOS image, plus movement of materials on the ground and change in illumination properties, there is a particularly strong change in this area that is not related building collapse.

a) Quickbird

b) IKONOS

Figure 7-8 Area 24 (a) Quickbird Image with Overlaid Edge Pixels (b) IKONOS Image with Overlain Edge Pixels

SECTION 8:
DISCUSSION, KEY FINDINGS AND FUTURE WORK

8.1 Discussion

After a major disaster, in order to perform timely and accurate change detection-based damage assessments, the remote sensing analyst is very much reliant on quick, comparable 'before' and 'after' datasets. Returning to the Tiered Reconnaissance framework described in Volume I (see also Section 1 of this Volume), in terms of Tier 2 and Tier 3 analysis (per-building and neighborhood levels) high resolution imagery is essential. Yet it is entirely possible that for a given sensor, no archive scenes will match recently acquired post-disaster imagery, or that it is not possible to acquire new imagery which matches archive imagery due to orbit procession or cloudy weather conditions. In this instance an 'ideal' change detection methodology cannot be used.

This chapter uniquely integrates high-resolution imagery acquired by two different satellites: (1) Quickbird and (2) IKONOS, with the goal of developing a truly *resilient* method of damage detection that is both *rapid* and *resourceful*. For exploratory multi-sensor research such as this, the Bam earthquake is a suitable case study, since buildings are predominantly similar in structure and exhibit distinctive bright adobe rooftops. A more complex urban environment would present a greater challenge for multi-sensor integration, and as such is more appropriate for future work.

The study examines the extent to which earthquake damage can be detected using very different pre- and post-disaster imagery characteristics, testing the hypothesis that significant non-damage-related changes between the IKONOS and Quickbird imagery are systematic and scene wide, and can therefore be negated out of the analysis. Sources of variability included sensor resolution, look angle and gain settings; differences that are entirely likely in a rapid-response situation. However, other factors also complicated the multi-sensor analysis. For instance, using the most affordable imagery, in this case entails standard level pre-processing, automatic black box atmospheric correction, and pre-pan-sharpening.

These multi-sensor variables created further complications in terms of spectral and textural comparisons. From initial visual analysis, significant differences were apparent between the available Quickbird and IKONOS imagery. These include differences not just related to the sensor, but related to the pre-processing regimes employed by the data provider prior to delivery. Accordingly, the pre-processing steps highlighted in figure 1-2 were undertaken to help account for the multi-sensor differences.

From table 8-1, overall, the processing steps were largely successfully substantially reducing the effect of systematic and scene-wide multi-sensor differences, to the extent that damage could be detected. However, they were unable to eliminate sources of variability; spatially varied factors such as the presence of cloud or haze and residual shadows continued to influence results obtained. Their complete removal requires further investigation.

Methodologically, this study investigated three different pixel-based spectral and textural damage detection techniques, at a Tier 2 neighborhood scale. Method 1 examined pre- and post-earthquake spectral differences, to determine whether a change detection signal could be detected using classification techniques. Method 2 followed Adams *et al.* (2004a) to examine the role of texture in pre-and post earthquake images, and more specifically whether the dissimilarity measure used to detect damage between Quickbird images, would also work with a multi-sensor change detection of Quickbird and IKONOS. Method 3 examined an edge-detection approach to detect change due to collapsed buildings.

Table 8-1 Processing Steps Adapted for Multi-Sensor Integration

Step	Description	Efficacy and Future Recommendations
Resampling and co-registration	The imagery was already georeferenced. However, to ensure a like-with-like comparison between building roofs, resampling of the 1m resolution IKONOS image to 60cm Quickbird resolution was required.	Co-registration helped to maximize spatial correspondence. Using nadir or near nadir imagery is recommended for future studies.
Pan-sharpening	The IKONOS image was delivered pre-pan sharpened, which presents a black box situation. Pansharpening was conducted on the Quickbird image to correspond	In the future it is recommended that bundle images are acquired from both sensors and pan-sharpening conducted in-house using the same algorithm
Histogram matching	To maximize spectral correspondence between the datasets, histogram matching was undertaken.	Some issues remain with shadows due to different look angles. As reported by Vu *et al.* (2005) a standard Quickbird image tends to have a blue tinge to it, which is not seen in the IKONOS image. Acquiring basic level imagery and conducting atmospheric correction and pansharpening in-house may help to mitigate sensor-related sources of change.
Masking	Urban masking was used to eliminate non-disaster-related sources of change between the images, such as vegetation seasonality and illumination conditions. Vegetation exclusion and roof inclusion masks focused the analysis on buildings, while eliminating other ground surface features and shadows.	As this study examines neighborhood statistics the analysis did not to be accurate to the building level. However, excluding large areas of potential misclassification is still good practice. Shadow removal was seen to help with this issue but did not completely eliminate it. A more detailed shadow examination is recommended in future studies.
Ortho-rectification	Ortho-rectification of the data was not undertaken.	It was not deemed necessary because the area of Bam is relatively flat, and in the absence of an accurate DEM, this processing step adds time but little if any accuracy.

Damage maps were created for each method to visually express spatial variations in the *extent* and *severity* of building collapse. At this time, remote sensing techniques successfully identify building collapse, and as such, the results can be used to produce various indicators including frequency of damaged pixels per city zone, or the frequency of urban damaged pixels. This general expression of damage occurrence and distribution is useful for rapid response activities, and could help guide field teams to the hardest hit areas. However, for more specific estimated of the *number* of damage buildings, an object-based approach is instead required (see Chapter 5). It is suggested that a damage map showing the percentage of collapsed buildings (see Chapter 5)

used in conjunction with a pixel-based map showing the general distribution of damage, would be of most use to emergency workers and planners.

Results for each method were aggregated and validated using several neighborhood scale techniques. For the spectral and edge-based analysis, damaged pixels were resampled into city zones following the Bam street network. These zones were of differing size and shape. For the textural analysis, damaged pixels were evaluated using a standard grid-based system of 120x120m. Whereas previous studies have employed street-based grids (Huyck *et al.*, 2003), the use of regularized grids is emerging in the literature (Saito *et al.*, 2004; Woo et al., 2005). Regularized grids performed well in this study, since they help minimize scale issues arising from differing zone sizes. In addition to scale issues, limitations of the validation datasets were found with comparing a damage area identified by pixel-based remote sensing results with a percentage of building destruction developed from the Yamazaki *et al.* (2004b) point samples. The area of building collapse (from pixel analysis) depends on the total area covered by buildings per zone, whereas the percentage of damaged structures instead depends on the number of buildings per zone, irrespective of their size. Variability in building footprint area across the city may therefore influence the total estimate of damage. Future work should explore techniques for limiting scale issues within pixel-based analysis.

Overall, this study found that it was possible to detect damage at a neighborhood level using a change detection methodology, and multi-sensor data sources from high resolution satellites. Table 8-2 summarizes general qualitative and quantitative characteristics identified using spectral, textural and edge-based methodologies, for sample neighborhoods in Bam dominated by damaged versus non-damaged structures.

Figure 8-1 compares the performance of the spectral and edge-based methods, in terms of the degree of correspondence between classified damage and the validation dataset developed by Yamazaki *et al.* (2004b), resampled into 40 city zones. As an indication of the accuracy of the classification, a) The frequency of correctly classified zones and b) the steepness of the curve between the correctly (at 0) and incorrectly classified zones (1 and above and -1 and below) are taken.

The ability to apply damage detection methodologies developed specifically for Bam to earthquake events elsewhere in the World is an important consideration. The city of Bam is characterized by predominantly adobe structures, with a distinctive blocky white appearance. The spectral analysis would prove difficult to equate to more complex towns, where the building stock is more varied in terms of composition and appearance. However, of the three techniques investigated it holds the greatest potential for distinguishing intermediate damage states between collapse and non-damage. Edge detection could prove useful as it works on image primitives not spectral properties, with careful calibration of the two input images so similar edges were picked up in both images. The applicability of textural analysis to different global locations requires further investigation, to determine if building collapse is universally characterized by a reduction in texture, or if this effect is limited to adobe structures where collapse results in homogenous rubble rather than blocky remnants.

Table 8-2 Summary of Qualitative and Quantitative Characteristics of Change Detection Measures, Associated with Extreme Damage and Non-Damaged Neighborhoods in Bam

Measure	Qualitative characteristics		Mean quantitative characteristics in sample zone	
	Extreme damage	Non-damage	Extreme damage	Non-damage
Spectral characteristics	Heterogeneous red or grey building debris. Visually resembles surrounding ground surface	Homogenous groups of white building roofs with distinct shadows at edges	<150DN	>150DN
Spectral difference	Decrease in pixel DN values in roof areas due to building collapse. Fewer white adobe roofs pointing towards the sensor. More brick or sand response – red / brown.	Limited change. Constant presence of white adobe roofs, blue industrial roofs. Surrounding ground more brown / sandy.	Difference >100DN	Difference ~ 75 DN due to scene-wide spectral offset
Dissimilarity characteristics	Low dissimilarity where jumbled rubble and sand is homogenous in color and blends with surrounding bare earth.	Highest dissimilarity seen around urban areas. High dissimilarity between roof edge and shadow, building and ground, building and vegetation.	Values in range 2-4	Values in range 1.5-2.5
Dissimilarity difference	Wider difference between 'before' and 'after' scenes.	Limited change. Sharp gradients of change remain between buildings and surroundings	Negative difference >1	Negative difference <0.6
Entropy characteristics	Low entropy between collapsed building rubble and ground.	Highest entropy seen around urban areas. High entropy between roof edge/shadow/ground/ vegetation. Low entropy in roof centre.	Values in range 3.5-4.5	Values in range 4.5-5.5
Entropy difference	Wider difference between 'before' and 'after' scenes.	Limited change. High entropy present in both pre- and post-earthquake images between buildings and surroundings	Negative difference ~0.2	Negative difference ~0.7
Correlation characteristics	High correlation between collapsed building rubble and ground.	Lowest correlation seen around urban areas. Low correlation between roof edge/shadow/building/ vegetation. High correlation in centre of building roofs.	Values tend towards zero	Negative values
Correlation difference	Wider difference between 'before' and 'after' scenes.	Limited change. Negative correlation present in both pre- and post-earthquake images between buildings and surroundings	Positive difference >0.7	Positive difference <0.2
Edge characteristics	Low frequency of edge pixels within jumbled piles of debris and rubble.	High frequency of edges associated with building walls.	Low. Mean ~50,000 edge pixels per zone	High. Mean >100,000 per zone
Edge difference	In total collapse area big drop in edge pixel count. In partially collapsed areas more disparate shorter edges.	Edges detected from edge of building roofs, also from cars, walls and other urban structures.	~50% reduction in the frequency of edge pixels.	N/A

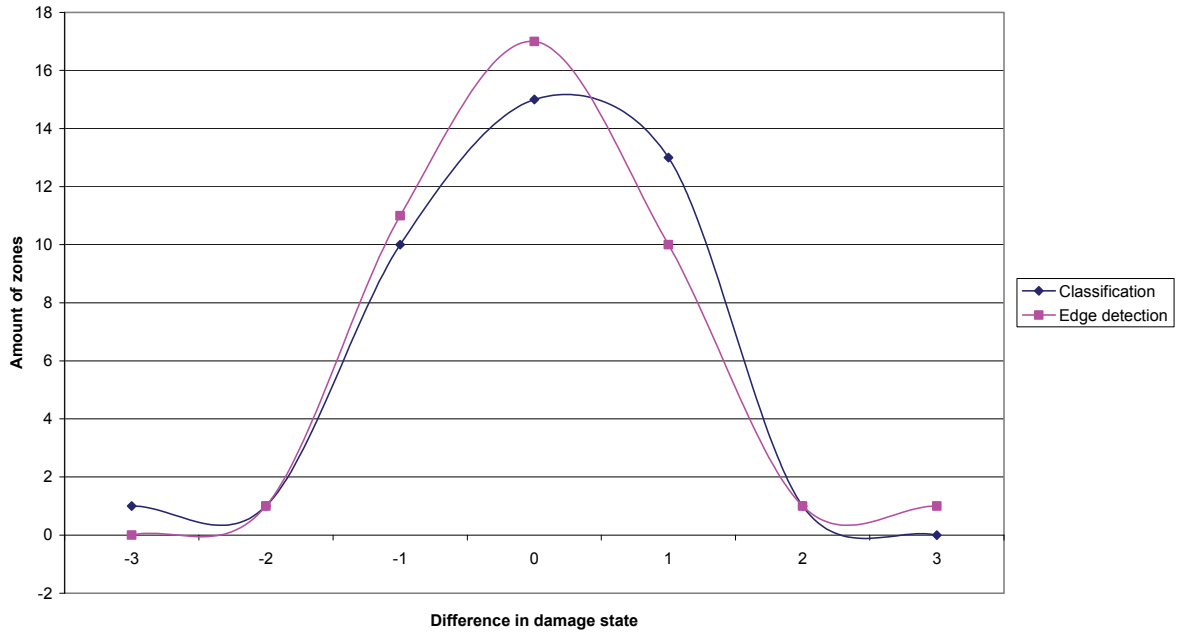

Figure 8-1 Difference in Performance of Spectral and Edge Detection Methods, in Terms of Difference Between Predicted and Validation Damage States

8.2 Key Findings

Considering the performance of the three different methodological approaches:

a) Key findings for Method 1: Spectral Analysis included:

- The spectrally-based damage assessment methodology successfully detected damage on a neighborhood scale using pre- and post-disaster input images acquired by two different high resolution optical satellites.
- The working hypothesis can be accepted that a lower spectral response was recorded from the debris of collapsed structures versus the homogenous roofs of non-damage buildings.
- From a qualitative visual comparison with the validation dataset from Yamazaki *et al.* (2004b) the supervised classification method performed well for adobe structures, identifying the main areas of heavy damage.
- Misclassifications appear to be in part due to multi-sensor differences that remain after the series of mitigation procedures employed during processing. This suggests that through pre-processing, some but not all, non-damage-related changes between the IKONOS and Quickbird imagery can be negated out of the analysis.
- Classified per-pixel damage can be mapped using a range of different summary statistics including the frequency of damage pixels per city zone, percent of urban damaged pixels per zone, or as a percent of damaged pixels per zone.

- Two methods of quantitative validation were explored, comprising an intersection analysis and a zone-based comparison. For the intersection analysis 72% of damage points fell within the areas classified as heavy damage. For the zone-based comparison, scale issues were an important consideration influencing the accuracies achieved using the three statistical measures. The percentage of damage pixels per city zone achieved the highest accuracy, with 15/40 zones correctly classified.
- These results suggest that a scale-independent measure of damage is urgently required for successful neighborhood scale damage mapping.

b) Key findings for Method 2: Textural Analysis included:

- Using textural measures such as entropy, dissimilarity and correlation can detect damage on a neighborhood scale using input images from different high resolution optical satellites. The output of this can be mapped as a classified amount of textural change per grid zone.
- The working hypothesis is rejected that chaotic piles of rubble associated with collapsed buildings exhibit poorly-defined edge structures and high textural variability. Alternative hypotheses are proposed that there is reduced chaos and lower dissimilarity, lower entropy and higher correlation within neighborhoods sustaining extreme building damage.
- From a qualitative visual comparison with the validation dataset from Yamazaki *et al.* (2004b) the dissimilarity, entropy and correlation textural measures method performed well for adobe structures, identifying the main areas of heavy damage.
- Using a 25x25 filter, misclassifications occurred within neighborhoods where a mixture of damaged versus non-damaged structures occurred. It may be more appropriate to determine the damage state of these mixed regions using an object-based approach.
- In the case of textural analysis, pre-processing techniques appear to have largely negated the effects of multi-sensor non-damage-related changes between the IKONOS and Quickbird imagery.
- A zone-based validation technique was explored, where the standard deviation of the mean textural measure for each zone was compared with the image-wide mean. The use of standard sized zones avoids the scale-related issues identified during the spectral validation exercise. The three texture measures all performed well. Dissimilarity produced the highest overall level of agreement. Entropy produced the best agreement when weighted by performance.
- These results suggest that textural measures and zonal mapping are useful techniques for neighborhood scale damage assessment.

c) Key findings for Method 3: Edge-based Analysis included:

- The edge detection methodology was partially successful in detecting damage on a neighborhood scale using input images from different high resolution optical satellites. The output can be mapped as a classified amount of change within city zones.

- The working hypothesis is accepted that collapsed buildings show fewer edges in the post-earthquake image, as distinct building boundaries are replaced by an indistinct and chaotic pattern of debris.
- However, from comparison with the validation dataset from Yamazaki *et al.* (2004b) misclassification and overestimation of damage occurs when the walls of collapsed buildings remain partially standing, and record an edge signature within the 'after' image.
- In the case of edge-based analysis, pre-processing techniques appear to have largely negated the effects of multi-sensor non-damage-related changes between the IKONOS and Quickbird imagery. However, haze/cloud remains an issue in the south-east of the city, suppressing edge signatures and causing an overestimation of damage.

8.3 Future Work

Two main areas of future work are identified:

1. For pre-processing to mitigate multi-sensor variation, using the component red, green, blue and near infrared bands of an imagery bundle, a Top Of Atmosphere (TOA) radiance measure could be calculated. This would produce pixel values that are more directly comparable between the datasets. Comparable pan-sharpening regimes and subsequent histogram matching routines may also prove beneficial.

2. In terms of change detection methodologies, the potential of image transformations such as IHS, PC and Wavelet, should be explored. Further, the integration of coarse pre-disaster building outlines obtained using software such as e-cognition may prove useful for mitigating scale effects and enabling a more accurate but still rapid neighbourhood damage assessment. Characterizing the building inventory of more cities around the World in GIS format is an important step towards this goal. The potential of remote sensing imagery and object-based analysis for inventory development is discussed in a separate MCEER report entitled 'Optimizing Object-based Segmentation Parameters for the Extraction of Buildings from VHR satellite imagery using Definiens Professional.'

SECTION 9:
REFERENCES

Adams, B.J., (2004), Improved disaster management through post-earthquake building damage assessment using multi-temporal satellite imagery, *Proceedings of the ISPRS XXth Congress Volume XXXV*, Istanbul.

Adams, B.J., (2005), Remote sensing technology – A coming of age, *Natural Hazards Observer*, **XXXIX(4)**: 1-3.

Adams, B.J. and Huyck, C.K., (2006), The emerging role of remote sensing technology in emergency management, In Taylor, C. and VanMarcke, E. (eds) *ASCE Monograph: Infrastructure risk Management Processes: Natural, Accidental, and Deliberate Hazards*, ASCE. P. 95-117.

Adams, B.J., Huyck, C.K., Mansouri, B., Eguchi, R.T. and Shinozuka, M., (2004a), Application of high-resolution optical satellite imagery for post-earthquake damage assessment: The 2003 Boumerdes (Algeria) and Bam (Iran) earthquakes, *MCEER Research and Accomplishments 2003-2004*, MCEER: Buffalo.

Adams, B.J., Huyck, C.K., Mio, M., Cho, S., Ghosh, S., Chung, H.C., Eguchi, R.T., Houshmand, B., Shinozuka, M., and Mansouri, B. (2004b) *The Bam (Iran) earthquake of December 26, 2003: Preliminary reconnaissance using remotely sensed data and the VIEWS system*, http://mceer.buffalo.edu/research/bam/default.asp.

Aoki, H., Matsuoka, M. and Yamazaki, F., (1998), Characteristics of satellite SAR images in the damaged areas due to the Hyogoken-Nanbu earthquake, *Proceedings of the 1998 Asian Conference on Remote Sensing*, http://www.gisdevelopment.net/aars/acrs/1998/ts3/ts3007.shtml.

Arciniegas, G.A., Bijker, W., Kerle N. and Tolpekin, V.A. (in press) Coherence- and amplitude-based analysis of seismogenic damage in Bam, Iran, using Envisat ASAR data, *IEEE Transactions on Geoscience and Remote Sensing, v. Special issue, Remote sensing for major disaster prevention, monitoring and assessment*.

Aschbacher, J. and Lichtenegger, J., (1990), Complementary nature of SAR and optical data: a case study in the Tropics. *Earth Observation Quarterly*, **31**, 4-8.

Boccippio D.J., Koshak W., Blakeslee R., Driscoll K., Mach D., Buechler D., Boeck W., Christian H.J. and Goodman, S.J., (2000), The Optical Transient Detector (OTD): Instrument Characteristics and Cross-Sensor Validation, *Journal of Atmospheric and Oceanic Technology,* **17(4)**:441-458.

Brisco, B., and Brown, R. J. (1995) Multidate SAR/TM synergism for crop classification in Western Canada. *Photogrammetric Engineering and Remote Sensing*, **61**: 1009-1014.

Chavez, P. S. (1987) Digital merging of Landsat TM and digitized NHAP data for 1 : 24 000

scale image mapping. *Photogrammetric Engineering and Remote Sensing*, **52**: 1637-1646.

Chiroiu, L. and Andre, G., (2001), *Damage assessment using high-resolution satellite imagery: application to 2001 Bhuj, India earthquake*, www.riskworld.com

Chiroiu, L., Adams, B.J. and Saito, K., (2006), Advanced techniques in modeling, response and recovery, In Olivera, C.S., Roca, A. and Goula, X. (eds.) *Assessing and Managing Earthquake Risk. Geoscientific and Engineering Knowledge for Earthquake Risk Mitigation: Developments, Tools, Techniques*, Springer: Netherlands, p. 427-448.

Chiroiu, L., Andre, G., Guillande, R. and Bahoken, F., (2002), Earthquake damage assessment using high-resolution satellite imagery, *Proceedings of the 7th U.S. National Conference on Earthquake Engineering*, Boston.

Comhaire, A. L., Ozer, A. and Jaspar, A., (1994), The contribution of ERS-1 and SPOT data in the morphologic and bathymetric study of the north sea and the Scheldt Estuary, *Proceedings of First ERS-1 Pilot Project Workshop*, Toledo, Spain, pp. 297± 302.

Corner, B.R., Narayanan, R.M. and Reichenbach, S E., (1999), Application of principal component analysis to multisensor classification, *Proceedings of the 27th AIPR Workshop: Advances in Computer-Assisted Recognition*.

Corves, C., (1994), Assessment of multi-temporal ERS-1 SAR Landsat TM data for mapping the Amazon river Foodplain. *Proceedings of First ERS-1 Pilot Project Workshop*,T oledo, Spain, 22± 24 June 1994, SP-365 (Paris: European Space Agency), pp. 129-132.

Dallemand, J. F., Lichtenegger, J., Kaufmann, V., Paudyal, D. R., and Reichert, A. (1992) Combined analysis of ERS-1 SAR and visible/infrared RS data for land cover/land use mapping in tropical zone: a case study in Guinea. *Space at the Service of our Environment, Proceedings First ERS-1 Symposium*, Cannes, France, 6-8 November 1992, SP-359 (Paris: European Space Agency), pp. 555-561.

EDM, (2000), *Report on the Kocaeli Turkey Earthquake of August 17th 1999, EDM Technical Report No. 6*, EDM: Miki.

Eguchi, R., Huyck, C., Adams, B., Mansouri, B., Houshmand, B. and Shinozuka, M., (2002), Earthquake damage detection algorithms using remote sensing data – Application to the August 17, 1999 Marmara, Turkey Earthquake, *Proceedings of the 7th U.S. National Conference on Earthquake Engineering*, Boston.

Eguchi, R., Huyck, C., Adams, B., Mansouri, B., Houshmand, B. and Shinozuka, M., (2003a), Earthquake damage detection algorithms using remotely sensed data – Application to the August 17, 1999 Marmara, Turkey earthquake, *Proceedings of the 7th EERI US/Japan Workshop on Urban earthquake Hazard Reduction*, Miami.

Eguchi, R., Huyck, C., Adams, B., Mansouri, B., Houshmand, B. and Shinozuka, M., (2003b), Resilient disaster response: Using remote Sensing technologies for post-earthquake damage detection, *MCEER Research and Accomplishments 2001-2003*, MCEER: Buffalo.

Eguchi, R., Huyck, C., Houshmand, B., Mansouri, B., Shinozuka, M., Yamazaki, F. Matsuoka, M. and Ulgen, S., (2000a), The Marmara earthquake: A view from space, *The Marmara, Turkey Earthquake of August 17, 1999: Reconnaissance Report Chapter 10, 151-169,* MCEER: Buffalo.

Eguchi, R., Huyck, C., Houshmand, B., Mansouri, B., Shinozuka, M., Yamazaki, F. Matsuoka, M. and Ulgen, S., (2000b), The Marmara, Turkey earthquake: Using advanced technology to conduct earthquake reconnaissance, *MCEER research and Accomplishments 1999-2000,* MCEER: Buffalo.

Ehlers, M., (1991), Multisensor image fusion techniques in remote sensing, *ISPRS Journal of Photogrammetry and Remote Sensing*, **46**, 19-30.

Estrada, M., Kohiyama, M. and Yamazaki, F., (2003), Damage detection method using middle-resolution optical satellite images based on normal fluctuation of digital numbers in multi-temporal images. Part 2: Numerical experiment to demonstrate digital numbers fluctuation using simulated middle-resolution images, *Proceedings of the 1st International Workshop on Remote Sensing for Disaster Response*, Newport Beach.

Estrada, M., Matsuoka, M. and Yamazaki, F., (2001b), Digital damage detection due to the 1999 Kocaeli, Turkey earthquake, *Bulletin of the Earthquake Resistant Structure Research Center*, **34**, 55-66.

Fisher R., Perkins S., Walker A., Wolfart E., (2003) *Sobel Edge Detector*, Available Online at: http://homepages.inf.ed.ac.uk/rbf/HIPR2/sobel.htm [accessed 4/11/07]

Gens R., (2004), *Geospatial Data Fusion*, http://www.asf.alaska.edu/educational/seminarpdf/2004/data_fusion.pdf Accessed 3/2/2007

Gianinetto, M., Villa, P., Lechi, G., (2006) Postflood Damage Evaluation Using Landsat TM and ETM+ Data Integrated With DEM, *GeoRS*, **44(1)**: 236-243.

Grünthal, G. (ed.): (1998) *European Macroseismic Scale 1998* (EMS-98). Cahiers du Centre Européen de Géodynamique et de Séismologie 15, Centre Européen de Géodynamique et de Séismologie, Luxembourg, 99 pp.

Gungor, O. and Shan, J., (2004), Evaluation of satellite image fusion using wavelet transform. *Proceedings of the ISPRS, commission VII, WGIII/6*, Istanbul, 2004, paper n° 236.

Guo, H. D. and Pinliang, D., (1989), Integrated MSS-SAR-SPOT-geophysical geochemical data for exploration geology in Yeder area. *CAS-IRSA*, 1-8

Gusella, L., Adams, B.J., Bitelli, G. and Huyck, C.K., (2005a), Object-oriented image understanding and post-earthquake damage assessment for the 2003 Bam, Iran, earthquake, *Earthquake Spectra*, **21(S1)**: 225-238.

Gusella, L., Huyck, C.K., Adams, B.J., Cho, S. and Chung, H., (2005b), Damage assessment with very-high resolution optical imagery following the December 26, 2003 Bam, Iran earthquake, *Proceedings of the 3rd International Workshop on Remote Sensing for Disaster Response*, Chiba, Japan. http://ares.tu.chiba-u.jp/workshop/Chiba-RS2005/Paper_Huyck_.pdf

Hall, D.L., (1992) *Mathematical Techniques in Multisensor Data Fusion*. Artech House, Boston, MA

Hall-Bey M. (2007) *What is texture?,* http://www.fp.ucalgary.ca/mhallbey/what_is_texture.htm Accessed 4/1/07

Harris J.R., Murray R. and Hirose, T., (1990), IHS transform for the integration of radar imagery with other remotely sensed data. *Photogrammetric Engineering and Remote Sensing*. **56**:1631-1641

Hellwich O., Heipke C. and Wessel, B., (2007), *Information for Mapping from Airborne SAR and Optical Imagery*, http://www.data-fusion.org/article.php?sid=83. Accessed 1/2/07

HIPR (2003) *Image Processing Learning Courses*, http://homepages.inf.ed.ac.uk/rbf/HIPR2/

Huyck, C.K. and Adams, B.J., (2004), Damage detection using regional edge dissimilarity of very high-resolution optical data. *Proceedings of the 2nd Workshop on Remote Sensing for Post-Disaster Response*, Newport Beach.

Huyck, C.K., Adams, B.J., Cho, S., Chung, H. and Eguchi, R.T., (2005), Towards rapid citywide damage mapping using neighborhood edge dissimilarities in very high-resolution optical satellite imagery – Application to the 2003 Bam, Iran, earthquake, *Earthquake Spectra*, **21(S1)**: 255-266.

Huyck, C.K, Mansouri, B., Eguchi, R.T., Houshmand, B., Castner, L. and Shinozuka, M., (2002), Earthquake damage detection algorithms using optical and ERS-SAR satellite data – Application to the August 17, 1999 Marmara, Turkey earthquake, P*roceedings of the 7th U.S. National Conference on Earthquake Engineering*, Boston.

Huyck, C.K., Adams, B.J. and Eguchi, R.T., (2003), An overview of post-earthquake reconnaissance using remote sensing, *Proceedings of the 1st International Workshop on Remote Sensing for Disaster Response*, Irvine.

Huyck, C.K., Adams, B.J., Cho, S., Eguchi, R.T., Mansouri, B. and Houshmand, B., (2004a), Methodologies for Post-earthquake Building Damage Detection Using SAR and Optical Remote Sensing: Application to the August 17, 1999 Marmara, Turkey Earthquake, *MCEER-04-0004 Technical Report*, MCEER: Buffalo.

Huyck, C.K., Adams, B.J. and Gusella, L., (2004b), Damage detection using neighborhood edge dissimilarity in very high-resolution optical data, *Proceedings of the 2nd International Workshop on Remote Sensing for Disaster Response*, Newport Beach, http://mceer-nt2.mceer.buffalo.edu/second_workshop/papers/05paper_huyck.pdf

Kaya, S., Curran, P. and Llewellyn, G., (2005), Post-earthquake building collapse: A comparison of government statistics and estimates derived from SPOT HRVIR data, *International Journal of Remote Sensing*, **26(13)**: 2731-2740.

Kaya, S., Llewellyn, G. and Curran, P., (2004), Displaying earthquake damage in urban areas using a vegetation-impervious-soil model and remotely sensed data, *Proceedings of the XXth ISPRS Congress*, Istanbul, http://www.isprs.org/istanbul2004/comm7/papers/125.pdf.

Kohiyama, M. and Yamazaki, F., (2005a), Damage detection for 2003 Bam, Iran earthquake using Terra-ASTER satellite imagery, *Earthquake Spectra*, **21(S1)**: 267-274.

Kohiyama, M. and Yamazaki, F., (2005b), Image fluctuation model for damage detection using middle resolution satellite imagery, *International Journal of Remote Sensing*, **26(24)**: 5603-5627.

Kohiyama, M., Estrada, M. and Yamazaki, F., (2003), Damage detection method using middle-resolution optical satellite images based on normal fluctuation of digital number s in multi-temporal images. Part 1: Formulation of the damage estimation method, *Proceedings of the 1st International Workshop on Remote Sensing for Disaster Response*, Irvine.

Kosaka N., Akiyama T., Tsai B. and Kojima T., (2005), Forest Type Classification Using Data Fusion of Multispectral and Panchromatic High-Resolution Satellite Imageries, *Proceedings of the 2005 Geoscience and Remote Sensing Symposium IGARSS '05*, **4**: 2980-2983

Kuehn, S., Benz, U. and Hurley, J., (2002), Efficient flood monitoring based on RADARSAT-1 images data and information fusion with object-oriented technology, *IEEE International Geoscience and Remote Sensing Symposium Proceedings,* 5, pp. 2862-8264.

Limpitlaw, D. and Gens, R., (2006), Dambo mapping for environmental monitoring using Landsat TM and SAR imagery: Case study in the Zambian Copperbelt, *International Journal of Remote Sensing*, **27(21)**: 4839 – 4845

Le Moigne J., Laporte N., Netanyahu N. S. (2001) Enhancement of Tropical Land Cover Mapping with Wavelet-Based Fusion and Unsupervised Clustering of SAR and Landsat Image Data, *SPIE Tolouse*, France 17-21 September 2001

Mangolini, M., Ranchin, T. and Wald, L., (1993), Fusion d'images SPOT multispectrale (XS) et panchromatique (P), et d'images radar. *From Optics to Radar, SPOT and ERS Applications, Conference Proceedings*, Paris: France, pp. 199-209.

Liao, M, Zhnag, L. and Lin, H. (2005) Change Detection in Multispectral Imagery from multisensor, *IEEE Int. Geoscience and Remote Sensing Symp*., Seoul, Korea, July 2005.

Mansouri, B. and Shinozuka, M., (2005), SAR image power calibration by urban texture: Application to the Bam earthquake using Envisat satellite ASAR data, *Proceedings of the 3rd International Workshop on Remote Sensing for Disaster Response*, Chiba.

Mansouri, B., Shinozuka, M., Huyck, C.K. and Houshmand, B., (2004), SAR complex data analysis for change detection for the Bam earthquake using Envisat satellite ASAR data, P*roceedings of the 2nd International Workshop on Remote Sensing for Disaster Response*, Newport Beach.

Mansouri, B., Shinozuka, M., Huyck, C.K. and Houshmand, B., (2005), Earthquake induced change detection in the 2003 Bam, Iran, earthquake by complex analysis using Envisat ASAR data, *Earthquake Spectra*, **21(S1)**: 275-284.

Matsuoka, M. and Yamazaki, F., (1998), Identification of damaged areas due to the 1995 Hyogoken-Nanbu earthquake using satellite optical images, *Proceedings of the 19th Asian Conference on Remote Sensing*, Manila.

Matsuoka, M. and Yamazaki, F., (1999), Characteristics of satellite images of damaged areas due to the 1995 Kobe earthquake. *Proceedings of the Second Conference on the Application of Remote Sensing and GIS for Disaster Management*, Washington D.C.

Matsuoka, M., and Yamazaki, F., (2000a) Interferometric characterization of areas damaged by the 1995 Kobe earthquake using satellite SAR images. *Proceedings of the 12th World Conference on Earthquake Engineering*, Auckland, New Zealand.

Matsuoka, M. and Yamazaki, F., (2000b), Satellite remote sensing of damaged areas due to the 1995 Kobe earthquake, In Toki, K. (ed) *Confronting Urban Earthquakes, Report of Fundamental Research on the Mitigation of Urban Disasters Caused by Near-field Earthquakes*, 259-262.

Matsuoka, M. and Yamazaki, F., (2003), Application of a methodology for detection building-damage area to recent earthquakes using SAR intensity images, *Proceedings of the 7th EERI US Japan Conference on Urban Earthquake Hazard Reduction*, Maui.

Matsuoka, M. and Yamazaki, F., (2004a), Use of SAR intensity imagery fr earthquake damage detection, *Proceedings of the 2nd International Workshop on Remote Sensing for Disaster Response*, Newport Beach.

Matsuoka, M. and Yamazaki, F., (2004b), Use of satellite SAR intensity imagery for detecting building areas damaged due to earthquakes, *Earthquake Spectra*, **20(3)**: 975-994.

Matsuoka, M. and Yamazaki, F., (2006), Use of SAR imagery for Monitoring areas damaged due to the 2006 mid Java, Indonesia earthquake, *Proceedings of the 4th International Workshop on Remote Sensing for Disaster Response*, Cambridge.

Mouat, D. A., Mahin, G. G. and Lancaster, J., (1993), Remote sensing techniques in the analysis of change detection, *Geocarto International*, **2**, 39-50

Nielsen A. A., (2002) Multiset canonical correlations analysis and multispectral, truly multitemporal remote sensing data. *IEEE Transactions on Image Processing*. **11(3)**:293-305

Neilsen, A.A., Conradsen, K. and Simpson, J.J., (1998), Multivariate Alteration Detection (MAD) and MAF postprocessing in multispectral, bitemporal image data: New Approaches to change detection studies, *Remote Sensing of Environment*, **4(1)**: 1-19

Niemeyer, I. and M.J. Canty, (2003), Pixel-Based and Object-Oriented Change Detection Analysis Using High-Resolution Imagery. Proc. 25th Symposium on Safeguards and Nuclear Material Management, Stockholm, Sweden, 13-15 May 2003 (CD-Rom)

Ozisik, D. and Kerle, N., (2004), Post-earthquake damage assessment using satellite and airborne data in the case of the 1999 Kocaeli earthquake, Turkey, *Proceedings of the XXth ISPRS Congress*, Istanbul.

Petit, C. and Lambin, E.F. (2001) Integration of multi-source remote sensing data for land cover change detection. *International Journal of Geographical Information Science* , **8(15)**: 785-803.

Price, J. C., (1987), Combining panchromatic and multispectral imagery from dual resolution satellite instruments, *Remote Sensing of Environment*, **21**, 119-128.

Pohl C. and Genderen, J.L.V., (1998), Multisensor image fusion in Remote Sensing: concepts, methods and applications, *International Journal of Remote Sensing*, **19(5)**: 823-854

Pohl, C., and van Genderen, J.L. (1994) Multisensor fusion : optimization and operationalisation for mapping applications, *SPIE conference on signal processing, sensor fusion and target recognition* : Vol. III, 4-8 April 1994, Orlando, USA, : SPIE proceedings series Vol. 2232, 1994, pp. 17-25

Pohl, C., Wang, Y., and Koopmans, B. N., 1994. The 1995 Flood in the Netherlands from Space, *ITC Journal*, **1994-4**: 414± 415.

Price, J. C., (1987), Combining panchromatic and multispectral imagery from dual resolution satellite instruments, *Remote Sensing of Environment*, **21**, 119-128.

Rathje E. and Crawford M., (2004), Using High Resolution Satellite Imagery To Detect Damage From The 2003 Northern Algeria Earthquake, *13th World Conference on Earthquake Engineering Conference Proceedings*.

Rathje, E., Crawford, M., Woo, K. and Neuenschwander, A. (2005) Damage patterns from satellite images of the 2003 Bam, Iran, earthquake, *Earthquake Spectra*, **21(S1)**: 295-307.

Rodarmel, C. Scott, L., Simerlink, D. and Walker, J. (2002) Multisensor fusion over the World Trade Center disaster site, *Optical Engineering*, **41(9)**: 2120-2128

RSI, (2002), *User's guide, ENVI version 3.6, 2nd edition,* RSI Inc., CO, US

Saito, K. and Spence, R.J., (2004), Application of texture analysis to high-resolution optical satellite images for mapping earthquake building damage distribution – a preliminary assessment, *Proceedings of the 2nd International Workshop on Remote Sensing for Disaster Response*, Newport Beach.

Saito, K. and Spence, R.J., (2005), Spatial autocorrelation characteristics of collapsed buildings in high-resolution optical satellite images - a preliminary assessment. *Proceedings of the 1st International Conference on Urban Disaster Reduction*, Kobe, Japan.

Saito, K., Spence, R.J., Going, C. and Markus, M., (2004), Using high-resolution satellite images for post-earthquake building damage assessment: a study following the 26.1.01 Gujurat earthquake, *Earthquake Spectra*, **20(1)**: 145-170.

Shettigara, V. K., (1992), A generalized component substitution technique for spatial enhancement of multispectral images using a higher resolution data set. P*hotogrammetric Engineering and Remote Sensing*, **58**: 561-567

Sonka M., Hlavac, V. Boyle, R. (1998) *Image Processing, Analysis, and Machine Vision - 2nd Edition*, PWS, Pacific Grove, CA, 800 p., ISBN 0-534-95393-X

Stramondo, S., Pierdicca, N., Chini, M. and Bignami, C., (2006a), Damage detection and surface effect mapping by integrating SAR and optical remote sensing, *Proceedings of the 4th International Workshop on Remote Sensing for Disaster Response*, Cambridge.

Stramondo, S., Bignami, C., Chini, M., Pierdicca, N. and Tertulliani, A., (2006b), Satellite radar and optical remote sensing for earthquake damage detection results from different case studies, *International Journal of Remote Sensing*, **27(20)**:4433-4447.

Suits, G., Malila, W. and Weller, T., (1988), Procedures for using signals from one sensor as substitutes for signals of another, *Remote Sensing of Environment*, **25**: 395-408.

Terraseer (2007) *About Jenk's Natural Breaks*, http://www.terraseer.com/help/stis/interface/map/classify/About_natural_breaks.htm

Tralli, D.M., (2000), *Assessment of Advanced Technologies for Loss Estimation*, MCEER: Buffalo.

Tu T.M., Lee Y.C., Chang C.P., Huang P.S. (2005) Adjustable intensity-hue-saturation and Brovey transform fusion technique for IKONOS/Quickbird Imagery. *Optical Engineering*, **44(11)**: 116201-p.1-10

Tu T.M., Lee Y.C., Huang P.S., Chang C.P. (2006) Modified smoothing filter based technique for IKONOS-Quickbird image fusion, *Optical Engineering*, **45(6)**: 066201 – p.1-8

Turker, M. and San, B.T., (2003), SPOT HRV data analysis for detecting earthquake-induced changes in Izmit, Turkey, *International Journal of Remote Sensing*, **24(12)**: 2439-2450.

USAID (2004) *Iran: estimated damage caused by the Bam earthquake*, http://www.reliefweb.int/rw/RWB.NSF/db900SID/SKAR-64GE3N?OpenDocument

Verma N., Rathore N.S. (2002) *Application of Remote Sensing and GIS in earthquake study: A case study of Bhuj earthquake 2001,* Available online at: http://www.gisdevelopment.net/aars/acrs/2002/hdm/252.pdf [accessed 21/8/2007]

Vu, T., Matsuoka, M. and Yamazaki, F. (2005) Preliminary results in development of an object-based image analysis method for earthquake damage assessment, *Proceedings of the 3rd International Workshop on Remote Sensing for Disaster Response*, Chiba, Japan. http://mceer.buffalo.edu/publications/workshop/05-SP03/Third_Workshop/default.asp

Wang, Z., Ziou, D.; Armenakis, C.; Li, D.; Qingquan, L. (2005) A comparative analysis of image fusion methods, IEEE Transactions on Geoscience and Remote Sensing, **43(6)**: 1391 – 1402

Ware, J.L., (2003), *Geospatial Data Fusion: Training GIS for Disaster Relief Operations*, http://gis.esri.com/library/userconf/proc03/p1097.pdf. Accessed 4/2/2007

Welch, R., Jordon, T. R. and Ehlers, M., (1985), Comparative evaluations of geodetic accuracy and cartographic potential of Landsat-4/5 TM image data. *Photogrammetric Engineering and Remote Sensing*, **51**: 1249-1262

Womble, J.A., Ghosh, S., Friedland, C.J., and Adams, B.J. (2006) Hurricane Katrina – Advanced Damage Detection: Integrating Remote-Sensing Images with VIEWS Field Reconnaissance, *Report of the Multidisciplinary Center for Earthquake Engineering Research*, University at Buffalo, http://mceer.buffalo.edu/publications/Katrina/06SP02-web.pdf.

Woo, K., Rathje, E. and Crawford, M., (2005), Comparison of earthquake damage evaluation using change detection and thematic classification, *Proceedings of the 3rd International Workshop on Remote Sensing for Disaster Response*, Chiba, Japan.

Yamazaki, F., (2001), Applications of remote sensing and GIS for damage assessment, *Proceedings of the Joint Workshop on Urban Safety Engineering*, Asian Institute of Technology, Bangkok.
Yamazaki, F., Kouchi, K., Matsuoka, M., Kohiyama, M. and Muraoka, N. (2004a) Damage detection from high-resolution satellite images for the 2003 Boumerdes, Algeria earthquake, P*roceedings of the 13th World Conference on Earthquake Engineering*, Vancouver.

Yamazaki, F., Yano, Y., Matsuoka, M. and Vu, T.T., (2004b), Building damage interpretation of the 2003 Bam, Iran earthquake, using Quickbird images, *Proceedings of the 2nd International Workshop on Remote Sensing for Disaster Response*, Newport Beach, USA.

Zhang, Y. (2004) Highlight Article: Understanding Image Fusion. *Photogrammetric Engineering & Remote Sensing*, **70(6)**: 657-661.

Zhukov, B., Oertel, D., Lanzl, F., Reinhackel, G. (1999) Unmixing-based multisensor multiresolution image fusion, , *IEEE Transactions on Geoscience and Remote Sensing*, **37(3)**:1212 - 1226

MCEER Technical Reports

MCEER publishes technical reports on a variety of subjects written by authors funded through MCEER. These reports are available from both MCEER Publications and the National Technical Information Service (NTIS). Requests for reports should be directed to MCEER Publications, MCEER, University at Buffalo, State University of New York, Red Jacket Quadrangle, Buffalo, New York 14261. Reports can also be requested through NTIS, 5285 Port Royal Road, Springfield, Virginia 22161. NTIS accession numbers are shown in parenthesis, if available.

NCEER-87-0001 "First-Year Program in Research, Education and Technology Transfer," 3/5/87, (PB88-134275, A04, MF-A01).

NCEER-87-0002 "Experimental Evaluation of Instantaneous Optimal Algorithms for Structural Control," by R.C. Lin, T.T. Soong and A.M. Reinhorn, 4/20/87, (PB88-134341, A04, MF-A01).

NCEER-87-0003 "Experimentation Using the Earthquake Simulation Facilities at University at Buffalo," by A.M. Reinhorn and R.L. Ketter, to be published.

NCEER-87-0004 "The System Characteristics and Performance of a Shaking Table," by J.S. Hwang, K.C. Chang and G.C. Lee, 6/1/87, (PB88-134259, A03, MF-A01). This report is available only through NTIS (see address given above).

NCEER-87-0005 "A Finite Element Formulation for Nonlinear Viscoplastic Material Using a Q Model," by O. Gyebi and G. Dasgupta, 11/2/87, (PB88-213764, A08, MF-A01).

NCEER-87-0006 "Symbolic Manipulation Program (SMP) - Algebraic Codes for Two and Three Dimensional Finite Element Formulations," by X. Lee and G. Dasgupta, 11/9/87, (PB88-218522, A05, MF-A01).

NCEER-87-0007 "Instantaneous Optimal Control Laws for Tall Buildings Under Seismic Excitations," by J.N. Yang, A. Akbarpour and P. Ghaemmaghami, 6/10/87, (PB88-134333, A06, MF-A01). This report is only available through NTIS (see address given above).

NCEER-87-0008 "IDARC: Inelastic Damage Analysis of Reinforced Concrete Frame - Shear-Wall Structures," by Y.J. Park, A.M. Reinhorn and S.K. Kunnath, 7/20/87, (PB88-134325, A09, MF-A01). This report is only available through NTIS (see address given above).

NCEER-87-0009 "Liquefaction Potential for New York State: A Preliminary Report on Sites in Manhattan and Buffalo," by M. Budhu, V. Vijayakumar, R.F. Giese and L. Baumgras, 8/31/87, (PB88-163704, A03, MF-A01). This report is available only through NTIS (see address given above).

NCEER-87-0010 "Vertical and Torsional Vibration of Foundations in Inhomogeneous Media," by A.S. Veletsos and K.W. Dotson, 6/1/87, (PB88-134291, A03, MF-A01). This report is only available through NTIS (see address given above).

NCEER-87-0011 "Seismic Probabilistic Risk Assessment and Seismic Margins Studies for Nuclear Power Plants," by Howard H.M. Hwang, 6/15/87, (PB88-134267, A03, MF-A01). This report is only available through NTIS (see address given above).

NCEER-87-0012 "Parametric Studies of Frequency Response of Secondary Systems Under Ground-Acceleration Excitations," by Y. Yong and Y.K. Lin, 6/10/87, (PB88-134309, A03, MF-A01). This report is only available through NTIS (see address given above).

NCEER-87-0013 "Frequency Response of Secondary Systems Under Seismic Excitation," by J.A. HoLung, J. Cai and Y.K. Lin, 7/31/87, (PB88-134317, A05, MF-A01). This report is only available through NTIS (see address given above).

NCEER-87-0014 "Modelling Earthquake Ground Motions in Seismically Active Regions Using Parametric Time Series Methods," by G.W. Ellis and A.S. Cakmak, 8/25/87, (PB88-134283, A08, MF-A01). This report is only available through NTIS (see address given above).

NCEER-87-0015 "Detection and Assessment of Seismic Structural Damage," by E. DiPasquale and A.S. Cakmak, 8/25/87, (PB88-163712, A05, MF-A01). This report is only available through NTIS (see address given above).

NCEER-87-0016 "Pipeline Experiment at Parkfield, California," by J. Isenberg and E. Richardson, 9/15/87, (PB88-163720, A03, MF-A01). This report is available only through NTIS (see address given above).

NCEER-87-0017 "Digital Simulation of Seismic Ground Motion," by M. Shinozuka, G. Deodatis and T. Harada, 8/31/87, (PB88-155197, A04, MF-A01). This report is available only through NTIS (see address given above).

NCEER-87-0018 "Practical Considerations for Structural Control: System Uncertainty, System Time Delay and Truncation of Small Control Forces," J.N. Yang and A. Akbarpour, 8/10/87, (PB88-163738, A08, MF-A01). This report is only available through NTIS (see address given above).

NCEER-87-0019 "Modal Analysis of Nonclassically Damped Structural Systems Using Canonical Transformation," by J.N. Yang, S. Sarkani and F.X. Long, 9/27/87, (PB88-187851, A04, MF-A01).

NCEER-87-0020 "A Nonstationary Solution in Random Vibration Theory," by J.R. Red-Horse and P.D. Spanos, 11/3/87, (PB88-163746, A03, MF-A01).

NCEER-87-0021 "Horizontal Impedances for Radially Inhomogeneous Viscoelastic Soil Layers," by A.S. Veletsos and K.W. Dotson, 10/15/87, (PB88-150859, A04, MF-A01).

NCEER-87-0022 "Seismic Damage Assessment of Reinforced Concrete Members," by Y.S. Chung, C. Meyer and M. Shinozuka, 10/9/87, (PB88-150867, A05, MF-A01). This report is available only through NTIS (see address given above).

NCEER-87-0023 "Active Structural Control in Civil Engineering," by T.T. Soong, 11/11/87, (PB88-187778, A03, MF-A01).

NCEER-87-0024 "Vertical and Torsional Impedances for Radially Inhomogeneous Viscoelastic Soil Layers," by K.W. Dotson and A.S. Veletsos, 12/87, (PB88-187786, A03, MF-A01).

NCEER-87-0025 "Proceedings from the Symposium on Seismic Hazards, Ground Motions, Soil-Liquefaction and Engineering Practice in Eastern North America," October 20-22, 1987, edited by K.H. Jacob, 12/87, (PB88-188115, A23, MF-A01). This report is available only through NTIS (see address given above).

NCEER-87-0026 "Report on the Whittier-Narrows, California, Earthquake of October 1, 1987," by J. Pantelic and A. Reinhorn, 11/87, (PB88-187752, A03, MF-A01). This report is available only through NTIS (see address given above).

NCEER-87-0027 "Design of a Modular Program for Transient Nonlinear Analysis of Large 3-D Building Structures," by S. Srivastav and J.F. Abel, 12/30/87, (PB88-187950, A05, MF-A01). This report is only available through NTIS (see address given above).

NCEER-87-0028 "Second-Year Program in Research, Education and Technology Transfer," 3/8/88, (PB88-219480, A04, MF-A01).

NCEER-88-0001 "Workshop on Seismic Computer Analysis and Design of Buildings With Interactive Graphics," by W. McGuire, J.F. Abel and C.H. Conley, 1/18/88, (PB88-187760, A03, MF-A01). This report is only available through NTIS (see address given above).

NCEER-88-0002 "Optimal Control of Nonlinear Flexible Structures," by J.N. Yang, F.X. Long and D. Wong, 1/22/88, (PB88-213772, A06, MF-A01).

NCEER-88-0003 "Substructuring Techniques in the Time Domain for Primary-Secondary Structural Systems," by G.D. Manolis and G. Juhn, 2/10/88, (PB88-213780, A04, MF-A01).

NCEER-88-0004 "Iterative Seismic Analysis of Primary-Secondary Systems," by A. Singhal, L.D. Lutes and P.D. Spanos, 2/23/88, (PB88-213798, A04, MF-A01).

NCEER-88-0005 "Stochastic Finite Element Expansion for Random Media," by P.D. Spanos and R. Ghanem, 3/14/88, (PB88-213806, A03, MF-A01).

NCEER-88-0006 "Combining Structural Optimization and Structural Control," by F.Y. Cheng and C.P. Pantelides, 1/10/88, (PB88-213814, A05, MF-A01).

NCEER-88-0007 "Seismic Performance Assessment of Code-Designed Structures," by H.H-M. Hwang, J-W. Jaw and H-J. Shau, 3/20/88, (PB88-219423, A04, MF-A01). This report is only available through NTIS (see address given above).

NCEER-88-0008 "Reliability Analysis of Code-Designed Structures Under Natural Hazards," by H.H-M. Hwang, H. Ushiba and M. Shinozuka, 2/29/88, (PB88-229471, A07, MF-A01). This report is only available through NTIS (see address given above).

NCEER-88-0009 "Seismic Fragility Analysis of Shear Wall Structures," by J-W Jaw and H.H-M. Hwang, 4/30/88, (PB89-102867, A04, MF-A01).

NCEER-88-0010 "Base Isolation of a Multi-Story Building Under a Harmonic Ground Motion - A Comparison of Performances of Various Systems," by F-G Fan, G. Ahmadi and I.G. Tadjbakhsh, 5/18/88, (PB89-122238, A06, MF-A01). This report is only available through NTIS (see address given above).

NCEER-88-0011 "Seismic Floor Response Spectra for a Combined System by Green's Functions," by F.M. Lavelle, L.A. Bergman and P.D. Spanos, 5/1/88, (PB89-102875, A03, MF-A01).

NCEER-88-0012 "A New Solution Technique for Randomly Excited Hysteretic Structures," by G.Q. Cai and Y.K. Lin, 5/16/88, (PB89-102883, A03, MF-A01).

NCEER-88-0013 "A Study of Radiation Damping and Soil-Structure Interaction Effects in the Centrifuge," by K. Weissman, supervised by J.H. Prevost, 5/24/88, (PB89-144703, A06, MF-A01).

NCEER-88-0014 "Parameter Identification and Implementation of a Kinematic Plasticity Model for Frictional Soils," by J.H. Prevost and D.V. Griffiths, to be published.

NCEER-88-0015 "Two- and Three- Dimensional Dynamic Finite Element Analyses of the Long Valley Dam," by D.V. Griffiths and J.H. Prevost, 6/17/88, (PB89-144711, A04, MF-A01).

NCEER-88-0016 "Damage Assessment of Reinforced Concrete Structures in Eastern United States," by A.M. Reinhorn, M.J. Seidel, S.K. Kunnath and Y.J. Park, 6/15/88, (PB89-122220, A04, MF-A01). This report is only available through NTIS (see address given above).

NCEER-88-0017 "Dynamic Compliance of Vertically Loaded Strip Foundations in Multilayered Viscoelastic Soils," by S. Ahmad and A.S.M. Israil, 6/17/88, (PB89-102891, A04, MF-A01).

NCEER-88-0018 "An Experimental Study of Seismic Structural Response With Added Viscoelastic Dampers," by R.C. Lin, Z. Liang, T.T. Soong and R.H. Zhang, 6/30/88, (PB89-122212, A05, MF-A01). This report is available only through NTIS (see address given above).

NCEER-88-0019 "Experimental Investigation of Primary - Secondary System Interaction," by G.D. Manolis, G. Juhn and A.M. Reinhorn, 5/27/88, (PB89-122204, A04, MF-A01).

NCEER-88-0020 "A Response Spectrum Approach For Analysis of Nonclassically Damped Structures," by J.N. Yang, S. Sarkani and F.X. Long, 4/22/88, (PB89-102909, A04, MF-A01).

NCEER-88-0021 "Seismic Interaction of Structures and Soils: Stochastic Approach," by A.S. Veletsos and A.M. Prasad, 7/21/88, (PB89-122196, A04, MF-A01). This report is only available through NTIS (see address given above).

NCEER-88-0022 "Identification of the Serviceability Limit State and Detection of Seismic Structural Damage," by E. DiPasquale and A.S. Cakmak, 6/15/88, (PB89-122188, A05, MF-A01). This report is available only through NTIS (see address given above).

NCEER-88-0023 "Multi-Hazard Risk Analysis: Case of a Simple Offshore Structure," by B.K. Bhartia and E.H. Vanmarcke, 7/21/88, (PB89-145213, A05, MF-A01).

NCEER-88-0024 "Automated Seismic Design of Reinforced Concrete Buildings," by Y.S. Chung, C. Meyer and M. Shinozuka, 7/5/88, (PB89-122170, A06, MF-A01). This report is available only through NTIS (see address given above).

NCEER-88-0025 "Experimental Study of Active Control of MDOF Structures Under Seismic Excitations," by L.L. Chung, R.C. Lin, T.T. Soong and A.M. Reinhorn, 7/10/88, (PB89-122600, A04, MF-A01).

NCEER-88-0026 "Earthquake Simulation Tests of a Low-Rise Metal Structure," by J.S. Hwang, K.C. Chang, G.C. Lee and R.L. Ketter, 8/1/88, (PB89-102917, A04, MF-A01).

NCEER-88-0027 "Systems Study of Urban Response and Reconstruction Due to Catastrophic Earthquakes," by F. Kozin and H.K. Zhou, 9/22/88, (PB90-162348, A04, MF-A01).

NCEER-88-0028 "Seismic Fragility Analysis of Plane Frame Structures," by H.H-M. Hwang and Y.K. Low, 7/31/88, (PB89-131445, A06, MF-A01).

NCEER-88-0029 "Response Analysis of Stochastic Structures," by A. Kardara, C. Bucher and M. Shinozuka, 9/22/88, (PB89-174429, A04, MF-A01).

NCEER-88-0030 "Nonnormal Accelerations Due to Yielding in a Primary Structure," by D.C.K. Chen and L.D. Lutes, 9/19/88, (PB89-131437, A04, MF-A01).

NCEER-88-0031 "Design Approaches for Soil-Structure Interaction," by A.S. Veletsos, A.M. Prasad and Y. Tang, 12/30/88, (PB89-174437, A03, MF-A01). This report is available only through NTIS (see address given above).

NCEER-88-0032 "A Re-evaluation of Design Spectra for Seismic Damage Control," by C.J. Turkstra and A.G. Tallin, 11/7/88, (PB89-145221, A05, MF-A01).

NCEER-88-0033 "The Behavior and Design of Noncontact Lap Splices Subjected to Repeated Inelastic Tensile Loading," by V.E. Sagan, P. Gergely and R.N. White, 12/8/88, (PB89-163737, A08, MF-A01).

NCEER-88-0034 "Seismic Response of Pile Foundations," by S.M. Mamoon, P.K. Banerjee and S. Ahmad, 11/1/88, (PB89-145239, A04, MF-A01).

NCEER-88-0035 "Modeling of R/C Building Structures With Flexible Floor Diaphragms (IDARC2)," by A.M. Reinhorn, S.K. Kunnath and N. Panahshahi, 9/7/88, (PB89-207153, A07, MF-A01).

NCEER-88-0036 "Solution of the Dam-Reservoir Interaction Problem Using a Combination of FEM, BEM with Particular Integrals, Modal Analysis, and Substructuring," by C-S. Tsai, G.C. Lee and R.L. Ketter, 12/31/88, (PB89-207146, A04, MF-A01).

NCEER-88-0037 "Optimal Placement of Actuators for Structural Control," by F.Y. Cheng and C.P. Pantelides, 8/15/88, (PB89-162846, A05, MF-A01).

NCEER-88-0038 "Teflon Bearings in Aseismic Base Isolation: Experimental Studies and Mathematical Modeling," by A. Mokha, M.C. Constantinou and A.M. Reinhorn, 12/5/88, (PB89-218457, A10, MF-A01). This report is available only through NTIS (see address given above).

NCEER-88-0039 "Seismic Behavior of Flat Slab High-Rise Buildings in the New York City Area," by P. Weidlinger and M. Ettouney, 10/15/88, (PB90-145681, A04, MF-A01).

NCEER-88-0040 "Evaluation of the Earthquake Resistance of Existing Buildings in New York City," by P. Weidlinger and M. Ettouney, 10/15/88, to be published.

NCEER-88-0041 "Small-Scale Modeling Techniques for Reinforced Concrete Structures Subjected to Seismic Loads," by W. Kim, A. El-Attar and R.N. White, 11/22/88, (PB89-189625, A05, MF-A01).

NCEER-88-0042 "Modeling Strong Ground Motion from Multiple Event Earthquakes," by G.W. Ellis and A.S. Cakmak, 10/15/88, (PB89-174445, A03, MF-A01).

NCEER-88-0043 "Nonstationary Models of Seismic Ground Acceleration," by M. Grigoriu, S.E. Ruiz and E. Rosenblueth, 7/15/88, (PB89-189617, A04, MF-A01).

NCEER-88-0044 "SARCF User's Guide: Seismic Analysis of Reinforced Concrete Frames," by Y.S. Chung, C. Meyer and M. Shinozuka, 11/9/88, (PB89-174452, A08, MF-A01).

NCEER-88-0045 "First Expert Panel Meeting on Disaster Research and Planning," edited by J. Pantelic and J. Stoyle, 9/15/88, (PB89-174460, A05, MF-A01).

NCEER-88-0046 "Preliminary Studies of the Effect of Degrading Infill Walls on the Nonlinear Seismic Response of Steel Frames," by C.Z. Chrysostomou, P. Gergely and J.F. Abel, 12/19/88, (PB89-208383, A05, MF-A01).

NCEER-88-0047 "Reinforced Concrete Frame Component Testing Facility - Design, Construction, Instrumentation and Operation," by S.P. Pessiki, C. Conley, T. Bond, P. Gergely and R.N. White, 12/16/88, (PB89-174478, A04, MF-A01).

NCEER-89-0001 "Effects of Protective Cushion and Soil Compliancy on the Response of Equipment Within a Seismically Excited Building," by J.A. HoLung, 2/16/89, (PB89-207179, A04, MF-A01).

NCEER-89-0002 "Statistical Evaluation of Response Modification Factors for Reinforced Concrete Structures," by H.H-M. Hwang and J-W. Jaw, 2/17/89, (PB89-207187, A05, MF-A01).

NCEER-89-0003 "Hysteretic Columns Under Random Excitation," by G-Q. Cai and Y.K. Lin, 1/9/89, (PB89-196513, A03, MF-A01).

NCEER-89-0004 "Experimental Study of `Elephant Foot Bulge' Instability of Thin-Walled Metal Tanks," by Z-H. Jia and R.L. Ketter, 2/22/89, (PB89-207195, A03, MF-A01).

NCEER-89-0005 "Experiment on Performance of Buried Pipelines Across San Andreas Fault," by J. Isenberg, E. Richardson and T.D. O'Rourke, 3/10/89, (PB89-218440, A04, MF-A01). This report is available only through NTIS (see address given above).

NCEER-89-0006 "A Knowledge-Based Approach to Structural Design of Earthquake-Resistant Buildings," by M. Subramani, P. Gergely, C.H. Conley, J.F. Abel and A.H. Zaghw, 1/15/89, (PB89-218465, A06, MF-A01).

NCEER-89-0007 "Liquefaction Hazards and Their Effects on Buried Pipelines," by T.D. O'Rourke and P.A. Lane, 2/1/89, (PB89-218481, A09, MF-A01).

NCEER-89-0008 "Fundamentals of System Identification in Structural Dynamics," by H. Imai, C-B. Yun, O. Maruyama and M. Shinozuka, 1/26/89, (PB89-207211, A04, MF-A01).

NCEER-89-0009 "Effects of the 1985 Michoacan Earthquake on Water Systems and Other Buried Lifelines in Mexico," by A.G. Ayala and M.J. O'Rourke, 3/8/89, (PB89-207229, A06, MF-A01).

NCEER-89-R010 "NCEER Bibliography of Earthquake Education Materials," by K.E.K. Ross, Second Revision, 9/1/89, (PB90-125352, A05, MF-A01). This report is replaced by NCEER-92-0018.

NCEER-89-0011 "Inelastic Three-Dimensional Response Analysis of Reinforced Concrete Building Structures (IDARC-3D), Part I - Modeling," by S.K. Kunnath and A.M. Reinhorn, 4/17/89, (PB90-114612, A07, MF-A01). This report is available only through NTIS (see address given above).

NCEER-89-0012 "Recommended Modifications to ATC-14," by C.D. Poland and J.O. Malley, 4/12/89, (PB90-108648, A15, MF-A01).

NCEER-89-0013 "Repair and Strengthening of Beam-to-Column Connections Subjected to Earthquake Loading," by M. Corazao and A.J. Durrani, 2/28/89, (PB90-109885, A06, MF-A01).

NCEER-89-0014 "Program EXKAL2 for Identification of Structural Dynamic Systems," by O. Maruyama, C-B. Yun, M. Hoshiya and M. Shinozuka, 5/19/89, (PB90-109877, A09, MF-A01).

NCEER-89-0015 "Response of Frames With Bolted Semi-Rigid Connections, Part I - Experimental Study and Analytical Predictions," by P.J. DiCorso, A.M. Reinhorn, J.R. Dickerson, J.B. Radziminski and W.L. Harper, 6/1/89, to be published.

NCEER-89-0016 "ARMA Monte Carlo Simulation in Probabilistic Structural Analysis," by P.D. Spanos and M.P. Mignolet, 7/10/89, (PB90-109893, A03, MF-A01).

NCEER-89-P017 "Preliminary Proceedings from the Conference on Disaster Preparedness - The Place of Earthquake Education in Our Schools," Edited by K.E.K. Ross, 6/23/89, (PB90-108606, A03, MF-A01).

NCEER-89-0017 "Proceedings from the Conference on Disaster Preparedness - The Place of Earthquake Education in Our Schools," Edited by K.E.K. Ross, 12/31/89, (PB90-207895, A012, MF-A02). This report is available only through NTIS (see address given above).

NCEER-89-0018 "Multidimensional Models of Hysteretic Material Behavior for Vibration Analysis of Shape Memory Energy Absorbing Devices, by E.J. Graesser and F.A. Cozzarelli, 6/7/89, (PB90-164146, A04, MF-A01).

NCEER-89-0019 "Nonlinear Dynamic Analysis of Three-Dimensional Base Isolated Structures (3D-BASIS)," by S. Nagarajaiah, A.M. Reinhorn and M.C. Constantinou, 8/3/89, (PB90-161936, A06, MF-A01). This report has been replaced by NCEER-93-0011.

NCEER-89-0020 "Structural Control Considering Time-Rate of Control Forces and Control Rate Constraints," by F.Y. Cheng and C.P. Pantelides, 8/3/89, (PB90-120445, A04, MF-A01).

NCEER-89-0021 "Subsurface Conditions of Memphis and Shelby County," by K.W. Ng, T-S. Chang and H-H.M. Hwang, 7/26/89, (PB90-120437, A03, MF-A01).

NCEER-89-0022 "Seismic Wave Propagation Effects on Straight Jointed Buried Pipelines," by K. Elhmadi and M.J. O'Rourke, 8/24/89, (PB90-162322, A10, MF-A02).

NCEER-89-0023 "Workshop on Serviceability Analysis of Water Delivery Systems," edited by M. Grigoriu, 3/6/89, (PB90-127424, A03, MF-A01).

NCEER-89-0024 "Shaking Table Study of a 1/5 Scale Steel Frame Composed of Tapered Members," by K.C. Chang, J.S. Hwang and G.C. Lee, 9/18/89, (PB90-160169, A04, MF-A01).

NCEER-89-0025 "DYNA1D: A Computer Program for Nonlinear Seismic Site Response Analysis - Technical Documentation," by Jean H. Prevost, 9/14/89, (PB90-161944, A07, MF-A01). This report is available only through NTIS (see address given above).

NCEER-89-0026 "1:4 Scale Model Studies of Active Tendon Systems and Active Mass Dampers for Aseismic Protection," by A.M. Reinhorn, T.T. Soong, R.C. Lin, Y.P. Yang, Y. Fukao, H. Abe and M. Nakai, 9/15/89, (PB90-173246, A10, MF-A02). This report is available only through NTIS (see address given above).

NCEER-89-0027 "Scattering of Waves by Inclusions in a Nonhomogeneous Elastic Half Space Solved by Boundary Element Methods," by P.K. Hadley, A. Askar and A.S. Cakmak, 6/15/89, (PB90-145699, A07, MF-A01).

NCEER-89-0028 "Statistical Evaluation of Deflection Amplification Factors for Reinforced Concrete Structures," by H.H.M. Hwang, J-W. Jaw and A.L. Ch'ng, 8/31/89, (PB90-164633, A05, MF-A01).

NCEER-89-0029 "Bedrock Accelerations in Memphis Area Due to Large New Madrid Earthquakes," by H.H.M. Hwang, C.H.S. Chen and G. Yu, 11/7/89, (PB90-162330, A04, MF-A01).

NCEER-89-0030 "Seismic Behavior and Response Sensitivity of Secondary Structural Systems," by Y.Q. Chen and T.T. Soong, 10/23/89, (PB90-164658, A08, MF-A01).

NCEER-89-0031 "Random Vibration and Reliability Analysis of Primary-Secondary Structural Systems," by Y. Ibrahim, M. Grigoriu and T.T. Soong, 11/10/89, (PB90-161951, A04, MF-A01).

NCEER-89-0032 "Proceedings from the Second U.S. - Japan Workshop on Liquefaction, Large Ground Deformation and Their Effects on Lifelines, September 26-29, 1989," Edited by T.D. O'Rourke and M. Hamada, 12/1/89, (PB90-209388, A22, MF-A03).

NCEER-89-0033 "Deterministic Model for Seismic Damage Evaluation of Reinforced Concrete Structures," by J.M. Bracci, A.M. Reinhorn, J.B. Mander and S.K. Kunnath, 9/27/89, (PB91-108803, A06, MF-A01).

NCEER-89-0034 "On the Relation Between Local and Global Damage Indices," by E. DiPasquale and A.S. Cakmak, 8/15/89, (PB90-173865, A05, MF-A01).

NCEER-89-0035 "Cyclic Undrained Behavior of Nonplastic and Low Plasticity Silts," by A.J. Walker and H.E. Stewart, 7/26/89, (PB90-183518, A10, MF-A01).

NCEER-89-0036 "Liquefaction Potential of Surficial Deposits in the City of Buffalo, New York," by M. Budhu, R. Giese and L. Baumgrass, 1/17/89, (PB90-208455, A04, MF-A01).

NCEER-89-0037 "A Deterministic Assessment of Effects of Ground Motion Incoherence," by A.S. Veletsos and Y. Tang, 7/15/89, (PB90-164294, A03, MF-A01).

NCEER-89-0038 "Workshop on Ground Motion Parameters for Seismic Hazard Mapping," July 17-18, 1989, edited by R.V. Whitman, 12/1/89, (PB90-173923, A04, MF-A01).

NCEER-89-0039 "Seismic Effects on Elevated Transit Lines of the New York City Transit Authority," by C.J. Costantino, C.A. Miller and E. Heymsfield, 12/26/89, (PB90-207887, A06, MF-A01).

NCEER-89-0040 "Centrifugal Modeling of Dynamic Soil-Structure Interaction," by K. Weissman, Supervised by J.H. Prevost, 5/10/89, (PB90-207879, A07, MF-A01).

NCEER-89-0041 "Linearized Identification of Buildings With Cores for Seismic Vulnerability Assessment," by I-K. Ho and A.E. Aktan, 11/1/89, (PB90-251943, A07, MF-A01).

NCEER-90-0001 "Geotechnical and Lifeline Aspects of the October 17, 1989 Loma Prieta Earthquake in San Francisco," by T.D. O'Rourke, H.E. Stewart, F.T. Blackburn and T.S. Dickerman, 1/90, (PB90-208596, A05, MF-A01).

NCEER-90-0002 "Nonnormal Secondary Response Due to Yielding in a Primary Structure," by D.C.K. Chen and L.D. Lutes, 2/28/90, (PB90-251976, A07, MF-A01).

NCEER-90-0003 "Earthquake Education Materials for Grades K-12," by K.E.K. Ross, 4/16/90, (PB91-251984, A05, MF-A05). This report has been replaced by NCEER-92-0018.

NCEER-90-0004 "Catalog of Strong Motion Stations in Eastern North America," by R.W. Busby, 4/3/90, (PB90-251984, A05, MF-A01).

NCEER-90-0005 "NCEER Strong-Motion Data Base: A User Manual for the GeoBase Release (Version 1.0 for the Sun3)," by P. Friberg and K. Jacob, 3/31/90 (PB90-258062, A04, MF-A01).

NCEER-90-0006 "Seismic Hazard Along a Crude Oil Pipeline in the Event of an 1811-1812 Type New Madrid Earthquake," by H.H.M. Hwang and C-H.S. Chen, 4/16/90, (PB90-258054, A04, MF-A01).

NCEER-90-0007 "Site-Specific Response Spectra for Memphis Sheahan Pumping Station," by H.H.M. Hwang and C.S. Lee, 5/15/90, (PB91-108811, A05, MF-A01).

NCEER-90-0008 "Pilot Study on Seismic Vulnerability of Crude Oil Transmission Systems," by T. Ariman, R. Dobry, M. Grigoriu, F. Kozin, M. O'Rourke, T. O'Rourke and M. Shinozuka, 5/25/90, (PB91-108837, A06, MF-A01).

NCEER-90-0009 "A Program to Generate Site Dependent Time Histories: EQGEN," by G.W. Ellis, M. Srinivasan and A.S. Cakmak, 1/30/90, (PB91-108829, A04, MF-A01).

NCEER-90-0010 "Active Isolation for Seismic Protection of Operating Rooms," by M.E. Talbott, Supervised by M. Shinozuka, 6/8/9, (PB91-110205, A05, MF-A01).

NCEER-90-0011 "Program LINEARID for Identification of Linear Structural Dynamic Systems," by C-B. Yun and M. Shinozuka, 6/25/90, (PB91-110312, A08, MF-A01).

NCEER-90-0012 "Two-Dimensional Two-Phase Elasto-Plastic Seismic Response of Earth Dams," by A.N. Yiagos, Supervised by J.H. Prevost, 6/20/90, (PB91-110197, A13, MF-A02).

NCEER-90-0013 "Secondary Systems in Base-Isolated Structures: Experimental Investigation, Stochastic Response and Stochastic Sensitivity," by G.D. Manolis, G. Juhn, M.C. Constantinou and A.M. Reinhorn, 7/1/90, (PB91-110320, A08, MF-A01).

NCEER-90-0014 "Seismic Behavior of Lightly-Reinforced Concrete Column and Beam-Column Joint Details," by S.P. Pessiki, C.H. Conley, P. Gergely and R.N. White, 8/22/90, (PB91-108795, A11, MF-A02).

NCEER-90-0015 "Two Hybrid Control Systems for Building Structures Under Strong Earthquakes," by J.N. Yang and A. Danielians, 6/29/90, (PB91-125393, A04, MF-A01).

NCEER-90-0016 "Instantaneous Optimal Control with Acceleration and Velocity Feedback," by J.N. Yang and Z. Li, 6/29/90, (PB91-125401, A03, MF-A01).

NCEER-90-0017 "Reconnaissance Report on the Northern Iran Earthquake of June 21, 1990," by M. Mehrain, 10/4/90, (PB91-125377, A03, MF-A01).

NCEER-90-0018 "Evaluation of Liquefaction Potential in Memphis and Shelby County," by T.S. Chang, P.S. Tang, C.S. Lee and H. Hwang, 8/10/90, (PB91-125427, A09, MF-A01).

NCEER-90-0019 "Experimental and Analytical Study of a Combined Sliding Disc Bearing and Helical Steel Spring Isolation System," by M.C. Constantinou, A.S. Mokha and A.M. Reinhorn, 10/4/90, (PB91-125385, A06, MF-A01). This report is available only through NTIS (see address given above).

NCEER-90-0020 "Experimental Study and Analytical Prediction of Earthquake Response of a Sliding Isolation System with a Spherical Surface," by A.S. Mokha, M.C. Constantinou and A.M. Reinhorn, 10/11/90, (PB91-125419, A05, MF-A01).

NCEER-90-0021 "Dynamic Interaction Factors for Floating Pile Groups," by G. Gazetas, K. Fan, A. Kaynia and E. Kausel, 9/10/90, (PB91-170381, A05, MF-A01).

NCEER-90-0022 "Evaluation of Seismic Damage Indices for Reinforced Concrete Structures," by S. Rodriguez-Gomez and A.S. Cakmak, 9/30/90, PB91-171322, A06, MF-A01).

NCEER-90-0023 "Study of Site Response at a Selected Memphis Site," by H. Desai, S. Ahmad, E.S. Gazetas and M.R. Oh, 10/11/90, (PB91-196857, A03, MF-A01).

NCEER-90-0024 "A User's Guide to Strongmo: Version 1.0 of NCEER's Strong-Motion Data Access Tool for PCs and Terminals," by P.A. Friberg and C.A.T. Susch, 11/15/90, (PB91-171272, A03, MF-A01).

NCEER-90-0025 "A Three-Dimensional Analytical Study of Spatial Variability of Seismic Ground Motions," by L-L. Hong and A.H.-S. Ang, 10/30/90, (PB91-170399, A09, MF-A01).

NCEER-90-0026 "MUMOID User's Guide - A Program for the Identification of Modal Parameters," by S. Rodriguez-Gomez and E. DiPasquale, 9/30/90, (PB91-171298, A04, MF-A01).

NCEER-90-0027 "SARCF-II User's Guide - Seismic Analysis of Reinforced Concrete Frames," by S. Rodriguez-Gomez, Y.S. Chung and C. Meyer, 9/30/90, (PB91-171280, A05, MF-A01).

NCEER-90-0028 "Viscous Dampers: Testing, Modeling and Application in Vibration and Seismic Isolation," by N. Makris and M.C. Constantinou, 12/20/90 (PB91-190561, A06, MF-A01).

NCEER-90-0029 "Soil Effects on Earthquake Ground Motions in the Memphis Area," by H. Hwang, C.S. Lee, K.W. Ng and T.S. Chang, 8/2/90, (PB91-190751, A05, MF-A01).

NCEER-91-0001 "Proceedings from the Third Japan-U.S. Workshop on Earthquake Resistant Design of Lifeline Facilities and Countermeasures for Soil Liquefaction, December 17-19, 1990," edited by T.D. O'Rourke and M. Hamada, 2/1/91, (PB91-179259, A99, MF-A04).

NCEER-91-0002 "Physical Space Solutions of Non-Proportionally Damped Systems," by M. Tong, Z. Liang and G.C. Lee, 1/15/91, (PB91-179242, A04, MF-A01).

NCEER-91-0003 "Seismic Response of Single Piles and Pile Groups," by K. Fan and G. Gazetas, 1/10/91, (PB92-174994, A04, MF-A01).

NCEER-91-0004 "Damping of Structures: Part 1 - Theory of Complex Damping," by Z. Liang and G. Lee, 10/10/91, (PB92-197235, A12, MF-A03).

NCEER-91-0005 "3D-BASIS - Nonlinear Dynamic Analysis of Three Dimensional Base Isolated Structures: Part II," by S. Nagarajaiah, A.M. Reinhorn and M.C. Constantinou, 2/28/91, (PB91-190553, A07, MF-A01). This report has been replaced by NCEER-93-0011.

NCEER-91-0006 "A Multidimensional Hysteretic Model for Plasticity Deforming Metals in Energy Absorbing Devices," by E.J. Graesser and F.A. Cozzarelli, 4/9/91, (PB92-108364, A04, MF-A01).

NCEER-91-0007 "A Framework for Customizable Knowledge-Based Expert Systems with an Application to a KBES for Evaluating the Seismic Resistance of Existing Buildings," by E.G. Ibarra-Anaya and S.J. Fenves, 4/9/91, (PB91-210930, A08, MF-A01).

NCEER-91-0008 "Nonlinear Analysis of Steel Frames with Semi-Rigid Connections Using the Capacity Spectrum Method," by G.G. Deierlein, S-H. Hsieh, Y-J. Shen and J.F. Abel, 7/2/91, (PB92-113828, A05, MF-A01).

NCEER-91-0009 "Earthquake Education Materials for Grades K-12," by K.E.K. Ross, 4/30/91, (PB91-212142, A06, MF-A01). This report has been replaced by NCEER-92-0018.

NCEER-91-0010 "Phase Wave Velocities and Displacement Phase Differences in a Harmonically Oscillating Pile," by N. Makris and G. Gazetas, 7/8/91, (PB92-108356, A04, MF-A01).

NCEER-91-0011 "Dynamic Characteristics of a Full-Size Five-Story Steel Structure and a 2/5 Scale Model," by K.C. Chang, G.C. Yao, G.C. Lee, D.S. Hao and Y.C. Yeh," 7/2/91, (PB93-116648, A06, MF-A02).

NCEER-91-0012 "Seismic Response of a 2/5 Scale Steel Structure with Added Viscoelastic Dampers," by K.C. Chang, T.T. Soong, S-T. Oh and M.L. Lai, 5/17/91, (PB92-110816, A05, MF-A01).

NCEER-91-0013 "Earthquake Response of Retaining Walls; Full-Scale Testing and Computational Modeling," by S. Alampalli and A-W.M. Elgamal, 6/20/91, to be published.

NCEER-91-0014 "3D-BASIS-M: Nonlinear Dynamic Analysis of Multiple Building Base Isolated Structures," by P.C. Tsopelas, S. Nagarajaiah, M.C. Constantinou and A.M. Reinhorn, 5/28/91, (PB92-113885, A09, MF-A02).

NCEER-91-0015 "Evaluation of SEAOC Design Requirements for Sliding Isolated Structures," by D. Theodossiou and M.C. Constantinou, 6/10/91, (PB92-114602, A11, MF-A03).

NCEER-91-0016 "Closed-Loop Modal Testing of a 27-Story Reinforced Concrete Flat Plate-Core Building," by H.R. Somaprasad, T. Toksoy, H. Yoshiyuki and A.E. Aktan, 7/15/91, (PB92-129980, A07, MF-A02).

NCEER-91-0017 "Shake Table Test of a 1/6 Scale Two-Story Lightly Reinforced Concrete Building," by A.G. El-Attar, R.N. White and P. Gergely, 2/28/91, (PB92-222447, A06, MF-A02).

NCEER-91-0018 "Shake Table Test of a 1/8 Scale Three-Story Lightly Reinforced Concrete Building," by A.G. El-Attar, R.N. White and P. Gergely, 2/28/91, (PB93-116630, A08, MF-A02).

NCEER-91-0019 "Transfer Functions for Rigid Rectangular Foundations," by A.S. Veletsos, A.M. Prasad and W.H. Wu, 7/31/91, to be published.

NCEER-91-0020 "Hybrid Control of Seismic-Excited Nonlinear and Inelastic Structural Systems," by J.N. Yang, Z. Li and A. Danielians, 8/1/91, (PB92-143171, A06, MF-A02).

NCEER-91-0021 "The NCEER-91 Earthquake Catalog: Improved Intensity-Based Magnitudes and Recurrence Relations for U.S. Earthquakes East of New Madrid," by L. Seeber and J.G. Armbruster, 8/28/91, (PB92-176742, A06, MF-A02).

NCEER-91-0022 "Proceedings from the Implementation of Earthquake Planning and Education in Schools: The Need for Change - The Roles of the Changemakers," by K.E.K. Ross and F. Winslow, 7/23/91, (PB92-129998, A12, MF-A03).

NCEER-91-0023 "A Study of Reliability-Based Criteria for Seismic Design of Reinforced Concrete Frame Buildings," by H.H.M. Hwang and H-M. Hsu, 8/10/91, (PB92-140235, A09, MF-A02).

NCEER-91-0024 "Experimental Verification of a Number of Structural System Identification Algorithms," by R.G. Ghanem, H. Gavin and M. Shinozuka, 9/18/91, (PB92-176577, A18, MF-A04).

NCEER-91-0025 "Probabilistic Evaluation of Liquefaction Potential," by H.H.M. Hwang and C.S. Lee," 11/25/91, (PB92-143429, A05, MF-A01).

NCEER-91-0026 "Instantaneous Optimal Control for Linear, Nonlinear and Hysteretic Structures - Stable Controllers," by J.N. Yang and Z. Li, 11/15/91, (PB92-163807, A04, MF-A01).

NCEER-91-0027 "Experimental and Theoretical Study of a Sliding Isolation System for Bridges," by M.C. Constantinou, A. Kartoum, A.M. Reinhorn and P. Bradford, 11/15/91, (PB92-176973, A10, MF-A03).

NCEER-92-0001 "Case Studies of Liquefaction and Lifeline Performance During Past Earthquakes, Volume 1: Japanese Case Studies," Edited by M. Hamada and T. O'Rourke, 2/17/92, (PB92-197243, A18, MF-A04).

NCEER-92-0002 "Case Studies of Liquefaction and Lifeline Performance During Past Earthquakes, Volume 2: United States Case Studies," Edited by T. O'Rourke and M. Hamada, 2/17/92, (PB92-197250, A20, MF-A04).

NCEER-92-0003 "Issues in Earthquake Education," Edited by K. Ross, 2/3/92, (PB92-222389, A07, MF-A02).

NCEER-92-0004 "Proceedings from the First U.S. - Japan Workshop on Earthquake Protective Systems for Bridges," Edited by I.G. Buckle, 2/4/92, (PB94-142239, A99, MF-A06).

NCEER-92-0005 "Seismic Ground Motion from a Haskell-Type Source in a Multiple-Layered Half-Space," A.P. Theoharis, G. Deodatis and M. Shinozuka, 1/2/92, to be published.

NCEER-92-0006 "Proceedings from the Site Effects Workshop," Edited by R. Whitman, 2/29/92, (PB92-197201, A04, MF-A01).

NCEER-92-0007 "Engineering Evaluation of Permanent Ground Deformations Due to Seismically-Induced Liquefaction," by M.H. Baziar, R. Dobry and A-W.M. Elgamal, 3/24/92, (PB92-222421, A13, MF-A03).

NCEER-92-0008 "A Procedure for the Seismic Evaluation of Buildings in the Central and Eastern United States," by C.D. Poland and J.O. Malley, 4/2/92, (PB92-222439, A20, MF-A04).

NCEER-92-0009 "Experimental and Analytical Study of a Hybrid Isolation System Using Friction Controllable Sliding Bearings," by M.Q. Feng, S. Fujii and M. Shinozuka, 5/15/92, (PB93-150282, A06, MF-A02).

NCEER-92-0010 "Seismic Resistance of Slab-Column Connections in Existing Non-Ductile Flat-Plate Buildings," by A.J. Durrani and Y. Du, 5/18/92, (PB93-116812, A06, MF-A02).

NCEER-92-0011 "The Hysteretic and Dynamic Behavior of Brick Masonry Walls Upgraded by Ferrocement Coatings Under Cyclic Loading and Strong Simulated Ground Motion," by H. Lee and S.P. Prawel, 5/11/92, to be published.

NCEER-92-0012 "Study of Wire Rope Systems for Seismic Protection of Equipment in Buildings," by G.F. Demetriades, M.C. Constantinou and A.M. Reinhorn, 5/20/92, (PB93-116655, A08, MF-A02).

NCEER-92-0013 "Shape Memory Structural Dampers: Material Properties, Design and Seismic Testing," by P.R. Witting and F.A. Cozzarelli, 5/26/92, (PB93-116663, A05, MF-A01).

NCEER-92-0014 "Longitudinal Permanent Ground Deformation Effects on Buried Continuous Pipelines," by M.J. O'Rourke, and C. Nordberg, 6/15/92, (PB93-116671, A08, MF-A02).

NCEER-92-0015 "A Simulation Method for Stationary Gaussian Random Functions Based on the Sampling Theorem," by M. Grigoriu and S. Balopoulou, 6/11/92, (PB93-127496, A05, MF-A01).

NCEER-92-0016 "Gravity-Load-Designed Reinforced Concrete Buildings: Seismic Evaluation of Existing Construction and Detailing Strategies for Improved Seismic Resistance," by G.W. Hoffmann, S.K. Kunnath, A.M. Reinhorn and J.B. Mander, 7/15/92, (PB94-142007, A08, MF-A02).

NCEER-92-0017 "Observations on Water System and Pipeline Performance in the Limón Area of Costa Rica Due to the April 22, 1991 Earthquake," by M. O'Rourke and D. Ballantyne, 6/30/92, (PB93-126811, A06, MF-A02).

NCEER-92-0018 "Fourth Edition of Earthquake Education Materials for Grades K-12," Edited by K.E.K. Ross, 8/10/92, (PB93-114023, A07, MF-A02).

NCEER-92-0019 "Proceedings from the Fourth Japan-U.S. Workshop on Earthquake Resistant Design of Lifeline Facilities and Countermeasures for Soil Liquefaction," Edited by M. Hamada and T.D. O'Rourke, 8/12/92, (PB93-163939, A99, MF-E11).

NCEER-92-0020 "Active Bracing System: A Full Scale Implementation of Active Control," by A.M. Reinhorn, T.T. Soong, R.C. Lin, M.A. Riley, Y.P. Wang, S. Aizawa and M. Higashino, 8/14/92, (PB93-127512, A06, MF-A02).

NCEER-92-0021 "Empirical Analysis of Horizontal Ground Displacement Generated by Liquefaction-Induced Lateral Spreads," by S.F. Bartlett and T.L. Youd, 8/17/92, (PB93-188241, A06, MF-A02).

NCEER-92-0022 "IDARC Version 3.0: Inelastic Damage Analysis of Reinforced Concrete Structures," by S.K. Kunnath, A.M. Reinhorn and R.F. Lobo, 8/31/92, (PB93-227502, A07, MF-A02).

NCEER-92-0023 "A Semi-Empirical Analysis of Strong-Motion Peaks in Terms of Seismic Source, Propagation Path and Local Site Conditions, by M. Kamiyama, M.J. O'Rourke and R. Flores-Berrones, 9/9/92, (PB93-150266, A08, MF-A02).

NCEER-92-0024 "Seismic Behavior of Reinforced Concrete Frame Structures with Nonductile Details, Part I: Summary of Experimental Findings of Full Scale Beam-Column Joint Tests," by A. Beres, R.N. White and P. Gergely, 9/30/92, (PB93-227783, A05, MF-A01).

NCEER-92-0025 "Experimental Results of Repaired and Retrofitted Beam-Column Joint Tests in Lightly Reinforced Concrete Frame Buildings," by A. Beres, S. El-Borgi, R.N. White and P. Gergely, 10/29/92, (PB93-227791, A05, MF-A01).

NCEER-92-0026 "A Generalization of Optimal Control Theory: Linear and Nonlinear Structures," by J.N. Yang, Z. Li and S. Vongchavalitkul, 11/2/92, (PB93-188621, A05, MF-A01).

NCEER-92-0027 "Seismic Resistance of Reinforced Concrete Frame Structures Designed Only for Gravity Loads: Part I - Design and Properties of a One-Third Scale Model Structure," by J.M. Bracci, A.M. Reinhorn and J.B. Mander, 12/1/92, (PB94-104502, A08, MF-A02).

NCEER-92-0028 "Seismic Resistance of Reinforced Concrete Frame Structures Designed Only for Gravity Loads: Part II - Experimental Performance of Subassemblages," by L.E. Aycardi, J.B. Mander and A.M. Reinhorn, 12/1/92, (PB94-104510, A08, MF-A02).

NCEER-92-0029 "Seismic Resistance of Reinforced Concrete Frame Structures Designed Only for Gravity Loads: Part III - Experimental Performance and Analytical Study of a Structural Model," by J.M. Bracci, A.M. Reinhorn and J.B. Mander, 12/1/92, (PB93-227528, A09, MF-A01).

NCEER-92-0030 "Evaluation of Seismic Retrofit of Reinforced Concrete Frame Structures: Part I - Experimental Performance of Retrofitted Subassemblages," by D. Choudhuri, J.B. Mander and A.M. Reinhorn, 12/8/92, (PB93-198307, A07, MF-A02).

NCEER-92-0031 "Evaluation of Seismic Retrofit of Reinforced Concrete Frame Structures: Part II - Experimental Performance and Analytical Study of a Retrofitted Structural Model," by J.M. Bracci, A.M. Reinhorn and J.B. Mander, 12/8/92, (PB93-198315, A09, MF-A03).

NCEER-92-0032 "Experimental and Analytical Investigation of Seismic Response of Structures with Supplemental Fluid Viscous Dampers," by M.C. Constantinou and M.D. Symans, 12/21/92, (PB93-191435, A10, MF-A03). This report is available only through NTIS (see address given above).

NCEER-92-0033 "Reconnaissance Report on the Cairo, Egypt Earthquake of October 12, 1992," by M. Khater, 12/23/92, (PB93-188621, A03, MF-A01).

NCEER-92-0034 "Low-Level Dynamic Characteristics of Four Tall Flat-Plate Buildings in New York City," by H. Gavin, S. Yuan, J. Grossman, E. Pekelis and K. Jacob, 12/28/92, (PB93-188217, A07, MF-A02).

NCEER-93-0001 "An Experimental Study on the Seismic Performance of Brick-Infilled Steel Frames With and Without Retrofit," by J.B. Mander, B. Nair, K. Wojtkowski and J. Ma, 1/29/93, (PB93-227510, A07, MF-A02).

NCEER-93-0002 "Social Accounting for Disaster Preparedness and Recovery Planning," by S. Cole, E. Pantoja and V. Razak, 2/22/93, (PB94-142114, A12, MF-A03).

NCEER-93-0003 "Assessment of 1991 NEHRP Provisions for Nonstructural Components and Recommended Revisions," by T.T. Soong, G. Chen, Z. Wu, R-H. Zhang and M. Grigoriu, 3/1/93, (PB93-188639, A06, MF-A02).

NCEER-93-0004 "Evaluation of Static and Response Spectrum Analysis Procedures of SEAOC/UBC for Seismic Isolated Structures," by C.W. Winters and M.C. Constantinou, 3/23/93, (PB93-198299, A10, MF-A03).

NCEER-93-0005 "Earthquakes in the Northeast - Are We Ignoring the Hazard? A Workshop on Earthquake Science and Safety for Educators," edited by K.E.K. Ross, 4/2/93, (PB94-103066, A09, MF-A02).

NCEER-93-0006 "Inelastic Response of Reinforced Concrete Structures with Viscoelastic Braces," by R.F. Lobo, J.M. Bracci, K.L. Shen, A.M. Reinhorn and T.T. Soong, 4/5/93, (PB93-227486, A05, MF-A02).

NCEER-93-0007 "Seismic Testing of Installation Methods for Computers and Data Processing Equipment," by K. Kosar, T.T. Soong, K.L. Shen, J.A. HoLung and Y.K. Lin, 4/12/93, (PB93-198299, A07, MF-A02).

NCEER-93-0008 "Retrofit of Reinforced Concrete Frames Using Added Dampers," by A. Reinhorn, M. Constantinou and C. Li, to be published.

NCEER-93-0009 "Seismic Behavior and Design Guidelines for Steel Frame Structures with Added Viscoelastic Dampers," by K.C. Chang, M.L. Lai, T.T. Soong, D.S. Hao and Y.C. Yeh, 5/1/93, (PB94-141959, A07, MF-A02).

NCEER-93-0010 "Seismic Performance of Shear-Critical Reinforced Concrete Bridge Piers," by J.B. Mander, S.M. Waheed, M.T.A. Chaudhary and S.S. Chen, 5/12/93, (PB93-227494, A08, MF-A02).

NCEER-93-0011 "3D-BASIS-TABS: Computer Program for Nonlinear Dynamic Analysis of Three Dimensional Base Isolated Structures," by S. Nagarajaiah, C. Li, A.M. Reinhorn and M.C. Constantinou, 8/2/93, (PB94-141819, A09, MF-A02).

NCEER-93-0012 "Effects of Hydrocarbon Spills from an Oil Pipeline Break on Ground Water," by O.J. Helweg and H.H.M. Hwang, 8/3/93, (PB94-141942, A06, MF-A02).

NCEER-93-0013 "Simplified Procedures for Seismic Design of Nonstructural Components and Assessment of Current Code Provisions," by M.P. Singh, L.E. Suarez, E.E. Matheu and G.O. Maldonado, 8/4/93, (PB94-141827, A09, MF-A02).

NCEER-93-0014 "An Energy Approach to Seismic Analysis and Design of Secondary Systems," by G. Chen and T.T. Soong, 8/6/93, (PB94-142767, A11, MF-A03).

NCEER-93-0015 "Proceedings from School Sites: Becoming Prepared for Earthquakes - Commemorating the Third Anniversary of the Loma Prieta Earthquake," Edited by F.E. Winslow and K.E.K. Ross, 8/16/93, (PB94-154275, A16, MF-A02).

NCEER-93-0016 "Reconnaissance Report of Damage to Historic Monuments in Cairo, Egypt Following the October 12, 1992 Dahshur Earthquake," by D. Sykora, D. Look, G. Croci, E. Karaesmen and E. Karaesmen, 8/19/93, (PB94-142221, A08, MF-A02).

NCEER-93-0017 "The Island of Guam Earthquake of August 8, 1993," by S.W. Swan and S.K. Harris, 9/30/93, (PB94-141843, A04, MF-A01).

NCEER-93-0018 "Engineering Aspects of the October 12, 1992 Egyptian Earthquake," by A.W. Elgamal, M. Amer, K. Adalier and A. Abul-Fadl, 10/7/93, (PB94-141983, A05, MF-A01).

NCEER-93-0019 "Development of an Earthquake Motion Simulator and its Application in Dynamic Centrifuge Testing," by I. Krstelj, Supervised by J.H. Prevost, 10/23/93, (PB94-181773, A-10, MF-A03).

NCEER-93-0020 "NCEER-Taisei Corporation Research Program on Sliding Seismic Isolation Systems for Bridges: Experimental and Analytical Study of a Friction Pendulum System (FPS)," by M.C. Constantinou, P. Tsopelas, Y-S. Kim and S. Okamoto, 11/1/93, (PB94-142775, A08, MF-A02).

NCEER-93-0021 "Finite Element Modeling of Elastomeric Seismic Isolation Bearings," by L.J. Billings, Supervised by R. Shepherd, 11/8/93, to be published.

NCEER-93-0022 "Seismic Vulnerability of Equipment in Critical Facilities: Life-Safety and Operational Consequences," by K. Porter, G.S. Johnson, M.M. Zadeh, C. Scawthorn and S. Eder, 11/24/93, (PB94-181765, A16, MF-A03).

NCEER-93-0023 "Hokkaido Nansei-oki, Japan Earthquake of July 12, 1993, by P.I. Yanev and C.R. Scawthorn, 12/23/93, (PB94-181500, A07, MF-A01).

NCEER-94-0001 "An Evaluation of Seismic Serviceability of Water Supply Networks with Application to the San Francisco Auxiliary Water Supply System," by I. Markov, Supervised by M. Grigoriu and T. O'Rourke, 1/21/94, (PB94-204013, A07, MF-A02).

NCEER-94-0002 "NCEER-Taisei Corporation Research Program on Sliding Seismic Isolation Systems for Bridges: Experimental and Analytical Study of Systems Consisting of Sliding Bearings, Rubber Restoring Force Devices and Fluid Dampers," Volumes I and II, by P. Tsopelas, S. Okamoto, M.C. Constantinou, D. Ozaki and S. Fujii, 2/4/94, (PB94-181740, A09, MF-A02 and PB94-181757, A12, MF-A03).

NCEER-94-0003 "A Markov Model for Local and Global Damage Indices in Seismic Analysis," by S. Rahman and M. Grigoriu, 2/18/94, (PB94-206000, A12, MF-A03).

NCEER-94-0004 "Proceedings from the NCEER Workshop on Seismic Response of Masonry Infills," edited by D.P. Abrams, 3/1/94, (PB94-180783, A07, MF-A02).

NCEER-94-0005 "The Northridge, California Earthquake of January 17, 1994: General Reconnaissance Report," edited by J.D. Goltz, 3/11/94, (PB94-193943, A10, MF-A03).

NCEER-94-0006 "Seismic Energy Based Fatigue Damage Analysis of Bridge Columns: Part I - Evaluation of Seismic Capacity," by G.A. Chang and J.B. Mander, 3/14/94, (PB94-219185, A11, MF-A03).

NCEER-94-0007 "Seismic Isolation of Multi-Story Frame Structures Using Spherical Sliding Isolation Systems," by T.M. Al-Hussaini, V.A. Zayas and M.C. Constantinou, 3/17/94, (PB94-193745, A09, MF-A02).

NCEER-94-0008 "The Northridge, California Earthquake of January 17, 1994: Performance of Highway Bridges," edited by I.G. Buckle, 3/24/94, (PB94-193851, A06, MF-A02).

NCEER-94-0009 "Proceedings of the Third U.S.-Japan Workshop on Earthquake Protective Systems for Bridges," edited by I.G. Buckle and I. Friedland, 3/31/94, (PB94-195815, A99, MF-A06).

NCEER-94-0010 "3D-BASIS-ME: Computer Program for Nonlinear Dynamic Analysis of Seismically Isolated Single and Multiple Structures and Liquid Storage Tanks," by P.C. Tsopelas, M.C. Constantinou and A.M. Reinhorn, 4/12/94, (PB94-204922, A09, MF-A02).

NCEER-94-0011 "The Northridge, California Earthquake of January 17, 1994: Performance of Gas Transmission Pipelines," by T.D. O'Rourke and M.C. Palmer, 5/16/94, (PB94-204989, A05, MF-A01).

NCEER-94-0012 "Feasibility Study of Replacement Procedures and Earthquake Performance Related to Gas Transmission Pipelines," by T.D. O'Rourke and M.C. Palmer, 5/25/94, (PB94-206638, A09, MF-A02).

NCEER-94-0013 "Seismic Energy Based Fatigue Damage Analysis of Bridge Columns: Part II - Evaluation of Seismic Demand," by G.A. Chang and J.B. Mander, 6/1/94, (PB95-18106, A08, MF-A02).

NCEER-94-0014 "NCEER-Taisei Corporation Research Program on Sliding Seismic Isolation Systems for Bridges: Experimental and Analytical Study of a System Consisting of Sliding Bearings and Fluid Restoring Force/Damping Devices," by P. Tsopelas and M.C. Constantinou, 6/13/94, (PB94-219144, A10, MF-A03).

NCEER-94-0015 "Generation of Hazard-Consistent Fragility Curves for Seismic Loss Estimation Studies," by H. Hwang and J-R. Huo, 6/14/94, (PB95-181996, A09, MF-A02).

NCEER-94-0016 "Seismic Study of Building Frames with Added Energy-Absorbing Devices," by W.S. Pong, C.S. Tsai and G.C. Lee, 6/20/94, (PB94-219136, A10, A03).

NCEER-94-0017 "Sliding Mode Control for Seismic-Excited Linear and Nonlinear Civil Engineering Structures," by J. Yang, J. Wu, A. Agrawal and Z. Li, 6/21/94, (PB95-138483, A06, MF-A02).

NCEER-94-0018 "3D-BASIS-TABS Version 2.0: Computer Program for Nonlinear Dynamic Analysis of Three Dimensional Base Isolated Structures," by A.M. Reinhorn, S. Nagarajaiah, M.C. Constantinou, P. Tsopelas and R. Li, 6/22/94, (PB95-182176, A08, MF-A02).

NCEER-94-0019 "Proceedings of the International Workshop on Civil Infrastructure Systems: Application of Intelligent Systems and Advanced Materials on Bridge Systems," Edited by G.C. Lee and K.C. Chang, 7/18/94, (PB95-252474, A20, MF-A04).

NCEER-94-0020 "Study of Seismic Isolation Systems for Computer Floors," by V. Lambrou and M.C. Constantinou, 7/19/94, (PB95-138533, A10, MF-A03).

NCEER-94-0021 "Proceedings of the U.S.-Italian Workshop on Guidelines for Seismic Evaluation and Rehabilitation of Unreinforced Masonry Buildings," Edited by D.P. Abrams and G.M. Calvi, 7/20/94, (PB95-138749, A13, MF-A03).

NCEER-94-0022 "NCEER-Taisei Corporation Research Program on Sliding Seismic Isolation Systems for Bridges: Experimental and Analytical Study of a System Consisting of Lubricated PTFE Sliding Bearings and Mild Steel Dampers," by P. Tsopelas and M.C. Constantinou, 7/22/94, (PB95-182184, A08, MF-A02).

NCEER-94-0023 “Development of Reliability-Based Design Criteria for Buildings Under Seismic Load,” by Y.K. Wen, H. Hwang and M. Shinozuka, 8/1/94, (PB95-211934, A08, MF-A02).

NCEER-94-0024 “Experimental Verification of Acceleration Feedback Control Strategies for an Active Tendon System,” by S.J. Dyke, B.F. Spencer, Jr., P. Quast, M.K. Sain, D.C. Kaspari, Jr. and T.T. Soong, 8/29/94, (PB95-212320, A05, MF-A01).

NCEER-94-0025 “Seismic Retrofitting Manual for Highway Bridges,” Edited by I.G. Buckle and I.F. Friedland, published by the Federal Highway Administration (PB95-212676, A15, MF-A03).

NCEER-94-0026 “Proceedings from the Fifth U.S.-Japan Workshop on Earthquake Resistant Design of Lifeline Facilities and Countermeasures Against Soil Liquefaction,” Edited by T.D. O’Rourke and M. Hamada, 11/7/94, (PB95-220802, A99, MF-E08).

NCEER-95-0001 "Experimental and Analytical Investigation of Seismic Retrofit of Structures with Supplemental Damping: Part 1 - Fluid Viscous Damping Devices," by A.M. Reinhorn, C. Li and M.C. Constantinou, 1/3/95, (PB95-266599, A09, MF-A02).

NCEER-95-0002 "Experimental and Analytical Study of Low-Cycle Fatigue Behavior of Semi-Rigid Top-And-Seat Angle Connections," by G. Pekcan, J.B. Mander and S.S. Chen, 1/5/95, (PB95-220042, A07, MF-A02).

NCEER-95-0003 "NCEER-ATC Joint Study on Fragility of Buildings," by T. Anagnos, C. Rojahn and A.S. Kiremidjian, 1/20/95, (PB95-220026, A06, MF-A02).

NCEER-95-0004 "Nonlinear Control Algorithms for Peak Response Reduction," by Z. Wu, T.T. Soong, V. Gattulli and R.C. Lin, 2/16/95, (PB95-220349, A05, MF-A01).

NCEER-95-0005 "Pipeline Replacement Feasibility Study: A Methodology for Minimizing Seismic and Corrosion Risks to Underground Natural Gas Pipelines," by R.T. Eguchi, H.A. Seligson and D.G. Honegger, 3/2/95, (PB95-252326, A06, MF-A02).

NCEER-95-0006 "Evaluation of Seismic Performance of an 11-Story Frame Building During the 1994 Northridge Earthquake," by F. Naeim, R. DiSulio, K. Benuska, A. Reinhorn and C. Li, to be published.

NCEER-95-0007 "Prioritization of Bridges for Seismic Retrofitting," by N. Basöz and A.S. Kiremidjian, 4/24/95, (PB95-252300, A08, MF-A02).

NCEER-95-0008 "Method for Developing Motion Damage Relationships for Reinforced Concrete Frames," by A. Singhal and A.S. Kiremidjian, 5/11/95, (PB95-266607, A06, MF-A02).

NCEER-95-0009 "Experimental and Analytical Investigation of Seismic Retrofit of Structures with Supplemental Damping: Part II - Friction Devices," by C. Li and A.M. Reinhorn, 7/6/95, (PB96-128087, A11, MF-A03).

NCEER-95-0010 "Experimental Performance and Analytical Study of a Non-Ductile Reinforced Concrete Frame Structure Retrofitted with Elastomeric Spring Dampers," by G. Pekcan, J.B. Mander and S.S. Chen, 7/14/95, (PB96-137161, A08, MF-A02).

NCEER-95-0011 "Development and Experimental Study of Semi-Active Fluid Damping Devices for Seismic Protection of Structures," by M.D. Symans and M.C. Constantinou, 8/3/95, (PB96-136940, A23, MF-A04).

NCEER-95-0012 "Real-Time Structural Parameter Modification (RSPM): Development of Innervated Structures," by Z. Liang, M. Tong and G.C. Lee, 4/11/95, (PB96-137153, A06, MF-A01).

NCEER-95-0013 "Experimental and Analytical Investigation of Seismic Retrofit of Structures with Supplemental Damping: Part III - Viscous Damping Walls," by A.M. Reinhorn and C. Li, 10/1/95, (PB96-176409, A11, MF-A03).

NCEER-95-0014 "Seismic Fragility Analysis of Equipment and Structures in a Memphis Electric Substation," by J-R. Huo and H.H.M. Hwang, 8/10/95, (PB96-128087, A09, MF-A02).

NCEER-95-0015 "The Hanshin-Awaji Earthquake of January 17, 1995: Performance of Lifelines," Edited by M. Shinozuka, 11/3/95, (PB96-176383, A15, MF-A03).

NCEER-95-0016 "Highway Culvert Performance During Earthquakes," by T.L. Youd and C.J. Beckman, available as NCEER-96-0015.

NCEER-95-0017 "The Hanshin-Awaji Earthquake of January 17, 1995: Performance of Highway Bridges," Edited by I.G. Buckle, 12/1/95, to be published.

NCEER-95-0018 "Modeling of Masonry Infill Panels for Structural Analysis," by A.M. Reinhorn, A. Madan, R.E. Valles, Y. Reichmann and J.B. Mander, 12/8/95, (PB97-110886, MF-A01, A06).

NCEER-95-0019 "Optimal Polynomial Control for Linear and Nonlinear Structures," by A.K. Agrawal and J.N. Yang, 12/11/95, (PB96-168737, A07, MF-A02).

NCEER-95-0020 "Retrofit of Non-Ductile Reinforced Concrete Frames Using Friction Dampers," by R.S. Rao, P. Gergely and R.N. White, 12/22/95, (PB97-133508, A10, MF-A02).

NCEER-95-0021 "Parametric Results for Seismic Response of Pile-Supported Bridge Bents," by G. Mylonakis, A. Nikolaou and G. Gazetas, 12/22/95, (PB97-100242, A12, MF-A03).

NCEER-95-0022 "Kinematic Bending Moments in Seismically Stressed Piles," by A. Nikolaou, G. Mylonakis and G. Gazetas, 12/23/95, (PB97-113914, MF-A03, A13).

NCEER-96-0001 "Dynamic Response of Unreinforced Masonry Buildings with Flexible Diaphragms," by A.C. Costley and D.P. Abrams," 10/10/96, (PB97-133573, MF-A03, A15).

NCEER-96-0002 "State of the Art Review: Foundations and Retaining Structures," by I. Po Lam, to be published.

NCEER-96-0003 "Ductility of Rectangular Reinforced Concrete Bridge Columns with Moderate Confinement," by N. Wehbe, M. Saiidi, D. Sanders and B. Douglas, 11/7/96, (PB97-133557, A06, MF-A02).

NCEER-96-0004 "Proceedings of the Long-Span Bridge Seismic Research Workshop," edited by I.G. Buckle and I.M. Friedland, to be published.

NCEER-96-0005 "Establish Representative Pier Types for Comprehensive Study: Eastern United States," by J. Kulicki and Z. Prucz, 5/28/96, (PB98-119217, A07, MF-A02).

NCEER-96-0006 "Establish Representative Pier Types for Comprehensive Study: Western United States," by R. Imbsen, R.A. Schamber and T.A. Osterkamp, 5/28/96, (PB98-118607, A07, MF-A02).

NCEER-96-0007 "Nonlinear Control Techniques for Dynamical Systems with Uncertain Parameters," by R.G. Ghanem and M.I. Bujakov, 5/27/96, (PB97-100259, A17, MF-A03).

NCEER-96-0008 "Seismic Evaluation of a 30-Year Old Non-Ductile Highway Bridge Pier and Its Retrofit," by J.B. Mander, B. Mahmoodzadegan, S. Bhadra and S.S. Chen, 5/31/96, (PB97-110902, MF-A03, A10).

NCEER-96-0009 "Seismic Performance of a Model Reinforced Concrete Bridge Pier Before and After Retrofit," by J.B. Mander, J.H. Kim and C.A. Ligozio, 5/31/96, (PB97-110910, MF-A02, A10).

NCEER-96-0010 "IDARC2D Version 4.0: A Computer Program for the Inelastic Damage Analysis of Buildings," by R.E. Valles, A.M. Reinhorn, S.K. Kunnath, C. Li and A. Madan, 6/3/96, (PB97-100234, A17, MF-A03).

NCEER-96-0011 "Estimation of the Economic Impact of Multiple Lifeline Disruption: Memphis Light, Gas and Water Division Case Study," by S.E. Chang, H.A. Seligson and R.T. Eguchi, 8/16/96, (PB97-133490, A11, MF-A03).

NCEER-96-0012 "Proceedings from the Sixth Japan-U.S. Workshop on Earthquake Resistant Design of Lifeline Facilities and Countermeasures Against Soil Liquefaction, Edited by M. Hamada and T. O'Rourke, 9/11/96, (PB97-133581, A99, MF-A06).

NCEER-96-0013 "Chemical Hazards, Mitigation and Preparedness in Areas of High Seismic Risk: A Methodology for Estimating the Risk of Post-Earthquake Hazardous Materials Release," by H.A. Seligson, R.T. Eguchi, K.J. Tierney and K. Richmond, 11/7/96, (PB97-133565, MF-A02, A08).

NCEER-96-0014 "Response of Steel Bridge Bearings to Reversed Cyclic Loading," by J.B. Mander, D-K. Kim, S.S. Chen and G.J. Premus, 11/13/96, (PB97-140735, A12, MF-A03).

NCEER-96-0015 "Highway Culvert Performance During Past Earthquakes," by T.L. Youd and C.J. Beckman, 11/25/96, (PB97-133532, A06, MF-A01).

NCEER-97-0001 "Evaluation, Prevention and Mitigation of Pounding Effects in Building Structures," by R.E. Valles and A.M. Reinhorn, 2/20/97, (PB97-159552, A14, MF-A03).

NCEER-97-0002 "Seismic Design Criteria for Bridges and Other Highway Structures," by C. Rojahn, R. Mayes, D.G. Anderson, J. Clark, J.H. Hom, R.V. Nutt and M.J. O'Rourke, 4/30/97, (PB97-194658, A06, MF-A03).

NCEER-97-0003 “Proceedings of the U.S.-Italian Workshop on Seismic Evaluation and Retrofit,” Edited by D.P. Abrams and G.M. Calvi, 3/19/97, (PB97-194666, A13, MF-A03).

NCEER-97-0004 "Investigation of Seismic Response of Buildings with Linear and Nonlinear Fluid Viscous Dampers," by A.A. Seleemah and M.C. Constantinou, 5/21/97, (PB98-109002, A15, MF-A03).

NCEER-97-0005 "Proceedings of the Workshop on Earthquake Engineering Frontiers in Transportation Facilities," edited by G.C. Lee and I.M. Friedland, 8/29/97, (PB98-128911, A25, MR-A04).

NCEER-97-0006 "Cumulative Seismic Damage of Reinforced Concrete Bridge Piers," by S.K. Kunnath, A. El-Bahy, A. Taylor and W. Stone, 9/2/97, (PB98-108814, A11, MF-A03).

NCEER-97-0007 "Structural Details to Accommodate Seismic Movements of Highway Bridges and Retaining Walls," by R.A. Imbsen, R.A. Schamber, E. Thorkildsen, A. Kartoum, B.T. Martin, T.N. Rosser and J.M. Kulicki, 9/3/97, (PB98-108996, A09, MF-A02).

NCEER-97-0008 "A Method for Earthquake Motion-Damage Relationships with Application to Reinforced Concrete Frames," by A. Singhal and A.S. Kiremidjian, 9/10/97, (PB98-108988, A13, MF-A03).

NCEER-97-0009 "Seismic Analysis and Design of Bridge Abutments Considering Sliding and Rotation," by K. Fishman and R. Richards, Jr., 9/15/97, (PB98-108897, A06, MF-A02).

NCEER-97-0010 "Proceedings of the FHWA/NCEER Workshop on the National Representation of Seismic Ground Motion for New and Existing Highway Facilities," edited by I.M. Friedland, M.S. Power and R.L. Mayes, 9/22/97, (PB98-128903, A21, MF-A04).

NCEER-97-0011 "Seismic Analysis for Design or Retrofit of Gravity Bridge Abutments," by K.L. Fishman, R. Richards, Jr. and R.C. Divito, 10/2/97, (PB98-128937, A08, MF-A02).

NCEER-97-0012 "Evaluation of Simplified Methods of Analysis for Yielding Structures," by P. Tsopelas, M.C. Constantinou, C.A. Kircher and A.S. Whittaker, 10/31/97, (PB98-128929, A10, MF-A03).

NCEER-97-0013 "Seismic Design of Bridge Columns Based on Control and Repairability of Damage," by C-T. Cheng and J.B. Mander, 12/8/97, (PB98-144249, A11, MF-A03).

NCEER-97-0014 "Seismic Resistance of Bridge Piers Based on Damage Avoidance Design," by J.B. Mander and C-T. Cheng, 12/10/97, (PB98-144223, A09, MF-A02).

NCEER-97-0015 “Seismic Response of Nominally Symmetric Systems with Strength Uncertainty,” by S. Balopoulou and M. Grigoriu, 12/23/97, (PB98-153422, A11, MF-A03).

NCEER-97-0016 “Evaluation of Seismic Retrofit Methods for Reinforced Concrete Bridge Columns,” by T.J. Wipf, F.W. Klaiber and F.M. Russo, 12/28/97, (PB98-144215, A12, MF-A03).

NCEER-97-0017 “Seismic Fragility of Existing Conventional Reinforced Concrete Highway Bridges,” by C.L. Mullen and A.S. Cakmak, 12/30/97, (PB98-153406, A08, MF-A02).

NCEER-97-0018 “Loss Asssessment of Memphis Buildings,” edited by D.P. Abrams and M. Shinozuka, 12/31/97, (PB98-144231, A13, MF-A03).

NCEER-97-0019 “Seismic Evaluation of Frames with Infill Walls Using Quasi-static Experiments,” by K.M. Mosalam, R.N. White and P. Gergely, 12/31/97, (PB98-153455, A07, MF-A02).

NCEER-97-0020 “Seismic Evaluation of Frames with Infill Walls Using Pseudo-dynamic Experiments,” by K.M. Mosalam, R.N. White and P. Gergely, 12/31/97, (PB98-153430, A07, MF-A02).

NCEER-97-0021 “Computational Strategies for Frames with Infill Walls: Discrete and Smeared Crack Analyses and Seismic Fragility,” by K.M. Mosalam, R.N. White and P. Gergely, 12/31/97, (PB98-153414, A10, MF-A02).

NCEER-97-0022 "Proceedings of the NCEER Workshop on Evaluation of Liquefaction Resistance of Soils," edited by T.L. Youd and I.M. Idriss, 12/31/97, (PB98-155617, A15, MF-A03).

MCEER-98-0001 "Extraction of Nonlinear Hysteretic Properties of Seismically Isolated Bridges from Quick-Release Field Tests," by Q. Chen, B.M. Douglas, E.M. Maragakis and I.G. Buckle, 5/26/98, (PB99-118838, A06, MF-A01).

MCEER-98-0002 "Methodologies for Evaluating the Importance of Highway Bridges," by A. Thomas, S. Eshenaur and J. Kulicki, 5/29/98, (PB99-118846, A10, MF-A02).

MCEER-98-0003 "Capacity Design of Bridge Piers and the Analysis of Overstrength," by J.B. Mander, A. Dutta and P. Goel, 6/1/98, (PB99-118853, A09, MF-A02).

MCEER-98-0004 "Evaluation of Bridge Damage Data from the Loma Prieta and Northridge, California Earthquakes," by N. Basoz and A. Kiremidjian, 6/2/98, (PB99-118861, A15, MF-A03).

MCEER-98-0005 "Screening Guide for Rapid Assessment of Liquefaction Hazard at Highway Bridge Sites," by T. L. Youd, 6/16/98, (PB99-118879, A06, not available on microfiche).

MCEER-98-0006 "Structural Steel and Steel/Concrete Interface Details for Bridges," by P. Ritchie, N. Kauhl and J. Kulicki, 7/13/98, (PB99-118945, A06, MF-A01).

MCEER-98-0007 "Capacity Design and Fatigue Analysis of Confined Concrete Columns," by A. Dutta and J.B. Mander, 7/14/98, (PB99-118960, A14, MF-A03).

MCEER-98-0008 "Proceedings of the Workshop on Performance Criteria for Telecommunication Services Under Earthquake Conditions," edited by A.J. Schiff, 7/15/98, (PB99-118952, A08, MF-A02).

MCEER-98-0009 "Fatigue Analysis of Unconfined Concrete Columns," by J.B. Mander, A. Dutta and J.H. Kim, 9/12/98, (PB99-123655, A10, MF-A02).

MCEER-98-0010 "Centrifuge Modeling of Cyclic Lateral Response of Pile-Cap Systems and Seat-Type Abutments in Dry Sands," by A.D. Gadre and R. Dobry, 10/2/98, (PB99-123606, A13, MF-A03).

MCEER-98-0011 "IDARC-BRIDGE: A Computational Platform for Seismic Damage Assessment of Bridge Structures," by A.M. Reinhorn, V. Simeonov, G. Mylonakis and Y. Reichman, 10/2/98, (PB99-162919, A15, MF-A03).

MCEER-98-0012 "Experimental Investigation of the Dynamic Response of Two Bridges Before and After Retrofitting with Elastomeric Bearings," by D.A. Wendichansky, S.S. Chen and J.B. Mander, 10/2/98, (PB99-162927, A15, MF-A03).

MCEER-98-0013 "Design Procedures for Hinge Restrainers and Hinge Sear Width for Multiple-Frame Bridges," by R. Des Roches and G.L. Fenves, 11/3/98, (PB99-140477, A13, MF-A03).

MCEER-98-0014 "Response Modification Factors for Seismically Isolated Bridges," by M.C. Constantinou and J.K. Quarshie, 11/3/98, (PB99-140485, A14, MF-A03).

MCEER-98-0015 "Proceedings of the U.S.-Italy Workshop on Seismic Protective Systems for Bridges," edited by I.M. Friedland and M.C. Constantinou, 11/3/98, (PB2000-101711, A22, MF-A04).

MCEER-98-0016 "Appropriate Seismic Reliability for Critical Equipment Systems: Recommendations Based on Regional Analysis of Financial and Life Loss," by K. Porter, C. Scawthorn, C. Taylor and N. Blais, 11/10/98, (PB99-157265, A08, MF-A02).

MCEER-98-0017 "Proceedings of the U.S. Japan Joint Seminar on Civil Infrastructure Systems Research," edited by M. Shinozuka and A. Rose, 11/12/98, (PB99-156713, A16, MF-A03).

MCEER-98-0018 "Modeling of Pile Footings and Drilled Shafts for Seismic Design," by I. PoLam, M. Kapuskar and D. Chaudhuri, 12/21/98, (PB99-157257, A09, MF-A02).

MCEER-99-0001 "Seismic Evaluation of a Masonry Infilled Reinforced Concrete Frame by Pseudodynamic Testing," by S.G. Buonopane and R.N. White, 2/16/99, (PB99-162851, A09, MF-A02).

MCEER-99-0002 "Response History Analysis of Structures with Seismic Isolation and Energy Dissipation Systems: Verification Examples for Program SAP2000," by J. Scheller and M.C. Constantinou, 2/22/99, (PB99-162869, A08, MF-A02).

MCEER-99-0003 "Experimental Study on the Seismic Design and Retrofit of Bridge Columns Including Axial Load Effects," by A. Dutta, T. Kokorina and J.B. Mander, 2/22/99, (PB99-162877, A09, MF-A02).

MCEER-99-0004 "Experimental Study of Bridge Elastomeric and Other Isolation and Energy Dissipation Systems with Emphasis on Uplift Prevention and High Velocity Near-source Seismic Excitation," by A. Kasalanati and M. C. Constantinou, 2/26/99, (PB99-162885, A12, MF-A03).

MCEER-99-0005 "Truss Modeling of Reinforced Concrete Shear-flexure Behavior," by J.H. Kim and J.B. Mander, 3/8/99, (PB99-163693, A12, MF-A03).

MCEER-99-0006 "Experimental Investigation and Computational Modeling of Seismic Response of a 1:4 Scale Model Steel Structure with a Load Balancing Supplemental Damping System," by G. Pekcan, J.B. Mander and S.S. Chen, 4/2/99, (PB99-162893, A11, MF-A03).

MCEER-99-0007 "Effect of Vertical Ground Motions on the Structural Response of Highway Bridges," by M.R. Button, C.J. Cronin and R.L. Mayes, 4/10/99, (PB2000-101411, A10, MF-A03).

MCEER-99-0008 "Seismic Reliability Assessment of Critical Facilities: A Handbook, Supporting Documentation, and Model Code Provisions," by G.S. Johnson, R.E. Sheppard, M.D. Quilici, S.J. Eder and C.R. Scawthorn, 4/12/99, (PB2000-101701, A18, MF-A04).

MCEER-99-0009 "Impact Assessment of Selected MCEER Highway Project Research on the Seismic Design of Highway Structures," by C. Rojahn, R. Mayes, D.G. Anderson, J.H. Clark, D'Appolonia Engineering, S. Gloyd and R.V. Nutt, 4/14/99, (PB99-162901, A10, MF-A02).

MCEER-99-0010 "Site Factors and Site Categories in Seismic Codes," by R. Dobry, R. Ramos and M.S. Power, 7/19/99, (PB2000-101705, A08, MF-A02).

MCEER-99-0011 "Restrainer Design Procedures for Multi-Span Simply-Supported Bridges," by M.J. Randall, M. Saiidi, E. Maragakis and T. Isakovic, 7/20/99, (PB2000-101702, A10, MF-A02).

MCEER-99-0012 "Property Modification Factors for Seismic Isolation Bearings," by M.C. Constantinou, P. Tsopelas, A. Kasalanati and E. Wolff, 7/20/99, (PB2000-103387, A11, MF-A03).

MCEER-99-0013 "Critical Seismic Issues for Existing Steel Bridges," by P. Ritchie, N. Kauhl and J. Kulicki, 7/20/99, (PB2000-101697, A09, MF-A02).

MCEER-99-0014 "Nonstructural Damage Database," by A. Kao, T.T. Soong and A. Vender, 7/24/99, (PB2000-101407, A06, MF-A01).

MCEER-99-0015 "Guide to Remedial Measures for Liquefaction Mitigation at Existing Highway Bridge Sites," by H.G. Cooke and J. K. Mitchell, 7/26/99, (PB2000-101703, A11, MF-A03).

MCEER-99-0016 "Proceedings of the MCEER Workshop on Ground Motion Methodologies for the Eastern United States," edited by N. Abrahamson and A. Becker, 8/11/99, (PB2000-103385, A07, MF-A02).

MCEER-99-0017 "Quindío, Colombia Earthquake of January 25, 1999: Reconnaissance Report," by A.P. Asfura and P.J. Flores, 10/4/99, (PB2000-106893, A06, MF-A01).

MCEER-99-0018 "Hysteretic Models for Cyclic Behavior of Deteriorating Inelastic Structures," by M.V. Sivaselvan and A.M. Reinhorn, 11/5/99, (PB2000-103386, A08, MF-A02).

MCEER-99-0019 "Proceedings of the 7th U.S.- Japan Workshop on Earthquake Resistant Design of Lifeline Facilities and Countermeasures Against Soil Liquefaction," edited by T.D. O'Rourke, J.P. Bardet and M. Hamada, 11/19/99, (PB2000-103354, A99, MF-A06).

MCEER-99-0020 "Development of Measurement Capability for Micro-Vibration Evaluations with Application to Chip Fabrication Facilities," by G.C. Lee, Z. Liang, J.W. Song, J.D. Shen and W.C. Liu, 12/1/99, (PB2000-105993, A08, MF-A02).

MCEER-99-0021 "Design and Retrofit Methodology for Building Structures with Supplemental Energy Dissipating Systems," by G. Pekcan, J.B. Mander and S.S. Chen, 12/31/99, (PB2000-105994, A11, MF-A03).

MCEER-00-0001 "The Marmara, Turkey Earthquake of August 17, 1999: Reconnaissance Report," edited by C. Scawthorn; with major contributions by M. Bruneau, R. Eguchi, T. Holzer, G. Johnson, J. Mander, J. Mitchell, W. Mitchell, A. Papageorgiou, C. Scaethorn, and G. Webb, 3/23/00, (PB2000-106200, A11, MF-A03).

MCEER-00-0002 "Proceedings of the MCEER Workshop for Seismic Hazard Mitigation of Health Care Facilities," edited by G.C. Lee, M. Ettouney, M. Grigoriu, J. Hauer and J. Nigg, 3/29/00, (PB2000-106892, A08, MF-A02).

MCEER-00-0003 "The Chi-Chi, Taiwan Earthquake of September 21, 1999: Reconnaissance Report," edited by G.C. Lee and C.H. Loh, with major contributions by G.C. Lee, M. Bruneau, I.G. Buckle, S.E. Chang, P.J. Flores, T.D. O'Rourke, M. Shinozuka, T.T. Soong, C-H. Loh, K-C. Chang, Z-J. Chen, J-S. Hwang, M-L. Lin, G-Y. Liu, K-C. Tsai, G.C. Yao and C-L. Yen, 4/30/00, (PB2001-100980, A10, MF-A02).

MCEER-00-0004 "Seismic Retrofit of End-Sway Frames of Steel Deck-Truss Bridges with a Supplemental Tendon System: Experimental and Analytical Investigation," by G. Pekcan, J.B. Mander and S.S. Chen, 7/1/00, (PB2001-100982, A10, MF-A02).

MCEER-00-0005 "Sliding Fragility of Unrestrained Equipment in Critical Facilities," by W.H. Chong and T.T. Soong, 7/5/00, (PB2001-100983, A08, MF-A02).

MCEER-00-0006 "Seismic Response of Reinforced Concrete Bridge Pier Walls in the Weak Direction," by N. Abo-Shadi, M. Saiidi and D. Sanders, 7/17/00, (PB2001-100981, A17, MF-A03).

MCEER-00-0007 "Low-Cycle Fatigue Behavior of Longitudinal Reinforcement in Reinforced Concrete Bridge Columns," by J. Brown and S.K. Kunnath, 7/23/00, (PB2001-104392, A08, MF-A02).

MCEER-00-0008 "Soil Structure Interaction of Bridges for Seismic Analysis," I. PoLam and H. Law, 9/25/00, (PB2001-105397, A08, MF-A02).

MCEER-00-0009 "Proceedings of the First MCEER Workshop on Mitigation of Earthquake Disaster by Advanced Technologies (MEDAT-1), edited by M. Shinozuka, D.J. Inman and T.D. O'Rourke, 11/10/00, (PB2001-105399, A14, MF-A03).

MCEER-00-0010 "Development and Evaluation of Simplified Procedures for Analysis and Design of Buildings with Passive Energy Dissipation Systems, Revision 01," by O.M. Ramirez, M.C. Constantinou, C.A. Kircher, A.S. Whittaker, M.W. Johnson, J.D. Gomez and C. Chrysostomou, 11/16/01, (PB2001-105523, A23, MF-A04).

MCEER-00-0011 "Dynamic Soil-Foundation-Structure Interaction Analyses of Large Caissons," by C-Y. Chang, C-M. Mok, Z-L. Wang, R. Settgast, F. Waggoner, M.A. Ketchum, H.M. Gonnermann and C-C. Chin, 12/30/00, (PB2001-104373, A07, MF-A02).

MCEER-00-0012 "Experimental Evaluation of Seismic Performance of Bridge Restrainers," by A.G. Vlassis, E.M. Maragakis and M. Saiid Saiidi, 12/30/00, (PB2001-104354, A09, MF-A02).

MCEER-00-0013 "Effect of Spatial Variation of Ground Motion on Highway Structures," by M. Shinozuka, V. Saxena and G. Deodatis, 12/31/00, (PB2001-108755, A13, MF-A03).

MCEER-00-0014 "A Risk-Based Methodology for Assessing the Seismic Performance of Highway Systems," by S.D. Werner, C.E. Taylor, J.E. Moore, II, J.S. Walton and S. Cho, 12/31/00, (PB2001-108756, A14, MF-A03).

MCEER-01-0001 "Experimental Investigation of P-Delta Effects to Collapse During Earthquakes," by D. Vian and M. Bruneau, 6/25/01, (PB2002-100534, A17, MF-A03).

MCEER-01-0002 "Proceedings of the Second MCEER Workshop on Mitigation of Earthquake Disaster by Advanced Technologies (MEDAT-2)," edited by M. Bruneau and D.J. Inman, 7/23/01, (PB2002-100434, A16, MF-A03).

MCEER-01-0003 "Sensitivity Analysis of Dynamic Systems Subjected to Seismic Loads," by C. Roth and M. Grigoriu, 9/18/01, (PB2003-100884, A12, MF-A03).

MCEER-01-0004 "Overcoming Obstacles to Implementing Earthquake Hazard Mitigation Policies: Stage 1 Report," by D.J. Alesch and W.J. Petak, 12/17/01, (PB2002-107949, A07, MF-A02).

MCEER-01-0005 "Updating Real-Time Earthquake Loss Estimates: Methods, Problems and Insights," by C.E. Taylor, S.E. Chang and R.T. Eguchi, 12/17/01, (PB2002-107948, A05, MF-A01).

MCEER-01-0006 "Experimental Investigation and Retrofit of Steel Pile Foundations and Pile Bents Under Cyclic Lateral Loadings," by A. Shama, J. Mander, B. Blabac and S. Chen, 12/31/01, (PB2002-107950, A13, MF-A03).

MCEER-02-0001 "Assessment of Performance of Bolu Viaduct in the 1999 Duzce Earthquake in Turkey" by P.C. Roussis, M.C. Constantinou, M. Erdik, E. Durukal and M. Dicleli, 5/8/02, (PB2003-100883, A08, MF-A02).

MCEER-02-0002 "Seismic Behavior of Rail Counterweight Systems of Elevators in Buildings," by M.P. Singh, Rildova and L.E. Suarez, 5/27/02. (PB2003-100882, A11, MF-A03).

MCEER-02-0003 "Development of Analysis and Design Procedures for Spread Footings," by G. Mylonakis, G. Gazetas, S. Nikolaou and A. Chauncey, 10/02/02, (PB2004-101636, A13, MF-A03, CD-A13).

MCEER-02-0004 "Bare-Earth Algorithms for Use with SAR and LIDAR Digital Elevation Models," by C.K. Huyck, R.T. Eguchi and B. Houshmand, 10/16/02, (PB2004-101637, A07, CD-A07).

MCEER-02-0005 "Review of Energy Dissipation of Compression Members in Concentrically Braced Frames," by K.Lee and M. Bruneau, 10/18/02, (PB2004-101638, A10, CD-A10).

MCEER-03-0001 "Experimental Investigation of Light-Gauge Steel Plate Shear Walls for the Seismic Retrofit of Buildings" by J. Berman and M. Bruneau, 5/2/03, (PB2004-101622, A10, MF-A03, CD-A10).

MCEER-03-0002 "Statistical Analysis of Fragility Curves," by M. Shinozuka, M.Q. Feng, H. Kim, T. Uzawa and T. Ueda, 6/16/03, (PB2004-101849, A09, CD-A09).

MCEER-03-0003 "Proceedings of the Eighth U.S.-Japan Workshop on Earthquake Resistant Design f Lifeline Facilities and Countermeasures Against Liquefaction," edited by M. Hamada, J.P. Bardet and T.D. O'Rourke, 6/30/03, (PB2004-104386, A99, CD-A99).

MCEER-03-0004 "Proceedings of the PRC-US Workshop on Seismic Analysis and Design of Special Bridges," edited by L.C. Fan and G.C. Lee, 7/15/03, (PB2004-104387, A14, CD-A14).

MCEER-03-0005 "Urban Disaster Recovery: A Framework and Simulation Model," by S.B. Miles and S.E. Chang, 7/25/03, (PB2004-104388, A07, CD-A07).

MCEER-03-0006 "Behavior of Underground Piping Joints Due to Static and Dynamic Loading," by R.D. Meis, M. Maragakis and R. Siddharthan, 11/17/03, (PB2005-102194, A13, MF-A03, CD-A00).

MCEER-04-0001 "Experimental Study of Seismic Isolation Systems with Emphasis on Secondary System Response and Verification of Accuracy of Dynamic Response History Analysis Methods," by E. Wolff and M. Constantinou, 1/16/04 (PB2005-102195, A99, MF-E08, CD-A00).

MCEER-04-0002 "Tension, Compression and Cyclic Testing of Engineered Cementitious Composite Materials," by K. Kesner and S.L. Billington, 3/1/04, (PB2005-102196, A08, CD-A08).

MCEER-04-0003 "Cyclic Testing of Braces Laterally Restrained by Steel Studs to Enhance Performance During Earthquakes," by O.C. Celik, J.W. Berman and M. Bruneau, 3/16/04, (PB2005-102197, A13, MF-A03, CD-A00).

MCEER-04-0004 "Methodologies for Post Earthquake Building Damage Detection Using SAR and Optical Remote Sensing: Application to the August 17, 1999 Marmara, Turkey Earthquake," by C.K. Huyck, B.J. Adams, S. Cho, R.T. Eguchi, B. Mansouri and B. Houshmand, 6/15/04, (PB2005-104888, A10, CD-A00).

MCEER-04-0005 "Nonlinear Structural Analysis Towards Collapse Simulation: A Dynamical Systems Approach," by M.V. Sivaselvan and A.M. Reinhorn, 6/16/04, (PB2005-104889, A11, MF-A03, CD-A00).

MCEER-04-0006 "Proceedings of the Second PRC-US Workshop on Seismic Analysis and Design of Special Bridges," edited by G.C. Lee and L.C. Fan, 6/25/04, (PB2005-104890, A16, CD-A00).

MCEER-04-0007 "Seismic Vulnerability Evaluation of Axially Loaded Steel Built-up Laced Members," by K. Lee and M. Bruneau, 6/30/04, (PB2005-104891, A16, CD-A00).

MCEER-04-0008 "Evaluation of Accuracy of Simplified Methods of Analysis and Design of Buildings with Damping Systems for Near-Fault and for Soft-Soil Seismic Motions," by E.A. Pavlou and M.C. Constantinou, 8/16/04, (PB2005-104892, A08, MF-A02, CD-A00).

MCEER-04-0009 "Assessment of Geotechnical Issues in Acute Care Facilities in California," by M. Lew, T.D. O'Rourke, R. Dobry and M. Koch, 9/15/04, (PB2005-104893, A08, CD-A00).

MCEER-04-0010 "Scissor-Jack-Damper Energy Dissipation System," by A.N. Sigaher-Boyle and M.C. Constantinou, 12/1/04 (PB2005-108221).

MCEER-04-0011 "Seismic Retrofit of Bridge Steel Truss Piers Using a Controlled Rocking Approach," by M. Pollino and M. Bruneau, 12/20/04 (PB2006-105795).

MCEER-05-0001 "Experimental and Analytical Studies of Structures Seismically Isolated with an Uplift-Restraint Isolation System," by P.C. Roussis and M.C. Constantinou, 1/10/05 (PB2005-108222).

MCEER-05-0002 "A Versatile Experimentation Model for Study of Structures Near Collapse Applied to Seismic Evaluation of Irregular Structures," by D. Kusumastuti, A.M. Reinhorn and A. Rutenberg, 3/31/05 (PB2006-101523).

MCEER-05-0003 "Proceedings of the Third PRC-US Workshop on Seismic Analysis and Design of Special Bridges," edited by L.C. Fan and G.C. Lee, 4/20/05, (PB2006-105796).

MCEER-05-0004 "Approaches for the Seismic Retrofit of Braced Steel Bridge Piers and Proof-of-Concept Testing of an Eccentrically Braced Frame with Tubular Link," by J.W. Berman and M. Bruneau, 4/21/05 (PB2006-101524).

MCEER-05-0005 "Simulation of Strong Ground Motions for Seismic Fragility Evaluation of Nonstructural Components in Hospitals," by A. Wanitkorkul and A. Filiatrault, 5/26/05 (PB2006-500027).

MCEER-05-0006 "Seismic Safety in California Hospitals: Assessing an Attempt to Accelerate the Replacement or Seismic Retrofit of Older Hospital Facilities," by D.J. Alesch, L.A. Arendt and W.J. Petak, 6/6/05 (PB2006-105794).

MCEER-05-0007 "Development of Seismic Strengthening and Retrofit Strategies for Critical Facilities Using Engineered Cementitious Composite Materials," by K. Kesner and S.L. Billington, 8/29/05 (PB2006-111701).

MCEER-05-0008 "Experimental and Analytical Studies of Base Isolation Systems for Seismic Protection of Power Transformers," by N. Murota, M.Q. Feng and G-Y. Liu, 9/30/05 (PB2006-111702).

MCEER-05-0009 "3D-BASIS-ME-MB: Computer Program for Nonlinear Dynamic Analysis of Seismically Isolated Structures," by P.C. Tsopelas, P.C. Roussis, M.C. Constantinou, R. Buchanan and A.M. Reinhorn, 10/3/05 (PB2006-111703).

MCEER-05-0010 "Steel Plate Shear Walls for Seismic Design and Retrofit of Building Structures," by D. Vian and M. Bruneau, 12/15/05 (PB2006-111704).

MCEER-05-0011 "The Performance-Based Design Paradigm," by M.J. Astrella and A. Whittaker, 12/15/05 (PB2006-111705).

MCEER-06-0001 "Seismic Fragility of Suspended Ceiling Systems," H. Badillo-Almaraz, A.S. Whittaker, A.M. Reinhorn and G.P. Cimellaro, 2/4/06 (PB2006-111706).

MCEER-06-0002 "Multi-Dimensional Fragility of Structures," by G.P. Cimellaro, A.M. Reinhorn and M. Bruneau, 3/1/06 (PB2007-106974, A09, MF-A02, CD A00).

MCEER-06-0003 "Built-Up Shear Links as Energy Dissipators for Seismic Protection of Bridges," by P. Dusicka, A.M. Itani and I.G. Buckle, 3/15/06 (PB2006-111708).

MCEER-06-0004 "Analytical Investigation of the Structural Fuse Concept," by R.E. Vargas and M. Bruneau, 3/16/06 (PB2006-111709).

MCEER-06-0005 "Experimental Investigation of the Structural Fuse Concept," by R.E. Vargas and M. Bruneau, 3/17/06 (PB2006-111710).

MCEER-06-0006 "Further Development of Tubular Eccentrically Braced Frame Links for the Seismic Retrofit of Braced Steel Truss Bridge Piers," by J.W. Berman and M. Bruneau, 3/27/06 (PB2007-105147).

MCEER-06-0007 "REDARS Validation Report," by S. Cho, C.K. Huyck, S. Ghosh and R.T. Eguchi, 8/8/06 (PB2007-106983).

MCEER-06-0008 "Review of Current NDE Technologies for Post-Earthquake Assessment of Retrofitted Bridge Columns," by J.W. Song, Z. Liang and G.C. Lee, 8/21/06 (PB2007-106984).

MCEER-06-0009 "Liquefaction Remediation in Silty Soils Using Dynamic Compaction and Stone Columns," by S. Thevanayagam, G.R. Martin, R. Nashed, T. Shenthan, T. Kanagalingam and N. Ecemis, 8/28/06 (PB2007-106985).

MCEER-06-0010 "Conceptual Design and Experimental Investigation of Polymer Matrix Composite Infill Panels for Seismic Retrofitting," by W. Jung, M. Chiewanichakorn and A.J. Aref, 9/21/06 (PB2007-106986).

MCEER-06-0011 "A Study of the Coupled Horizontal-Vertical Behavior of Elastomeric and Lead-Rubber Seismic Isolation Bearings," by G.P. Warn and A.S. Whittaker, 9/22/06 (PB2007-108679).

MCEER-06-0012 "Proceedings of the Fourth PRC-US Workshop on Seismic Analysis and Design of Special Bridges: Advancing Bridge Technologies in Research, Design, Construction and Preservation," Edited by L.C. Fan, G.C. Lee and L. Ziang, 10/12/06 (PB2007-109042).

MCEER-06-0013 "Cyclic Response and Low Cycle Fatigue Characteristics of Plate Steels," by P. Dusicka, A.M. Itani and I.G. Buckle, 11/1/06 06 (PB2007-106987).

MCEER-06-0014 "Proceedings of the Second US-Taiwan Bridge Engineering Workshop," edited by W.P. Yen, J. Shen, J-Y. Chen and M. Wang, 11/15/06 (PB2008-500041).

MCEER-06-0015 "User Manual and Technical Documentation for the REDARS^{TM} Import Wizard," by S. Cho, S. Ghosh, C.K. Huyck and S.D. Werner, 11/30/06 (PB2007-114766).

MCEER-06-0016 "Hazard Mitigation Strategy and Monitoring Technologies for Urban and Infrastructure Public Buildings: Proceedings of the China-US Workshops," edited by X.Y. Zhou, A.L. Zhang, G.C. Lee and M. Tong, 12/12/06 (PB2008-500018).

MCEER-07-0001 "Static and Kinetic Coefficients of Friction for Rigid Blocks," by C. Kafali, S. Fathali, M. Grigoriu and A.S. Whittaker, 3/20/07 (PB2007-114767).

MCEER-07-0002 "Hazard Mitigation Investment Decision Making: Organizational Response to Legislative Mandate," by L.A. Arendt, D.J. Alesch and W.J. Petak, 4/9/07 (PB2007-114768).

MCEER-07-0003 "Seismic Behavior of Bidirectional-Resistant Ductile End Diaphragms with Unbonded Braces in Straight or Skewed Steel Bridges," by O. Celik and M. Bruneau, 4/11/07 (PB2008-105141).

MCEER-07-0004 "Modeling Pile Behavior in Large Pile Groups Under Lateral Loading," by A.M. Dodds and G.R. Martin, 4/16/07(PB2008-105142).

MCEER-07-0005 "Experimental Investigation of Blast Performance of Seismically Resistant Concrete-Filled Steel Tube Bridge Piers," by S. Fujikura, M. Bruneau and D. Lopez-Garcia, 4/20/07 (PB2008-105143).

MCEER-07-0006 "Seismic Analysis of Conventional and Isolated Liquefied Natural Gas Tanks Using Mechanical Analogs," by I.P. Christovasilis and A.S. Whittaker, 5/1/07.

MCEER-07-0007 "Experimental Seismic Performance Evaluation of Isolation/Restraint Systems for Mechanical Equipment – Part 1: Heavy Equipment Study," by S. Fathali and A. Filiatrault, 6/6/07 (PB2008-105144).

MCEER-07-0008 "Seismic Vulnerability of Timber Bridges and Timber Substructures," by A.A. Sharma, J.B. Mander, I.M. Friedland and D.R. Allicock, 6/7/07 (PB2008-105145).

MCEER-07-0009 "Experimental and Analytical Study of the XY-Friction Pendulum (XY-FP) Bearing for Bridge Applications," by C.C. Marin-Artieda, A.S. Whittaker and M.C. Constantinou, 6/7/07 (PB2008-105191).

MCEER-07-0010 "Proceedings of the PRC-US Earthquake Engineering Forum for Young Researchers," Edited by G.C. Lee and X.Z. Qi, 6/8/07 (PB2008-500058).

MCEER-07-0011 "Design Recommendations for Perforated Steel Plate Shear Walls," by R. Purba and M. Bruneau, 6/18/07, (PB2008-105192).

MCEER-07-0012 "Performance of Seismic Isolation Hardware Under Service and Seismic Loading," by M.C. Constantinou, A.S. Whittaker, Y. Kalpakidis, D.M. Fenz and G.P. Warn, 8/27/07, (PB2008-105193).

MCEER-07-0013 "Experimental Evaluation of the Seismic Performance of Hospital Piping Subassemblies," by E.R. Goodwin, E. Maragakis and A.M. Itani, 9/4/07, (PB2008-105194).

MCEER-07-0014 "A Simulation Model of Urban Disaster Recovery and Resilience: Implementation for the 1994 Northridge Earthquake," by S. Miles and S.E. Chang, 9/7/07, (PB2008-106426).

MCEER-07-0015 "Statistical and Mechanistic Fragility Analysis of Concrete Bridges," by M. Shinozuka, S. Banerjee and S-H. Kim, 9/10/07, (PB2008-106427).

MCEER-07-0016 "Three-Dimensional Modeling of Inelastic Buckling in Frame Structures," by M. Schachter and AM. Reinhorn, 9/13/07, (PB2008-108125).

MCEER-07-0017 "Modeling of Seismic Wave Scattering on Pile Groups and Caissons," by I. Po Lam, H. Law and C.T. Yang, 9/17/07 (PB2008-108150).

MCEER-07-0018 "Bridge Foundations: Modeling Large Pile Groups and Caissons for Seismic Design," by I. Po Lam, H. Law and G.R. Martin (Coordinating Author), 12/1/07 (PB2008-111190).

MCEER-07-0019 "Principles and Performance of Roller Seismic Isolation Bearings for Highway Bridges," by G.C. Lee, Y.C. Ou, Z. Liang, T.C. Niu and J. Song, 12/10/07 (PB2009-110466).

MCEER-07-0020 "Centrifuge Modeling of Permeability and Pinning Reinforcement Effects on Pile Response to Lateral Spreading," by L.L Gonzalez-Lagos, T. Abdoun and R. Dobry, 12/10/07 (PB2008-111191).

MCEER-07-0021 "Damage to the Highway System from the Pisco, Perú Earthquake of August 15, 2007," by J.S. O'Connor, L. Mesa and M. Nykamp, 12/10/07, (PB2008-108126).

MCEER-07-0022 "Experimental Seismic Performance Evaluation of Isolation/Restraint Systems for Mechanical Equipment – Part 2: Light Equipment Study," by S. Fathali and A. Filiatrault, 12/13/07 (PB2008-111192).

MCEER-07-0023 "Fragility Considerations in Highway Bridge Design," by M. Shinozuka, S. Banerjee and S.H. Kim, 12/14/07 (PB2008-111193).

MCEER-07-0024 "Performance Estimates for Seismically Isolated Bridges," by G.P. Warn and A.S. Whittaker, 12/30/07 (PB2008-112230).

MCEER-08-0001 "Seismic Performance of Steel Girder Bridge Superstructures with Conventional Cross Frames," by L.P. Carden, A.M. Itani and I.G. Buckle, 1/7/08, (PB2008-112231).

MCEER-08-0002 "Seismic Performance of Steel Girder Bridge Superstructures with Ductile End Cross Frames with Seismic Isolators," by L.P. Carden, A.M. Itani and I.G. Buckle, 1/7/08 (PB2008-112232).

MCEER-08-0003 "Analytical and Experimental Investigation of a Controlled Rocking Approach for Seismic Protection of Bridge Steel Truss Piers," by M. Pollino and M. Bruneau, 1/21/08 (PB2008-112233).

MCEER-08-0004 "Linking Lifeline Infrastructure Performance and Community Disaster Resilience: Models and Multi-Stakeholder Processes," by S.E. Chang, C. Pasion, K. Tatebe and R. Ahmad, 3/3/08 (PB2008-112234).

MCEER-08-0005 "Modal Analysis of Generally Damped Linear Structures Subjected to Seismic Excitations," by J. Song, Y-L. Chu, Z. Liang and G.C. Lee, 3/4/08 (PB2009-102311).

MCEER-08-0006 "System Performance Under Multi-Hazard Environments," by C. Kafali and M. Grigoriu, 3/4/08 (PB2008-112235).

MCEER-08-0007 "Mechanical Behavior of Multi-Spherical Sliding Bearings," by D.M. Fenz and M.C. Constantinou, 3/6/08 (PB2008-112236).

MCEER-08-0008 "Post-Earthquake Restoration of the Los Angeles Water Supply System," by T.H.P. Tabucchi and R.A. Davidson, 3/7/08 (PB2008-112237).

MCEER-08-0009 "Fragility Analysis of Water Supply Systems," by A. Jacobson and M. Grigoriu, 3/10/08 (PB2009-105545).

MCEER-08-0010 "Experimental Investigation of Full-Scale Two-Story Steel Plate Shear Walls with Reduced Beam Section Connections," by B. Qu, M. Bruneau, C-H. Lin and K-C. Tsai, 3/17/08 (PB2009-106368).

MCEER-08-0011 "Seismic Evaluation and Rehabilitation of Critical Components of Electrical Power Systems," S. Ersoy, B. Feizi, A. Ashrafi and M. Ala Saadeghvaziri, 3/17/08 (PB2009-105546).

MCEER-08-0012 "Seismic Behavior and Design of Boundary Frame Members of Steel Plate Shear Walls," by B. Qu and M. Bruneau, 4/26/08 . (PB2009-106744).

MCEER-08-0013 "Development and Appraisal of a Numerical Cyclic Loading Protocol for Quantifying Building System Performance," by A. Filiatrault, A. Wanitkorkul and M. Constantinou, 4/27/08 (PB2009-107906).

MCEER-08-0014 "Structural and Nonstructural Earthquake Design: The Challenge of Integrating Specialty Areas in Designing Complex, Critical Facilities," by W.J. Petak and D.J. Alesch, 4/30/08 (PB2009-107907).

MCEER-08-0015 "Seismic Performance Evaluation of Water Systems," by Y. Wang and T.D. O'Rourke, 5/5/08 (PB2009-107908).

MCEER-08-0016 "Seismic Response Modeling of Water Supply Systems," by P. Shi and T.D. O'Rourke, 5/5/08 (PB2009-107910).

MCEER-08-0017 "Numerical and Experimental Studies of Self-Centering Post-Tensioned Steel Frames," by D. Wang and A. Filiatrault, 5/12/08 (PB2009-110479).

MCEER-08-0018 "Development, Implementation and Verification of Dynamic Analysis Models for Multi-Spherical Sliding Bearings," by D.M. Fenz and M.C. Constantinou, 8/15/08 (PB2009-107911).

MCEER-08-0019 "Performance Assessment of Conventional and Base Isolated Nuclear Power Plants for Earthquake Blast Loadings," by Y.N. Huang, A.S. Whittaker and N. Luco, 10/28/08 (PB2009-107912).

MCEER-08-0020 "Remote Sensing for Resilient Multi-Hazard Disaster Response – Volume I: Introduction to Damage Assessment Methodologies," by B.J. Adams and R.T. Eguchi, 11/17/08.

MCEER-08-0021 "Remote Sensing for Resilient Multi-Hazard Disaster Response – Volume II: Counting the Number of Collapsed Buildings Using an Object-Oriented Analysis: Case Study of the 2003 Bam Earthquake," by L. Gusella, C.K. Huyck and B.J. Adams, 11/17/08.

MCEER-08-0022 "Remote Sensing for Resilient Multi-Hazard Disaster Response – Volume III: Multi-Sensor Image Fusion Techniques for Robust Neighborhood-Scale Urban Damage Assessment," by B.J. Adams and A. McMillan, 11/17/08.

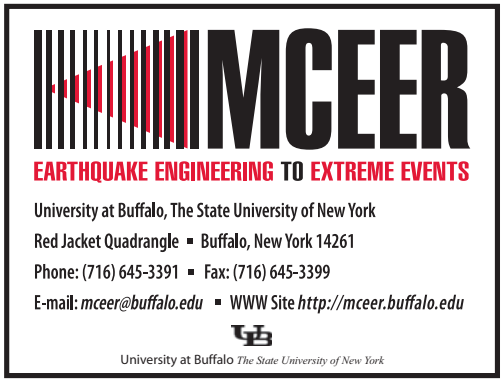

ISSN 1520-295X